



**Phthalocyanine and Subphthalocyanine Hybrid  
Macrocycles: Improved Accessibility and  
Synthetic Control via new Intermediates**

Jacob Gretton

This thesis is submitted in fulfilment of the requirements of the degree of  
Doctor of Philosophy at the University of East Anglia

School of Chemistry  
University of East Anglia, Norwich, United Kingdom

September 2022

©This copy of the thesis has been supplied on the condition that anyone who consults it, is understood to recognise that its copyright rests with the author and that no quotation from the thesis, nor any information derived therefrom, may be published without the author's prior written consent.

## Declaration

The research described in this thesis is, to the best of my knowledge, original except where due reference has been made.

Jacob Gretton

This thesis is dedicated to my beloved parents  
Svetlana & Adam Gretton

# Abstract

This thesis is concerned with the development of synthetic pathways towards tetrabenzoporphyrin/phthalocyanine hybrid macrocycles, specifically TBTAPs and SubTBDAPs. Initial investigations further explored the latest synthetic procedures developed by the Cammidge group, which revealed the formation of unexpected products during previous work. Further development of these procedures utilizing a variety of control mechanisms successfully facilitated more selective and higher yielding procedures for ABBA and ABBB TBTAP derivatives, as well as novel ABA SubTBDAP systems. This work revealed new mechanistic insights into both macrocyclization pathways.

New intermediates were identified by this work, which were key to understanding TBTAP macrocyclization at a mechanistic level. Synthetic pathways were developed to facilitate access to a variety of new intermediates, which can be considered to be partially pre-assembled macrocycles. This methodology offers an exciting basis for future work, and may be developed to facilitate the controlled and step-wise assembly of hybrid macrocycles.

Finally, the newly developed species facilitated the development of new TBTAP and SubTBDAP synthetic routes to produce novel macrocycles. These novel precursors and pathways possess numerous advantages; TBTAPs and SubTBDAPs were obtained in much greater yields than previously possible, new substitution patterns can now be selectively obtained, and macrocyclization occurs with milder conditions, potentially allowing synthetic access to TBTAPs and SubTBDAPs bearing thermally sensitive functional groups.

## **Access Condition and Agreement**

Each deposit in UEA Digital Repository is protected by copyright and other intellectual property rights, and duplication or sale of all or part of any of the Data Collections is not permitted, except that material may be duplicated by you for your research use or for educational purposes in electronic or print form. You must obtain permission from the copyright holder, usually the author, for any other use. Exceptions only apply where a deposit may be explicitly provided under a stated licence, such as a Creative Commons licence or Open Government licence.

Electronic or print copies may not be offered, whether for sale or otherwise to anyone, unless explicitly stated under a Creative Commons or Open Government license. Unauthorised reproduction, editing or reformatting for resale purposes is explicitly prohibited (except where approved by the copyright holder themselves) and UEA reserves the right to take immediate 'take down' action on behalf of the copyright and/or rights holder if this Access condition of the UEA Digital Repository is breached. Any material in this database has been supplied on the understanding that it is copyright material and that no quotation from the material may be published without proper acknowledgement.

# Acknowledgements

Firstly, I would like to thank Prof Andrew N. Cammidge for his continuous support throughout my journey as an undergraduate and PhD student at UEA. During my studies he has mentored me professionally and personally, and allowed me to thrive through the fantastic research he continuously drives forward. He is an exceptional example of a teacher, leader, and scientific mind.

I must also thank Dr Isabelle Fernandes for her extremely valuable experimental insights; working alongside you has been a pleasure, truly a wizard of this dark art we call macrocyclization! I would additionally like to thank all members, past and present, of lab 3.17, as well as the entirety of floor 3 for always providing a brilliant environment to work and share ideas.

Dr Philip Wilson, Dr Colin Macdonald, the HPC team, and the technical staff behind the scenes must be thanked for running and maintaining the instrumentation and equipment that is so critical to my own work, and the work of the entire department. Special thanks to Mark and Pete, taking the time to stop for a chat definitely helped keep me sane during the long days. This project would not have been possible without funding from UEA & the faculty of science, to which I am deeply grateful.

To my family I owe the deepest gratitude; from my earliest memories mum and dad nurtured my fascination for science and engineering, despite the large quantity of electronics dismantled and promptly broken. Thank you for teaching me the value of a curious and open mind, I would not be the person I am today without you both. I would like to extend this gratitude to the entire Cosford gang; my kind & wonderful sister Anna and grandmother Corinne, as well as Dan, Meg, Andy, Isabelle and Ben.

Finally, thank you to the exemplary selection of people that I am privileged to call my friends; Connor, Adam, Jake, Matt, Millie, Katie, Ant, Laura, Tess, Scott, Aby, and the rest of the crew. I doubt I would've been able to do this without your support. Despite half of the last 4 years being peppered with lockdowns and doom I have so many memories of truly excellent times, here's to many more adventures, shindigs and shenanigans!

# Contents

<b>List of Figures</b>	<b>12</b>
<b>1 Natural and synthetic macrocycles: synthesis, properties and applications</b>	<b>1</b>
1.1 Structure of Porphyrinoids and common hybrids . . . . .	1
1.2 Electronic structure of porphyrinoids . . . . .	4
1.3 Synthesis . . . . .	5
1.3.1 Porphyrins . . . . .	5
1.3.2 Phthalocyanines . . . . .	6
1.3.3 Subphthalocyanines . . . . .	8
1.3.4 TBTAPs and SubTBDAPs . . . . .	9
1.4 Functionalisation methods . . . . .	10
1.4.1 Peripheral and non-peripheral substitution . . . . .	10
1.4.2 Metalation and axial substitution . . . . .	11
1.4.3 <i>Meso</i> substitution . . . . .	13
1.4.4 Multichromophore arrays and complexes . . . . .	14
1.5 Current and potential applications . . . . .	14
1.5.1 OPVs . . . . .	14
1.5.2 NLOs . . . . .	16
1.5.3 Photocatalysis, photochemistry and PDT . . . . .	16
1.5.4 Molecular sensors . . . . .	17
1.5.5 SMMs . . . . .	19
<b>2 Investigations into TBTAP formation</b>	<b>20</b>
2.1 Introduction . . . . .	20
2.1.1 History of synthetic routes to TBTAPs . . . . .	20
2.1.2 Recent application and advances . . . . .	26
2.1.3 Recent advances in the Cammidge group . . . . .	26
2.2 Aims of this work . . . . .	33
2.2.1 Conditions screen . . . . .	33
2.2.2 Metal screen . . . . .	34
2.2.3 Intermediate targets . . . . .	34
2.3 Results and Discussion . . . . .	34
2.3.1 Aminoisoindoline synthesis . . . . .	34
2.3.2 Repeat of TBTAP procedure . . . . .	37
2.3.3 Repeat of TBTAP synthesis producing both 2:2 and 3:1 TBTAPs . . . . .	39
2.3.4 All in addition with varying reagent ratios . . . . .	43
2.3.5 Addition rates . . . . .	45

2.3.6	Metals . . . . .	46
2.4	Intermediate targets . . . . .	50
2.4.1	Target intermediates and methods . . . . .	50
2.4.2	Previously examined intermediates . . . . .	53
2.4.3	Dimethoxyisindolines, reactivity and potential stepwise construction . . . . .	55
2.4.4	Synthesis of target condensation products . . . . .	56
2.4.5	Protection method . . . . .	68
2.4.6	Summary of new synthetic methodology and future work	76
2.5	TBTAP synthesis from novel intermediate materials . . . . .	77
2.5.1	Unsubstituted derivatives . . . . .	77
2.5.2	Substituted TBTAPs via derivatives of <b>(30)</b> . . . . .	79
2.5.3	Discussion and mechanisms . . . . .	85
2.6	Conclusions and future work . . . . .	93
2.6.1	Synthetic methods for selective synthesis of 2:2 and 3:1 TBTAPs . . . . .	93
2.6.2	Synthetic methods for stepwise assembly of macro- cyclic building blocks . . . . .	95
2.6.3	Future work . . . . .	97
<b>3</b>	<b>Mechanistic investigations into SubTBDAP formation</b>	<b>100</b>
3.1	Introduction . . . . .	100
3.2	Aims . . . . .	102
3.2.1	Peripherally and non-peripherally substituted Sub- TBDAPs via conventional pathways . . . . .	102
3.2.2	SubTBDAP synthesis from newly developed species . .	104
3.3	Results and discussion . . . . .	106
3.3.1	Repeat of previously optimised procedures . . . . .	106
3.3.2	Attempted synthesis of non-peripherally substituted SubTBDAPs via conventional pathways . . . . .	108
3.3.3	Peripherally substituted SubTBDAPs via conven- tional pathways . . . . .	112
3.3.4	Attempted SubTBDAP synthesis from ‘trimer’ . . . . .	116
3.3.5	SubTBDAP from unsubstituted dimer . . . . .	116
3.4	Conclusions and future work . . . . .	119
<b>4</b>	<b>DFT studies on key proposed structures and pathways</b>	<b>121</b>
4.1	Introduction . . . . .	121
4.1.1	Aims . . . . .	121
4.1.2	Pathways to be targeted . . . . .	121
4.1.3	Methods . . . . .	122
4.2	Aminoisindoline homocondensation . . . . .	122
4.3	Synthesis of dimethoxyisindolines . . . . .	124
4.4	Synthesis of <b>(30)</b> and equilibrium . . . . .	126
4.5	Homocondensations of <b>(30)</b> at different positions . . . . .	128
4.6	Conclusions . . . . .	131

<b>5</b>	<b>Experimental</b>	<b>132</b>
5.1	General Methods . . . . .	132
5.2	Phthalonitriles and bromobenzonitriles . . . . .	132
5.2.1	6,7-Dicyano-1,2,3,4-tetrahydro-1,1,4,4-tetramethylnaphthalene ( <b>14</b> ) . . . . .	132
5.2.2	6-Bromo-7-cyano-1,2,3,4-tetrahydro-1,1,4,4-tetramethylnaphthalene . . . . .	135
5.2.3	4,5-Diphenoxyphtalonitrile . . . . .	136
5.2.4	4,5-Dimethoxyphtalonitrile . . . . .	136
5.2.5	2-Bromo-4,5-dimethoxybenzonitrile . . . . .	138
5.2.6	4,5-Dimethylphtalonitrile . . . . .	138
5.2.7	2-Bromo-4,5-dimethylbenzonitrile . . . . .	139
5.2.8	3,6-Diphenylphtalonitrile . . . . .	140
5.3	Amidines and aminoisoindolines . . . . .	142
5.3.1	( <i>Z</i> )-1-(Phenylmethylene)-1 <i>H</i> -isoindol-3-amine . . . . .	142
5.3.2	( <i>Z</i> )-1-[(4-Methoxybenzylidene)]-5,5,8,8-tetramethyl-5 <i>H</i> ,6 <i>H</i> ,7 <i>H</i> ,8 <i>H</i> -benzo[ <i>f</i> ]isoindol-3-amine . . . . .	144
5.3.3	( <i>Z</i> )-5,6-Dimethoxy-1-[(4-methoxy)benzylidene]-1 <i>H</i> -isoindol-3-amine . . . . .	146
5.4	Dimethoxyindolines . . . . .	147
5.4.1	1-Imino-3,3-dimethoxyisoindoline ( <b>29</b> ) . . . . .	147
5.4.2	N-Boc 1-imino-3,3-dimethoxyisoindoline ( <b>34</b> ) . . . . .	148
5.4.3	1-Imino-5,5,8,8-tetramethyl-5 <i>H</i> ,6 <i>H</i> ,7 <i>H</i> ,8 <i>H</i> -12,12-dimethoxyisoindoline ( <b>31</b> ) . . . . .	148
5.4.4	NBoc 1-Imino-5,5,8,8-tetramethyl-5 <i>H</i> ,6 <i>H</i> ,7 <i>H</i> ,8 <i>H</i> -12,12-dimethoxyisoindoline ( <b>36</b> ) . . . . .	149
5.4.5	1-Imino-4,5-diphenoxy-8,8-dimethoxyisoindoline . . . . .	150
5.4.6	1-Imino-3,3-dimethoxybenzo( <i>F</i> )isoindoline ( <b>41</b> ) . . . . .	150
5.5	Aminoisoindoline & dimethoxyisoindoline dimeric condensation products . . . . .	151
5.5.1	Condensation product ( <b>30</b> ) . . . . .	151
5.5.2	Condensation product ( <b>25</b> ) . . . . .	153
5.5.3	Condensation product ( <b>42</b> ) . . . . .	154
5.5.4	Condensation product ( <b>43</b> ) . . . . .	155
5.5.5	NBoc protected condensation product ( <b>35</b> ) . . . . .	156
5.5.6	NBoc protected condensation product ( <b>37</b> ) . . . . .	157
5.6	Trimeric condensation products . . . . .	158
5.6.1	Condensation product ( <b>33</b> ) . . . . .	158
5.6.2	Condensation product ( <b>40</b> ) . . . . .	159
5.7	TBTAPs . . . . .	161
5.7.1	MgTBTAP ( <b>16</b> ) . . . . .	161
5.7.2	2:2 MgTBTAP ( <b>18</b> ) . . . . .	162
5.7.3	3:1 MgTBTAP ( <b>19</b> ) . . . . .	163
5.7.4	3:1 ZnTBTAP ( <b>24</b> ) . . . . .	165
5.7.5	1:3 MgTBTAP ( <b>53</b> ) . . . . .	166
5.7.6	3:1 MgTBTAP ( <b>54</b> ) . . . . .	167
5.8	SubTBDAPs . . . . .	169
5.8.1	SubTBDAP-OPh ( <b>46</b> ) . . . . .	169
5.8.2	Naphthyl-SubTBDAP-OPh ( <b>47</b> ) . . . . .	171

<b>6 Appendix</b>	<b>181</b>
6.1 Publications . . . . .	181

# List of Abbreviations

Ar	Aromatic
BINAP	2,2'-Bis(diphenylphosphino)-1,1'-binaphthyl
br	Broad
C	Celsius
<i>cis</i> -TBDAP	<i>cis</i> -Tetrabenzodiazaporphyrin
COF	Covalent Organic Framework
COSY	Correlation Spectroscopy
d	Doublet
dd	Doublet of Doublets
dt	Doublet of Triplets
ddd	Doublet of Doublet of Doublets
D-A	Donor Acceptor
DABCO	1,4-Diazabicyclo[2.2.2]octane
DBU	1,8-Diazabicyclo[5.4.0]undec-7-ene
DCM	Dichloromethane
DFT	Density Functional Theory
DMF	Dimethylformamide
DMSO	Dimethylsulfoxide
DPPF	1,1'-Bis(diphenylphosphino)ferrocene
DSSC	Dye Sensitized Solar Cell
EtOAc	Ethyl Acetate
Et <sub>2</sub> O	Diethyl ether
eq	Equivalents
HCl	Hydrochloric acid
HOMO	Highest Occupied Molecular Orbital
IR	Infrared
<i>i</i> -Pr	Iso-propyl
<i>i</i> -PrOH	Isopropyl alcohol

J	Coupling Constant
K	Kelvin
LED	Light Emitting Diode
LUMO	Lowest Unoccupied Molecular Orbital
M	Metal
m	Multiplet
MALDI-TOF	Matrix Assisted Laser Desorption/Ionization - Time Of Flight
MeOH	Methanol
MS	Mass Spectroscopy
MOF	Metal Organic Framework
m/z	Mass over Charge
NBO	Natural Bond Orbital
NLO	Non-linear Optics
NMR	Nuclear Magnetic Resonance
OFET	Organic Field Effect Transistor
OLED	Organic Light Emitting Diode
OPV	Organic photovoltaic
Pc	Phthalocyanine
PCE	Power Conversion Efficiency
PDT	Photodynamic therapy
PE	Petroleum Ether
PS	Photosensitizer
Por	Porphyrin
ppm	Parts Per Million
SAT	Sitting Atop
SM	Starting Material
SMM	Single Molecule Magnet
SubPc	Subphthalocyanine
SubPor	Subporphyrin
SubTBDAP	Subtribenzodiazaporphyrin
TBMAP	Tetrabenzomonoazaporphyrin
TBTAP	Tetrabenzotriazaporphyrin
TBP	Tetrabenzoporphyrin
<i>t</i> -Bu	Tert-butyl
THF	Tetrahydrofuran

TLC	Thin Layer Chromatography
TPP	Tetraphenylporphyrin
<i>trans</i> -TBDAP	<i>trans</i> -Tetrabenzodiazaporphyrin

# List of Figures

1.1	Structures of porphyrin (Por) <b>(1)</b> and phthalocyanine (Pc) <b>(2)</b> . . .	1
1.2	Structures of subphthalocyanine <b>(3)</b> and superphthalocyanine <b>(4)</b> . . . . .	2
1.3	Tetrabenzoporphyrin/Pc parent structure with the <i>meso</i> positions labelled. The attached table describes the <i>meso</i> -substitution and species obtained. . . . .	3
1.4	Subphthalocyanine <b>(5)</b> , tribenzosubporphyrin <b>(6)</b> , SubTB-DAP <b>(7)</b> . . . . .	4
1.5	Electronic transitions in porphyrinoids described by the Gouterman four-orbital model. . . . .	5
1.6	Structures of heme B <b>(8)</b> and chlorophyll $c_1$ <b>(9)</b> . . . . .	6
1.7	Optimised geometry of SubPcB-Cl showing the conical conformation of the macrocycle resulting from the tetrahedral geometry of the central boron atom. . . . .	8
1.8	An example of a perturbed phthalocyanine, distortion of the macrocyclic ring and electron rich phenyl groups red shift the absorbance to the near IR (790 nm). . . . .	10
1.9	An example of a peripherally annulated phthalocyanine (para-tautomer shown). . . . .	11
1.10	An example of a ytterbium SAT complex (left and center) compared to the planar magnesium porphyrin (right), conformational differences between the two are clearly visible. <sup>60</sup> (Hydrogens omitted for clarity.) . . . . .	12
1.11	Crystal structure of a tetraphenylporphyrin europium phthalocyanine double decker compound (hydrogens omitted for clarity). <sup>61</sup> . . . . .	12
1.12	An example of a photocatalytic system for hydrogen production. <sup>62</sup>	13
1.13	Some examples of aminoisoindoline derivatives previously synthesised. <sup>64,65</sup> . . . . .	13
1.14	A DFT optimised structure of a multichromophore array produced by the Cammidge group, electronic coupling of the chromophores (Pc and SubPc) affords absorbance across the entire solar spectrum (hydrogens and hexyl chains omitted for clarity, grey = carbon, red = oxygen, blue = nitrogen, pink = boron, blue/grey = silicon). <sup>32</sup> . . . . .	15
1.15	An example of a multichromophore array for application in OPV devices. <sup>71</sup> . . . . .	16

1.16	An example of a dihydrobenzoporphyrim used as a photosensitizer for PDT. <sup>90</sup> . . . . .	17
1.17	Phthalocyanine tetrasulfonic acid is an example of an optical sensor for copper ions, producing a significant spectral and fluorescence change selectively for copper ions. <sup>95</sup> . . . . .	18
1.18	The structure of Mn12-ac, the first discovered SMM system (Mn <sup>III</sup> = purple, Mn <sup>IV</sup> = green, carbon = grey, oxygen = red). <sup>96</sup>	19
2.1	The structure of TBTAP, R = H, Ar, alkyl. . . . .	20
2.2	Results obtained by Cammidge <i>et al.</i> , SM 1 = 3,6-dihexylphthalonitrile, SM 2 = 3,6-didecylphthalonitrile, ratio = MeMgBr : phthalonitrile. . . . .	23
2.3	An example of a platinum coordinated TBMAP complex, this species displays very strong NIR emission at room temperature. <sup>107</sup> . . . . .	26
2.4	Table of SubTBDAP derivatives synthesised during previous studies. <sup>64</sup> . . . . .	30
2.5	<sup>1</sup> H NMR spectrum of <i>p</i> -methoxyphenylaminoisindoline ( <b>13</b> ), with the characteristic Z alkene proton at 6.7 ppm, and strong methoxy signal at 3.84 ppm. . . . .	36
2.6	<sup>1</sup> H NMR spectrum of TBTAP ( <b>16</b> ). Note the characteristic deshielding of some macrocyclic protons caused by ring current phenomena of porphyrinoids. . . . .	38
2.7	UV-Vis spectra of TBTAP ( <b>16</b> ). . . . .	38
2.8	<sup>1</sup> H NMR spectrum of TBTAP ( <b>18</b> ), with an expansion of the aliphatic region. THF- <i>d</i> <sub>8</sub> was used as the NMR solvent, with a residual solvent peak visible at 1.72 ppm. . . . .	41
2.9	<sup>1</sup> H NMR spectrum of TBTAP ( <b>19</b> ), with an expansion of the aliphatic region. The reduction in symmetry is clearly seen in both the aromatic and alkyl regions of the spectrum. . . . .	42
2.10	UV-Vis spectra of MgTBTAPs ( <b>18</b> ) and ( <b>19</b> ). . . . .	43
2.11	Table of results for all in addition of reagents with varying ratios. . . . .	44
2.12	Two equivalents of condensation product ( <b>20</b> ) coordinated to metal. . . . .	47
2.13	<sup>1</sup> H NMR spectra of novel 3:1 Zn TBTAP ( <b>24</b> ). . . . .	49
2.14	UV-Vis spectra of ZnTBTAP ( <b>24</b> ), displaying a very similar absorbance profile to the identically substituted 3:1 MgTBTAP ( <b>19</b> ). . . . .	49
2.15	Condensation product ( <b>25</b> ) of aminoisindoline ( <b>13</b> ) and the 6,7-dicyanotetrahydrotetramethylnaphthalene ( <b>14</b> ) identified by MALDI-TOF analysis of crude reaction mixtures. . . . .	50
2.16	Possible intermediate ( <b>25</b> ) identified by MALDI-TOF with a m/z of 488. . . . .	50
2.17	An ABCD TBTAP bearing different substituents on each ring, 2:2 TBTAP ( <b>18</b> ) would be considered an ABBA system, and 3:1 TBTAP ( <b>19</b> ) an ABBB system. . . . .	52
2.18	<sup>1</sup> H NMR spectra of dimethoxyisindoline ( <b>29</b> ). . . . .	57
2.19	<sup>1</sup> H NMR spectra of product ( <b>30</b> ). . . . .	60
2.20	UV-Visible spectra of condensation products ( <b>30</b> ) and ( <b>32</b> ). . . . .	60

2.21	Condensation products <b>(32)</b> and <b>(33)</b> identified by MALDI-TOF and $^1\text{H}$ NMR. The unsubstituted parent structure of <b>(33)</b> was previously discovered during SubTB-DAP synthesis and its structure confirmed by x-ray crystallography. . . . .	61
2.22	$^1\text{H}$ NMR spectra of product <b>(32)</b> , with an expansion of the aromatic region. Residual solvent peaks for $\text{CDCl}_3$ and DCM are visible at 7.26 ppm, 5.32 ppm and 1.56 ppm. . . . .	62
2.23	$^1\text{H}$ NMR spectra of product <b>(33)</b> , with expansions of the methoxy signal and alkyl region. . . . .	63
2.24	UV-visible spectra of product <b>(33)</b> , again a brown material with wide absorbance. . . . .	63
2.25	Derivatives chosen and synthesised for the work in section 2.5, Ar = <i>p</i> -methoxybenzene. . . . .	67
2.26	$^1\text{H}$ NMR spectra of dimethoxy condensation product <b>(42)</b> . . . . .	67
2.27	$^1\text{H}$ NMR spectra of dimethoxy condensation product <b>(43)</b> . . . . .	68
2.28	NMR of unsubstituted NBoc dimethoxyisoindoline <b>(34)</b> in $\text{CDCl}_3$ , with an expansion of the clear signals for the methoxy and <i>t</i> -butyl fragments. . . . .	71
2.29	$^1\text{H}$ NMR of <b>(35)</b> in $\text{CDCl}_3$ . . . . .	72
2.30	MALDI-TOF evidence for the formation of <b>(40)</b> (611 $m/z$ ) from <b>(30)</b> (378 $m/z$ ), via a possible intermediate comprising of two units of <b>(30)</b> (755 $m/z$ ) before elimination of 1,3-diiminoisoindoline. . . . .	78
2.31	Suite of aminoisoindoline and dimethoxyisoindoline derivatives chosen for this work. . . . .	81
2.32	Parent structure <b>(30)</b> with substitution positions shown, with a table of synthesised derivatives. . . . .	83
2.33	The $^1\text{H}$ NMR spectra of 1:3 dimethoxy TBTAP <b>(53)</b> and 3:1 TBTAP <b>(54)</b> . . . . .	84
2.34	UV-Visible absorption spectra of MgTBTAPs <b>(53)</b> and <b>(54)</b> . . . . .	85
2.35	MALDI-TOF analysis of crude reaction mixtures from <b>(30)</b> . . . . .	89
2.36	Table of masses observed and likely corresponding structures. . . . .	90
2.37	Structures of intermediates proposed in figures 2.92 and 2.93. These structures both have an exact mass of 756.30. . . . .	91
2.38	Structure of the hypothesised intermediate resulting from the condensation of <b>(30)</b> and <b>(40)</b> , with an exact mass of 989.38. . . . .	91
2.39	MALDI-TOF MS spectra of crude reaction mixture after 40 minutes at 220°C. . . . .	92
2.40	Table of masses observed and likely corresponding structures. . . . .	92
2.41	Positions susceptible to nucleophilic attack. . . . .	98
3.1	The ‘trimer’ condensation product of phthalonitrile and aminoisoindoline previously isolated and characterised. <sup>64</sup> . . . . .	104
3.2	$^1\text{H}$ NMR spectra of SubTBDAP-OPh <b>(46)</b> . . . . .	107
3.3	MALDI-TOF spectra of SubTBDAP <b>(46)</b> . . . . .	108
3.4	MALDI-TOF spectra for diphenyl-SubTBDAP <b>(55)</b> . Again the parent ion (745 $m/z$ ) and [SubTBDAP-B] <sup>+</sup> (652 $m/z$ ) peaks are visible. . . . .	111

3.5	UV-Vis spectra of SubTBDAP-OPh ( <b>46</b> ) and naphthyl substituted SubTBDAP-OPh ( <b>47</b> ). . . . .	114
3.6	<sup>1</sup> H NMR of naphthyl-SubTBDAP ( <b>47</b> ) . . . . .	114
4.1	Potential energy diagram for the reaction presented above. . . . .	123
4.2	Potential energy diagram for dimethoxyisoindoline formation. Solvent = methanol. . . . .	125
4.3	Potential energy diagram for the formation of diisopropylisoindoline. Solvent = iso-propanol. . . . .	126
4.4	Hypothesised 6-membered cyclic transition state for the condensation of aminoisoindoline and methoxyisoindoline. . . . .	127
4.5	Potential energy diagram for the pathway presented above. . . . .	128
4.6	NBO analysis of charge distribution in ( <b>30</b> ). Red indicates increased electron density, green indicates reduced electron density, and black indicates neutral. . . . .	129
4.7	Potential energy diagram for the pathway presented in scheme 4.7. . . . .	131
5.1	2,5-Dichloro-2,5-dimethylhexane . . . . .	133
5.2	1,1,4,4-Tetramethyl-1,2,3,4-tetrahydronaphthalene . . . . .	133
5.3	6,7-Dibromo-1,1,4,4-tetramethyl-1,2,3,4-tetrahydronaphthalene . . . . .	134
5.4	6,7-Dicyano-1,1,4,4-tetramethyl-1,2,3,4-tetrahydronaphthalene . . . . .	135
5.5	6,7-Dicyano-1,1,4,4-tetramethyl-1,2,3,4-tetrahydronaphthalene . . . . .	135
5.6	4,5-Diphenoxyphthalonitrile . . . . .	136
5.7	1,2-Dibromo-4,5-dimethoxybenzene . . . . .	137
5.8	4,5-Dimethoxyphthalonitrile . . . . .	137
5.9	2-Bromo-4,5-dimethoxybenzotrile . . . . .	138
5.10	1,2-Dibromo-4,5-dimethylbenzene . . . . .	138
5.11	4,5-Dimethylphthalonitrile . . . . .	139
5.12	2-Bromo-4,5-dimethylbenzotrile . . . . .	140
5.13	Phthalonitrile-3,6-ditriflate . . . . .	140
5.14	3,6-Diphenylphthalonitrile . . . . .	141
5.15	2-Bromobenzamidine hydrochloride . . . . .	142
5.16	(Z)-1-(Phenylmethylene)-1 <i>H</i> -isoindol-3-amine . . . . .	143
5.17	(Z)-1-[(4-Methoxy)benzylidene]-1 <i>H</i> -isoindol-3-amine . . . . .	143
5.18	1,1,4,4-Tetramethyl-1,2,3,4-tetrahydronaphthamidine hydrochloride . . . . .	144
5.19	(Z)-1-[(4-Methoxybenzylidene)]-5,5,8,8-tetramethyl-5 <i>H</i> ,6 <i>H</i> ,7 <i>H</i> ,8 <i>H</i> -benzo[ <i>f</i> ]isoindol-3-amine . . . . .	145
5.20	2-Bromo-4,5-dimethoxybenzamidine hydrochloride . . . . .	146
5.21	(Z)-5,6-Dimethoxy-1-[(4-methoxy)benzylidene]-1 <i>H</i> -isoindol-3-amine . . . . .	146
5.22	1-Imino-3,3-dimethoxyisoindoline . . . . .	147
5.23	N-Boc 1-imino-3,3-dimethoxyisoindoline . . . . .	148
5.24	1-Imino-5,5,8,8-tetramethyl-5 <i>H</i> ,6 <i>H</i> ,7 <i>H</i> ,8 <i>H</i> -12,12-dimethoxyisoindoline . . . . .	149
5.25	NBoc 1-Imino-5,5,8,8-tetramethyl-5 <i>H</i> ,6 <i>H</i> ,7 <i>H</i> ,8 <i>H</i> -12,12-dimethoxyisoindoline ( <b>36</b> ) . . . . .	149
5.26	1-Imino-4,5-diphenoxy-8,8-dimethoxyisoindoline . . . . .	150
5.27	1-Imino-3,3-dimethoxybenzo(F)isoindoline . . . . .	151

5.28	Condensation product ( <b>30</b> ) . . . . .	152
5.29	Condensation product ( <b>25</b> ) . . . . .	153
5.30	Condensation product ( <b>42</b> ) . . . . .	154
5.31	Condensation product ( <b>43</b> ) . . . . .	155
5.32	NBoc protected condensation product ( <b>35</b> ) . . . . .	156
5.33	NBoc protected condensation product ( <b>37</b> ) . . . . .	157
5.34	Condensation product ( <b>33</b> ) . . . . .	158
5.35	Condensation product ( <b>40</b> ) . . . . .	159
5.36	MgTBTAP ( <b>16</b> ) . . . . .	161
5.37	2:2 MgTBTAP ( <b>18</b> ) . . . . .	162
5.38	3:1 MgTBTAP ( <b>19</b> ) . . . . .	164
5.39	3:1 ZnTBTAP ( <b>24</b> ) . . . . .	165
5.40	1:3 MgTBTAP ( <b>53</b> ) . . . . .	166
5.41	3:1 MgTBTAP ( <b>54</b> ) . . . . .	168
5.42	SubTBDAP-OPh ( <b>46</b> ) . . . . .	169
5.43	Naphthyl-SubTBDAP-OPh ( <b>47</b> ) . . . . .	171

# List of Schemes

1.1	Porphyrin synthesis developed by Rothermund, R = phenyl. . . .	6
1.2	Generic scheme for the synthesis of phthalocyanines. . . . .	7
1.3	Phthalocyanine macrocyclization mechanism proposed by McGaff <i>et al.</i> <sup>46</sup> . . . . .	7
1.4	The first synthesis of SubPcB-Cl from phthalonitrile and BCl <sub>3</sub> . <sup>47</sup>	8
1.5	Synthesis of aminoisindolines from 2-bromobenzonitriles. . . . .	9
1.6	Previously hypothesised sequence of events in TBTAP formation	9
1.7	Synthesis of substituted Pcs, R=H, Aryl, Alkyl, Ether, Thiol, Amine, Halide etc. . . . .	11
1.8	The first example of a cross coupling reaction utilizing a bromo TBTAP derivative. <sup>63</sup> . . . . .	14
2.1	Macrocyclization pathway proposed by Barrett in 1939. . . . .	21
2.2	Leznoff and McKeown's reported synthesis of TBTAP derivatives, successfully synthesised derivatives listed below. <sup>23</sup> . . . . .	22
2.3	Galanin <i>et al.</i> synthesis of <i>meso</i> substituted TBTAPs. R = ethyl, hexyl and dodecyl. . . . .	23
2.4	Derivatives synthesised by Kalashnikov <i>et al.</i> , R = H, <i>o</i> -Me, <i>m</i> -Me, <i>p</i> -Me, <i>p</i> -OMe. . . . .	24
2.5	The Cammidge <i>et al.</i> synthesis of TBTAPs afforded by the co-macrocyclization of aminoisindoline and phthalonitrile. . . . .	24
2.6	Pathways to 2-bromobenzonitriles and phthalonitriles. . . . .	25
2.7	Aminoisindoline synthesis from 2-bromobenzonitriles. . . . .	25
2.8	Cammidge <i>et al.</i> synthesis of non-peripherally alkyl substituted TBTAPs, R = C <sub>6</sub> H <sub>13</sub> . <sup>26</sup> . . . . .	27
2.9	The utilization of aminoisindolines as a TBTAP precursor by Cammidge <i>et al.</i> <sup>28</sup> . . . . .	28
2.10	The further optimised Cammidge <i>et al.</i> synthesis of TBTAPs afforded by the co-macrocyclization of aminoisindoline and phthalonitrile, utilising DABCO and syringe pump addition of reagents. <sup>29</sup> . . . . .	29
2.11	The Cammidge <i>et al.</i> synthesis of SubTBDAPs utilising aminoisindoline precursors, followed by apical substitution of phenol, or directly through use of B(OPh) <sub>3</sub> . <sup>64</sup> . . . . .	30
2.12	The previously hypothesised TBTAP macrocyclization pathway. New derivatives explored: R = H, OMe, OHx, ODc, 1,1,4,4-tetramethylcyclohexane and OPh. . . . .	31
2.13	Initial condensation of phthalonitrile with aminoisindoline. . . .	32

2.14	Homocondensation of two units of the dimer species, forming the 2+2 open chain species, with elimination of ammonia, that macrocyclizes to form 2:2 TBTAPs. . . . .	32
2.15	Macrocyclization of the open chain oligomer presented in the previous figure. . . . .	32
2.16	Synthesis of amidine hydrochloride from 2-bromobenzonitrile. . .	35
2.17	Sonogashira cross coupling cycle adapted from a recent review. <sup>116</sup> L = BINAP, B = DBU, R <sub>1</sub> = benzonitrile, X = Br. . . . .	35
2.18	Domino 5-exo- <i>dig</i> cyclization facilitated under the same reaction conditions to yield aminoisindoline and regenerate L <sub>2</sub> PdCl <sub>2</sub> . . .	36
2.19	Scheme for the repeat of the previously optimised TBTAP synthesis.	37
2.20	Hypothesised mechanism for the homocondensation of aminoisindoline to form azadipyrromethene ( <b>17</b> ). . . . .	39
2.21	Scheme for the previous TBTAP investigations revealing the formation of two different TBTAP derivatives. The original study obtained 2:2 TBTAP ( <b>18</b> ) in 14 % yield, and 3:1 TBTAP ( <b>19</b> ) in 1 % yield. . . . .	40
2.22	Hypothesised homocondensation of the condensation product ( <b>20</b> ) to yield tetramer ( <b>21</b> ). . . . .	44
2.23	Nucleophilic attack of phthalonitrile by aminoisindoline to produce the condensation product ( <b>20</b> ). . . . .	45
2.24	Hypothesised consecutive addition of phthalonitrile to form the 4 membered open chain oligomer and macrocyclization to form the 3:1 TBTAP. . . . .	45
2.25	Selective 3:1 ZnBr <sub>2</sub> mediated TBTAP synthesis utilizing aminoisindoline ( <b>13</b> ) and 6,7-dicyano-1,2,3,4-tetrahydro-1,1,4,4-tetramethylnaphthalene ( <b>14</b> ) to form TBTAP ( <b>24</b> ). . .	48
2.26	Hypothesised homocondensation of the condensation product ( <b>25</b> ), selectively building the potential 2:2 TBTAP precursor ( <b>26</b> ). . .	51
2.27	Proposed stepwise formation of ABCC system ( <b>27</b> ) from ( <b>20</b> ) and phthalonitrile. . . . .	52
2.28	Proposed macrocyclization of pre assembled ABCC system ( <b>27</b> ) facilitated by an Mg template ion with elimination of ammonia. .	53
2.29	Templating and macrocyclization of two units of azadipyrromethene to yield TBDAP. . . . .	54
2.30	Macrocyclization of ( <b>28</b> ) to yield SubTBDAP with elimination of an aromatic fragment. . . . .	55
2.31	Scheme for the synthesis of dimethoxyisindoline ( <b>29</b> ). <sup>121</sup> . . . .	55
2.32	Condensation of dimethoxyisindoline with aminoisindoline to yield condensation product ( <b>30</b> ). . . . .	56
2.33	Proposed mechanism for the formation of dimethoxyisindoline ( <b>29</b> ). . . . .	56
2.34	Scheme for the synthesis of dimethoxyisindoline ( <b>31</b> ). . . . .	57
2.35	Failed dimethoxyisindoline derivatives. . . . .	58
2.36	Successful synthesis of target condensation product ( <b>30</b> ). . . . .	59
2.37	Summary of hypothesised equilibria between starting materials, ( <b>32</b> ) and ( <b>33</b> ). . . . .	64
2.38	The hypothesised reverse reaction for aminoisindoline addition to ( <b>32</b> ) to form ( <b>33</b> ), driven by methanol rather than ammonia. .	65

2.39	The hypothesised formation of a dimethoxy substituted analogue of aminoisoindoline ( <b>13</b> ). . . . .	65
2.40	Hypothesised mechanism for formation of ( <b>32</b> ) from aminoisoindoline and dimethoxyisoindoline ( <b>31</b> ). Removing methanol from the reaction mixture should prevent the reverse reaction occurring, driving the formation of ( <b>32</b> ). . . . .	66
2.41	Strategy for the formation of condensation product ( <b>30</b> ) via NBoc protected dimethoxyisoindolines. . . . .	69
2.42	Strategy for the stepwise construction of ABCD systems utilising NBoc protected dimethoxyisoindolines. Successive deprotection and addition of further protected dimethoxyisoindoline should facilitate the stepwise construction of such systems. . . . .	69
2.43	Proposed mechanism for the glycerol mediated Boc protection of amines. Glycerol acts as a solvent but also has a catalytic effect by stabilising intermediate species. <sup>122</sup> . . . . .	70
2.44	Scheme for the synthesis of NBoc protected product ( <b>35</b> ) from NBoc protected dimethoxyisoindoline, Ar = <i>para</i> -methoxytoluene. . . . .	72
2.45	Generic mechanism for protonation and elimination of isobutene from NBoc protected amines. . . . .	73
2.46	Generic mechanism for the decarboxylation to yield the deprotected amine. . . . .	73
2.47	Hypothesised nucleophilic attack by TFA resulting in the decomposition of the structure. . . . .	74
2.48	Deprotonation and elimination to regenerate the <i>t</i> -butoxide anion, followed by addition of hydroxide facilitated by 1eq of H <sub>2</sub> O. . . . .	74
2.49	Final elimination of CO <sub>2</sub> to yield the unprotected product ( <b>30</b> ) . . . . .	75
2.50	Hypothesised equilibrium for the addition of <i>t</i> -BuO. . . . .	75
2.51	Scheme for the synthesis of, and <sup>1</sup> H NMR spectra for ( <b>37</b> ). . . . .	76
2.52	The hypothesised mechanism for the formation of ( <b>40</b> ) with elimination of 1,3-diiminoisoindoline. . . . .	78
2.53	Formation of MgTBTAP from ( <b>30</b> ) in toluene or <i>p</i> -xylene at reflux. . . . .	79
2.54	Hypothesised homocondensation of ( <b>30</b> ), followed by coordination by magnesium, macrocyclization and aromatisation to yield MgTBTAP ( <b>16</b> ). . . . .	80
2.55	Hypothesised coordination of two units of ( <b>30</b> ) to magnesium, followed by condensation, macrocyclization and aromatisation to yield MgTBTAP. . . . .	80
2.56	Unexpected formation of 3:1 MgTBTAP ( <b>19</b> ) from ( <b>32</b> ). . . . .	82
2.57	Formation of 3:1 TBTAPs from derivatives of ( <b>30</b> ) in <i>p</i> -xylene at reflux. . . . .	83
2.58	The hypothesised mechanism for the formation of ( <b>40</b> ) with elimination of 1,3-diiminoisoindoline. . . . .	86
2.59	Hypothesised mechanism for the condensation of two units of ( <b>30</b> ) with elimination of aminoisoindoline. . . . .	86
2.60	Hypothesised mechanism for the addition of one more unit of ( <b>30</b> ) to the 3 membered chain with elimination of aminoisoindoline. . . . .	87
2.61	Pathways to be analysed by MALDI-TOF MS. . . . .	88
2.62	Selective synthesis of 2:2 substituted ABBA MgTBTAP and 3:1 ABBA ZnTBTAP systems. . . . .	94
2.63	Synthesis of 3:1 ABBA TBTAP systems from derivatives of ( <b>30</b> ) . . . . .	94

2.64	Summary of synthetic methods to <b>(30)</b> and derivatives. . . . .	96
2.65	Formation of <b>(40)</b> and derivatives from aminoisindolines and dimethoxyindolines. . . . .	96
2.66	Scheme for the formation of <b>(40)</b> with elimination of 1,3-diiminoisindoline. . . . .	97
2.67	Scheme for the synthesis of symmetrical TBTAPs from symmetrical derivatives of <b>(30)</b> . . . . .	98
2.68	Potential macrocyclization of trimeric side products to SubTBDAPs. . . . .	99
3.1	Synthesis of SubPc-Cl and SubTBDAP-Cl from aminoisindoline and phthalonitrile under optimum SubPc-Cl formation conditions. . . . .	100
3.2	Synthesis of SubPc-OPh via addition of phenol to the reaction mixture. . . . .	101
3.3	Synthesis of SubPc-OR derivatives from borates, R = OMe, OPh, OBu, <i>Oi-Pr</i> . . . . .	101
3.4	Synthesis of symmetrical peripherally ( $R_2$ ) and non-peripherally ( $R_1$ ) substituted SubPcs. . . . .	102
3.5	An example of a tri-substituted SubPc, designed as a nanoparticle encapsulant during previous work in the Cammidge group. The ability to include easily displaceable halide substituents at the peripheral positions opens up the possibility of palladium catalysed cross-coupling reactions to further functionalise the macrocycle. . . . .	103
3.6	Formation of substituted SubTBDAPs, the symmetrical homomacrocyclization SubPc products are also expected to be produced as side products. . . . .	104
3.7	A potential SubTBDAP formation pathway. . . . .	105
3.8	Scheme for SubTBDAP formation . . . . .	106
3.9	Non-peripheral phenyl substituted SubPc synthesis. The hexaphenyl SubPc was not thermally/kinetically accessible, tetraphenyl SubPc was synthesised in poor yield, and diphenyl SubPc was synthesised in good yield. This clearly shows the trend of significantly decreased yield as steric crowding increases. . . . .	109
3.10	Scheme and proposed product for this SubTBDAP reaction. . . . .	110
3.11	Scheme for the formation of diphenyl SubTBDAP, the expected side products are SubTBDAP, SubPc, diphenyl SubPc, and tetraphenyl SubPc. The two possible regioisomers of diphenyl SubTBDAP are also shown. . . . .	110
3.12	Scheme for the synthesis of peripherally substituted SubTBDAPs. . . . .	112
3.13	Successful synthesis of naphthyl substituted SubTBDAP <b>(47)</b> . . . . .	113
3.14	Proposed macrocyclization of the ‘trimer’ to SubTBDAP with elimination of an aromatic fragment. . . . .	115
3.15	Failed synthesis of SubTBDAPs from trimers. . . . .	116
3.16	Successful and highly yielding synthesis of SubTBDAP from condensation product <b>(30)</b> . . . . .	117
3.17	The proposed reaction mechanism between two units of <b>(30)</b> to form the alternative open chain ABB trimeric structure. . . . .	118
3.18	Hypothesised macrocyclization of the open chain ABB ‘trimer’ to yield SubTBDAP with elimination of ammonia. . . . .	118

3.19	Synthesis of Cs, ABA, SubTBDAPs from aminoisoindoline and phthalonitrile. . . . .	119
3.20	Synthesis of SubTBDAP derivatives from <b>(30)</b> , with the hypothesised substitution pattern shown. . . . .	120
4.1	Initial proton transfer to form the more activated imine B. . . . .	122
4.2	Homocondensation with elimination of ammonia to form azadipyrromethene C, which further tautomerizes to final structure D. . . . .	123
4.3	Series of equilibria that form dimethoxyisoindoline. . . . .	124
4.4	Formation of isopropylisoindoline. . . . .	125
4.5	Dissociation of dimethoxyisoindoline to methoxyisoindoline and methanol. . . . .	126
4.6	Tautomerization to form the final condensation product D. . . . .	127
4.7	Scheme for the formation of various products from two units of condensation dimer <b>(30)</b> . . . . .	130

# Chapter 1

## Natural and synthetic macrocycles: synthesis, properties and applications

### 1.1 Structure of Porphyrinoids and common hybrids

Porphyrinoids are a class of large, macrocyclic compounds that are not only ubiquitous in nature, but extensively studied in a vast range of scientific and medical fields. They possess a fascinating range of properties<sup>1</sup> and ability to be functionalised and tuned to meet the requirements of various applications. At the heart of modern porphyrinoid research there are two main classes of compounds: the naturally occurring porphyrins, referred to as the ‘pigments of life’, and the synthetic analogues, phthalocyanines (figure 1.1).

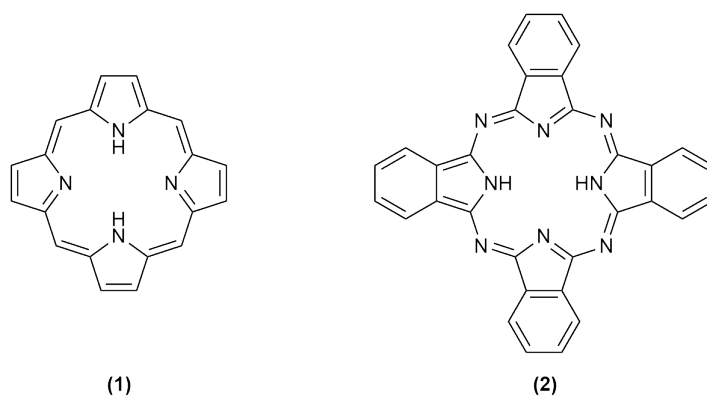


Figure 1.1: Structures of porphyrin (Por) (1) and phthalocyanine (Pc) (2).

Porphyrins and phthalocyanines share a defining feature of porphyrinoids, an extended Hückel aromatic  $\pi$  electron system, delocalised above and below

the plane of the ring.<sup>2</sup> For Por and Pc the  $\pi$  system comprises of 18 electrons, however many examples of contracted or expanded porphyrinoids exist - all exhibiting Hückel aromaticity. These  $\pi$  systems give rise to many of the optical and electronic properties that result in porphyrinoids being so widely and extensively studied. Subphthalocyanine and superphthalocyanine (figure 1.2) form  $14\text{-}\pi$  and  $22\text{-}\pi$  electron systems respectively.<sup>3,4</sup> The size of the  $\pi$  system and functionalisation of macrocycles lend these compounds to extensive tunability and diverse application. These extended, aromatic  $\pi$  systems give rise to remarkably strong molar extinction coefficients, excellent thermal and photochemical stability, as well as exhibiting rare photochemical phenomena such as two photon excitations and various NLO properties.<sup>5-11</sup>

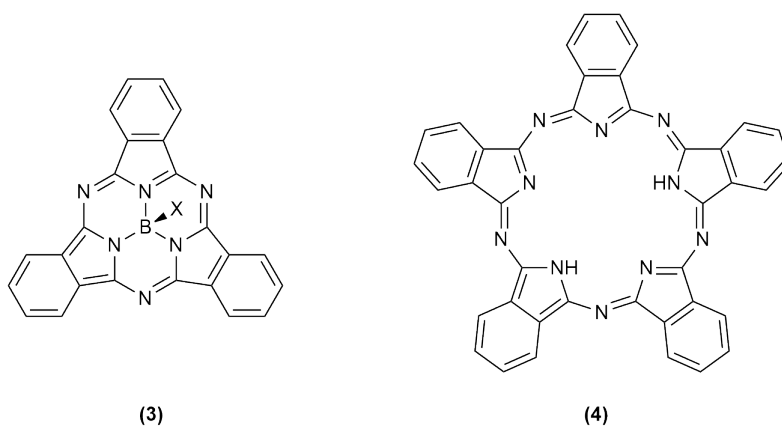
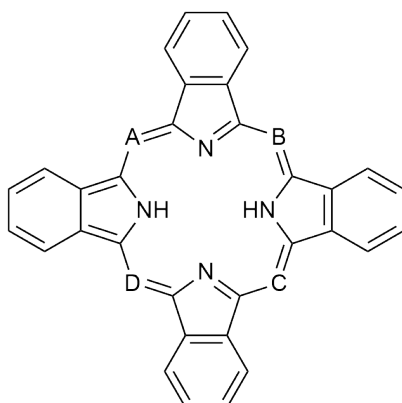


Figure 1.2: Structures of subphthalocyanine **(3)** and superphthalocyanine **(4)**.

Individually these porphyrinoids have been extensively researched as highly functional organic materials; driven by the demand for more controllable systems, hybrid porphyrinoids have received significant attention in recent years.<sup>12-14</sup> These compounds bridge the gap between porphyrin and phthalocyanine type systems by controlling the substitution of *meso* positions on the core; porphyrins bear carbon, phthalocyanines bear nitrogen, and hybrids a mixture of the two. Shown below (figure 1.3) is a tetrabenzoporphyrin/phthalocyanine core, with *meso* positions labelled and a description of the resulting hybrid. The inclusion of *meso*  $sp^2$  hybridised carbon atoms in these structures allows easy functionalisation or integration of such macrocycles to more complex systems.



Meso Substitution	Species
A=B=C=D = Nitrogen	Phthalocyanine
A=B=C = Nitrogen, D = Carbon	TetraBenzoTriAzaPorphyrin (TBTAP)
A=B = Nitrogen, C=D = Carbon	<i>cis</i> -TetraBenzoDiAzaPorphyrin ( <i>cis</i> -TBDAP)
A=C = Nitrogen, B=D = Carbon	<i>trans</i> -TetraBenzoDiAzaPorphyrin ( <i>trans</i> -TBDAP)
A = Nitrogen, B=C=D = Carbon	TetraBenzoMonoAzaPorphyrin (TBMAP)
A=B=C=D = Carbon	TetraBenzoPorphyrin (TBP)

Figure 1.3: Tetraenzoporphyrin/Pc parent structure with the *meso* positions labelled. The attached table describes the *meso*-substitution and species obtained.

While TBTAP was first isolated and characterised in the 1930s during early developments in phthalocyanine chemistry,<sup>15–17</sup> a lack of controllable synthetic routes meant that further research was somewhat sporadic. Between 1939 and the late 1980s various properties of hybrid structures were explored as methods and instrumentation developed,<sup>18–22</sup> with all research using the original 1939 synthesis from Barrett *et al.*<sup>17</sup> Between 1990 and 2000 some novel procedures to *meso*-substituted TBTAPs were developed, opening the door to more interesting derivatives and applications.<sup>23,24</sup> In recent years the Cambridge group has been at the forefront of developing synthetic routes to these hybrids, publishing numerous routes to TBTAPs, TBDAPs and TBMAPs over the last decade or so.<sup>25–29</sup> Following these synthetic developments, in 2015 the group was able to produce the first examples of a new hybrid macrocycle that bridges subporphyrins and subphthalocyanines, SubTBDAPs (figure 1.4).<sup>30</sup> As with Pc/Por hybrids, the inclusion of *meso* sp<sup>2</sup> hybridised carbon allows functionalisation and further integration into larger systems.

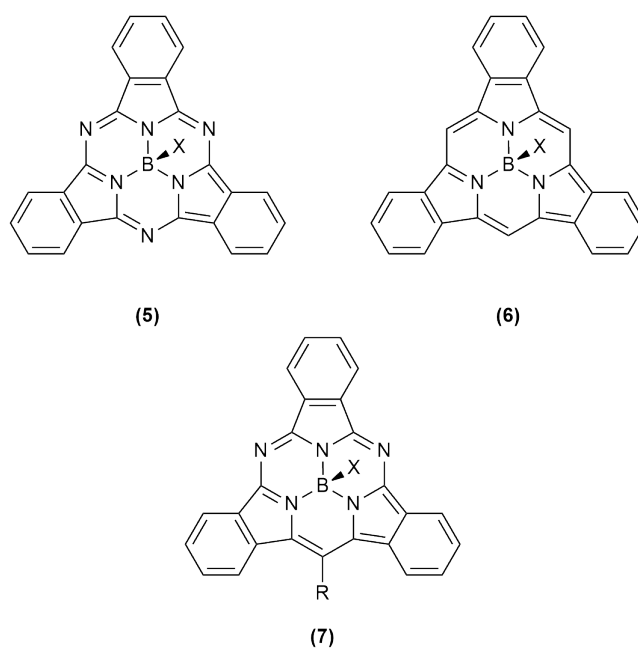


Figure 1.4: Subphthalocyanine (5), tribenzosubporphyrin (6), SubTBDAP (7).

## 1.2 Electronic structure of porphyrinoids

The unique electronic structures of the previously discussed species are responsible for a wide range of fascinating and useful photochemical and photophysical properties. The large, delocalised  $\pi$  systems present lend themselves to very high molar extinction coefficients upon interaction with light. Porphyrins, phthalocyanines, and subphthalocyanines display similar UV-visible excitation profiles, consisting of two main regions. These are the Soret band (B band) and Q band, which are typically found between 380 - 500 nm, and 500-750 nm respectively. The presence of two distinct bands were explained by the Gouterman four-orbital model.<sup>31</sup> First applied in 1959, this model suggests transitions occur between the two highest energy  $\pi$  orbitals and the two lowest energy  $\pi^*$  orbitals (figure 1.5), giving rise to the multiple strong  $\pi \rightarrow \pi^*$  transitions observed.

Porphyrinoids display complementary absorption profiles, and a combination of chromophores from all 3 classes discussed above may effectively cover almost all of the visible spectrum. Porphyrins display a strong Soret band (350-450 nm), this complements the Q band of phthalocyanines (600-800 nm), and combined with the strong Q band displayed by subphthalocyanines (500-600 nm), may allow efficient harvesting of light throughout most of the 350-800 nm range.<sup>32</sup> This makes porphyrinoids extremely interesting candidates for application in sensitized light harvesting systems, such as dye sensitized solar cells, or synthetic photosynthesis systems. The fast electron and energy transfer processes associated with these macrocycles further lends porphyrinoids to these applica-

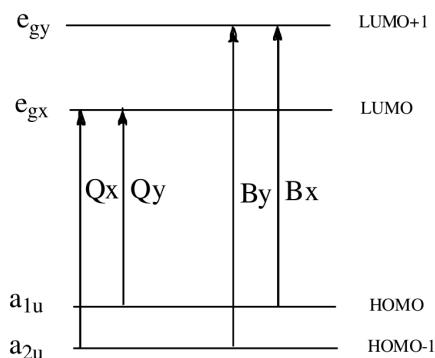


Figure 1.5: Electronic transitions in porphyrinoids described by the Gouterman four-orbital model.

tions.

With porphyrinoid chemistry now being a large and diverse field, a comprehensive range of options exist with respect to producing electronically  $\pi$  linked systems. Porphyrinoids may be covalently and electronically linked to various substrates, supramolecular structures, macrocycles, and transition metal complexes. This results in the ability to easily form electronically complex and useful structures with countless applications, outlined in section 1.5.

## 1.3 Synthesis

### 1.3.1 Porphyrins

Porphyrins represent an extremely important family of naturally occurring tetrapyrrole macrocycles. In nature the ability of porphyrins and derivatives to bind metals and absorb light is central to their evolutionary integration. Such examples include the heme cofactor (figure 1.6), which plays a key role in many cellular processes spanning multiple classes of organism. These include oxygen transportation, energy metabolism, detoxification and even sensing of environmental changes.<sup>33–36</sup> Chlorophyll (figure 1.6) is another porphyrin based complex that is key to life as we know it, present in almost all plants and responsible for capturing solar energy and facilitating photosynthesis.<sup>37</sup>

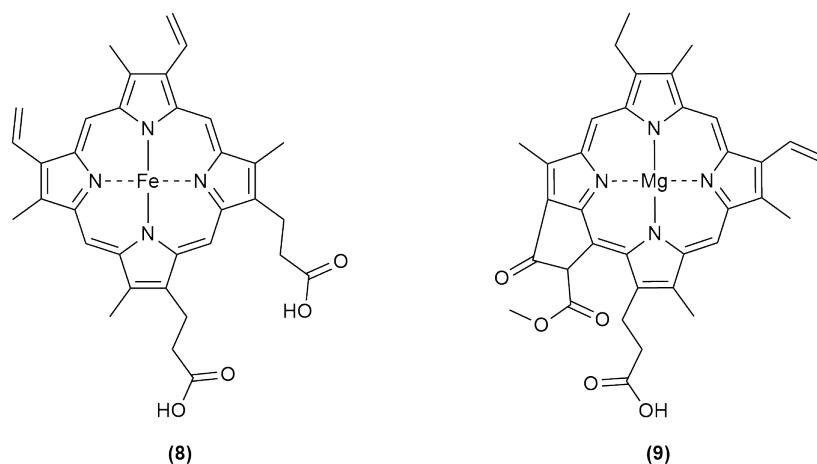
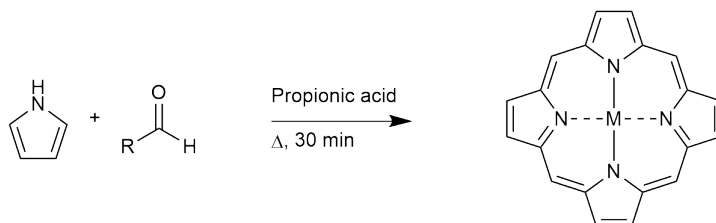


Figure 1.6: Structures of heme B (8) and chlorophyll c<sub>1</sub> (9).

While numerous synthetic procedures for porphyrins exist, the most famously employed is the condensation of pyrrole and an aldehyde to produce tetraphenylporphyrins (TPP, scheme 1.1). Initially developed by Rothermund,<sup>38,39</sup> and later refined further by Adler, Longo and for asymmetric derivatives by Lindsey,<sup>40,41</sup> this procedure affords porphyrins easily, quickly and in adequate yields.

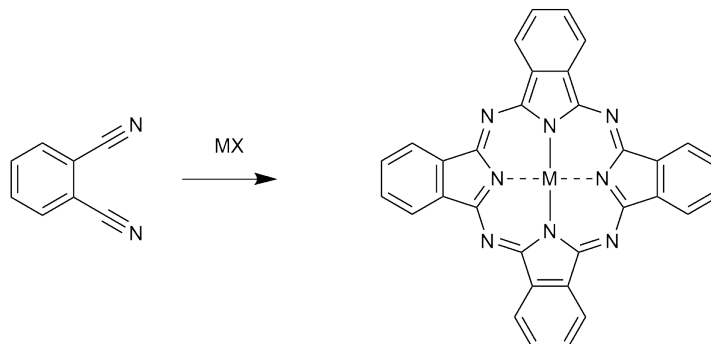


Scheme 1.1: Porphyrin synthesis developed by Rothermund, R = phenyl.

### 1.3.2 Phthalocyanines

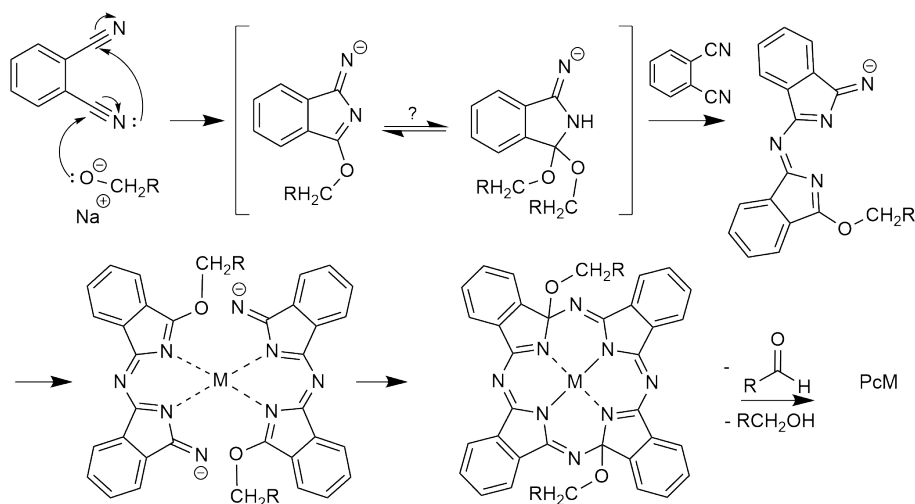
Phthalocyanines, unlike porphyrins, do not occur in nature. These systems were first discovered and characterised in the early 1900s, as a side product from the industrial synthesis of phthalimide from ammonia and phthalic anhydride.<sup>42</sup> This intensely blue material was characterised as iron tetrabenzotetraazaporphyrin, or iron phthalocyanine, and displayed exceptional thermal and photochemical stability, lending itself well to use as a colourant. Throughout the 1930s the work of Dent, Linstead and Lowe yielded the first Pc synthesis from phthalonitrile, as well as various metallated derivatives and x-ray crystal structures, confirming the molecular configuration (scheme 1.2).<sup>43–45</sup> Phthalocyanines are still used as colourants to this day, however with advances

in synthetic chemistry their application has become ever more intriguing and diverse.



Scheme 1.2: Generic scheme for the synthesis of phthalocyanines.

Phthalocyanines may be synthesised by the macrocyclization of a variety of isoindoline type materials, commonly 1,3-diiminoisoindolines or phthalonitriles, in the presence of a template ion to form symmetrical Pcs. Asymmetrical Pcs are currently prepared by statistical condensation of different isoindoline or phthalonitrile derivatives, giving a mixture of products and hence poor yield for the target material. The proposed mechanism for Pc macrocyclization via the very common sodium alkoxide mediated pathway is shown in scheme 1.3.<sup>46</sup>



Scheme 1.3: Phthalocyanine macrocyclization mechanism proposed by McGaff *et al.*<sup>46</sup>

### 1.3.3 Subphthalocyanines

First synthesised in 1972 by Meller and Ossko,<sup>47</sup> SubPcs have received relatively little attention compared to phthalocyanines and porphyrins. Discovered by accident while attempting to form boron phthalocyanine, boron subphthalocyanine comprises of 3 isoindoline fragments cyclized and coordinated to a tetrahedral boron atom. This smaller ring, combined with the tetrahedral boron creates a unique, non-planar structure compared to other porphyrinoids,<sup>48</sup> as well as significantly varying optical properties. Currently, no SubPcs have been synthesised with a template other than boron, which bears an axial ligand. The bowl like structure of SubPcB-Cl is shown in figure 1.7 below. Like phthalocyanines, SubPcs may be synthesised from a selection of isoindoline type species, but most commonly employed is phthalonitrile (scheme 1.4).

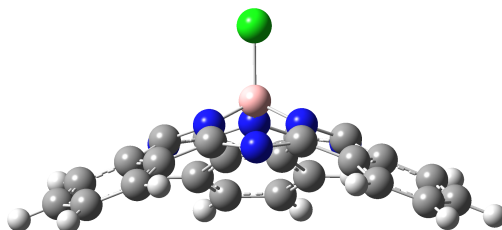
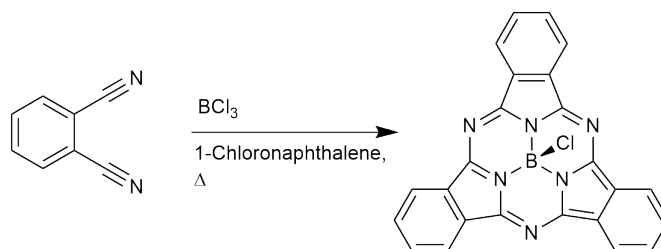


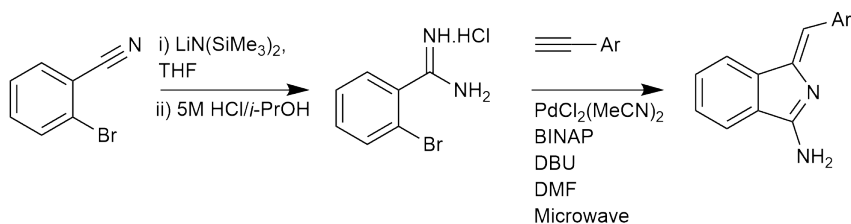
Figure 1.7: Optimised geometry of SubPcB-Cl showing the conical conformation of the macrocycle resulting from the tetrahedral geometry of the central boron atom.



Scheme 1.4: The first synthesis of SubPcB-Cl from phthalonitrile and  $\text{BCl}_3$ .<sup>47</sup>

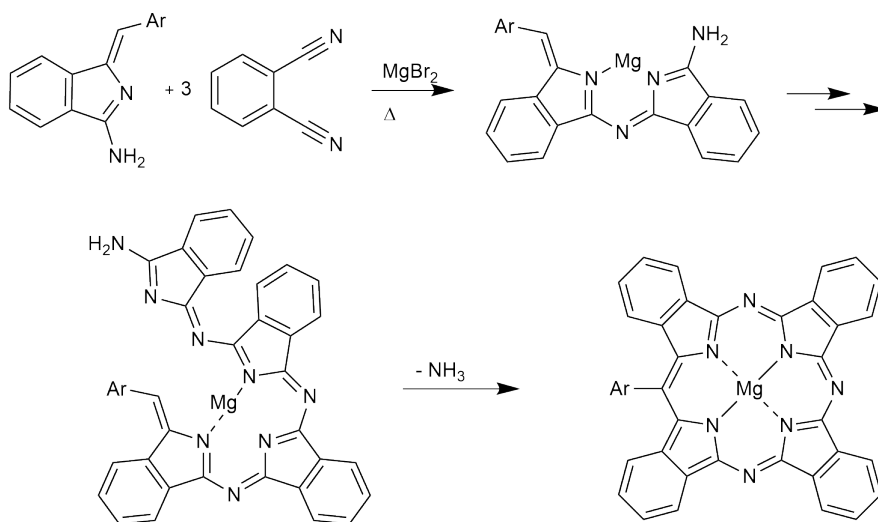
### 1.3.4 TBTAPs and SubTBDAPs

Driven by the Cammidge groups' advances in hybrid chemistry, TBTAPs and SubTBDAPs can conveniently be synthesised from common starting materials.<sup>29</sup> The development of aminoisindoline precursors (scheme 1.5) has allowed controllable and easy functionalisation of the *meso* position for both TBTAPs and SubTBDAPs; these aminoisindolines may be reacted with phthalonitrile in the presence of  $\text{MgBr}_2$  to yield TBTAPs, and boron sources such as  $\text{BCl}_3$  or  $\text{B}(\text{OPh})_3$  to yield SubTBDAPs.



Scheme 1.5: Synthesis of aminoisindolines from 2-bromobenzonitriles.

In TBTAP synthesis the role of the aminoisindoline has been hypothesised to act as an initiator to the macrocyclization process, attacking phthalonitrile in sequence to build the open chain oligomer, templated around magnesium. Elimination of ammonia facilitates the final macrocyclization and aromatisation step to yield  $\text{MgTBTAP}$  as shown below (scheme 1.6).<sup>28</sup>



Scheme 1.6: Previously hypothesised sequence of events in TBTAP formation

## 1.4 Functionalisation methods

The development of porphyrinoid synthesis has enabled a plethora of functionalisation methods, allowing the creation of a diverse range of structurally and electronically altered porphyrinoids. This tuneability is critical to optimisation of these species in almost all applications utilising highly functional organic materials.

### 1.4.1 Peripheral and non-peripheral substitution

Functionalisation of starting materials in porphyrinoid synthesis can be utilised to produce functionalised porphyrinoids with interesting properties. Electron donating or withdrawing groups may be added to alter the electronics of the macrocycle, increase solubility, reduce symmetry, or even utilise steric hindrance to alter the macrocycle structure.<sup>49–53</sup> In the example below (figure 1.8) the presence of non-peripheral phenyl groups significantly distorts the macrocycle structure and red-shifts the UV-Vis spectrum.

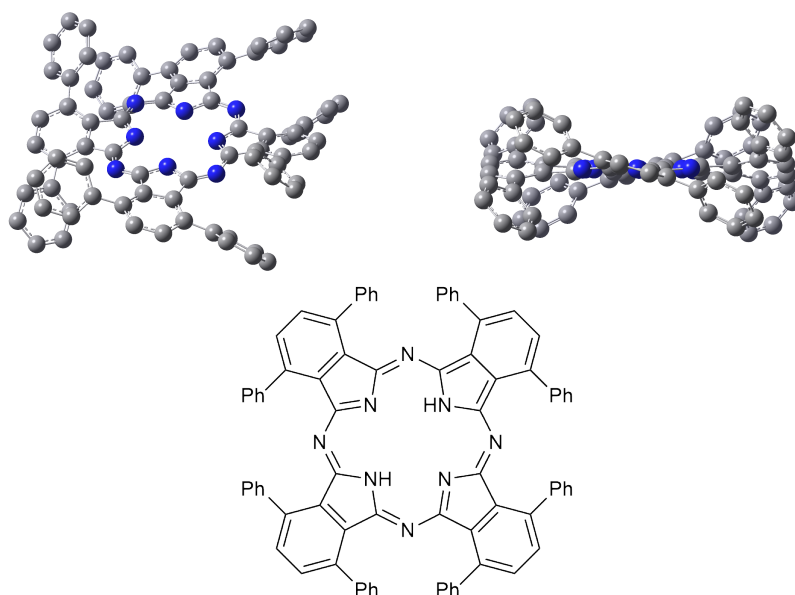
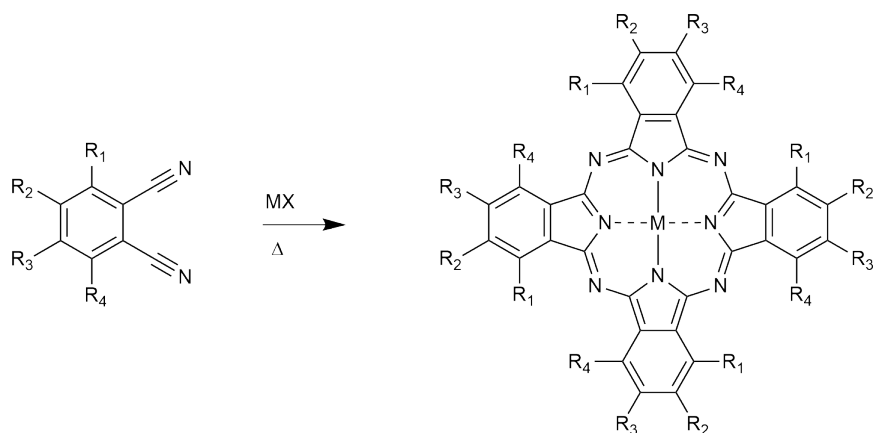


Figure 1.8: An example of a perturbed phthalocyanine, distortion of the macrocyclic ring and electron rich phenyl groups red shift the absorbance to the near IR (790 nm).

Unlike with asymmetric porphyrin derivatives, which have been successfully synthesised using stepwise approaches,<sup>54</sup> asymmetrical Pcs are synthesised by statistical condensation of 2 or more phthalonitriles. This leads to a large number of often difficult to separate products, and low yield for the target compound. Asymmetric phthalonitrile derivatives eg.  $R_2 = \text{Aryl}$ ,  $R_1 = R_3 = R_4 = \text{H}$  (scheme 1.7), also produce structural isomers, complicating synthesis further.



Scheme 1.7: Synthesis of substituted Pcs, R=H, Aryl, Alkyl, Ether, Thiol, Amine, Halide etc.

An extension of peripheral substitution is annulation of peripheral ring structures, leading to many highly interesting extended species (figure 1.9). This strategy can be used to build electronically conjugated, two-dimensional, supra-molecular frameworks. Particular attention has been received with respect to the development of metal organic frameworks (MOFs) and covalent organic frameworks (COFs), which show potential as gas storage solutions. Applications in OFETs, OPVs, PDT, photocatalysis and many more high technology fields have also been investigated.<sup>55–59</sup>

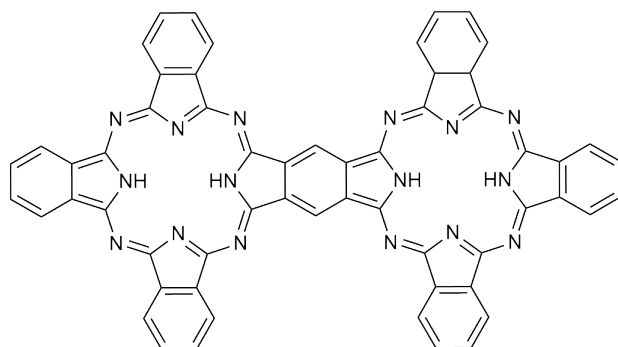


Figure 1.9: An example of a peripherally annulated phthalocyanine (para- tautomer shown).

#### 1.4.2 Metalation and axial substitution

Phthalocyanines, porphyrins, subphthalocyanines and related hybrid structures all share the common property of being excellent ligands. This allows a vast range of metals to be inserted into most porphyrinoids, the only exception being SubPc and SubTBDAP, where currently only boron coordinated species

have been synthesised. These coordinated metals can be functionalised with further ligands, be they commonly employed organic ligands, or other macrocycles. This opens a diverse range of options with respect to integration of these porphyrinoids to other systems, such as multichromophore arrays.

A wide variety of metals spanning the majority of the periodic table may be inserted into Pcs and Pors. The metal used may be selected to control properties such as geometry of the complex, electronic and electrochemical attributes, as well as properties such as spin. The size of metal ion dictates the formation of planar complexes or distorted *sitting-atop* (SAT) complexes. Shown in figure 1.10 are example complexes displaying these conformational differences.

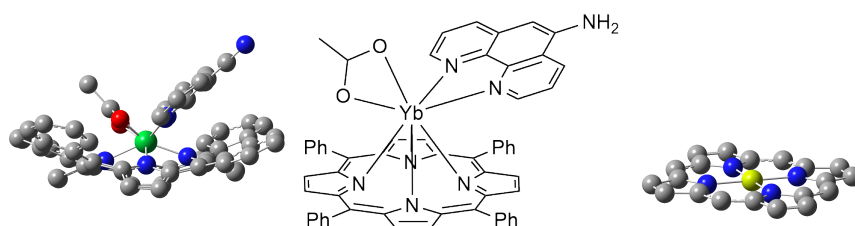


Figure 1.10: An example of a ytterbium SAT complex (left and center) compared to the planar magnesium porphyrin (right), conformational differences between the two are clearly visible.<sup>60</sup> (Hydrogens omitted for clarity.)

SAT conformations lend themselves to the formation of double and triple decker species, with two macrocycles coordinated to a single, large metal ion. These type of complexes have received significant attention for their potential applications in molecular machine systems such as molecular gyroscopes, single molecule magnets (SMMs) and supramolecular assemblies. Shown in figure 1.11 is an example of a porphyrin/phthalocyanine based double decker complex, again displaying the *sitting-atop* geometry.

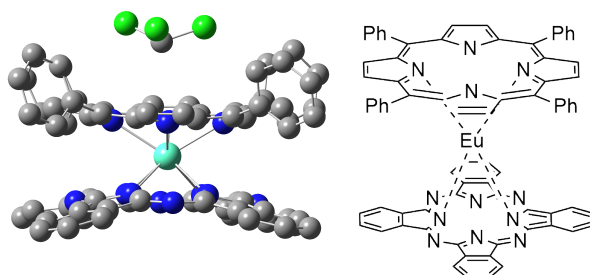


Figure 1.11: Crystal structure of a tetraphenylporphyrin europium phthalocyanine double decker compound (hydrogens omitted for clarity).<sup>61</sup>

Photocatalytic systems, an example of which is shown in figure 1.12, have received significant research effort in recent years due to their potential to afford

green and low energy synthetic transformations, as well as for fuel production, pollutant photodegradation etc. As with transition metal catalysis a metal center is normally required to bind the target substrate and facilitate the chemical transformation. The vast array of metals that can be utilised once again allow wide tuning potential and application.

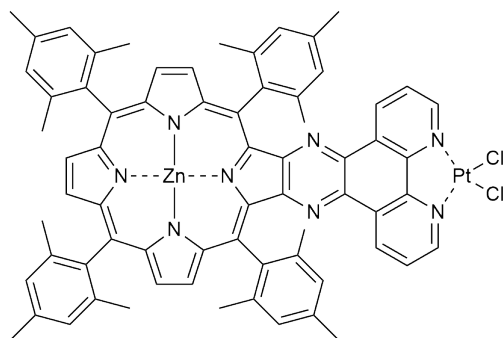


Figure 1.12: An example of a photocatalytic system for hydrogen production.<sup>62</sup>

### 1.4.3 *Meso* substitution

Porphyrins are commonly synthesised as tetra *meso* substituted derivatives from precursors such as benzaldehyde. Asymmetric *meso* substituted porphyrins such as TPP-OH (tetraphenylporphyrin bearing a single *meso*-phenol group and 3 *meso* phenyl groups) may be synthesised by statistical condensation. In hybrid structures the integration of a *meso*  $sp^2$  carbon, with easily altered aromatic groups from aminoindoline precursors provides further options for functionalisation. Other chromophores may be integrated directly, or aryl groups containing functional groups to allow further cross coupling reactions may be included. Both of these methods have been developed and utilised by the Cammidge group in previous studies. Shown in figure 1.13 are examples of the scope of aminoindolines synthesised by previous work, as well as the first example of a cross coupling reaction involving a TBTAP (scheme 1.8).<sup>63</sup>

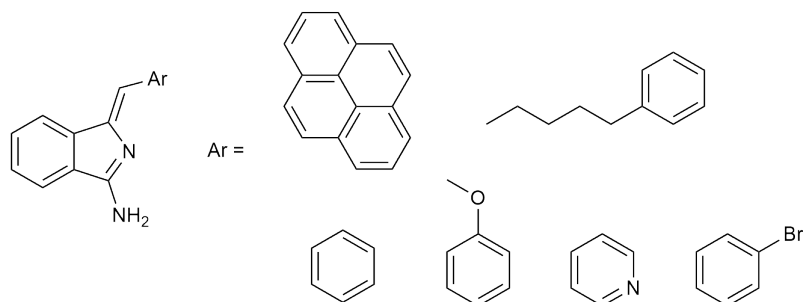
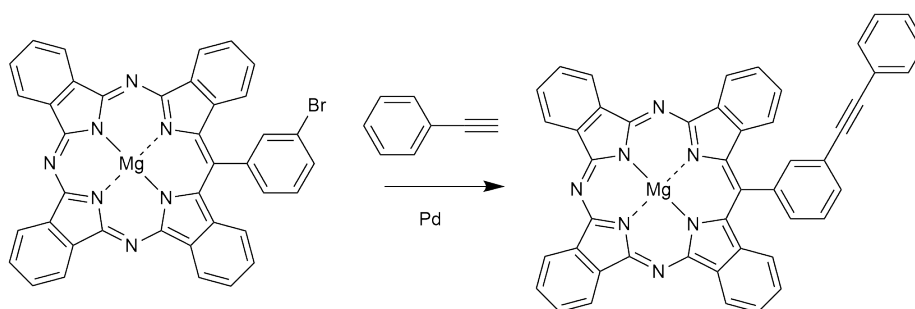


Figure 1.13: Some examples of aminoindoline derivatives previously synthesised.<sup>64,65</sup>



Scheme 1.8: The first example of a cross coupling reaction utilizing a bromo TBTAP derivative.<sup>63</sup>

#### 1.4.4 Multichromophore arrays and complexes

The range of synthetically accessible porphyrinoids, as well as their versatility in functionalisation and formation of more complex species, has yielded a ‘toolkit’ for the controlled construction of so called multichromophore arrays. Multichromophore systems are constructed from electronically linked fragments serving different purposes. For example, a system could consist of peripheral ‘antenna’ fragments designed to collect solar energy; with electron transfer or cascade processes ‘funneling’ energy to a central fragment designed to facilitate a photocatalytic transformation. These systems obviously require careful design and tuning to achieve the desired electron transfer characteristics etc, however a well designed system can achieve incredibly efficient results.

Multichromophore arrays have found application as biomimetic light harvesters,<sup>66</sup> non-linear optical materials,<sup>67</sup> functional dyes and fluorophores,<sup>68</sup> energy funnels and cascades,<sup>69,70</sup> and donor-acceptor pairs.

### 1.5 Current and potential applications

#### 1.5.1 OPVs

The emerging field of Organic PhotoVoltaics (OPVs) has received extraordinary research effort over the last 20-30 years, with some of the latest advances opening the doors to highly efficient, cheap, environmentally friendly and easily manufactured OPV devices with novel properties.<sup>71,72</sup> Some of these properties include the ability to achieve high power conversion efficiencies (PCEs) from basically transparent panels.<sup>73</sup>

Early OPVs were extremely inefficient compared to their silicon based counterparts of the day; early examples of organic dye based OPVs recorded efficiencies as low as a fraction of a percent with porphyrinoids such as chlorophyll and magnesium phthalocyanine (MgPc).<sup>74</sup> 1% PCE was achieved for a phthalocyanine based OPV in 1986,<sup>75</sup> which represented a significant advance in efficiency, and paved the way towards OPVs that would eventually compete with silicon based devices.

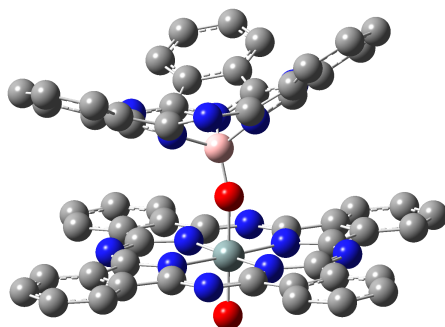


Figure 1.14: A DFT optimised structure of a multichromophore array produced by the Cammidge group, electronic coupling of the chromophores (Pc and SubPc) affords absorbance across the entire solar spectrum (hydrogens and hexyl chains omitted for clarity, grey = carbon, red = oxygen, blue = nitrogen, pink = boron, blue/grey = silicon).<sup>32</sup>

Performance in OPVs is influenced and limited by a number of factors such as low light absorption in the red/IR regions, poor charge transport, and poor photochemical stability over extended time periods. These problems have been addressed over the years with the synthesis of highly specialised materials, use of advanced material combinations to create well matched donor-acceptor (D-A) pairs, and development of more controlled self assembly or thin film deposition methods. The requirements for highly efficient organic molecules for OPVs are strong light absorption and charge transport characteristics;<sup>76</sup> these properties are usually afforded by the presence of delocalised  $\pi$  and  $\pi^*$  systems in the organic molecule. From these requirements it is logical to conclude that most porphyrinoids would make excellent candidates as photosensitisers (PS), and indeed, porphyrinoids have found themselves at the center of OPV development. Recently the Cammidge group developed a multichromophore array that effectively absorbs light across almost the entirety of the solar spectrum - a so called 'black chromophore', shown in figure 1.14.

The complementary properties of porphyrinoids with themselves and other common D-A components such as fullerene or other conjugated organics, in addition to an incredibly diverse suite of functionalisation and integration options, has facilitated the development of many unique and interesting solutions to the problems described above. Figure 1.15 shows an example of a multichromophore array, a porphyrin bearing four naphthalene diimide fragments via electronically conjoined bridges. The extension of the  $\pi$  system pushes absorbance into the near IR, drastically improving PCEs in the studied OPV from 1% to 5-8%.<sup>71</sup> This is a single example of the plethora of ways chromophores can be tailored to improve a specific system.

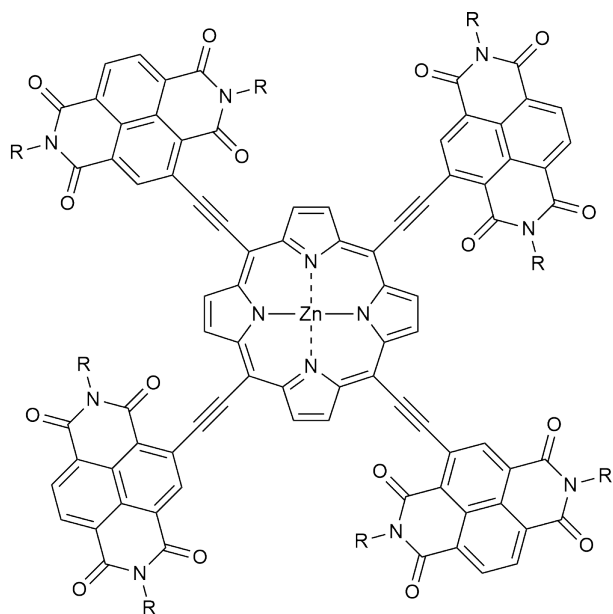


Figure 1.15: An example of a multichromophore array for application in OPV devices.<sup>71</sup>

### 1.5.2 NLOs

The rapidly expanding field of non-linear optics (NLOs) has significantly contributed to the development of countless indispensable optical and electronic devices that provide the foundations for modern telecommunications, computing, electronics and more. These devices can be organised into three categories: development of advanced and specialised lasers, material interactions such as spectroscopy, machining and analysis, and finally information technology such as data storage, sensors and signal processing. Early NLO research utilised inorganic structures such as  $\beta$ -barium borate or potassium niobate, materials that are still used today; however since 1990 attention has shifted towards organic  $\pi$  conjugated systems, driven by developments in flexible and versatile chemical synthesis.<sup>77–80</sup> Naturally, porphyrinoids have received significant attention in NLO development, where molecular modification can be used to control primary (NLO susceptibility etc) and secondary (solubility, absorption, stability etc) NLO properties.<sup>49</sup>

### 1.5.3 Photocatalysis, photochemistry and PDT

Solar radiation is an abundant and renewable source of energy. If effectively captured on large scale and used not only to produce electricity, but also for green and efficient chemical transformations; it offers a plethora of solutions to the problems associated with modern energy and industrial demands. These include renewable energy production,<sup>81–83</sup> processing of pollutants or chemical waste,<sup>84–86</sup> green chemical transformations, and photodynamic therapies (PDT) for the treatment of cancers and other conditions.<sup>87–89</sup> Due to their

large delocalised  $\pi$  systems and fast electron transfer characteristics various porphyrinoids have found significant application in this field, an example of a commercial porphyrin based PDT sensitizer is shown in figure 1.16.

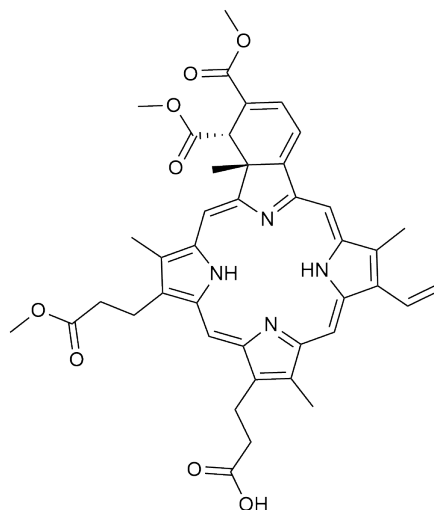


Figure 1.16: An example of a dihydrobenzoporphyrin used as a photosensitizer for PDT.<sup>90</sup>

The photocatalytic production of hydrogen has been studied extensively due to its application as a clean and renewable fuel not only in internal combustion engines, but also electricity producing hydrogen fuel cells. The widespread application of hydrogen as a fuel would have a huge impact on global greenhouse emissions. Currently hydrogen is most commonly produced electrolytically, its cleanliness as a fuel therefore relies on the use of renewably sourced electricity; photocatalytic production allows the direct production of hydrogen from water and solar radiation, minimising infrastructure requirements and likely increasing efficiency.<sup>91–93</sup>

Photocatalytic systems have been shown to efficiently degrade toxic compounds such as phenols, dyes and numerous organic compounds, this could lead to efficient and passive treatment of waste water from a variety of industrial processes, significantly reducing pollution and processing costs and complexity.<sup>84–86</sup> Photodynamic therapies exploit the ability of porphyrinoids to convert triplet to singlet oxygen upon irradiation with light. A porphyrinoid combined with an appropriate delivery method can effectively localise to tumours in a patient; combined with targeted light irradiation this method provides a precise way to induce controlled necrosis of target cells with minimal side effects.<sup>87–89</sup>

#### 1.5.4 Molecular sensors

Recent increases in pollution and decreases in air quality are factors contributing to the need for effective monitoring and analysis of hazardous gasses

and chemicals; the development of new sensing materials and organic semiconductors is resulting in increased resolution, sensitivity and versatility. Molecular sensors can be described by 3 elements: binding and recognition, transduction, and measurement. Systems may be produced to detect ions, gasses, proteins, DNA/RNA and other fragments. Recognition and transduction can occur via a number of mechanisms such as electrochemical, mechanical or optical.<sup>94</sup> Shown in figure 1.17 is an example of a system that can be used to selectively detect copper ions.

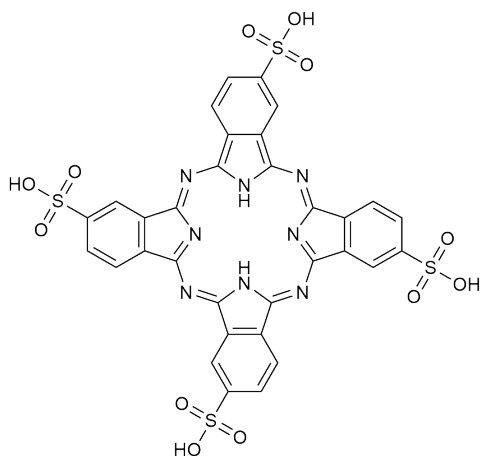


Figure 1.17: Phthalocyanine tetrasulfonic acid is an example of an optical sensor for copper ions, producing a significant spectral and fluorescence change selectively for copper ions.<sup>95</sup>

To facilitate binding of an analyte a good ligand must be present in the system; macrocycles are often employed for detection of ions and gasses as they are often not only good ligands, but may also be modified to improve selectivity or sensitivity. Commonly employed for this type of detection are switchable fluorophores, where fluorescence emission changes with concentration of the target ion or gas. This emission may easily be measured and correlated to concentration.

### 1.5.5 SMMs

In the early 1990s a significant transition metal complex was discovered (figure 1.18); when cooled with liquid helium this complex retained magnetisation for extended periods of time, giving rise to the field of single molecule magnets, or SMMs.<sup>96</sup> As an advance from traditional bulk ferromagnetic materials in applications such as data storage, SMMs may potentially allow huge increases in data density compared with traditional data storage technologies. Molecular spintronics is another development with large potential ramifications for computing and storage densities; this field uses SMM materials to bridge the disciplines of spintronics and molecular electronics, resulting in the ability to manipulate and control the spin and charge of molecules in such devices.<sup>97</sup>

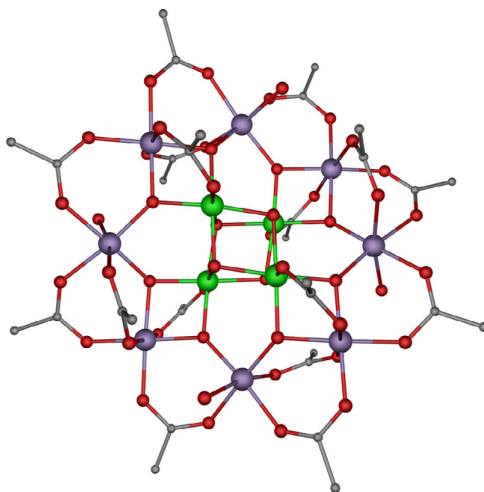


Figure 1.18: The structure of Mn<sub>12</sub>-ac, the first discovered SMM system (Mn<sup>III</sup> = purple, Mn<sup>IV</sup> = green, carbon = grey, oxygen = red).<sup>96</sup>

Since their inception, lanthanide ions have found themselves at the heart of SMM research due to their large spin values and easy integration in organometallic complexes. Of particular interest are macrocyclic double and triple decker compounds enclosing lanthanide ions (figure 1.11); these species may not only function as molecular gyroscopes, but can also produce SMMs with high spin and exceptionally high anisotropic barriers, vastly increasing the feasibility of integration and utilisation in real world systems.<sup>98</sup>

## Chapter 2

# Investigations into TBTAP formation

### 2.1 Introduction

#### 2.1.1 History of synthetic routes to TBTAPs

Over the last few decades developments in the synthetic chemistry of porphyrins and phthalocyanines have enabled straight forward synthetic access to a vast range of increasingly complex functionalised porphyrinoids, with a wide variety of uses and tuneability for specific applications. Tetrabenzotriazaporphyrins (TBTAPs, figure 2.1) represent one class of possible hybrid structures between porphyrins and phthalocyanines, bearing 3 nitrogen atoms and 1 carbon atom at the *meso* positions as described in section 1.1. While TBTAP was first discovered and characterised in the 1930s,<sup>16</sup> lack of controllable and reliable synthetic routes significantly hindered further research into these fascinating macrocycles compared to the development enjoyed by porphyrins and phthalocyanines.

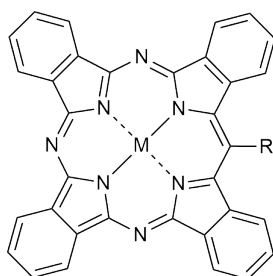
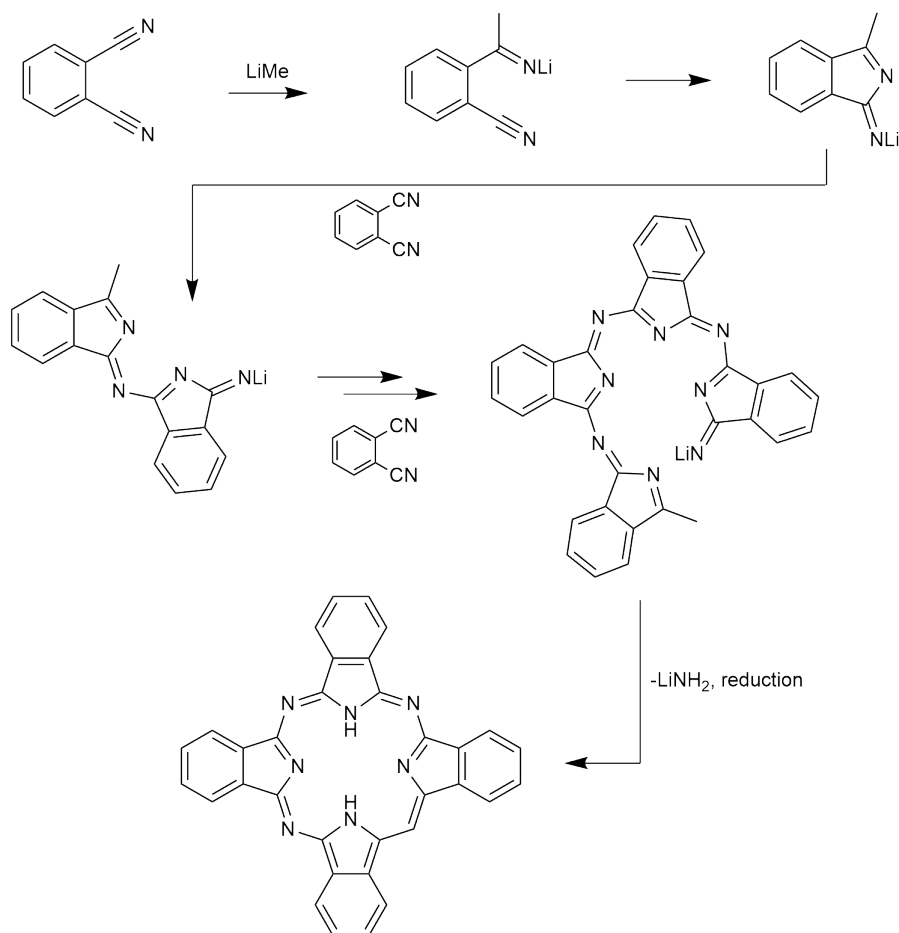


Figure 2.1: The structure of TBTAP, R = H, Ar, alkyl.

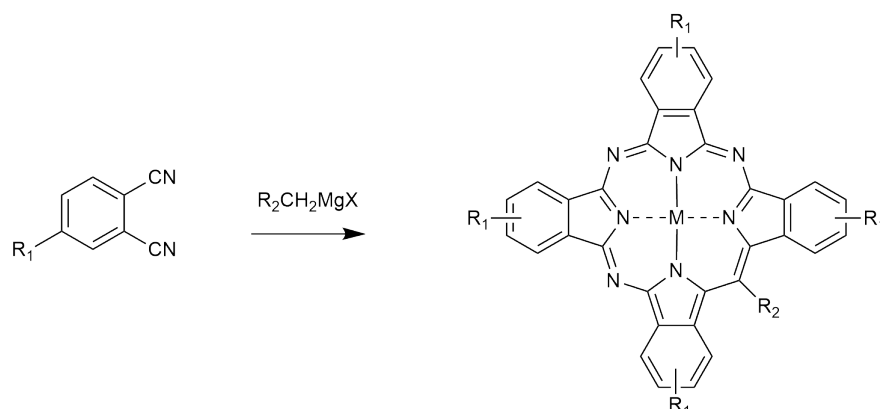
Following the work from Fischer in 1936 and Helbeger in 1937 that described the formation of unknown macrocyclic pigments consisting of four pyrrole rings linked by a mixture of methine and nitrogen fragments, TBTAP was successfully isolated in very poor yield and the structure determined in 1939 by Barrett

*et al.*<sup>16,99</sup> This procedure utilised the Grignard reagent MeMgI and phthalonitrile as reactants. Further mechanistic investigations utilizing methyllithium as the initiating nucleophile suggested the macrocyclization pathway proceeds via the formation of a nucleophilic isoindoline analogue that attacks 3 more units of phthalonitrile until a 4 membered open chain is formed; this undergoes macrocyclization and aromatization with elimination of lithium amide to yield TBAP, the proposed pathway is shown in scheme 2.1.



Scheme 2.1: Macrocyclization pathway proposed by Barrett in 1939.

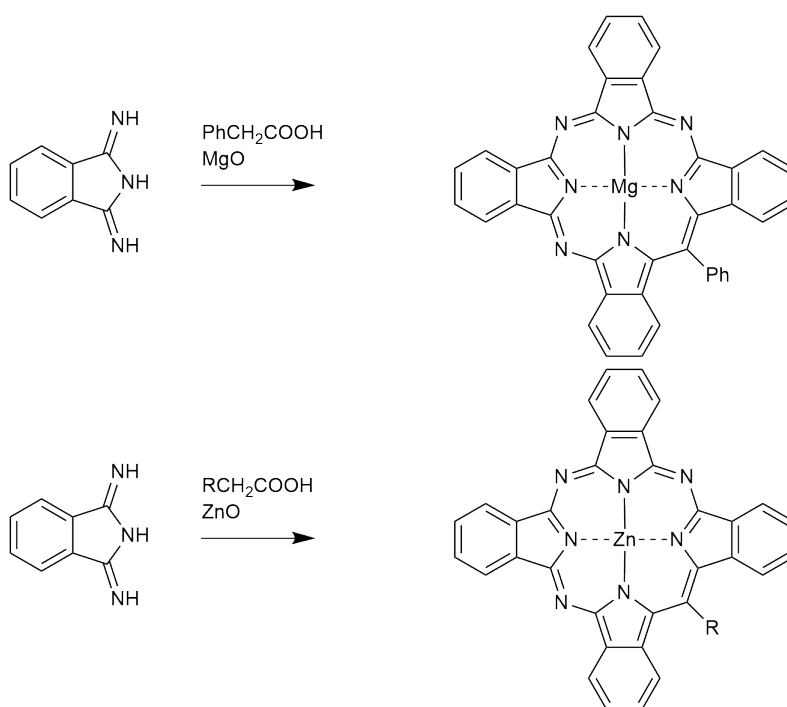
This confirmation of structure and a controllable (albeit low yielding) synthetic procedure for TBAP opened the door to examining various spectroscopic and electronic properties of these unique species, however it was not until 50 years later that the first examples of *meso* functionalised TBAPs were synthesised by Leznoff and McKeown.<sup>23</sup> This synthetic route utilised alkyl and phenyl Grignard reagents to insert functional groups at the *meso* position of the resulting TBAPs (scheme 2.2).



Scheme 2.2: Leznoff and McKeown's reported synthesis of TBTAP derivatives, successfully synthesised derivatives listed below.<sup>23</sup>

R <sub>1</sub> , R <sub>2</sub> and X	TBTAP produced
R <sub>1</sub> = <i>t</i> -BuO, R <sub>2</sub> = Propyl, X = Br	R <sub>1</sub> = <i>t</i> -BuO, R <sub>2</sub> = Propyl, M=Mg
R <sub>1</sub> = <i>t</i> -BuO, R <sub>2</sub> = <i>n</i> -Pentadecane, X = Cl	R <sub>1</sub> = <i>t</i> -BuO, R <sub>2</sub> = <i>n</i> -Pentadecane, M=H <sub>2</sub>
R <sub>1</sub> = <i>t</i> -Bu, R <sub>2</sub> = <i>n</i> -Pentadecane, X = Cl	R <sub>1</sub> = <i>t</i> -Bu, R <sub>2</sub> = <i>n</i> -Pentadecane, M=H <sub>2</sub>
R <sub>1</sub> = H, R <sub>2</sub> = <i>n</i> -Pentadecane, X = Cl	R <sub>1</sub> = H, R <sub>2</sub> = <i>n</i> -Pentadecane, M=Mg
R <sub>1</sub> = <i>t</i> -Bu, R <sub>2</sub> = Ph, X = Cl	R <sub>1</sub> = <i>t</i> -Bu, R <sub>2</sub> = Ph, M=H <sub>2</sub>
R <sub>1</sub> = H, R <sub>2</sub> = Ph, X = Cl	R <sub>1</sub> = H, R <sub>2</sub> = Ph, M=Mg

New procedures were developed for the synthesis of magnesium *meso*-phenyl substituted TBTAPs and zinc *meso*-alkyl substituted TBTAPs by Galanin *et al* in 2002 and 2004 respectively.<sup>24,100</sup> These procedures utilised carboxylic acid derivatives to facilitate the inclusion of a *meso* carbon atom, 1,3-diiminoisindoline and metal oxides as template/macrocyclization reagents (scheme 2.3).



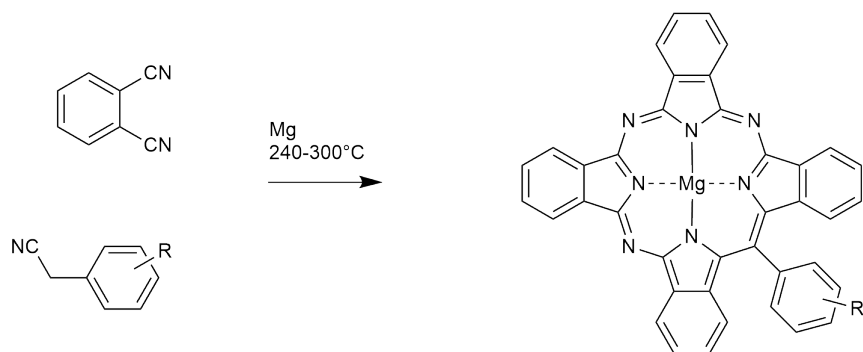
Scheme 2.3: Galanin *et al.* synthesis of *meso* substituted TBTAPs. R = ethyl, hexyl and dodecyl.

In 2011 the Cammidge group explored and refined the synthesis of hybrid porphyrinoids from Grignard reagents: it was found that varying the ratio of MeMgBr gave more selective access to TBTAPs, TBDAPs, TBMAPs and TBP from 3,6-dialkyl phthalonitrile derivatives. In contrast the use of 4,5-dialkyl phthalonitriles resulted in mixtures of Pc and TBTAP (figure 2.2).<sup>26</sup>

Starting material	Ratio	Pc-H <sub>2</sub>	TBTAP-H <sub>2</sub>	<i>cis</i> -TBDAP-H <sub>2</sub>	TBMAP-H <sub>2</sub>	TBP-H <sub>2</sub>
1	1:4	nd	nd	nd	nd	nd
1	1:1	trace	24%	14%	trace	nd
1	2:1	trace	27%	9%	3%	trace
1	3:1	nd	18%	8%	4%	1%
1	4:1	nd	trace	trace	trace	12%
1	5:1	nd	nd	nd	nd	1%
2	2:1	trace	13%	5%	3%	1%

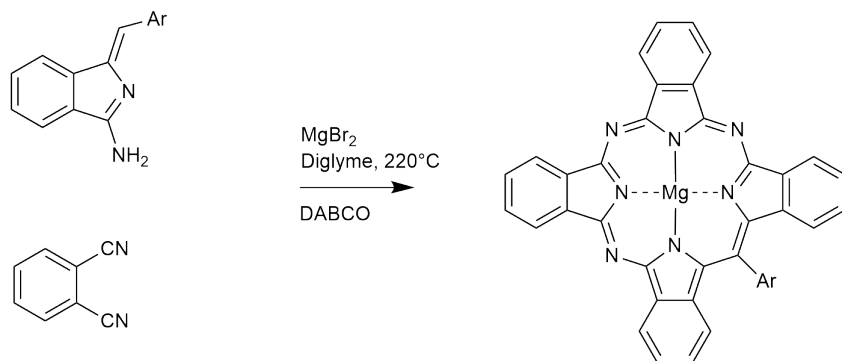
Figure 2.2: Results obtained by Cammidge *et al.*, SM 1 = 3,6-dihexylphthalonitrile, SM 2 = 3,6-didecylphthalonitrile, ratio = MeMgBr : phthalonitrile.

In the same year Kalashnikov *et al.* reported the synthesis of a series of *meso*-aryl substituted TBTAPs from phthalonitrile and arylacetonitriles (scheme 2.4). While this procedure gave new control over the *meso* substitution, yields remained around 10%.<sup>101</sup>



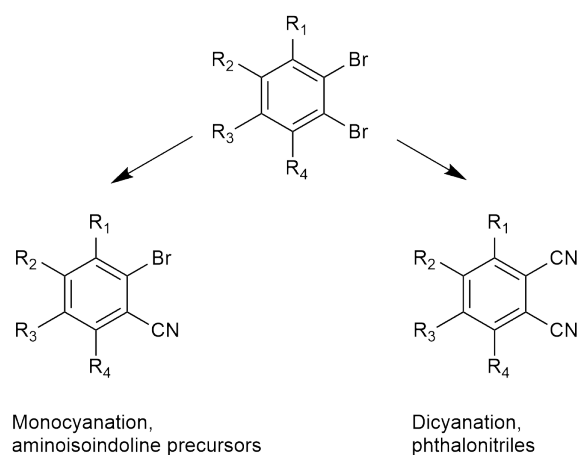
Scheme 2.4: Derivatives synthesised by Kalashnikov *et al.*, R = H, *o*-Me, *m*-Me, *p*-Me, *p*-OMe.

In 2013 the Cammidge group published a new procedure for TBTAP synthesis, utilising aminoisoindoline precursors (scheme 2.5). This synthesis affords TBTAPs in good yield, with control of *meso* substitution from the aminoisoindoline, and peripheral and non-peripheral substitution from the phthalonitrile. This procedure has since been refined and optimised to yield a wide range of functionalised TBTAPs in 20-40% yield.<sup>28,29</sup>



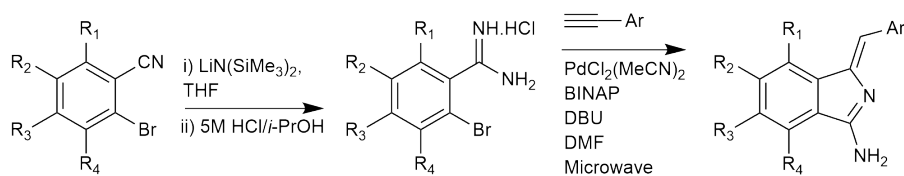
Scheme 2.5: The Cammidge *et al.* synthesis of TBTAPs afforded by the macrocyclization of aminoisoindoline and phthalonitrile.

Substituted aminoisoindolines can conveniently be synthesised from the same 1,2-dibromobenzene starting materials as substituted phthalonitriles (scheme 2.6), differing only in the production of 2-bromobenzonitriles for the synthesis of aminoisoindolines, or 1,2-dibenzonitriles to produce phthalonitriles. The wide range of commercially available ethynylaryls used in aminoisoindoline synthesis also allow for a large selection of aminoisoindoline derivatives, and therefore *meso* substituted TBTAPs to be easily and selectively synthesised in relatively high yields (scheme 2.7).



Scheme 2.6: Pathways to 2-bromobenzonitriles and phthalonitriles.

From 2-bromonitriles aminoisoindolines are synthesised via an initial treatment with  $\text{LiN}(\text{SiMe}_3)_2$ , producing an intermediate amidine hydrochloride upon hydrolysis with  $\text{HCl}/i\text{-PrOH}$ . This amidine hydrochloride is then coupled with an ethynylaryl utilizing copper free Sonogashira conditions, an in-situ 5-*exo-dig* cyclization produces the final aminoisoindoline product (scheme 2.7).



Scheme 2.7: Aminoisoindoline synthesis from 2-bromobenzonitriles.

### 2.1.2 Recent application and advances

Despite the relatively low levels of research attention ( $\sim 100$  pieces of literature relating to TBTAPs since 1930), these remarkable macrocycles have resulted in many patents and papers relating to their utilisation in high technology and optoelectronic fields over recent years.

Patented medical applications of TBTAPs and related hybrid porphyrinoids include use as fluorescent markers/probes for hybridization and immunoassays<sup>102</sup> and in linked porphyrinoid/anti-cancer structures.<sup>103</sup> In optoelectronic fields patents have been recently granted relating to the use of TBTAPs as donor materials in OPVs, absorbers for DSSCs, emitters for red and NIR OLEDs (figure 2.3), absorbers for hydrogenations and improved black inks.<sup>104–107</sup>

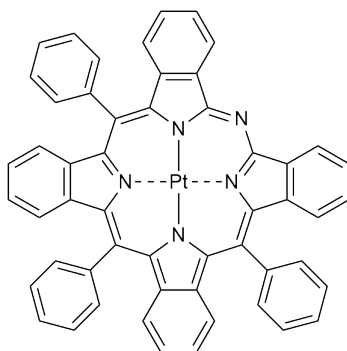


Figure 2.3: An example of a platinum coordinated TBMAP complex, this species displays very strong NIR emission at room temperature.<sup>107</sup>

Recent studies have also shown the potential of TBTAP type materials in various other applications such as thin films for liquid crystals and organic field effect transistors,<sup>108,109</sup> phosphorescent metal complexes for NIR fluorophores and sensing oxygen,<sup>110</sup> and theoretical as well as experimental studies suggesting good potential for application in DSSCs/OPVs.<sup>111</sup>

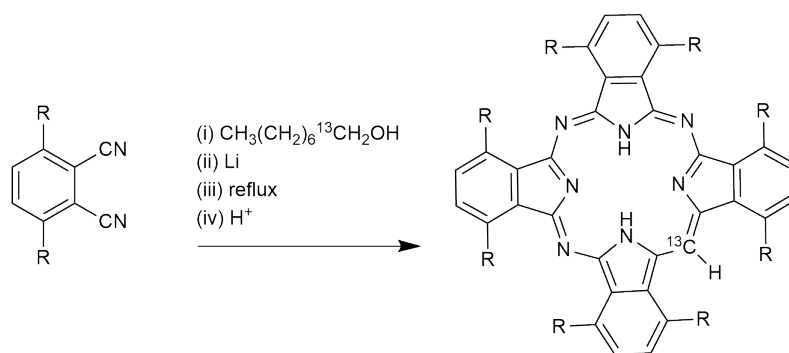
The diverse integration of TBTAPs and related macrocycles in high technology and cutting edge applications highlights the adaptability of hybrid species. As with the advance of evermore controlled and sophisticated Pc and Por synthesis, it can be expected that further development of hybrid synthetic routes and derivatives will facilitate more specialised and highly specific/tuned application.

### 2.1.3 Recent advances in the Cammidge group

As detailed previously, the Cammidge group have made significant progress with respect to the development of high yielding procedures for the synthesis of various hybrid porphyrinoids, with aminoisindoline precursors being utilised to produce TBTAPs and SubTBDAPs in relatively high yields. However it has

become clear that the macrocyclization of these species is still not well understood at a mechanistic level, with a range of side products produced. Gaining insight into mechanistic events and steps will aid the development of future procedures, potentially facilitating better yields, control, and more selective synthesis of asymmetric derivatives in place of statistical condensations.

Some of the first mechanistic investigations into TBTAP formation from the Cammidge group focused on the unexpected synthesis of non-peripherally alkyl substituted TBTAPs from phthalonitriles under conditions that would normally yield phthalocyanines (scheme 2.8). The only possible source for the methine carbon in the reaction was from the solvent, and  $^{13}\text{C}$  labelling experiments revealed this to be the source of the *meso* carbon atom. This unexpected result demonstrates some of the complexities in the macrocyclization process.

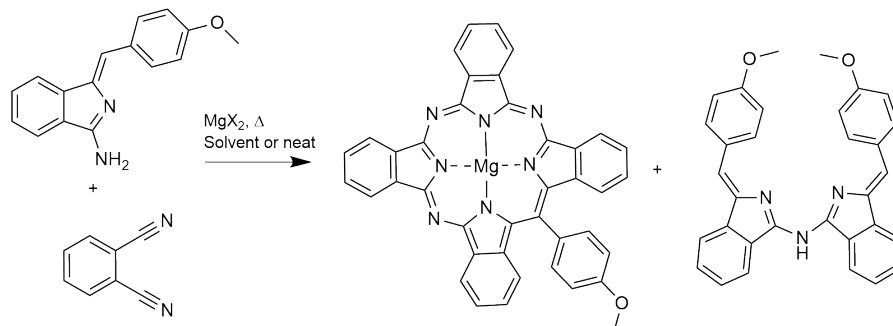


Scheme 2.8: Cammidge *et al* synthesis of non-peripherally alkyl substituted TBTAPs, R =  $\text{C}_6\text{H}_{13}$ .<sup>26</sup>

The 2011 investigations by Cammidge *et al.* provided convenient synthetic routes to a range of hybrid macrocycles by varying the quantities of Grignard reagent to phthalonitrile. As detailed previously, higher quantities of Grignard reagent resulted in more aza bridges replaced with methine bridges in the resulting macrocycles.<sup>112</sup> Therefore, methine bridges were clearly being inserted by the Grignard reagent, but the exact mechanistic steps that resulted in integration of carbon bridges remained unknown.

In 2013 the Cammidge group published procedures for the synthesis of TBTAPs utilizing aminoisoindoline precursors.<sup>28</sup> These precursors are Ar-C analogues of diiminoisoindoline, commonly employed in the synthesis of phthalocyanines. It was reasoned these analogues would have similar reactivity to diiminoisoindoline and therefore be integrated in the macrocyclization process, potentially providing easy inclusion of an aryl bearing *meso* carbon atom. The first attempt at this reaction utilised aminoisoindoline and diiminoisoindoline, with  $\text{MgBr}_2$  as a template ion. Unfortunately the self-condensation products Pc and azadipyrromethene were produced in significant yields. In principle, the azadipyrromethene can also act as a TBTAP or TBDAP precursor, however

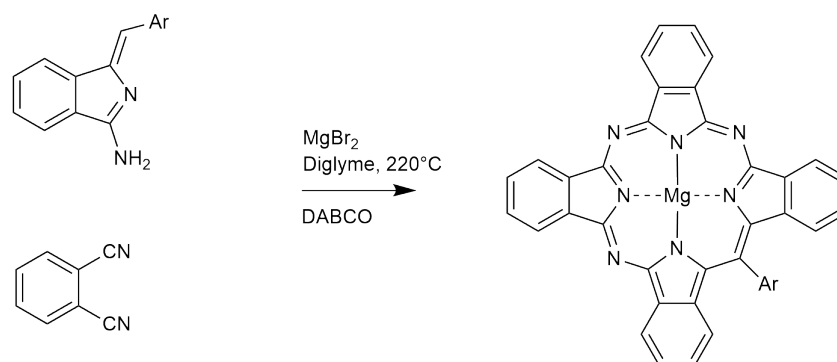
various attempts to re-subject the isolated compound to the reaction conditions have not yielded any macrocyclic products.



Scheme 2.9: The utilization of aminoisoindolines as a TBTAP precursor by Cammidge *et al.*<sup>28</sup>

By considering the reactivity of the substrates used, the procedure was refined through the utilization of the less reactive phthalonitrile instead of di-aminoisoindoline. At 220°C the formation of Pc can be significantly reduced while aminoisoindoline still initiates the macrocyclization with phthalonitrile, giving a competitive rate of TBTAP formation (scheme 2.9). However the reaction remains a delicate balance between competing pathways, and the use of functionally modified reagents can alter the relative yields of products due to electronic, steric, and/or as of yet unknown factors.

Further improvements to yield were obtained through careful optimisation of the procedure.<sup>29</sup> In an attempt to minimise azadipyrromethene formation, a 1:1 solution of aminoisoindoline and phthalonitrile was added to a solution of phthalonitrile (3 eq) in diglyme over a period of 1 hour using a syringe pump. This procedure minimises the concentration of aminoisoindoline in solution and therefore promotes macrocyclization over homocondensation. Subsequently, DABCO (1,4-diazabicyclo[2.2.2]octane), is also added to the reaction. It was found that aminoisoindoline coordinated the central cavity of the MgTBTAP product, DABCO displaces the aminoisoindoline and allows complete reaction of the starting material, hence improving yield. These subtle but carefully conceived modifications to the procedure have allowed synthesis of TBTAPs in up to 40% yield (scheme 2.10).

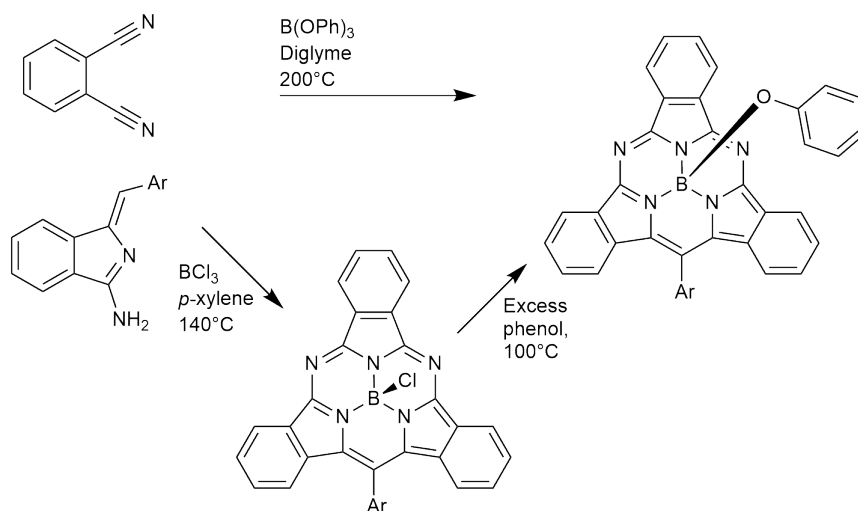


Scheme 2.10: The further optimised Cammidge *et al* synthesis of TBTDAPs afforded by the co-macrocyclization of aminoindoline and phthalonitrile, utilising DABCO and syringe pump addition of reagents.<sup>29</sup>

### Adaptation to SubTBDDAP synthesis

Subphthalocyanines are synthesised in cyclization processes analogous to the macrocyclization of Pcs; phthalonitrile is used as a precursor and a template ion utilised to facilitate the polymerisation of phthalonitrile in an open chain around the template. Once the chain reaches 4 members for Pcs, or 3 members for SubPcs, macrocyclization and aromatization occurs to form the product. Literature only describes cyclotrimerization and SubPc formation using boron as a template ion, all other ions are too large and promote Pc formation.<sup>113</sup> Given the similarities in the macrocyclizations, a co-macrocyclization utilising aminoindoline and phthalonitrile around boron was the next logical progression for this new precursor.

SubTBDDAP was first successfully isolated and characterised in 2015 from the cyclotrimerization of aminoindoline and phthalonitrile facilitated by boron trichloride.<sup>64</sup> The expected product, SubTBDDAP-BCl, was observed by MALDI-TOF analysis, along with the corresponding SubTBDDAP-BOH and [SubTBDDAP-B]<sup>+</sup> fragments. The instability of the apical ligand is well documented for SubPc species, and as expected, attempts to isolate the new SubTBDDAP-BCl species resulted in hydrolysis of the apical site if water was present, or the production of SubTBDDAP-BOMe if methanol was used during workup. This degradation of the target species complicates isolation and purification, so the procedure was adapted to include treatment with excess phenol after the initial reaction period (scheme 2.11). This step converts the apical position to an -OPh fragment, which is significantly more stable and allowed satisfactory purification and isolation of the target molecules.



Scheme 2.11: The Cammidge *et al.* synthesis of SubTBDAPs utilising aminoindoline precursors, followed by apical substitution of phenol, or directly through use of  $B(OPh)_3$ .<sup>64</sup>

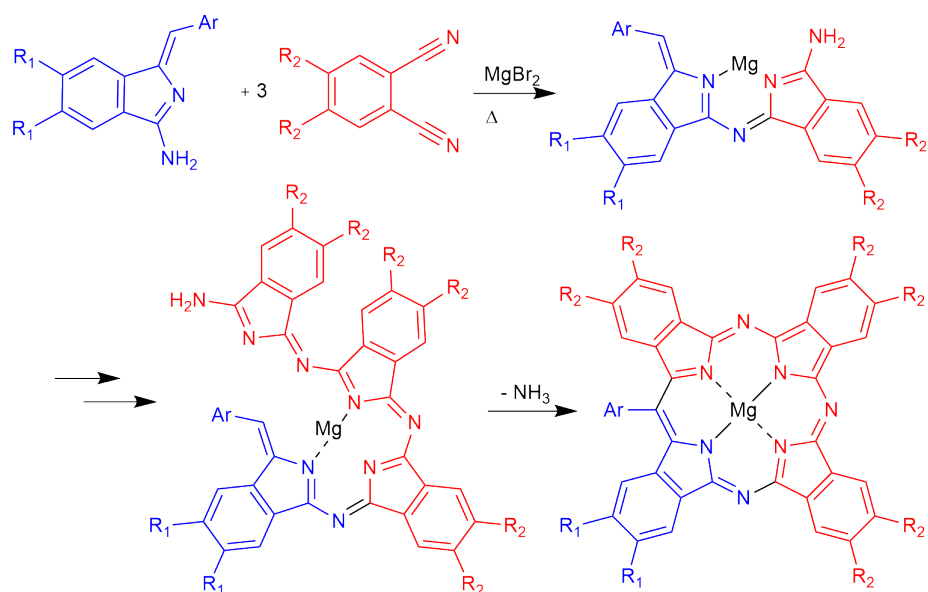
Ar =	Axial substituent =
Ph	OPh
Ph	OMe
Ph	O <i>i</i> Pr
Ph	OBu
<i>p</i> -MeOPh	OMe
<i>p</i> - <i>n</i> -pentylPh	OPh
<i>p</i> -MeOPh	OPh
<i>p</i> -CF <sub>3</sub> Ph	OPh

Figure 2.4: Table of SubTBDAP derivatives synthesised during previous studies.<sup>64</sup>

As with TBTAP synthesis the aminoindoline used controls the substitution at the *meso* position, and the straight forward preparation of aminoindoline derivatives allows a wide range of functionalities to be included at the *meso* position. During development of the synthesis, the versatility of axial and *meso* functionalisation was explored, along with a procedure for direct axial substitution utilizing different borates in the reaction (scheme 2.11). A wide range of SubTBDAPs were produced, bearing substituted aryl and heterocyclic functionalities at the *meso* position, and a variety of alkoxy and phenoxy functionalities at the axial position (figure 2.4).

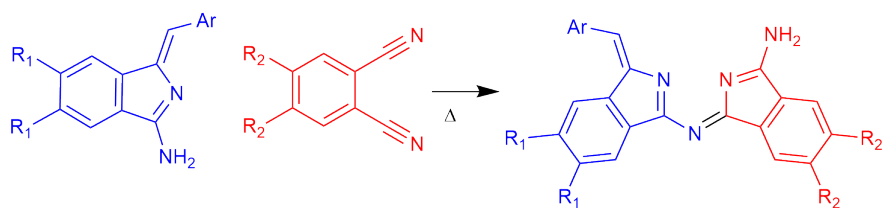
### Mixed TBTAP products utilizing substituted phthalonitriles or aminoisoindolines

With the assumption that the proposed mechanism of aminoisoindoline initiating TBTAP macrocyclization with phthalonitrile was correct, the group progressed with exploring TBTAPs functionalised at the peripheral positions. This previous work not only served to produce new TBTAP derivatives, but also to essentially ‘tag’ each ring of the macrocycle to determine which starting material it had originated from. Based on the previously assumed mechanism 3:1 TBTAPs were expected to be produced, with 3 isoindoline units originating from phthalonitrile, and one from aminoisoindoline as shown in scheme 2.12.

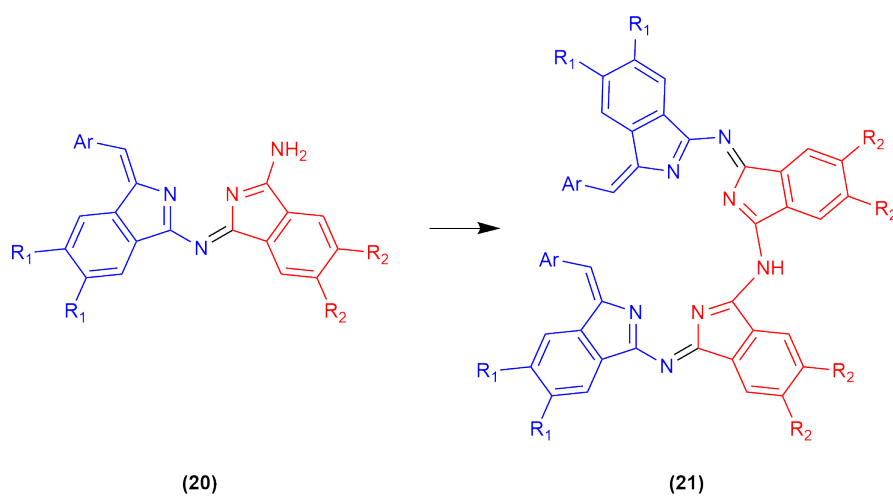


Scheme 2.12: The previously hypothesised TBTAP macrocyclization pathway. New derivatives explored: R = H, OMe, OHx, ODc, 1,1,4,4-tetramethylcyclohexane and OPh.

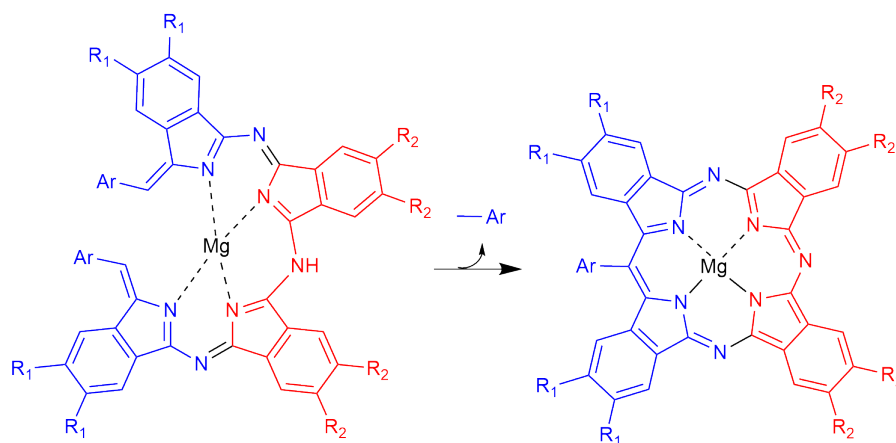
Unexpectedly, most experiments produced 2:2 TBTAPs as the major product, both from substituted phthalonitriles and aminoisoindolines. This suggests an entirely different reaction pathway to the previous hypothesis, not previously observed due to both the aminoisoindolines and phthalonitriles used being unsubstituted, and therefore producing unsubstituted MgTBTAP regardless. These results suggest the formation of a dimeric species, followed by homocondensation, and finally elimination of an aromatic fragment from the aminoisoindoline followed by aromatization. A hypothesised pathway is shown in schemes 2.13 - 2.15.



Scheme 2.13: Initial condensation of phthalonitrile with aminoisindoline.



Scheme 2.14: Homocondensation of two units of the dimer species, forming the 2+2 open chain species, with elimination of ammonia, that macrocyclizes to form 2:2 TBTAPs.



Scheme 2.15: Macrocyclization of the open chain oligomer presented in the previous figure.

This discovery has significant implications for the development of TBTAP synthesis, and is the first evidence of the possibility of multiple reaction pathways in TBTAP synthesis utilising aminoisoindolines. Gaining an understanding of this pathway could allow for better control over reactions, higher yields, easier access to asymmetric derivatives and the development of new precursors or controlled synthesis of reaction intermediates.

## 2.2 Aims of this work

This work aims to explore these apparent multiple reaction pathways in TBTAP formation. By altering reaction conditions and parameters it is anticipated more selective and higher yielding syntheses that favour a single pathway may be developed. If reaction intermediates can be identified this may allow controlled synthesis of pre assembled porphyrinoids, stepping away from traditional macrocyclization pathways and the reliance on low yielding statistical condensation of asymmetric derivatives. By gaining understanding of the TBTAP macrocyclization mechanisms and the role of aminoisoindoline, these unique macrocycles will see more widespread research and application as enjoyed by the parent porphyrinoids.

### 2.2.1 Conditions screen

The most recent iteration of the Cammidge *et al.* TBTAP synthesis utilizing aminoisoindoline is a fairly sophisticated procedure. To a preheated solution (220°C) of phthalonitrile (3 eq) and MgBr<sub>2</sub> in diglyme, a solution of phthalonitrile (1 eq) and aminoisoindoline (1 eq) was added dropwise with a syringe pump over 1 hr. The mixture was refluxed for 30 min before a final solution of phthalonitrile (1 eq) and DABCO (1.5 eq) was added over 1 hr. The reaction was then finally refluxed for a further 30 mins before workup and isolation of TBTAP.

It was found that by adding the aminoisoindoline slowly, and thus minimising the concentration and therefore homocondensation of this precursor, the yield of TBTAP was improved. However addition rate could alter the ratios of intermediates initially present in the reaction, and therefore the dominant pathway and products. Thus this is a key parameter for further exploration. As well as addition speeds, the ratios of reagents used are also to be investigated for the same reasons.

The hypothesis moving into this work was that using a 1:1 ratio of phthalonitrile:aminoisoindoline, faster addition rates, or a combination of both strategies would initially promote the formation of the previously hypothesised ‘dimer’ (**20**) (scheme 2.13). The large concentration of this intermediate would then promote 2:2 formation as shown in schemes 2.14 and 2.15. The inverse was also hypothesised, with slower addition and large excesses of phthalonitrile expected to favour the stepwise condensation and macrocyclization of 3:1 TBTAPs as shown in scheme 2.12.

### 2.2.2 Metal screen

Currently explorations of aminoisoindoline mediated TBTAP macrocyclization have only been undertaken with  $\text{MgBr}_2$ . Given the likelihood of multiple possible reaction pathways leading to TBTAPs, and potentially other hybrid macrocyclic products, the metal used is a key parameter to explore. The role of metals in these reactions is as a template ion, with the macrocycle being built around it and the coordination effects reducing the entropic demands of cyclizing a large macrocycle. The size of the metal ion used and the relative energies of various coordination geometries is likely to have a significant effect on the reaction outcome.

### 2.2.3 Intermediate targets

Identification of intermediate targets is essential to the development of more controlled TBTAP synthesis; a probable useful material is the condensation product of aminoisoindoline and phthalonitrile described above that likely leads to the formation of 2:2 TBTAPs. The aim is that by developing and expanding the suite of precursors and synthetic strategies, a wide range of complex derivatives will become more accessible via new synthetic methodologies and species.

## 2.3 Results and Discussion

### 2.3.1 Aminoisoindoline synthesis

The first step in these investigations began with synthesising the required aminoisoindoline reagents, and repeating previously optimised reactions for TBTAP formation as control experiments. Aminoisoindolines are readily synthesised from amidines via a Sonogashira coupling followed by a 5-*exo-dig* cycloisomerization domino reaction; and amidines are easily synthesised from 2-bromobenzonitriles via treatment with  $\text{LiN}(\text{SiMe}_3)_2$  to form the corresponding 2-bromobenzamidine.

#### Amidine synthesis

A procedure for the synthesis of amidines was described by Boéré and colleagues in 1987 (scheme 2.16), and is a high yielding, straight forward synthesis from easily accessible 2-bromobenzonitriles and commercially available materials (1M anhydrous solutions of  $\text{LiN}(\text{SiMe}_3)_2$  in THF may be purchased readily).<sup>114</sup> This procedure has been employed by the Cammidge group for the synthesis of a range of structurally and electronically diverse amidines with excellent success.

The reaction proceeds in  $\text{Et}_2\text{O}$  or THF readily at room temperature to form the lithium bis(trimethylsilyl)benzamidine intermediate, this intermediate may be reacted to form tris(trimethylsilyl)benzamidine derivatives, or hydrolysed with  $\text{HCl}/i\text{-PrOH}$  to produce the desired amidine hydrochloride salt. The free-base amidines tend to form oils and waxes, meaning purification must be performed via distillation or column chromatography. The hydrochloride salts are

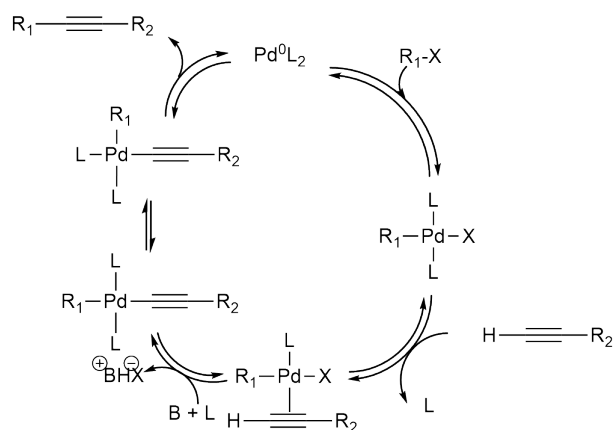


Scheme 2.16: Synthesis of amidine hydrochloride from 2-bromobenzonitrile.

advantageous as they readily precipitate from the reaction in high purity and yield, allowing quick and easy isolation.

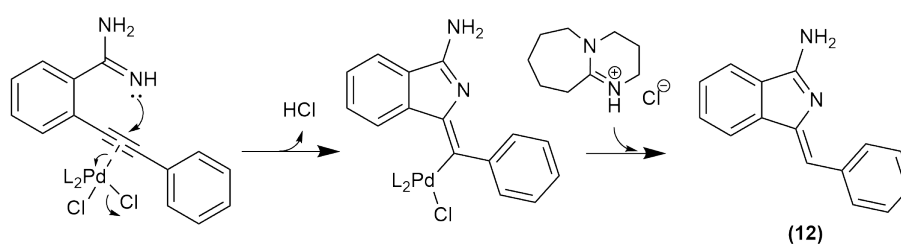
### Cross coupling mechanism

The next step in the synthesis of these aminoisindolines is a one-pot palladium mediated, copper free Sonogashira cross-coupling, followed by a cycloisomerization, developed by Cuny *et al.*<sup>115</sup> This one-pot synthesis was carried out in a microwave reactor vial under microwave irradiation. Amidine hydrochloride and aryl acetylene are coupled via catalytic palladium utilising BINAP as the ligand, DBU as base, and DMF as solvent.



Scheme 2.17: Sonogashira cross coupling cycle adapted from a recent review.<sup>116</sup> L = BINAP, B = DBU, R<sub>1</sub> = benzonitrile, X = Br.

Microwave irradiation at 120°C facilitates the initial Sonogashira cross coupling described above (scheme 2.17), the intermediate undergoes a 5-exo-*dig* cycloisomerization in situ to produce the target aminoisindoline (scheme 2.18). The reaction selectively produces the Z-alkene geometry, as determined by NOSEY NMR during the original studies.<sup>115</sup> Aqueous work up and purification by column chromatography using silica gel yielded the desired aminoisindolines in 60-90% yield.



Scheme 2.18: Domino 5-*exo-dig* cyclization facilitated under the same reaction conditions to yield aminoindoline and regenerate  $L_2PdCl_2$ .

### NMR and characterisation

While a range of aminoindoline derivatives incorporating various aryl functionalities have been previously synthesised by the Cammidge group, for this work simple phenyl and *p*-methoxyphenyl derivatives shall be employed. Utilizing 2-bromobenzonitrile as the amidine precursor, with phenylacetylene and 4-methoxyphenylacetylene respectively as alkynes. The *p*-methoxyphenyl aminoindoline is advantageous in that there is a strong and clear methoxy NMR peak (figure 2.5). When investigating intermediate compounds this will allow easy determination of the presence of aminoindoline fragments. The identity of the aminoindoline was also confirmed by  $^{13}C$  NMR and MALDI-TOF.

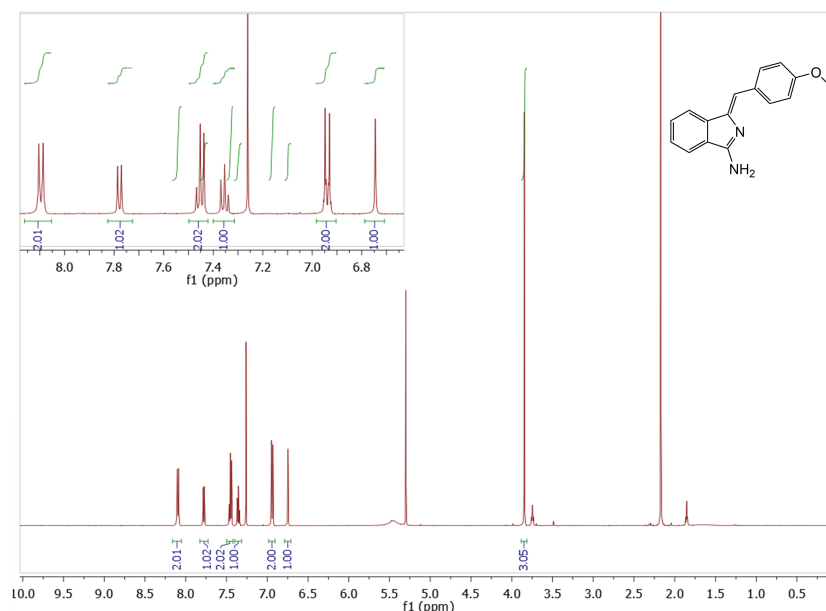
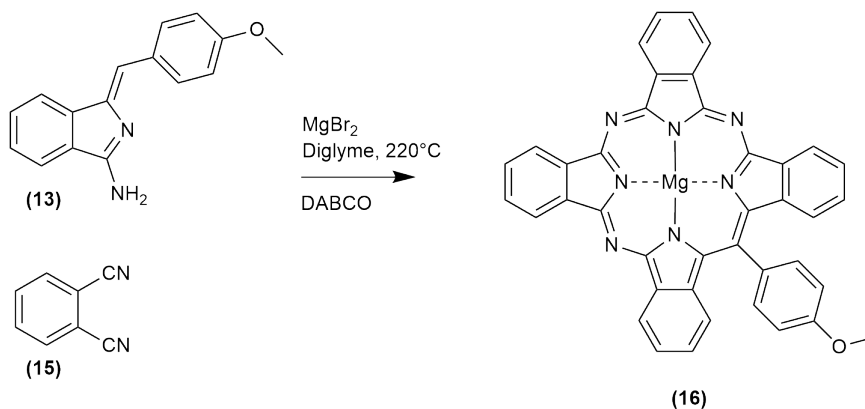


Figure 2.5:  $^1H$  NMR spectrum of *p*-methoxyphenylaminoindoline (**13**), with the characteristic *Z* alkene proton at 6.7 ppm, and strong methoxy signal at 3.84 ppm.

### 2.3.2 Repeat of TBTAP procedure

With the required aminoisoindolines synthesised easily and in good yields, and the identity confirmed by  $^1\text{H}$  NMR,  $^{13}\text{C}$  NMR and MALDI-TOF MS, the next step in investigations was to repeat the previously published TBTAP synthesis (scheme 2.19).<sup>29</sup>



Scheme 2.19: Scheme for the repeat of the previously optimised TBTAP synthesis.

#### Result and yield

The desired TBTAP was successfully synthesised utilising the controlled addition methodology previously described. After the reaction conditions and workup the crude product was subjected to silica gel chromatography, which after recrystallisation of the main green fraction yielded the pure MgTBTAP (16) product expected.

As well as the expected TBTAP trace quantities of MgPc were produced, as well as a quantity of the azadipyrromethene homocondensation product of aminoisoindoline. The yield of TBTAP was somewhat lower than previously reported, around 20%. The reaction was repeated but no significant improvements to yield were obtained.

#### Characterisation

The NMR (figure 2.6), UV-Vis (figure 2.7) and MALDI-TOF data is concordant with previously reported data, confirming the successful synthesis of MgTBTAP (16). The NMR data shows the characteristic de-shielded protons, a shift caused by ring current phenomena in aromatic macrocycles.<sup>117</sup> The UV-Vis spectra clearly shows the characteristic Soret and Q bands associated with 18- $\pi$  electron macrocycles,  $\lambda_{\text{max}}$  values also agree with the literature values for MgTBTAP (16).<sup>12</sup>

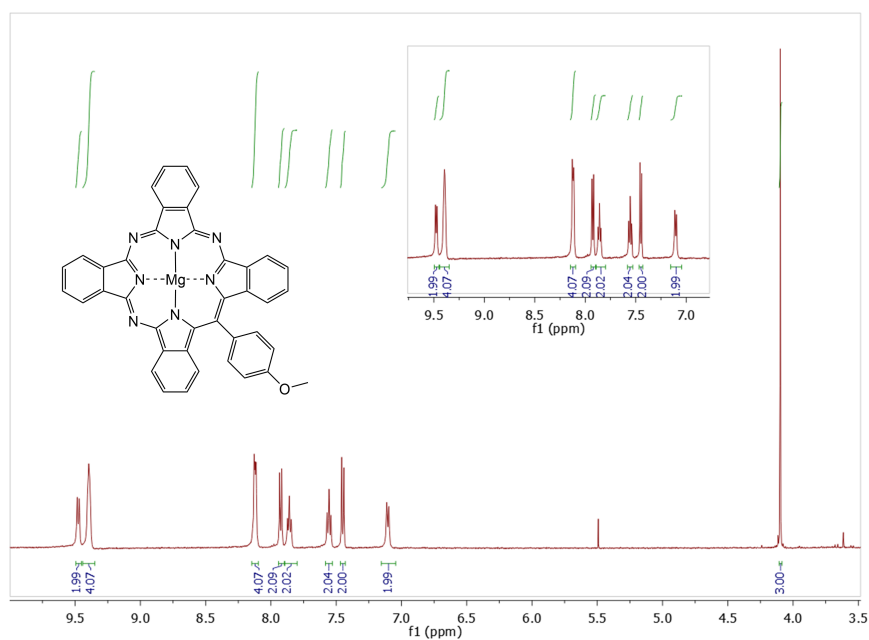


Figure 2.6: <sup>1</sup>H NMR spectrum of TBTPAP (**16**). Note the characteristic deshielding of some macrocyclic protons caused by ring current phenomena of porphyrinoids.

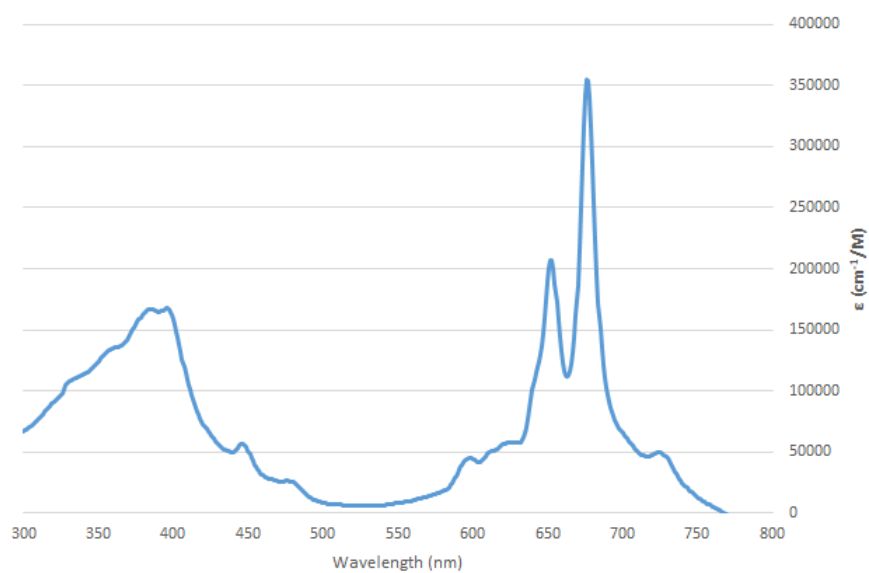
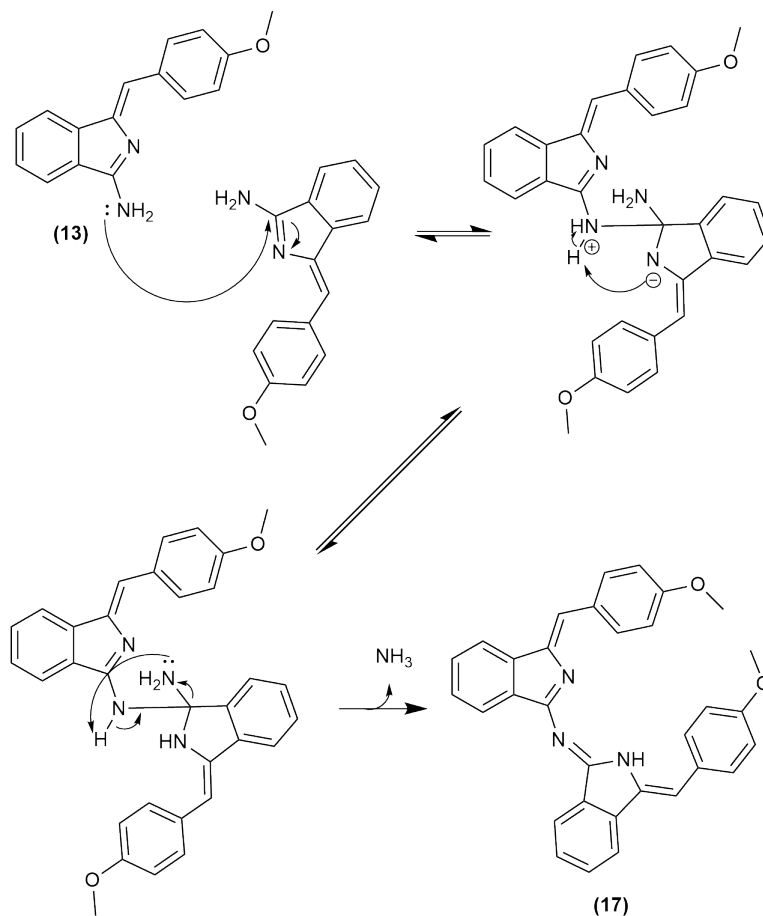


Figure 2.7: UV-Vis spectra of TBTPAP (**16**).

### Aminoisoindoline homocondensation mechanism

The mechanism for the homocondensation of aminoisoindoline is shown below (scheme 2.20). As well as having a nucleophilic amine, the  $\alpha$  carbon is also an electrophilic center. This facilitates the nucleophilic attack of one molecule by another, eliminating ammonia to yield the homocondensation product. While this can be mitigated by slow addition of aminoisoindoline some homocondensation still occurs, reducing yield. This reaction likely proceeds with coordination of  $Mg^{2+}$  under TBTAP reaction conditions, however may also be synthesised by reflux in toluene without  $Mg^{2+}$ .

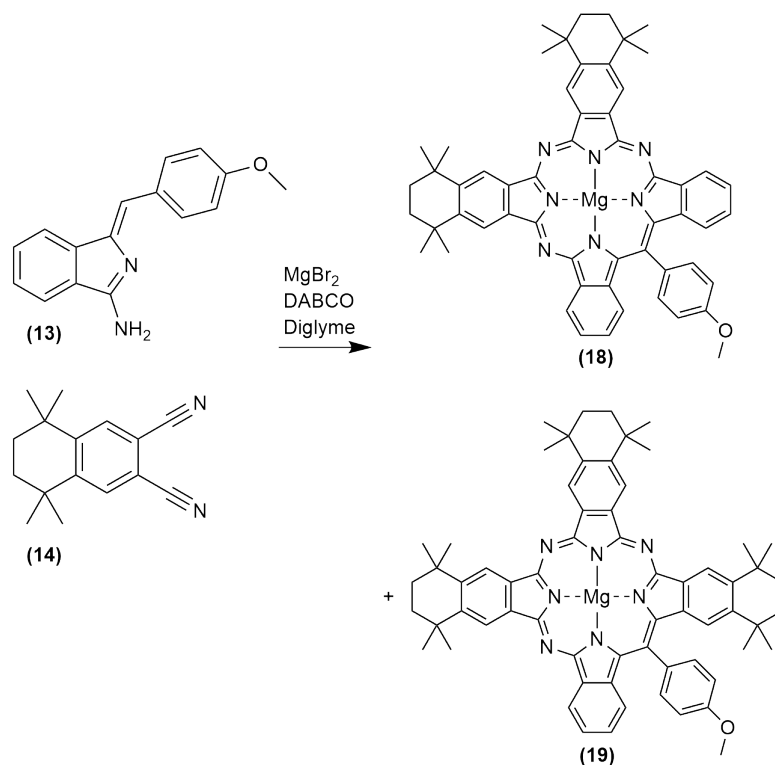


Scheme 2.20: Hypothesised mechanism for the homocondensation of aminoisoindoline to form azadipyrromethene (17).

### 2.3.3 Repeat of TBTAP synthesis producing both 2:2 and 3:1 TBTAPs

As previously described recent work within the Cammidge group revealed unexpected peculiarities during explorations of peripherally substituted TBTAP

derivatives. Most derivatives synthesised produced exclusively 2:2 TBTAPs, with the exception of 1,2,3,4-tetrahydro-1,1,4,4-tetramethylnaphthyl derivatives, which produced a mixture of 2:2 and 3:1 TBTAP (scheme 2.21). This derivative was chosen for this study in an attempt to gain control over the competing pathways.



Scheme 2.21: Scheme for the previous TBTAP investigations revealing the formation of two different TBTAP derivatives. The original study obtained 2:2 TBTAP (18) in 14 % yield, and 3:1 TBTAP (19) in 1 % yield.

The previously optimised slow addition procedure was repeated utilising 6,7-dicyano-1,2,3,4-tetrahydro-1,1,4,4-tetramethylnaphthalene (14) as the phthalonitrile. After the final reflux period the crude was worked up as previously described. A second column chromatography utilising PE:THF:MeOH (10:3:1) yielded two green fractions that were isolated and recrystallised from DCM/MeOH. The first of the two green fractions yielded 7.7 mg of the 3:1 TBTAP (19) (2.0 % yield), and the second fraction 10.3 mg of the 2:2 TBTAP (18) (3.0 % yield). The products identities were confirmed by <sup>1</sup>H NMR, MALDI-TOF and UV-vis spectroscopy.

It is notable that the yields obtained vary significantly from the previous studies results, however the reaction was repeated and the same yields of 3.0 % and 2.0 % for TBTAP (18) and TBTAP (19) respectively were obtained.

With the harsh conditions required to achieve macrocyclization of TBTAPs it is possible minor variations in experimental parameters, such as variance in different temperature probes, could contribute to a drastically reduced rate of product formation.

## Results and yields

As previously described, a mixture of 3:1 and 2:2 TBTAPs were produced by the reaction in a roughly 2:3 ratio. This procedure and result is therefore a good place to begin procedural modifications. The yields of both products are however very low, this may be due to steric or electronic effects. This is a well known trend in phthalocyanine chemistry, with sterically demanding or electronically deactivated phthalonitriles requiring higher temperatures or longer reaction times to achieve good yields of macrocyclization.

## NMR

The identities of the 3:1 and 2:2 products were confirmed by NMR and MALDI-TOF and agreed with previous experimental data. Evidence of the reduction of symmetry in the 3:1 TBTAP (**19**) (figure 2.9) is clear in the NMR spectrum compared to the 2:2 TBTAP (**18**) (figure 2.8). The aliphatic region is also complicated in the 3:1 spectrum due to the reduction in symmetry.

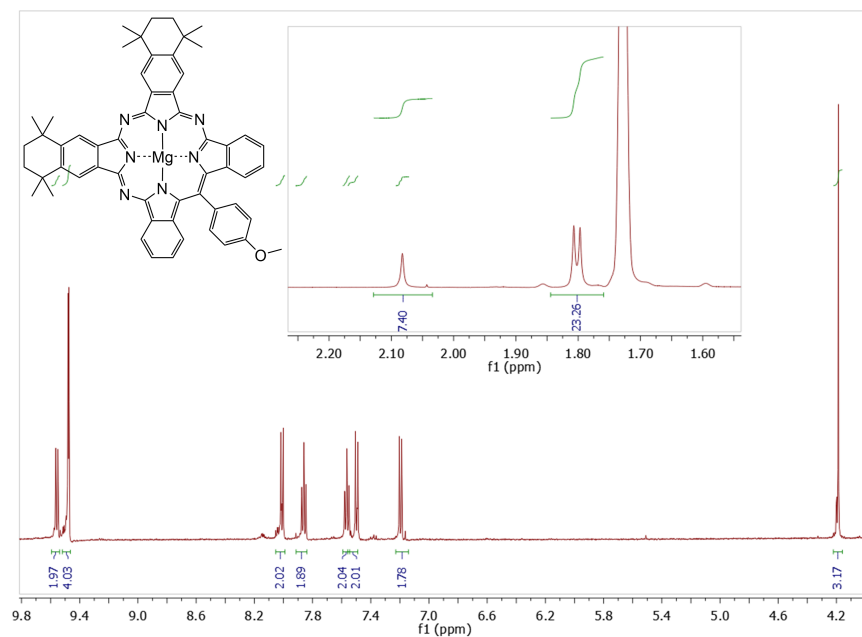


Figure 2.8:  $^1\text{H}$  NMR spectrum of TBTAP (**18**), with an expansion of the aliphatic region.  $\text{THF-}d_8$  was used as the NMR solvent, with a residual solvent peak visible at 1.72 ppm.

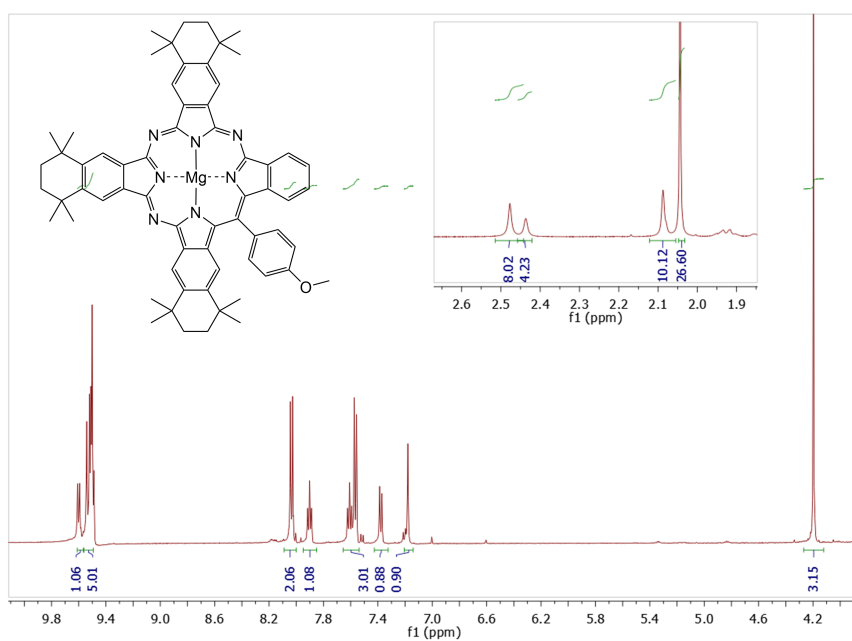


Figure 2.9: <sup>1</sup>H NMR spectrum of TBTAP (**19**), with an expansion of the aliphatic region. The reduction in symmetry is clearly seen in both the aromatic and alkyl regions of the spectrum.

The UV-Vis spectra (figure 2.10) represent a typical MgTBTAP spectra, a slight red shift is present due to the tetrahydrotetramethylnaphthyl substituents, increasing between the 2:2 substituted MgTBTAP (**18**) and 3:1 substituted MgTBTAP (**19**).

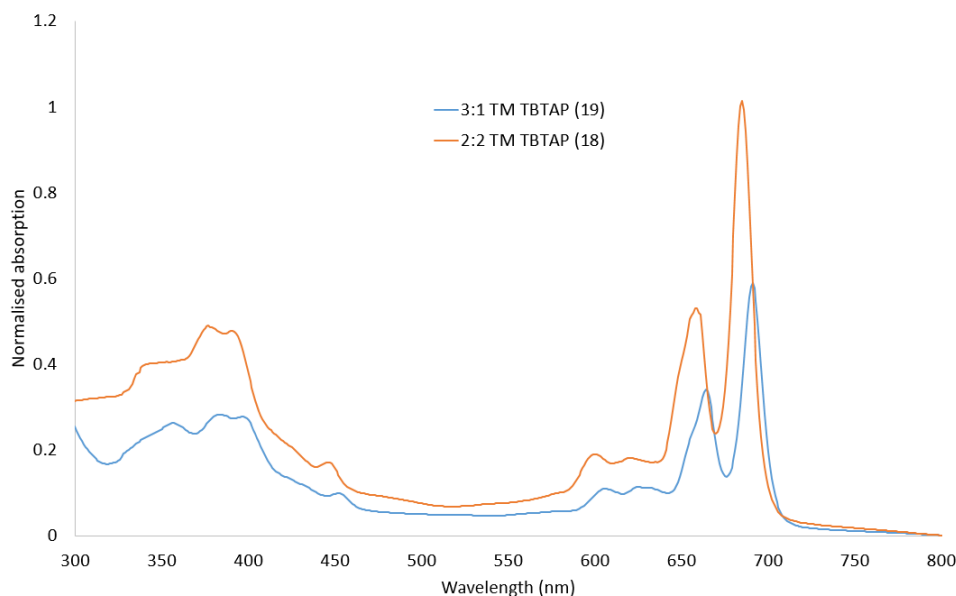
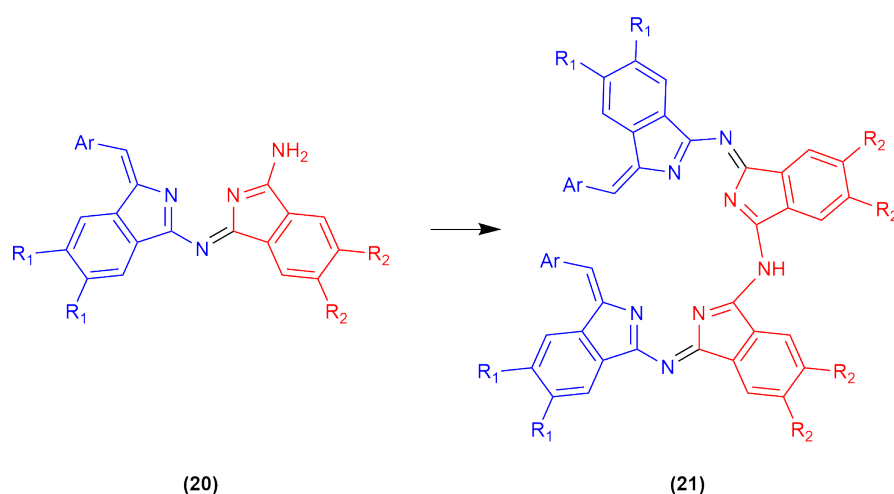


Figure 2.10: UV-Vis spectra of MgTBTAPs (**18**) and (**19**).

### 2.3.4 All in addition with varying reagent ratios

From the initial procedure, and with clear evidence of two competing reaction pathways, the first modifications were attempted to promote 2:2 TBTAP formation. It was reasoned that by not using a syringe pump for controlled addition of aminoisoindoline, and instead adding all reagents at the start of the reaction, the higher concentration of aminoisoindoline present would react with the phthalonitrile in a 1:1 ratio. This would produce a large concentration of the hypothesised condensation product (**20**) shown in scheme 2.22, and therefore promote the theoretical 2+2 addition to form tetramer (**21**), resulting in 2:2 TBTAPs.

Reagent ratios were also an important factor to consider. Large excesses of phthalonitrile and a relatively low concentration of aminoisoindoline may be considered analogous to the syringe pump addition method described previously. To promote the 2+2 condensation the theoretically optimum reagent ratios are 1:1, so this was first to be investigated. 1:2 and 2:1 ratios of aminoisoindoline:phthalonitrile were also investigated.



Scheme 2.22: Hypothesised homocondensation of the condensation product (20) to yield tetramer (21).

Ratio of aminoisindoline:phthalonitrile	Products produced & yield
2:1	2:2 TBTAP (5.5 %), azadipyrromethene (85 %)
1:1	2:2 TBTAP (8.1 %), 3:1 TBTAP (trace), azadipyrromethene (24 %)
1:2	2:2 TBTAP (6.8 %), 3:1 TBTAP (trace), azadipyrromethene (13 %)

Figure 2.11: Table of results for all in addition of reagents with varying ratios.

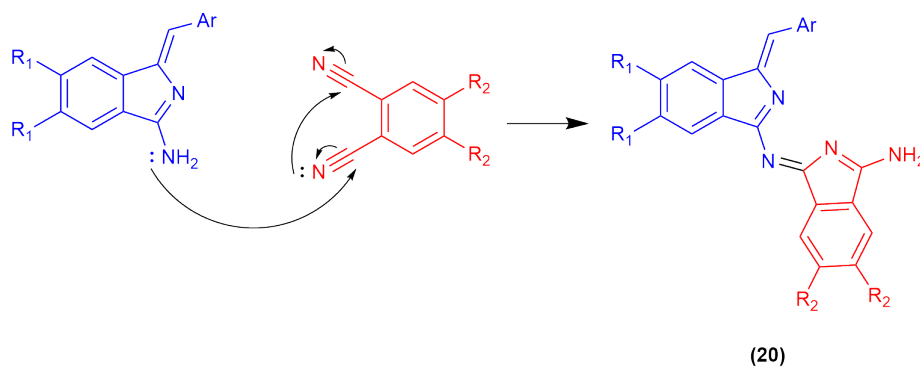
## Results

6,7-Dicyano-1,2,3,4-tetrahydro-1,1,4,4-tetramethylnaphthalene (14), aminoisindoline (13), DABCO and MgBr<sub>2</sub> were suspended in 3 mL of diglyme and the mixture heated for 3 hours at 220°C in an oil bath, resulting in a very intensely green material being formed. Purification was performed as described by the standard procedures. The reactions utilise 1.6 mmol total of phthalonitrile + aminoisindoline in varying ratios.

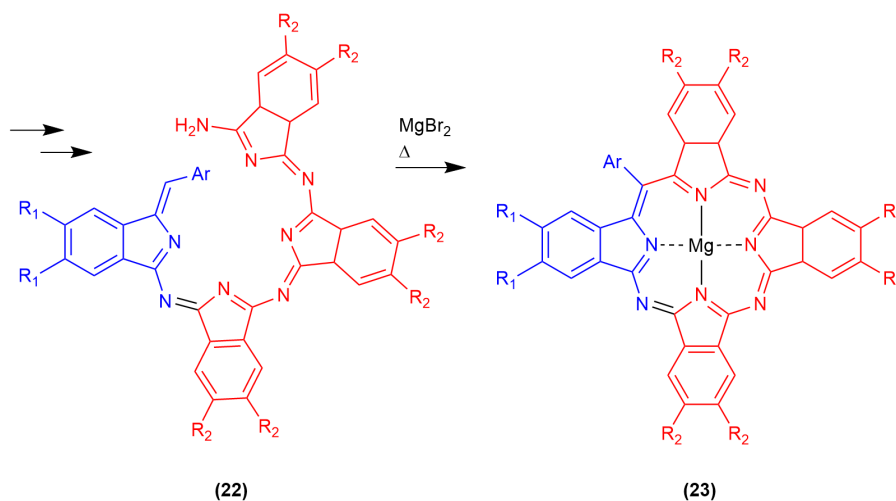
The results presented in figure 2.11 appear to support the hypothesis presented, with all in reactions all producing exclusively 2:2 TBTAP products. Exclusive access to 2:2 TBTAPs is very useful as it simplifies purification; in some cases 2:2 and 3:1 TBTAPs have very similar retention factors on TLC or silica gel chromatography. Yield for this reaction is also significantly improved for this product at 8% compared to 3% from the initial mixed reaction.

### 2.3.5 Addition rates

With the previous procedural modifications producing exclusively the 2:2 TB-TAP (**18**), the next logical step in our investigations was to increase the addition time to determine if the 3:1 TBTAP (**19**) could be selectively synthesised by the same hypothesis. It was postulated that slower addition of aminoisindoline and the resulting low concentrations of this initiating precursor would encourage the sequential condensation of 3 units of phthalonitrile (scheme 2.23 and 2.24). This would form the open chain 3:1 TBTAP (**22**), which after macrocyclization would produce the desired 3:1 TBTAP (**23**).



Scheme 2.23: Nucleophilic attack of phthalonitrile by aminoisindoline to produce the condensation product (**20**).



Scheme 2.24: Hypothesised consecutive addition of phthalonitrile to form the 4 membered open chain oligomer and macrocyclization to form the 3:1 TBTAP.

The investigations began with repeating the previous procedure as described in section 2.3.3 to ensure reliability and repeatability of the result. The procedure produced both TBTAP (**18**) and TBTAP (**19**) as expected utilising the standard 1 hr addition time for the first aminoisoindoline solution and the same initial 1:3 ratio of aminoisoindoline:phthalonitrile, with 2 additional equivalents of phthalonitrile added with the solutions of aminoisoindoline and DABCO. The ratio of products was 2:3 of TBTAP (**19**) and TBTAP (**18**) respectively.

With a total of 5 equivalents of phthalonitrile added through syringe pump additions it was deemed not necessary to increase the amount of phthalonitrile used to encourage 3:1 formation, but rather investigate slower addition times. A 3 hour addition time was chosen.

To a solution of phthalonitrile and  $\text{MgBr}_2$  suspended in 0.5 mL diglyme and heated to  $220^\circ\text{C}$  in an oil bath was added a solution of aminoisoindoline and phthalonitrile in diglyme (1 mL). The solution was added over 3 hours using a syringe pump. Followed by a further solution of DABCO and phthalonitrile, added over 3 hours. The dark green residue was purified by the standard procedure.

## Results

With slow addition and hence a longer reaction time, 15.3 mg (3.9 %) of 3:1 TBTAP (**19**) and 20.7 mg (6.0 %) of 2:2 TBTAP (**18**) was isolated. This again gives a product ratio of 2:3, the same as the standard procedure. It is therefore clear that addition times longer than 1 hr have no effect on the pathways that form the two products. The yield of both products was doubled however.

The identical ratio of products suggests a macrocyclization pathway different to those initially hypothesised. Rather than a stepwise formation of a linear open chain species that undergoes macrocyclization, it appears likely that an initial condensation product is formed that then undergoes a complex set of equilibrium pathways with a delicate thermodynamic balance (explored throughout later experiments in chapter 2). This could explain why previous studies of peripherally substituted TBTAPs produced 2:2 TBTAPs for most derivatives, and only the synthesis of tetrahydro-tetramethylnaphthalene TBTAPs result in 3:1 formation; however at this stage the factors that drive 3:1 TBTAP formation remain unknown.

### 2.3.6 Metals

Synthesis of TBTAPs have previously been reported utilizing either magnesium or zinc as template ions. The latest advances utilising aminoisoindolines by the Cammidge group have thus far only explored the use of  $\text{MgBr}_2$  as a template ion. Given the crucial role of template ions in reducing entropic barriers and templating components in macrocyclizations it seems logical to explore the effects different ions may have of the competing pathways.

With the hypothesised pathways previously presented, it appears logical that 3:1 TBTAP formation via an open chain oligomer consisting of 1 aminoisoindoline and 3 phthalonitrile fragments would favour a square planar geometry around the metal center. The previously presented hypothesised pathway for 2:2 formation (scheme 2.22) shows a homocondensation of an initially produced species (**20**), followed by macrocyclization. It was also hypothesised that this may occur as a pericyclic process between two units coordinated to a metal in a tetrahedral arrangement as shown below (figure 2.12). Both possibilities must be considered, and therefore different template ions that favour different geometries must be explored.

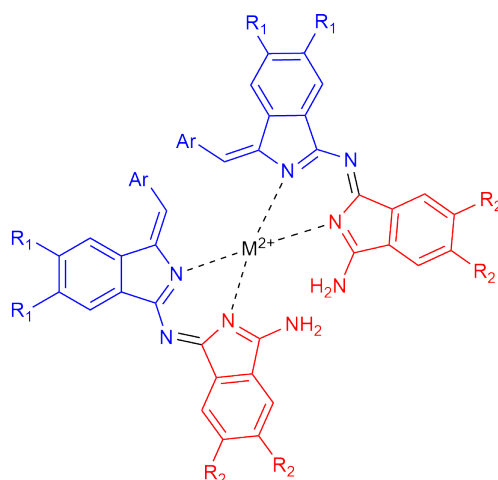
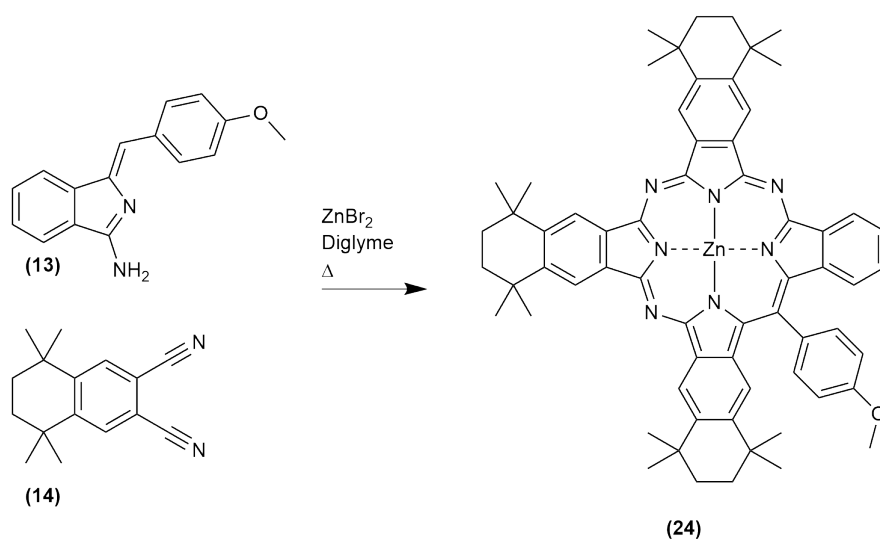


Figure 2.12: Two equivalents of condensation product (**20**) coordinated to metal.

With magnesium's use as a template ion in TBTAP synthesis well researched and documented, other ions were chosen with either square planar geometry with larger or smaller ionic radii, or tetrahedral geometry with similar ionic radii. Zinc was chosen as the  $Zn^{2+}$  ion favours a tetrahedral geometry and has a similar ionic radii to  $Mg^{2+}$  (74 and 72 pm respectively). Nickel and palladium were selected as both 2+ ions favour square planar configurations, and have ionic radii smaller and larger than  $Mg^{2+}$  (70 and 86 pm respectively). The sources of these ions were  $MgBr_2$ ,  $ZnBr_2$ ,  $NiBr_2$  and  $PdCl_2$ .

Zinc was the first ion to be tested, the standard TBTAP addition procedure was utilised. To a solution of 6,7-dicyanotetrahydrotetramethylnaphthalene (**14**) and  $ZnBr_2$  in diglyme was added a solution of aminoisoindoline (**13**) and 6,7-dicyanotetrahydrotetramethylnaphthalene (**14**) in diglyme over a period of 1 hour. A further solution of DABCO and 6,7-dicyanotetrahydrotetramethylnaphthalene (**14**) was added over 30 minutes. TLC revealed a large amount of aminoisoindoline homocondensation initially, followed by the appearance of a green spot. The crude material was worked up as normal to yield exclusively the 3:1 TBTAP (**24**) in 12 mg yield (3.0 %) (scheme 2.25).



Scheme 2.25: Selective 3:1 ZnBr<sub>2</sub> mediated TBTAP synthesis utilizing aminoisoindoline (**13**) and 6,7-dicyano-1,2,3,4-tetrahydro-1,1,4,4-tetramethylnaphthalene (**14**) to form TBTAP (**24**).

Zinc was chosen for its tetrahedral geometry, the expected result was that the tetrahedral geometry would favourably facilitate 2:2 TBTAP formation via the previously proposed intermediates, however the opposite result was obtained. The first experiment produced exclusively 3:1 TBTAP (**24**), confirmed by NMR, UV-vis and MALDI-TOF (figure 2.13 and 2.14). With previous variation of addition rate with MgBr<sub>2</sub> mediated macrocyclization having a significant effect on product ratios this was the next parameter to investigate with ZnBr<sub>2</sub> mediated macrocyclization.

The next experiment consisted of an all in reaction not utilizing slow addition of reagents, with ZnBr<sub>2</sub> as the metal. As with previous MgBr<sub>2</sub> mediated synthesis all reagents were suspended in diglyme and heated at reflux for approximately 3 hours. The crude product was purified and TBTAPs isolated with the standard work up procedure. This reaction also produced exclusively 3:1 TBTAP (**24**) in 14 mg yield (3.4 %).

A 3 hour syringe pump addition was also tried as with previous experiments. This also gave exclusively 3:1 TBTAP (**24**) in a higher yield (23 mg, 5.7 %). It appears yields may be improved with longer reaction times. Alternatively, the use of a higher boiling point solvent such as 1,2,3-trichlorobenzene, or the use of a sealed glass tube as the reaction vessel to obtain reaction temperatures greater than the boiling point of diglyme under atmospheric conditions may improve yields further.

NiBr<sub>2</sub> and PdCl<sub>2</sub> were tested with various addition procedures. All attempts failed to yield any macrocyclization products.

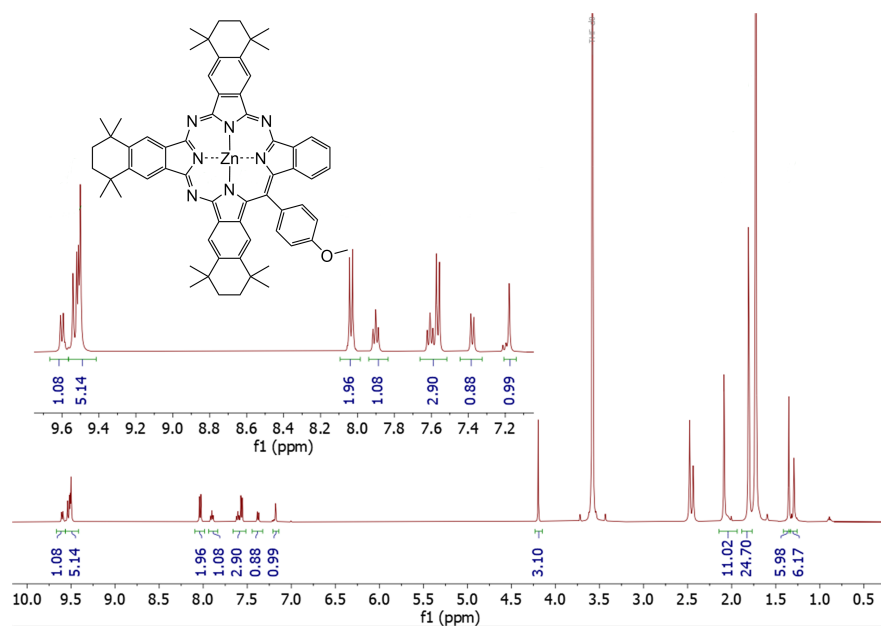


Figure 2.13:  $^1\text{H}$  NMR spectra of novel 3:1 Zn TBATP (**24**).

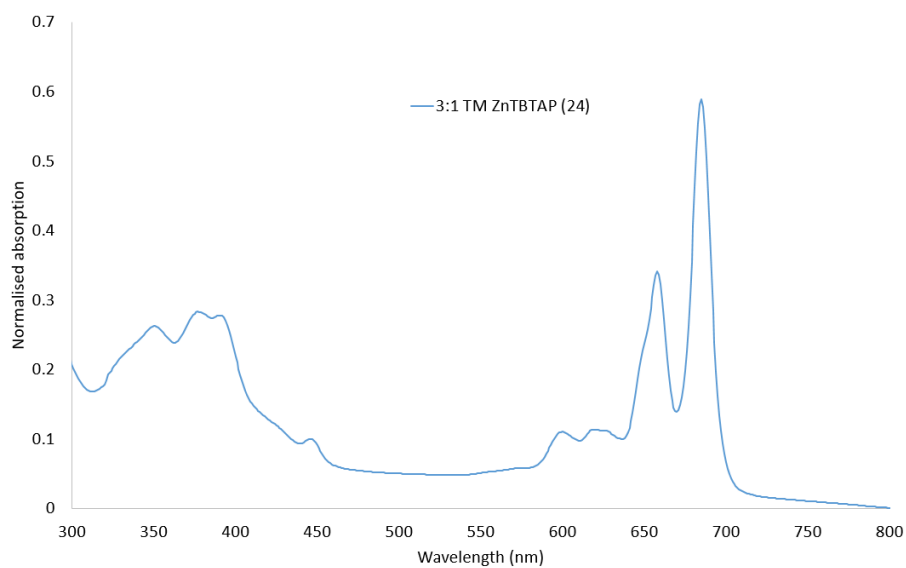
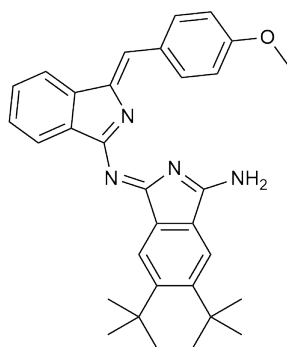


Figure 2.14: UV-Vis spectra of ZnTBATP (**24**), displaying a very similar absorbance profile to the identically substituted 3:1 MgTBATP (**19**).

## 2.4 Intermediate targets

### 2.4.1 Target intermediates and methods

During experiments modifying conditions, reagents and metals, MALDI spectra of crude reaction mixtures regularly revealed unknown possible intermediates. A recurring peak of interest was seen at approx 490 m/z (figure 2.16), present in all reactions, identifying this likely intermediate could reveal mechanistic insight. The peak most likely corresponds to the condensation of aminoisoindoline (**13**) with one equivalent of the phthalonitrile (**14**) used, and a proposed structure shown in figure 2.15.



(25)

Figure 2.15: Condensation product (**25**) of aminoisoindoline (**13**) and the 6,7-dicyanotetrahydro-1H-naphthalene (**14**) identified by MALDI-TOF analysis of crude reaction mixtures.

This structure was proposed earlier in the discussion as the likely first step in the macrocyclization process.<sup>28</sup> With clear evidence of this species the next logical step was to target its synthesis selectively. Reactions could then be performed utilizing this pre-assembled part of the macrocycle via a number of conceivable routes.

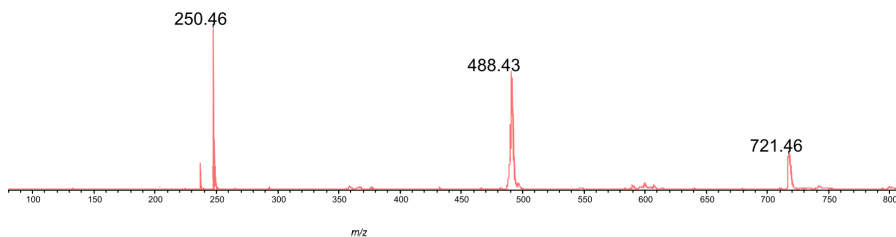
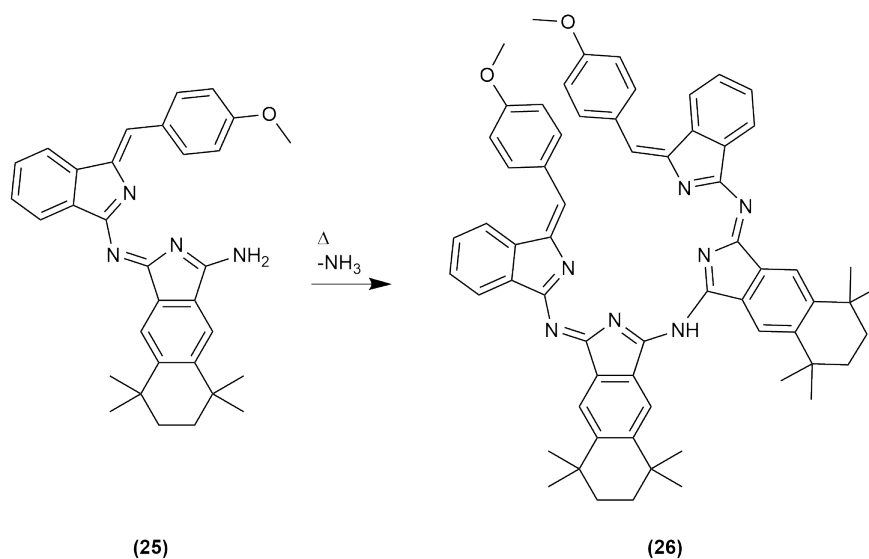


Figure 2.16: Possible intermediate (**25**) identified by MALDI-TOF with a m/z of 488.

It was hypothesised that structure **(25)** could be reacted in a homocondensation analogous to aminoindoline homocondensation to form the 4 membered open chain oligomer **(26)** (scheme 2.26), that may then be macrocyclized with magnesium. Alternatively **(25)** may be reacted with additional phthalonitrile to build TBTAPs in a more stepwise manner. This exciting prospect could allow far more control over complex derivatives, and the potential to construct ABCD systems (controlled substitution at each ring position as shown in figure 2.17) selectively with much higher yields and easier purification than statistical condensation.



Scheme 2.26: Hypothesised homocondensation of the condensation product **(25)**, selectively building the potential 2:2 TBTAP precursor **(26)**.

Shown in scheme 2.26 is the potential controlled synthesis of an open chain ABBA system, templated with magnesium and macrocyclized with the elimination of an aromatic fragment; this route would facilitate controlled synthesis of ABBA 2:2 TBTAP systems in likely far greater yields. Below (schemes 2.27 and 2.28) is shown a scheme for reacting **(20)** with further phthalonitrile, this would facilitate the controlled formation of AABB or ABCC TBTAP systems, depending on the substitution of condensation product **(20)**.

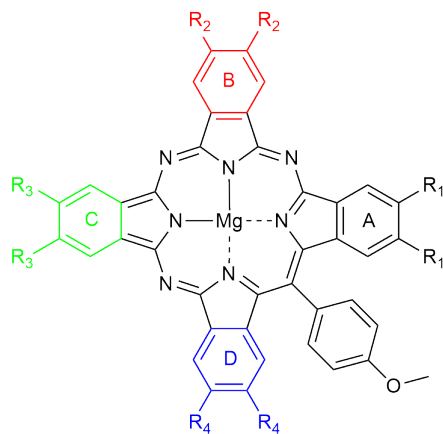
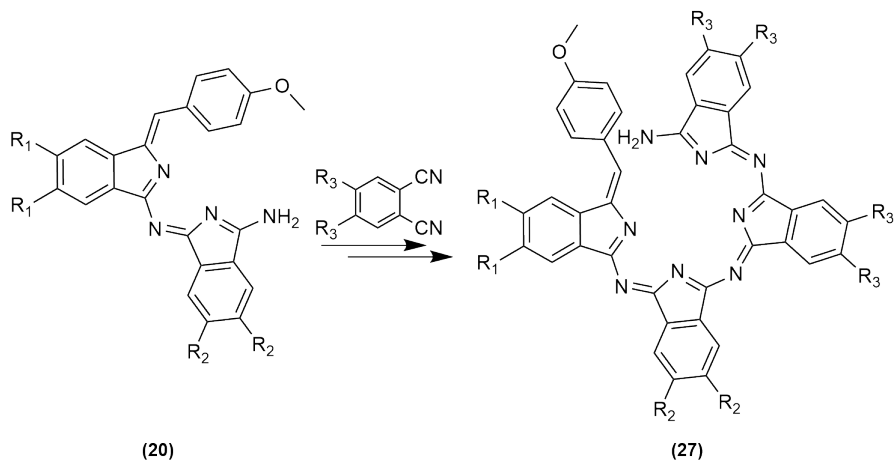
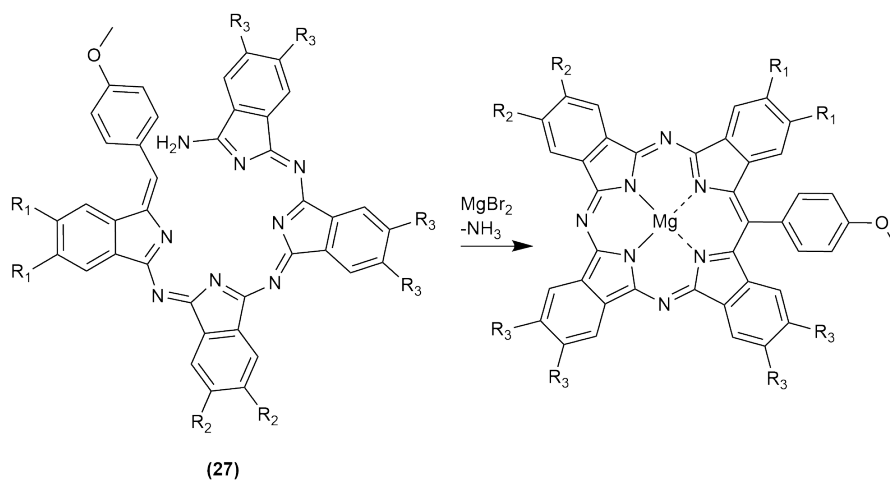


Figure 2.17: An ABCD TBTAP bearing different substituents on each ring, 2:2 TBTAP (**18**) would be considered an ABBA system, and 3:1 TBTAP (**19**) an ABBB system.



Scheme 2.27: Proposed stepwise formation of ABCC system (**27**) from (**20**) and phthalonitrile.

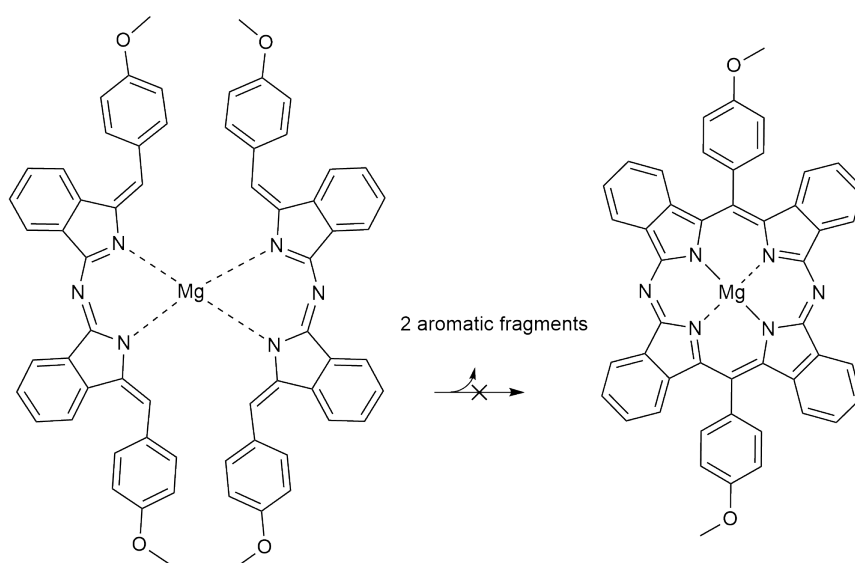


Scheme 2.28: Proposed macrocyclization of pre assembled ABCC system (27) facilitated by an Mg template ion with elimination of ammonia.

#### 2.4.2 Previously examined intermediates

Previous work in the Cambridge group has identified a range of thermodynamic ‘dead ends’ in the macrocyclization of TBTAPs and SubTBDAPs. These are isolable intermediates or side products that have been identified and characterised in previous work. When re-subjected to the reaction conditions none of these structures were successful in producing macrocyclic products. Despite the lack of product formation, these compounds are still essential to understanding macrocyclization mechanisms as they provide valuable insight into pathways that do not result in macrocyclic products.

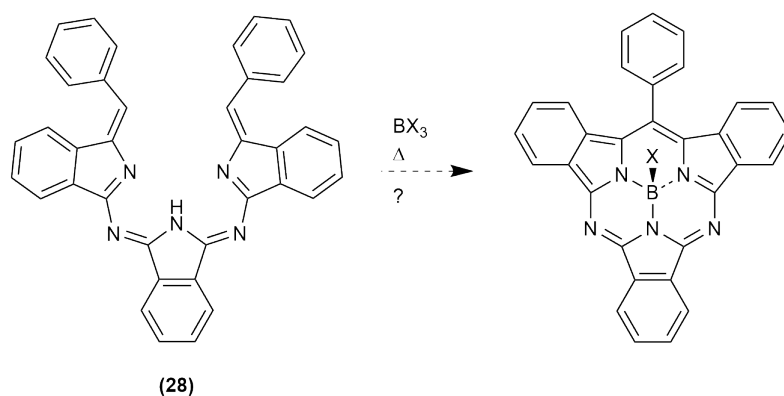
Aminoindoline homocondensation products have been looked at extensively as potential intermediates. Formation of 2:2 TBTAPs as previously described involve the elimination of an aromatic fragment upon macrocyclization, it is therefore possible to conceive a pathway by which two units of this condensation product eliminate two aromatic fragments to yield TBDAPs as shown in scheme 2.29.



Scheme 2.29: Templating and macrocyclization of two units of azadipyrromethene to yield TBDAP.

Various attempts at this reaction have not yielded any hybrid products, TB-DAPs or otherwise, therefore it is logical to conclude that building TBTAPs or other hybrids from higher order intermediates most likely requires the elimination of ammonia for macrocyclization to occur. Azadipyrromethenes have also been re-subjected to the reaction conditions for SubTBDAP formation with no success.

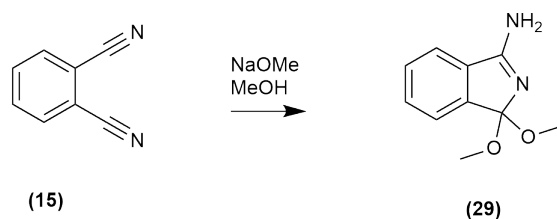
Previous studies on SubTBDAP formation isolated and identified a similar ‘trimeric’ material, the condensation product of one unit of phthalonitrile condensed with two units of aminoisoindoline, shown below. It is once again easy to conceive a pathway by which elimination of an aromatic fragment and complexation with a boron source yields a SubTBDAP. In previous work, it appeared this material reduced in concentration during the reaction, however it is unknown if this is due to macrocyclization, equilibria, or decomposition of the material. Investigations in this work will aim to selectively synthesise these materials and subject them to the SubTBDAP formation conditions previously optimised (scheme 2.30).



Scheme 2.30: Macrocyclization of **(28)** to yield SubTBDAP with elimination of an aromatic fragment.

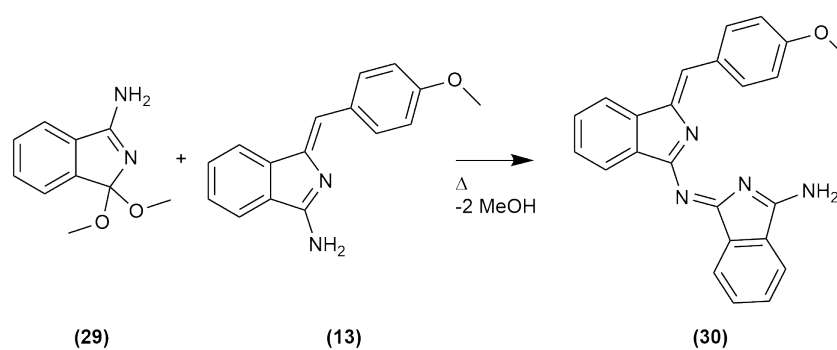
### 2.4.3 Dimethoxyisindolines, reactivity and potential stepwise construction

To synthesise the target condensation products **(25)** & **(30)**, as well as other proposed intermediates/pathways, a phthalonitrile analogue with increased reactivity is required to selectively condense with aminoisindoline while avoiding further polymerisation or macrocyclization. The literature reveals the use of dimethoxyisindolines in various low temperature and selective macrocycle synthesis.<sup>118–120</sup> Dimethoxyisindolines are easily synthesised from phthalonitriles and sodium methoxide as shown in scheme 2.31. The resulting species is highly activated towards nucleophilic attack due to the ability of the methoxy groups to dissociate, forming a highly reactive intermediate.



Scheme 2.31: Scheme for the synthesis of dimethoxyisindoline **(29)**.<sup>121</sup>

It was predicted that dimethoxyisindolines would react readily with aminoisindoline to form the target species **(30)** (scheme 2.32). It is also feasible that from product **(30)**, if controllable, a stepwise ABCC open chain oligomer may be synthesised (scheme 2.27 - 2.28), allowing controlled synthesis of ABCC TBTAP systems.

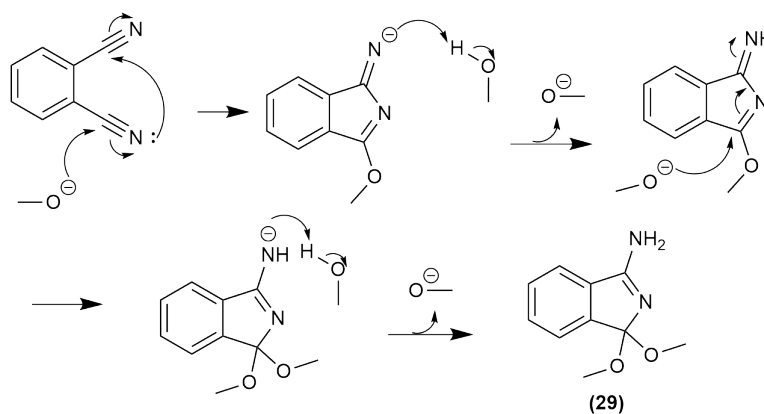


Scheme 2.32: Condensation of dimethoxyisoindoline with aminoisoindoline to yield condensation product (30).

## 2.4.4 Synthesis of target condensation products

### Dimethoxyisoindoline synthesis and derivatives

Synthesis of the target materials began with the formation of the required dimethoxyisoindolines. Following known procedures previously developed at UEA, a solution of sodium methoxide was produced using methanol and sodium metal.<sup>121</sup> Phthalonitrile was added to this solution and stirred at room temperature overnight. The resulting pale green precipitate was filtered and washed with water to yield the required dimethoxyisoindoline via a quick and simple procedure. The formation mechanism is shown below (scheme 2.33), in methanol the methoxide anion is regenerated, therefore sodium methoxide may be used in catalytic, sub-stoichiometric quantities, the precipitation of the product (29) from the reaction solution drives the reaction to completion.



Scheme 2.33: Proposed mechanism for the formation of dimethoxyisoindoline (29).

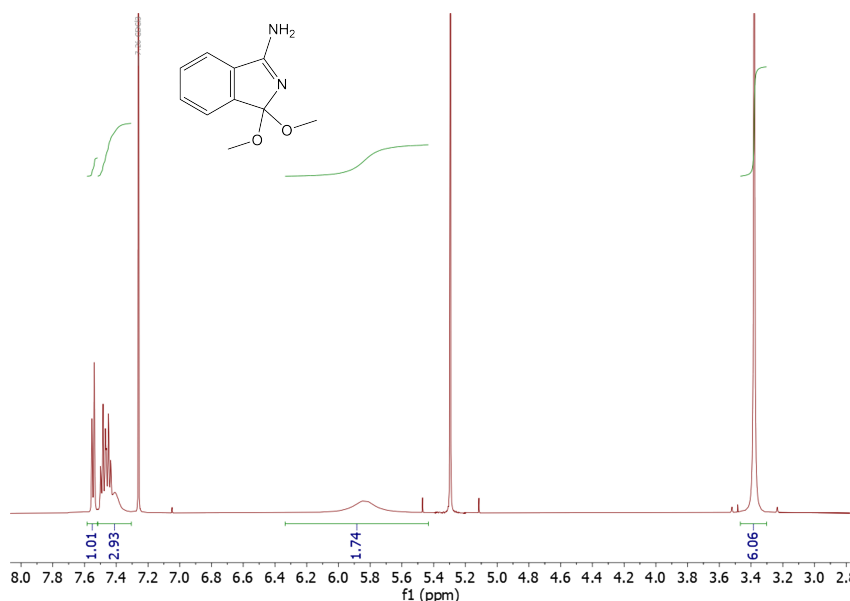
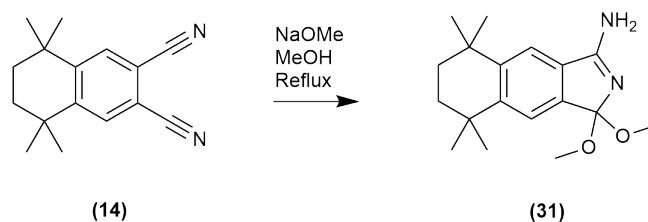


Figure 2.18:  $^1\text{H}$  NMR spectra of dimethoxyisoindoline (**29**).

Following the synthesis of the unsubstituted dimethoxyisoindoline (**29**), 6,7-dicyanotetrahydrotetramethylnaphthalene (**14**) was added to a solution of sodium methoxide in methanol and stirred overnight (scheme 2.34). Upon completion the precipitate was filtered and washed with water to yield the desired dimethoxyisoindoline (**31**). The yield, however, was significantly lower compared to unsubstituted dimethoxyisoindoline (**29**). The reaction is likely to be driven forward by the precipitation of the target dimethoxyisoindoline from the reaction mixture. Tetrahydrotetramethylnaphthalene derivatives are likely to have higher solubility, and therefore precipitate from the reaction less readily. The solvent volume was reduced for subsequent reactions which improved the yield of dimethoxyisoindoline (**31**).

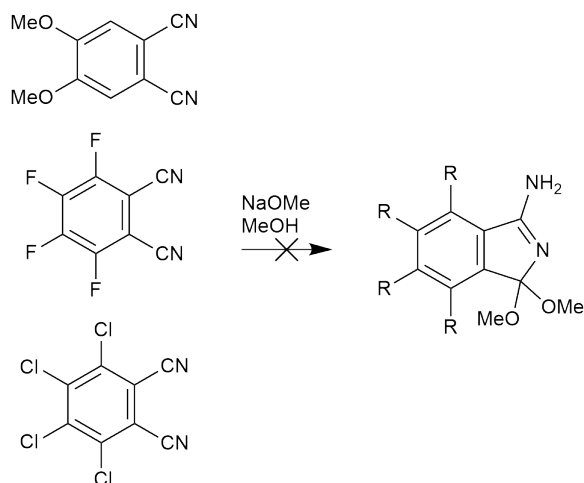


Scheme 2.34: Scheme for the synthesis of dimethoxyisoindoline (**31**).

The procedure was also expanded to produce 4,5-diphenoxydimethoxyisoindoline and dimethoxy-benz[*f*]isoindoline (**41**), which again was synthesised in acceptable yield. However, these derivatives appear to

exemplify the scope of the procedure; other more electronically demanding phthalonitriles were attempted (scheme 2.35), however did not yield isolable products. Complicated mixtures were often obtained on TLC, sometimes with highly coloured red/orange compounds present suggesting condensation to higher order oligomers. This may be driven by increased electronic activation of intermediate species, producing oligomers, or by high solubility of the targeted products meaning the target materials do not precipitate readily from the reaction.

It is possible the procedure may be adapted to facilitate a wider range of dimethoxyisindoline derivatives in future work through a number of options. Low temperature conditions may be useful in controlling unwanted side products as well as encouraging the target dimethoxyisindoline to precipitate from the reaction mixture. Additionally stoichiometric quantities of NaOMe in an alternative solvent may yield the target materials.



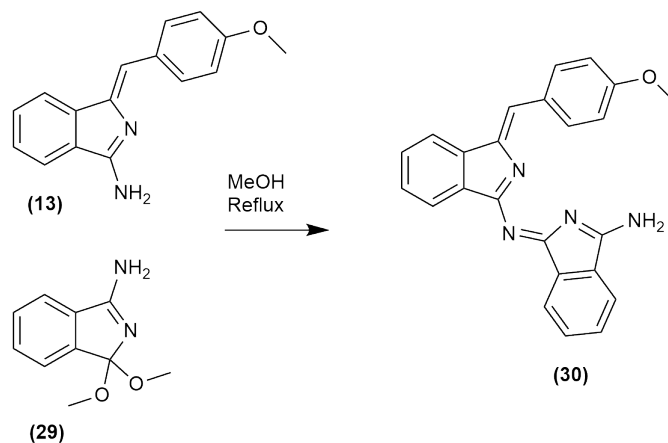
Scheme 2.35: Failed dimethoxyisindoline derivatives.

### Dimethoxyisindoline properties

While the dimethoxyisindolines described above were synthesised in good yields and able to be characterised, they possess some disadvantageous properties. Isolated dimethoxyisindolines will slowly turn yellow/green due to decomposition and the formation of condensation products, this process is greatly accelerated on exposure to light. The dimethoxyisindolines will also cyclize to form Pcs in very high yield at temperatures as low as 60° C, meaning subsequent reaction conditions must be carefully considered.

### Condensation products

Following the successful synthesis of the dimethoxyisoindoline (**29**) and a selection of derivatives, the next step was a condensation reaction between (**29**) and aminoisoindoline (**13**). Utilizing previously developed but as yet unpublished procedures by the Cammidge group, a first attempt was performed using an equimolar ratio of aminoisoindoline and dimethoxyisoindoline in methanol at reflux. With aminoisoindoline generally undergoing homocondensation in higher boiling solvents such as toluene this was not expected as a side reaction. After addition and heating a dark red solution was formed. Initial TLC results appeared promising, with a new dark red/orange spot quickly appearing. The reaction was continued overnight and upon completion a dark orange precipitate had formed, this was filtered and recrystallised from ethyl acetate/hexane to yield the desired compound (**30**) (scheme 2.36).



Scheme 2.36: Successful synthesis of target condensation product (**30**).

### Characterisation of (**30**)

Structure (**30**) is a red/brown compound with broad UV-visible absorbance and extremely weak fluorescence emission. The structure has a  $\lambda_{\text{max}}$  of around 260 nm and molar extinction coefficient in the order of  $1.5 \times 10^4$  (figure 2.20). The  $^1\text{H}$  NMR spectrum is concordant with the structure proposed (figure 2.19).

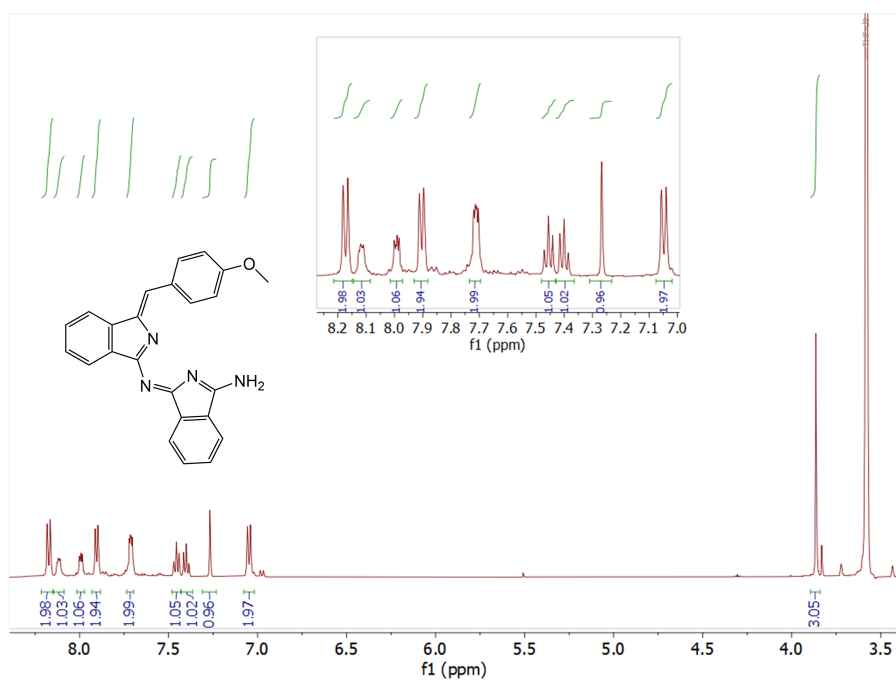


Figure 2.19:  $^1\text{H}$  NMR spectra of product (30).

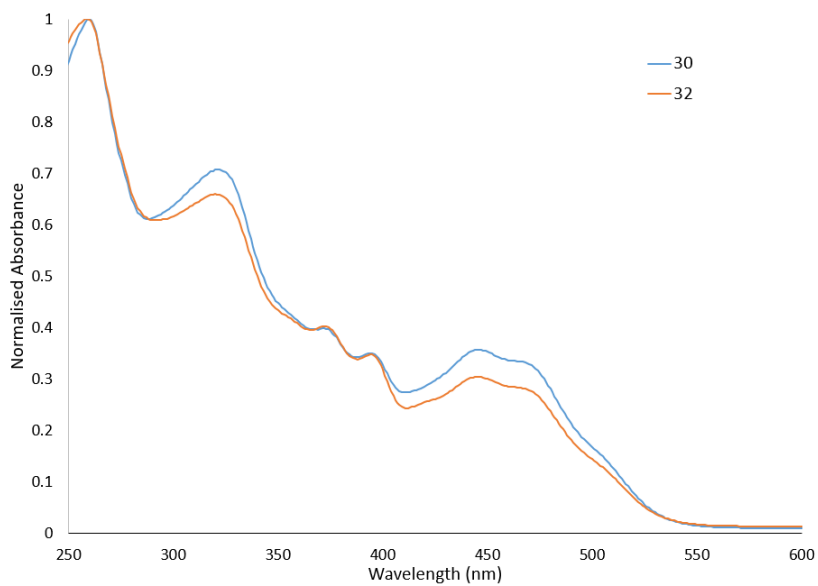


Figure 2.20: UV-Visible spectra of condensation products (30) and (32).

## Substituted derivatives

Substituted derivatives were then targeted, starting with the tetramethyltetrahydronaphthalene (**14**) derivatives discussed earlier. By targeting and synthesising this species it was anticipated it may be used to selectively synthesise the 2:2 TBTAP (**18**) derivative observed in previous experiments. The hypothesised scheme is shown in scheme 2.26.

Dimethoxyisoidoline (**31**), synthesised previously, was then reacted with aminoisoidoline (**13**) as discussed in this section. Initial results looked similarly encouraging, however after 24 hrs no precipitate had formed, and TLC indicated the presence of both aminoisoidoline starting material as well as a significant quantity of an unknown dark brown material, and the dark orange/red material that was likely to be the desired product (**32**). Isolation of these fractions was performed by column chromatography and the materials characterised by MALDI-TOF and  $^1\text{H}$  NMR.

MALDI-TOF analysis revealed the presence of the targeted product (**32**) with a peak at 489 m/z. The aminoisoidoline (**13**) starting material was present at 251 m/z, and a peak at 722 m/z for the unknown brown material. This mass suggests the condensation of one equivalent of dimethoxyisoidoline with two equivalents of aminoisoidoline.  $^1\text{H}$  NMR also revealed a structure with higher symmetry than the target species (**32**) and concordant with the structure shown below (figure 2.21, product **33**). Condensation products (**32**) and (**33**) are characterised below (figure 2.22-2.24, the UV-vis spectra of (**32**) is shown above in figure 2.20.

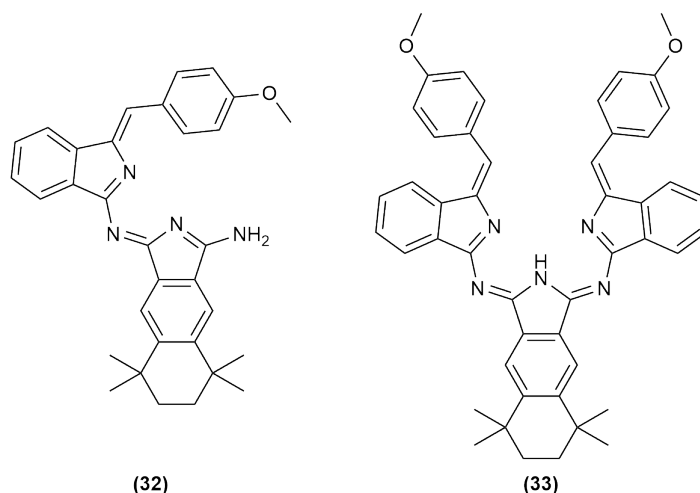


Figure 2.21: Condensation products (**32**) and (**33**) identified by MALDI-TOF and  $^1\text{H}$  NMR. The unsubstituted parent structure of (**33**) was previously discovered during SubTBDAP synthesis and its structure confirmed by x-ray crystallography.

Characterisation of **(32)** and **(33)**.

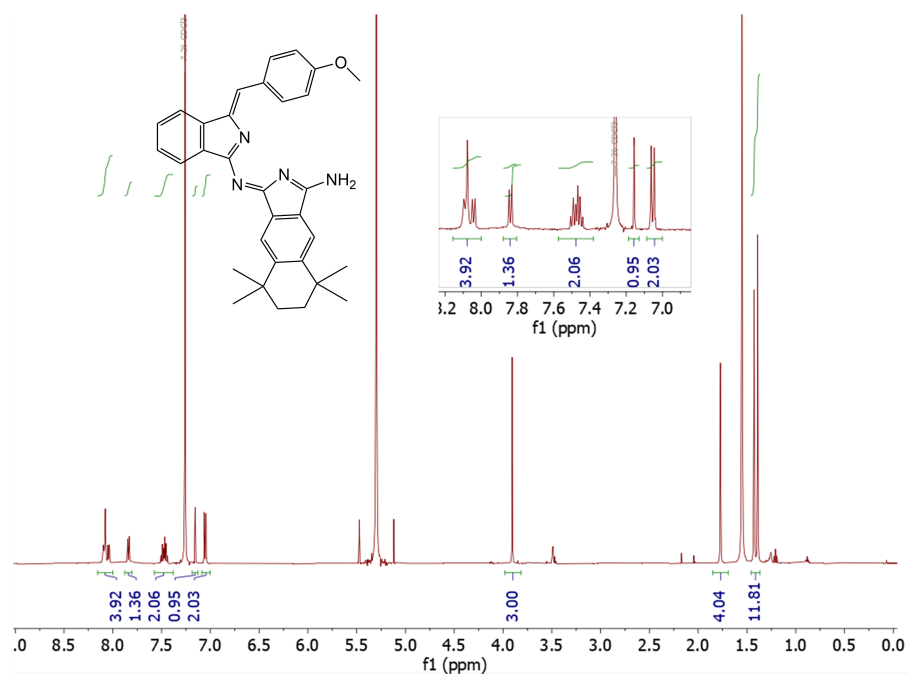


Figure 2.22: <sup>1</sup>H NMR spectra of product **(32)**, with an expansion of the aromatic region. Residual solvent peaks for CDCl<sub>3</sub> and DCM are visible at 7.26 ppm, 5.32 ppm and 1.56 ppm.

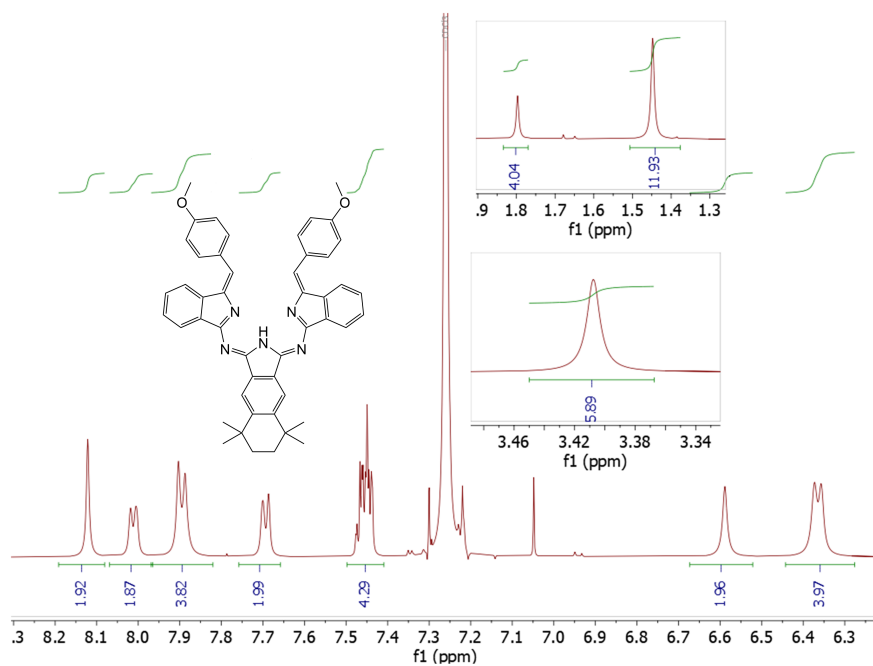


Figure 2.23: <sup>1</sup>H NMR spectra of product **(33)**, with expansions of the methoxy signal and alkyl region.

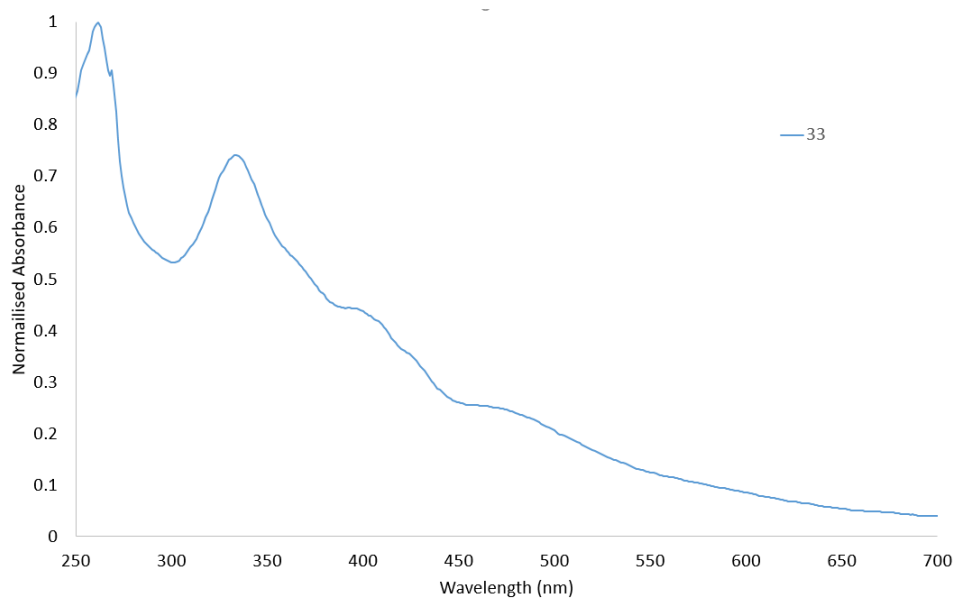
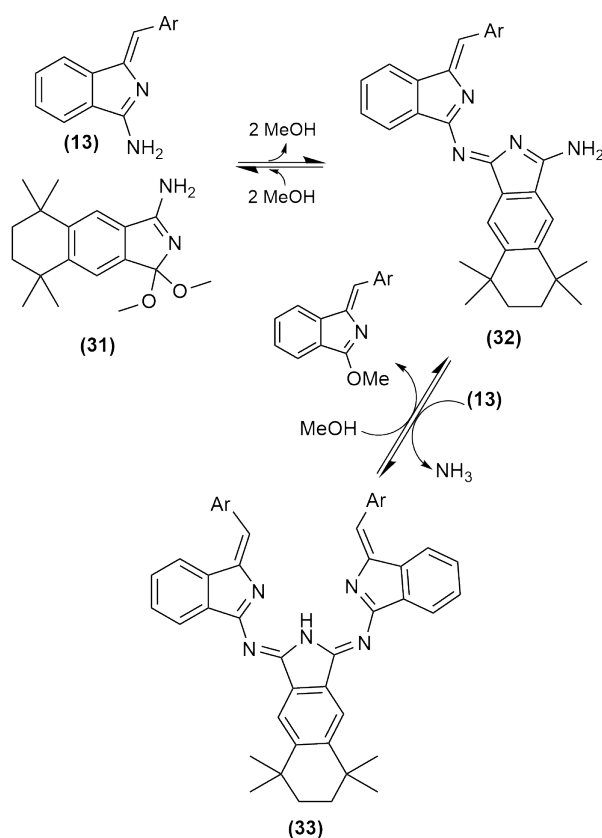


Figure 2.24: UV-visible spectra of product **(33)**, again a brown material with wide absorbance.

### Mechanistic discussion

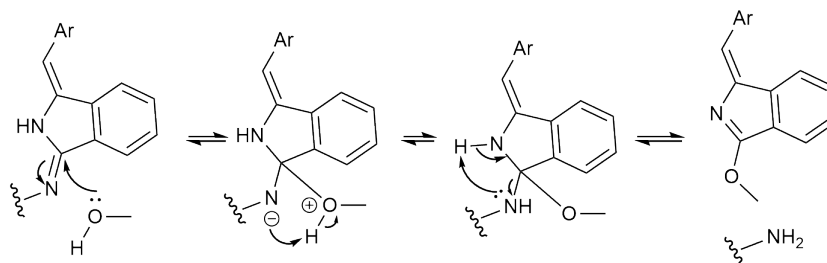
At this stage it appears that once produced, **(32)** reacts preferentially with more aminoisoindoline **(13)** to form species **(33)** (scheme 2.37). Procedural modifications were employed to try and overcome this and successfully synthesise **(32)** in good yields. Room temperature was tried over reflux conditions. This produced a roughly 1:1 mixture of **(32)**:**(33)**. Syringe pump addition of aminoisoindoline was also attempted. It was observed after all reactions that starting material remained, and a mixture of products was quickly obtained, but then ratios stayed consistent. This implies an equilibrium exists between the products. Given the volatility of ammonia it is expected the reaction would be driven towards **(33)**, however the reverse reaction to reform **(32)** could also be driven by methanol, producing a methoxyisoindoline (scheme 2.38 and 2.39).



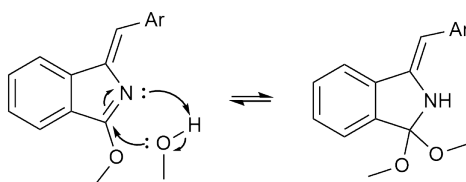
Scheme 2.37: Summary of hypothesised equilibria between starting materials, **(32)** and **(33)**.

With clear evidence of an equilibrium, it was reasoned that removing methanol from the reaction would drive the reaction towards the desired product **(32)** by reducing the rate of reverse reaction. After the initial condensation of **(32)** this modification will limit the quantity of aminoisoindoline **(13)** present in the reaction, hence reducing the probability of further condensation to **(33)**.

With **(32)** forming at RT in methanol due to the increased reactivity of the dimethoxyisindoline it may be possible to thermodynamically limit or eliminate the formation of the unwanted product **(33)**, significantly improving yield.



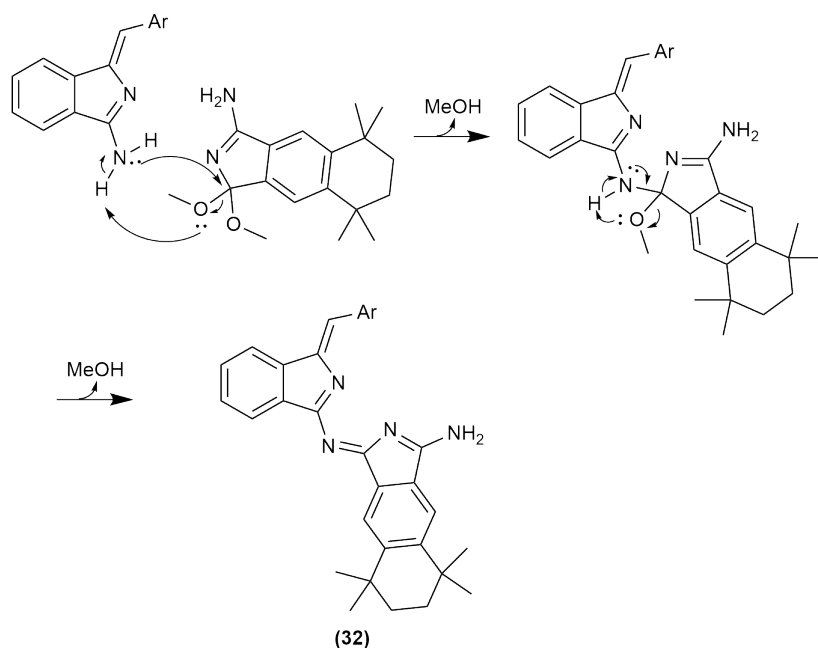
Scheme 2.38: The hypothesised reverse reaction for aminoisindoline addition to **(32)** to form **(33)**, driven by methanol rather than ammonia.



Scheme 2.39: The hypothesised formation of a dimethoxy substituted analogue of aminoisindoline **(13)**.

As discussed previously, elimination of methanol from the reaction mixture through the use of an alternative, non-nucleophilic, solvent should reduce the rate of reverse reaction significantly. By reducing or eliminating reverse reactions that regenerate aminoisindoline from the product the reaction should follow the designed pathway, whereby the highly activated dimethoxyisindoline undergoes nucleophilic attack by the amine group in aminoisindoline to selectively form **(32)** as shown in scheme 2.40.

DCM was selected as a solvent due to the excellent solubility of both aminoisindolines and substituted dimethoxyisindolines, and non-nucleophilic nature of the solvent. Oven dried molecular sieves were employed to capture methanol produced by the reaction and thus prevent reverse reactions, and the solution heated to reflux at 40°C. The adaptation resulted in much higher yields of the desired product **(32)** (50-60 % vs 20-30 %), and in most cases purification was achieved by simple recrystallisation due to the generally reduced solubility of product **(32)** compared to starting materials and side product **(33)**. The procedure was also reliable with a range of derivatives, producing moderate to good yields. **(33)** and derivatives of, were still produced by the reactions, albeit in much lower quantity. This is due to **(32)** still being susceptible to nucleophilic attack by aminoisindoline.



Scheme 2.40: Hypothesised mechanism for formation of **(32)** from aminoisoindoline and dimethoxyisoindoline **(31)**. Removing methanol from the reaction mixture should prevent the reverse reaction occurring, driving the formation of **(32)**.

### Final procedure and scope of functionalisation

The final procedure for producing condensation products **(30)** and derivatives utilised the anhydrous DCM at reflux with molecular sieves method outlined in the previous section. This procedure was successful at producing a wide range of derivatives in moderate to good yields. The limits of the procedure currently appear to be the range of dimethoxyisoindolines and aminoisoindolines synthetically available. Several derivatives were selected and utilised in the work in section 2.5, outlined in figure 2.25.

The  $^1\text{H}$  NMR spectra of condensation products **(42)** and **(43)** are shown in figures 2.26 and 2.27.

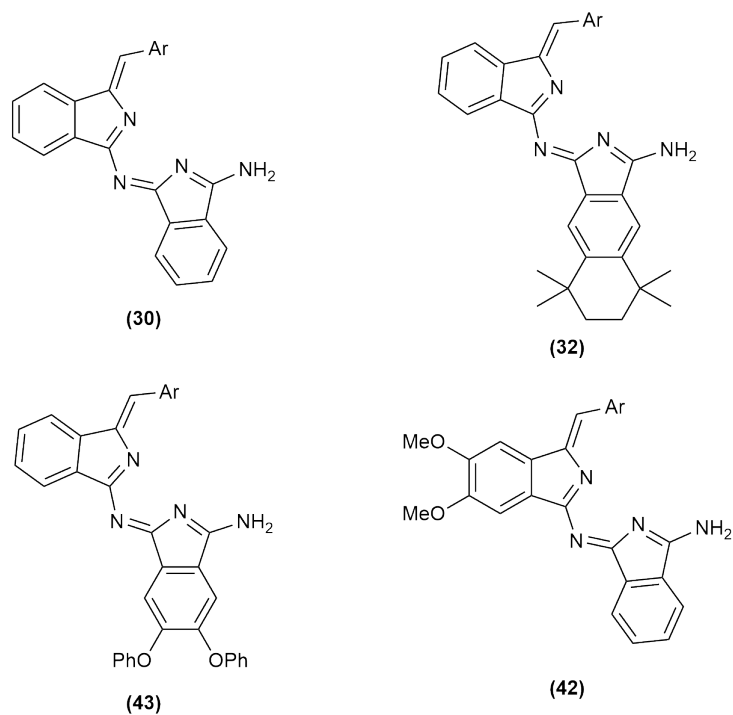


Figure 2.25: Derivatives chosen and synthesised for the work in section 2.5, Ar = *p*-methoxybenzene.

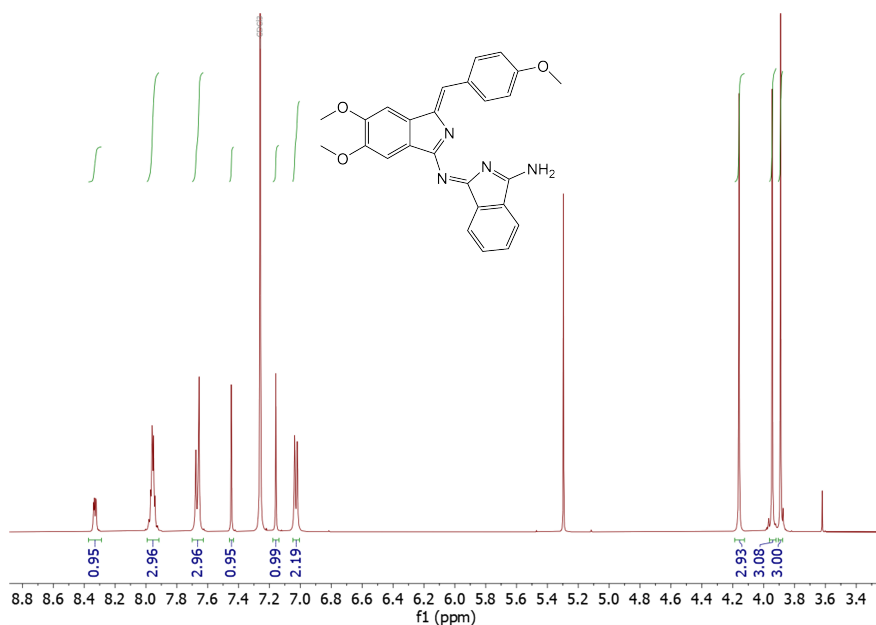


Figure 2.26: <sup>1</sup>H NMR spectra of dimethoxy condensation product (42).

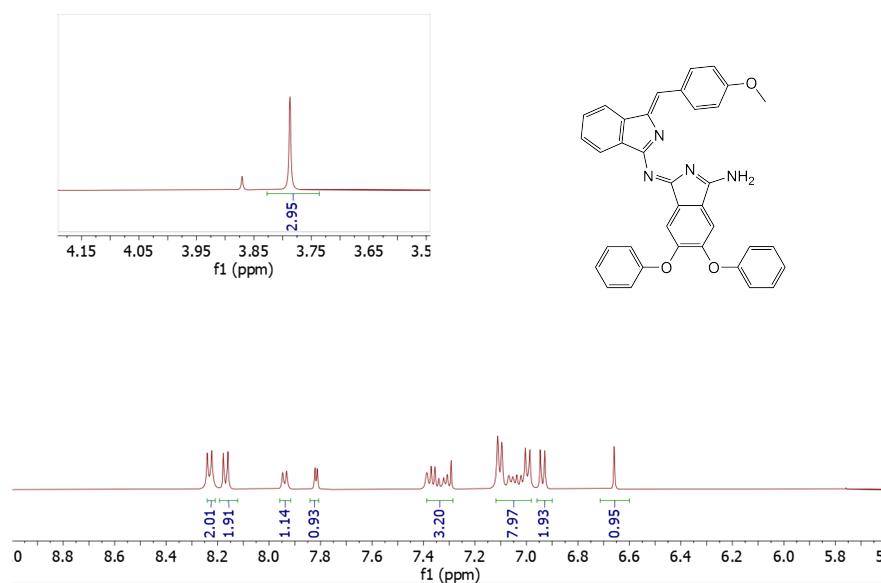
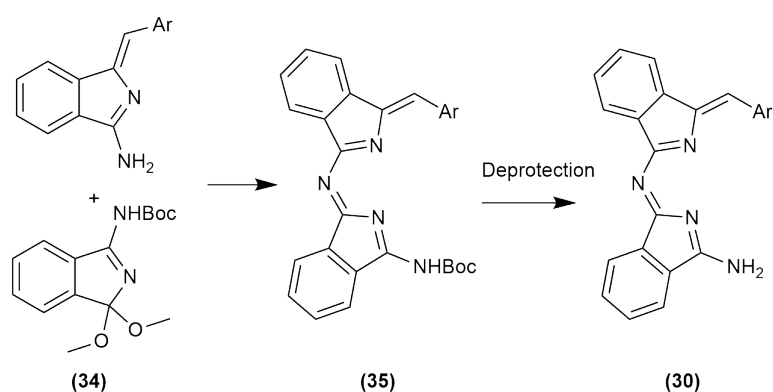


Figure 2.27:  $^1\text{H}$  NMR spectra of dimethoxy condensation product (**43**).

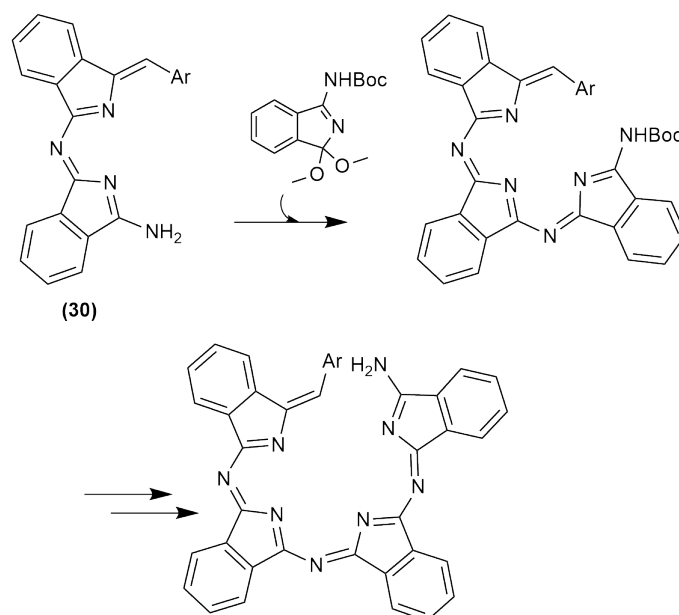
## 2.4.5 Protection method

### Protection of dimethoxyisoindolines

Due to the occasionally poor yields and mixed products obtained for substituted condensation products, and with the ultimate goal of stepwise synthesis of ABCD TBTAP macrocycles, it was decided to explore the use of a nitrogen protecting group on the amine of the dimethoxyisoindoline derivatives. It was reasoned that by using a protecting group, dimeric species, as well as a range of open chain 3 and 4 membered oligomers may be synthesised in a stepwise and selective manner (scheme 2.41 - 42). The same pathway could potentially be used to form templates for SubTBDAP synthesis as well as TBTAP synthesis, and may lead to similar advances in Pc synthesis. *Tert*-butoxycarbonyl (BOC) was chosen as the protecting group due to its application with a vast range of amine derivatives and relatively mild protection and de-protection methods. A scheme for condensation of this protected dimethoxyisoindoline with aminoisoindoline is shown in scheme 2.41.



Scheme 2.41: Strategy for the formation of condensation product **(30)** via N-Boc protected dimethoxyisindolines.

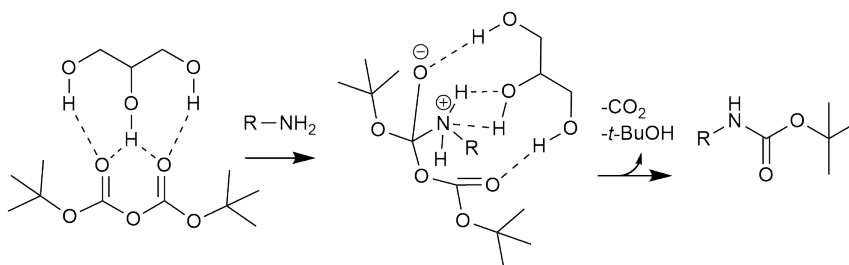


Scheme 2.42: Strategy for the stepwise construction of ABCD systems utilising N-Boc protected dimethoxyisindolines. Successive deprotection and addition of further protected dimethoxyisindoline should facilitate the stepwise construction of such systems.

The first step in this targeted synthetic pathway was to establish synthetic protocol for N-Boc protection of dimethoxyisindolines. Due to the activated reactivity of the dimethoxyisindoline, caution was required with using solvents such as alcohols or water at elevated temperature as they may substitute the methoxy positions. 3 procedures were selected from literature to attempt with dimethoxyisindolines. All 3 methods utilised di-*tert*-butyl dicarbonate as the

Boc source, readily available from commercial sources. Two procedures simply utilised di-*tert*-butyl dicarbonate in H<sub>2</sub>O and glycerol respectively. The final procedure attempted utilised di-*tert*-butyl dicarbonate in DMF with Et<sub>3</sub>N as a base.<sup>122–124</sup>

Attempts with the H<sub>2</sub>O and DMF solvated procedures were unsuccessful, with no product isolated. Attempts utilizing di-*tert*-butyl dicarbonate in a solution of glycerol were successful. Dimethoxyisoindoline was added to the solution of di-*tert*-butyl dicarbonate in glycerol and stirred at RT overnight, the initial suspension dissolved to form a clear solution overnight. After 24 hours the mixture was extracted 3 times with EtOAc:hexane (1:9), the extracts were dried and concentrated to yield the desired protected dimethoxyisoindoline. Glycerol has the role of a solvent and a catalyst for the reaction, stabilising the di-*tert*-butyl dicarbonate and the intermediate structure shown in scheme 2.43.<sup>122</sup>



Scheme 2.43: Proposed mechanism for the glycerol mediated Boc protection of amines. Glycerol acts as a solvent but also has a catalytic effect by stabilising intermediate species.<sup>122</sup>

This procedure appeared versatile in protecting both the unsubstituted and substituted dimethoxyisoindoline derivatives. The protected dimethoxyisoindolines are easily characterised by NMR, with distinctive signals for the two methoxy substituents, and the *tert*-butyl substituent (figure 2.28).

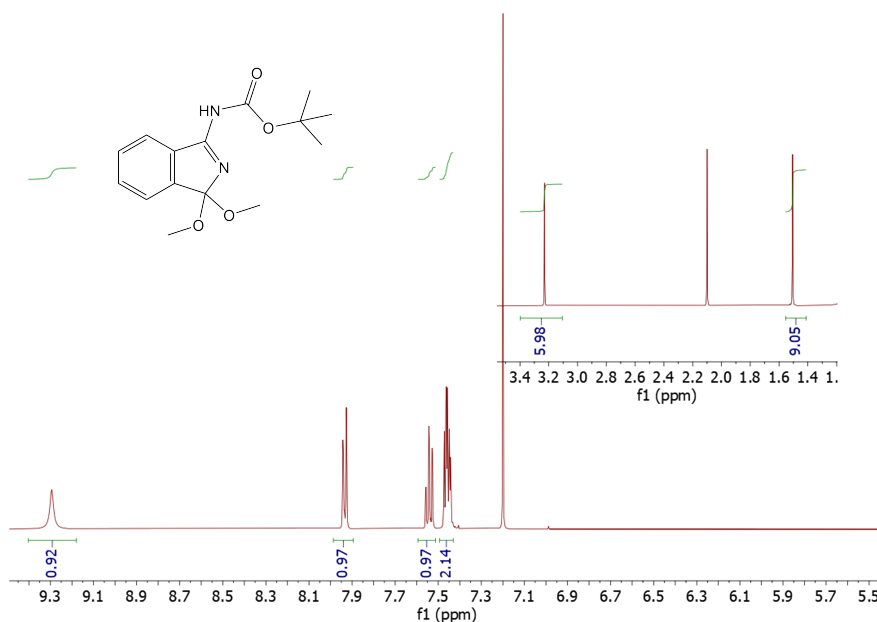
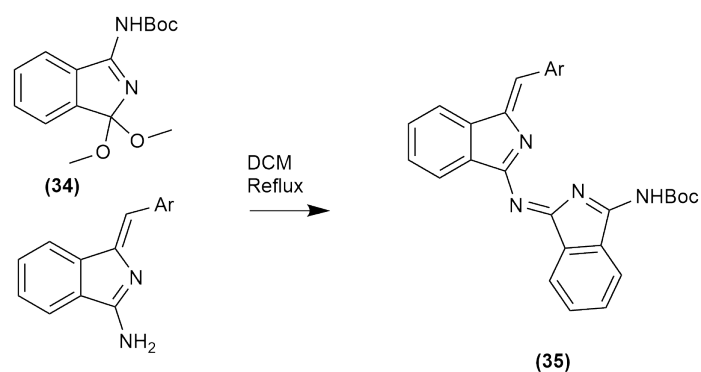


Figure 2.28: NMR of unsubstituted NBoc dimethoxyisindoline (**34**) in  $\text{CDCl}_3$ , with an expansion of the clear signals for the methoxy and *t*-butyl fragments.

### Synthesis of condensation products via protected dimethoxyisindolines

With NBoc protected dimethoxyisindolines successfully synthesised, the next step was to repeat the previous synthetic procedures utilizing the protected dimethoxyisindoline in the hope of achieving controllable synthesis of the protected product (**35**) with minimal side product formation. Reflux in methanol gave the desired product in 35 % yield, reflux in DCM yielded (**35**) in upwards of 70 %. The scheme for the reaction is shown in scheme 2.44. The procedure appeared versatile with both substituted NBoc dimethoxyisindolines as well as the parent NBoc dimethoxyisindoline (**34**). The  $^1\text{H}$  NMR clearly shows a structure concordant with that of the protected product (**35**), with the *t*-Bu signal clearly present (figure 2.29).



Scheme 2.44: Scheme for the synthesis of NBoc protected product **(35)** from NBoc protected dimethoxyisoindoline, Ar = *para*-methoxytoluene.

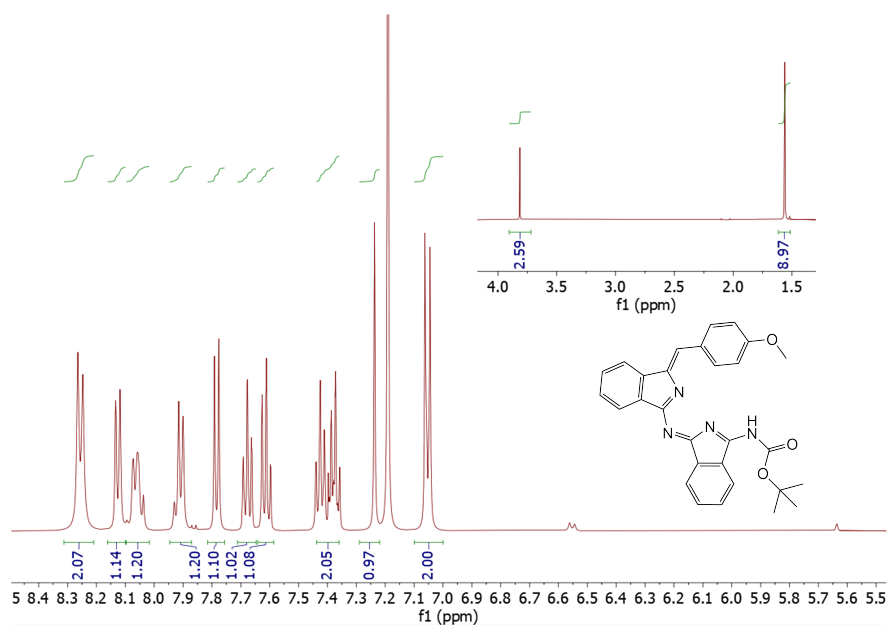
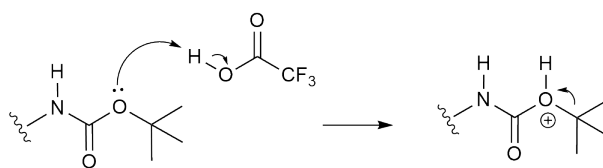


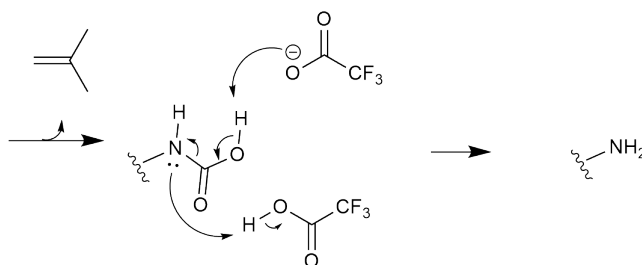
Figure 2.29: <sup>1</sup>H NMR of **(35)** in CDCl<sub>3</sub>.

A de-protection method was required to remove the Boc functionality from the terminal amine for subsequent condensations or TBTP synthesis. Most commonly employed are acids such as HCl or TFA. These acids facilitate quick and simple de-protection with the elimination of CO<sub>2</sub> and isobutene as shown in schemes 2.45 and 2.46.



Scheme 2.45: Generic mechanism for protonation and elimination of isobutene from NBoc protected amines.

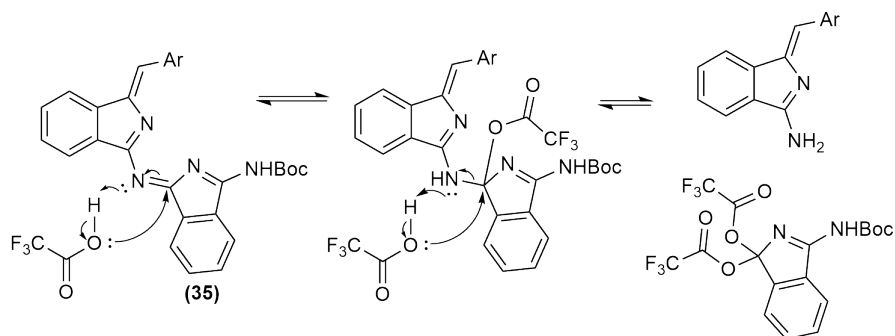
After initial protonation follows elimination of the isobutane carbocation, which rearranges to isobutene. While this elimination may be slow the volatility of the isobutene product causes it to quickly leave solution, irreversibly driving the reaction towards the product.



Scheme 2.46: Generic mechanism for the decarboxylation to yield the deprotected amine.

While actual attempts to de-protect the NBoc protected condensation product (**35**) using both HCl in dioxane and TFA in DCM looked initially promising on TLC, the reaction quickly produced a complicated mixture of products on TLC, suggesting decomposition of the material. It is feasible that protonation followed by nucleophilic attack by the TFA conjugate base could decompose the structure as shown in scheme 2.47.

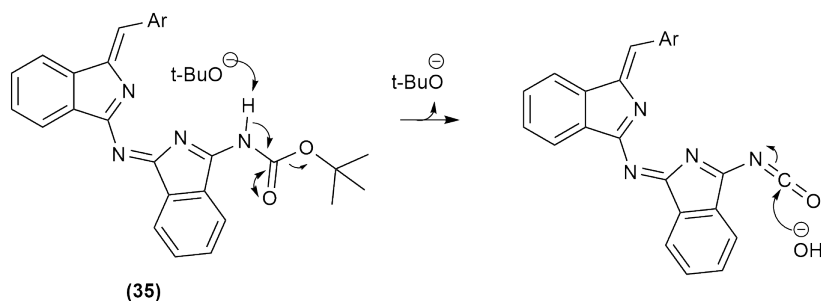
Several attempts were tried with both acid catalysed methods; often a small amount of product was isolable, however the majority of the material decomposed. Following this, milder, non-nucleophilic reagents and methods were investigated.



Scheme 2.47: Hypothesised nucleophilic attack by TFA resulting in the decomposition of the structure.

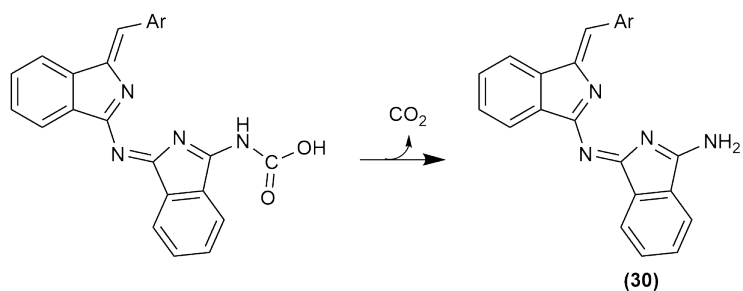
An  $I_2$  catalysed RT solvent free and solvated de-protection procedure was investigated, however no de-protected product was obtained using NBoc protected product (**35**). Intriguingly, methods for both the protection and de-protection of Boc protected amines catalysed by  $I_2$  under near identical conditions are presented in literature.<sup>125,126</sup>

Literature revealed base catalysed de-protection also, specifically the NaOtBu/  $H_2O$  facilitated de-protection of NBoc amines in THF, via an isocyanate intermediate as shown in scheme 2.48.<sup>127</sup>

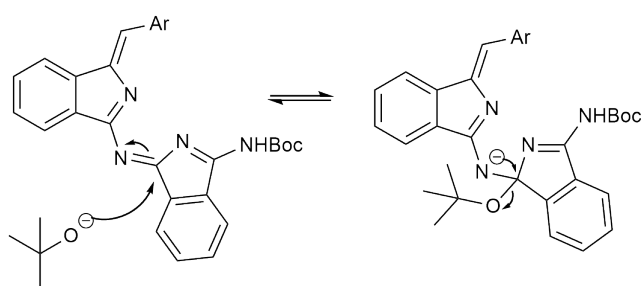


Scheme 2.48: Deprotonation and elimination to regenerate the *t*-butoxide anion, followed by addition of hydroxide facilitated by 1eq of  $H_2O$ .

Following deprotonation and the formation of the isocyanate intermediate, attack of the isocyanate by hydroxide forms a carbamic acid that then undergoes decarboxylation to yield the de-protected product (scheme 2.49). It is also expected that the butoxide anion will attack (**35**) in a manner analogous to TFA (scheme 2.50), however the use of an aprotic solvent, 1 eq of  $H_2O$  and basic conditions prevents decomposition of the product.



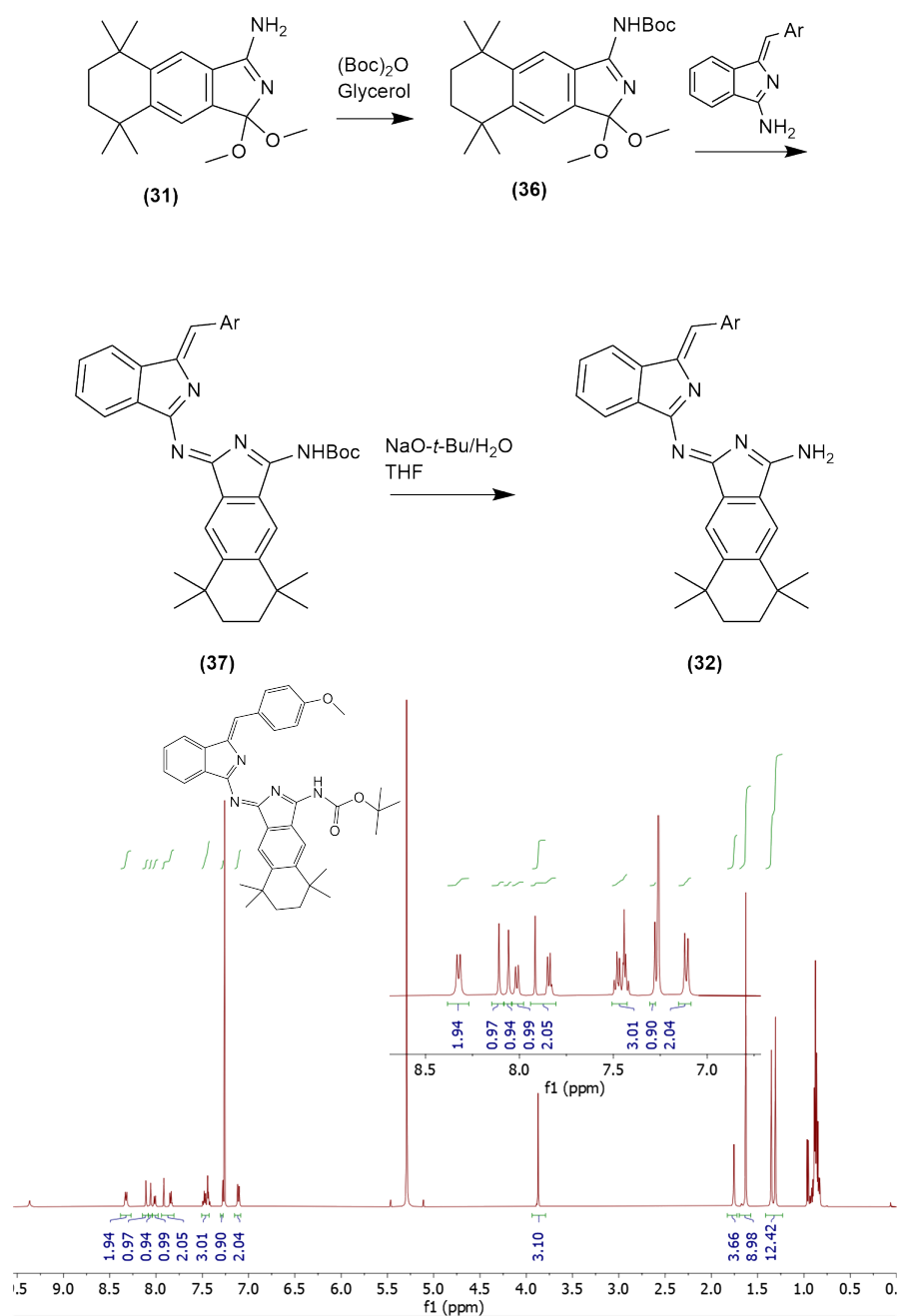
Scheme 2.49: Final elimination of CO<sub>2</sub> to yield the unprotected product **(30)**



Scheme 2.50: Hypothesised equilibrium for the addition of *t*-BuO.

Reflux of the protected **(35)** in THF, with NaO-*t*-Bu/H<sub>2</sub>O for 4 hours yielded the de-protected product **(30)** in good yield, with minimal decomposition or side product formation.

With this synthetic methodology developed it was also applied to the synthesis of tetrahydrotetramethyl derivative **(32)**, which previously preferentially reacted to form the trimeric species **(33)** seen in the previous section. Utilising the Boc protected dimethoxyisoindoline afforded the protected condensation product **(37)** in approx 60% yield, and subsequent deprotection yielded the target product **(32)** (scheme 2.51).



Scheme 2.51: Scheme for the synthesis of, and <sup>1</sup>H NMR spectra for (37).

## 2.4.6 Summary of new synthetic methodology and future work

This work has developed a selection of powerful new methodology to obtain two novel classes of condensation product, (30) and (33). While these struc-

tures have previously been observed as side products in numerous studies and projects within the Cammidge group, any further mechanistic studies have been restricted by a lack of access to these materials. Straightforward synthetic access to these species has facilitated the work on TBTAP synthesis in section 2.5 and SubTBDAP synthesis in chapter 3, however a plethora of potential pathways to Por/Pc hybrids as well as other porphyrinoids can be conceived, reaching far beyond the scope of this work.

## 2.5 TBTAP synthesis from novel intermediate materials

### 2.5.1 Unsubstituted derivatives

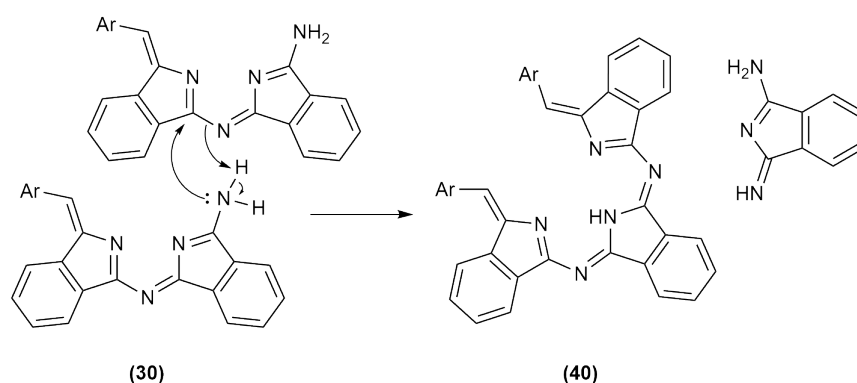
With synthetic pathways to the target intermediates reliably established experiments could begin targeting 2:2 substituted TBTAPs and other species from these intermediates.

#### Aims

The aim of these experiments was to synthesise and isolate the homocondensation product of 2 units of **(30)**, and macrocyclize this species with magnesium to yield TBTAPs in a stepwise manner. The dimeric species are expected to undergo homocondensation via a pathway analogous to aminoisoindoline homocondensation, outlined previously. Experiments began with subjecting **(30)** to mild conditions that should yield the desired condensation, namely mild heating in toluene with and without 0.5 eq of MgBr<sub>2</sub>.

Heating **(30)** with or without MgBr<sub>2</sub> at low temperature (60°C) did however not yield the desired product, but instead the displacement product **(40)**, as evidenced by MALDI-TOF and the appearance of a brown spot on TLC. In toluene, without the presence of methanol or other nucleophilic solvents that could drive a reverse reaction as previously discussed, the formation of **(40)** implies **(30)** must be reacting with itself to yield **(40)** and 1,3-diiminoisoindoline as shown in scheme 2.52.

Clear evidence for the formation of **(40)** was visible on TLC, and the material was able to be isolated and its identity also confirmed by NMR. While the MALDI data appears to support these conclusions (figure 2.30), the peak identified as a possible intermediate species (755 m/z) could alternatively be a [2M] MALDI-TOF dimer of material **(30)**.



Scheme 2.52: The hypothesised mechanism for the formation of (40) with elimination of 1,3-diminoisindoline.

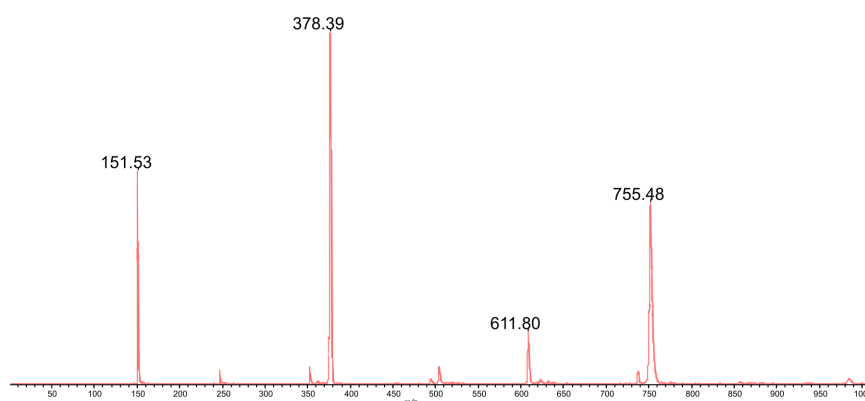
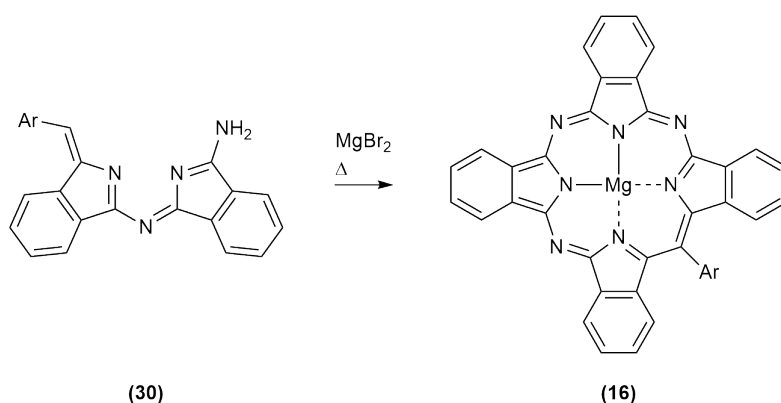


Figure 2.30: MALDI-TOF evidence for the formation of (40) (611 m/z) from (30) (378 m/z), via a possible intermediate comprising of two units of (30) (755 m/z) before elimination of 1,3-diminoisindoline.

With this result occurring at 60°C, and a slow rate of reaction with starting material still present after 2 days, higher temperatures were employed. Toluene at reflux was employed for the next reaction, with all other TBTAP macrocyclization pathways requiring 180-220°C or more macrocyclization was not expected at this temperature. After reflux overnight however an intensely green solution had formed, this was worked up and purified to yield MgTBTAP (16), albeit in low yield (3.0 %), a significant quantity of (40) was also produced by the reaction.

What is notable about this synthesis is the low temperature required to achieve macrocyclization from (30), while the reaction was slow the use of a low temperature may be useful in controlling side reactions etc, and may give



Scheme 2.53: Formation of MgTBTAP from **(30)** in toluene or *p*-xylene at reflux.

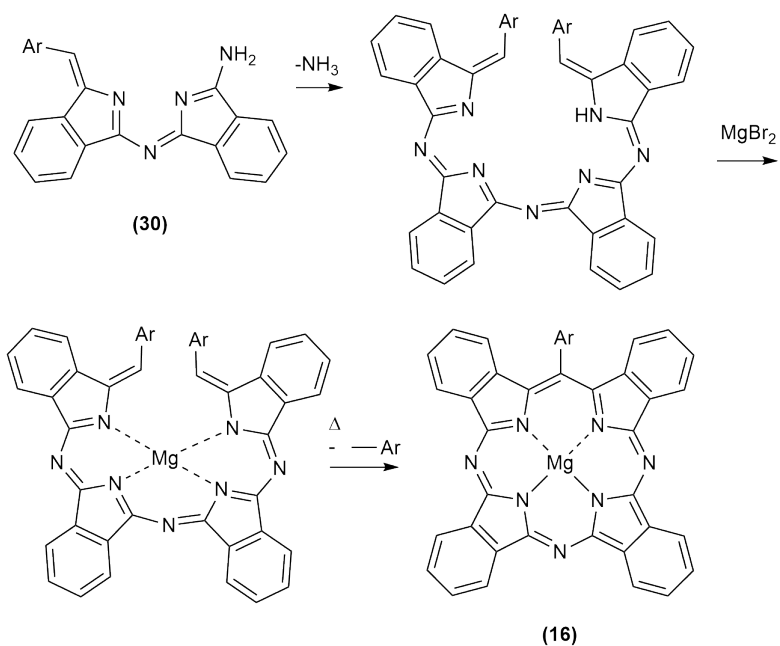
better selectivity for the synthesis of substituted derivatives. It appears at this stage that the higher temperature utilised by this reaction facilitates the condensation and macrocyclization as designed, with macrocyclization occurring rapidly so any intermediates were not observable by MALDI-TOF. Subsequent experiments focused on optimisation of TBTAP synthesis from these precursors.

The next experiment utilised a higher boiling point solvent, *p*-xylene, at reflux with the expectation a higher temperature will give better yields of TBTAP **(16)**. **(30)** was reacted at reflux with 0.5 eq of MgBr<sub>2</sub> for 3 hours. The reaction was then worked up and purified by the standard procedure, yielding MgTBTAP in excellent yield (40 %). **(40)** was produced as a side product (19%). This procedure is therefore a significant progression for the synthesis of parent structure MgTBTAP, giving exceptional yields with mild conditions (scheme 2.53).

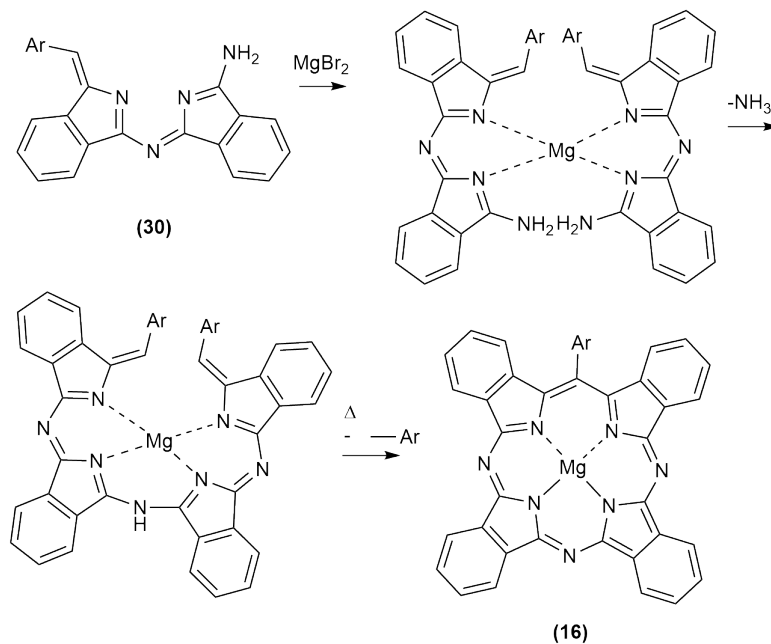
With an apparently far cleaner synthesis with fewer and easily characterisable side products, a clearer picture of the reaction pathway and dynamics can be formed. This will be analysed in depth by computational methods in a later chapter. If a thermodynamic landscape can be deduced modifications to the procedure and starting material may be employed to additionally activate the desired macrocyclization pathway, giving higher yields and more selectivity.

### 2.5.2 Substituted TBTAPs via derivatives of **(30)**

With the previous experiments producing MgTBTAP in exceptional yield it appears at this stage that two units of **(30)** either undergo homocondensation followed by coordination to magnesium and subsequent macrocyclization, or alternatively two units of **(30)** coordinate magnesium and undergo condensation and macrocyclization in two discrete steps, or as a pericyclic process. These proposed pathways are shown in schemes 2.54 and 2.55. The pericyclic mechanism is not shown, however would proceed via simultaneous elimination of ammonia and an aromatic fragment from the second structure in scheme 2.55.



Scheme 2.54: Hypothesised hemocondensation of **(30)**, followed by coordination by magnesium, macrocyclization and aromatisation to yield MgTBTAP **(16)**.



Scheme 2.55: Hypothesised coordination of two units of **(30)** to magnesium, followed by condensation, macrocyclization and aromatisation to yield MgTBTAP **(16)**.

As can clearly be seen from the proposed mechanism this pathway should selectively produce 2:2 TBTAPs, making it a selective and high yielding route to 2:2 TBATPs. To verify this the reaction must be performed with substituted derivatives, so each ring may be ‘tagged’ to reveal its origin.

As described earlier in the chapter, aminoisoindolines, phthalonitriles and hence dimethoxyisoindolines may be synthesised via the same pathways, giving convenient access to a suite of derivatives and hence variations of **(30)**. Derivatives chosen are shown in figure 2.31, from this accessible selection 9 different variations of **(30)** may be synthesised, giving access to a suite of ABBA and some symmetrically substituted TBTAPs through the use of symmetrically substituted derivatives of **(30)**.

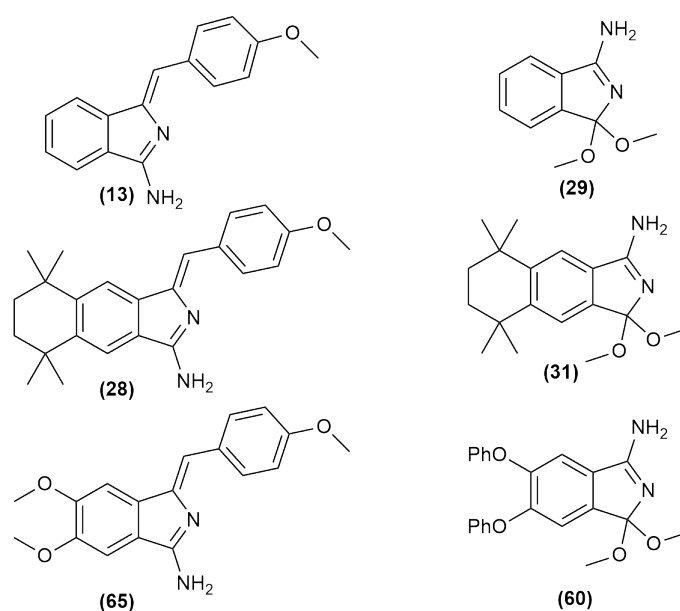
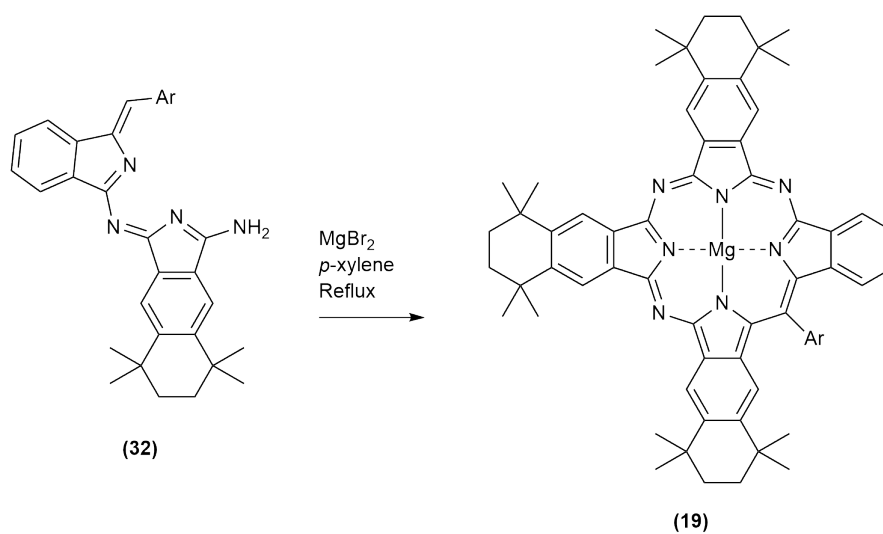


Figure 2.31: Suite of aminoisoindoline and dimethoxyisoindoline derivatives chosen for this work.

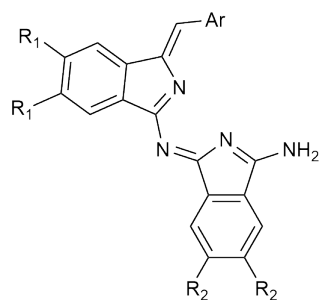
Initial investigations began with the tetrahydrotetramethylnaphthyl derivative **(32)** and the formation TBTAP from this species. **(32)** was reacted in *p*-xylene at reflux with 0.5 eq of  $\text{MgBr}_2$ . Again a dark green solution was formed, which was worked up and purified to yield the MgTBTAP product. From the previous experiments the 2:2 MgTBTAP product **(18)** was expected, however MALDI-TOF and NMR revealed that in fact 3:1 MgTBTAP **(19)** was formed in 31% yield by this reaction as shown in scheme 2.56. The reaction was repeated several times under varying conditions and solvents and the same result was obtained, albeit in slightly varying yields. Again, the reaction produced the ABA condensation material **(33)** in approx 20 % yields.



Scheme 2.56: Unexpected formation of 3:1 MgTBTAP (**19**) from (**32**).

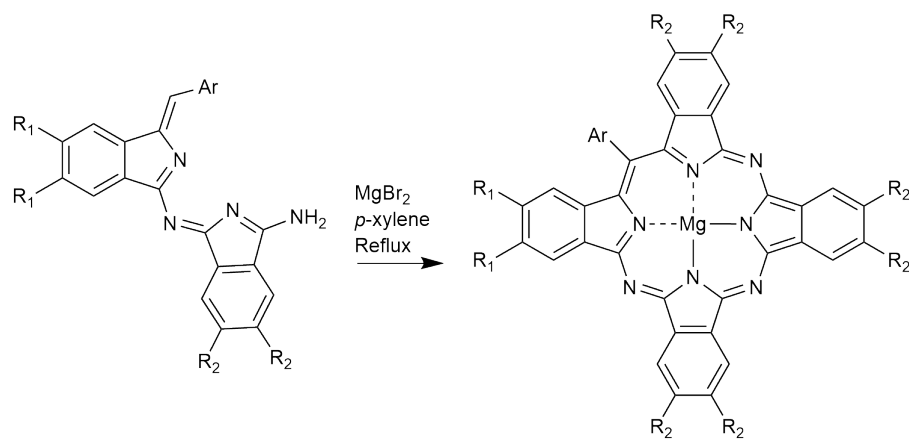
With this unexpected result the reaction needed to be repeated with differently substituted dimers in case sterics or electronics of the condensation species was influencing the outcome. A variety of derivatives of (**30**) were synthesised and tested utilizing tetrahydrotetramethylnaphthyl, diphenoxy and dimethoxy substitution, the derivatives utilised are shown in figure 2.32.

All derivatives described in figure 2.32 were subjected the the same reaction conditions previously optimised. All derivatives successfully reacted to form the unexpected 3:1 MgTBTAPs, as confirmed by MALDI-TOF and NMR spectroscopy. Trace amounts of 2:2 TBTAP were normally detectable by MALDI-TOF, however the major product in all cases was 3:1 TBTAP (scheme 2.57).



R <sub>1</sub>	R <sub>2</sub>

Figure 2.32: Parent structure (**30**) with substitution positions shown, with a table of synthesised derivatives.



Scheme 2.57: Formation of 3:1 TBTAPs from derivatives of (**30**) in *p*-xylene at reflux.

Figures 2.33 and 2.34 show the <sup>1</sup>H NMR spectra of novel 3:1 MgTBTAPs (**53**) and (**54**). Again the NMR spectra of both materials clearly show ABBB type TBTAPs due to the reduction in symmetry.

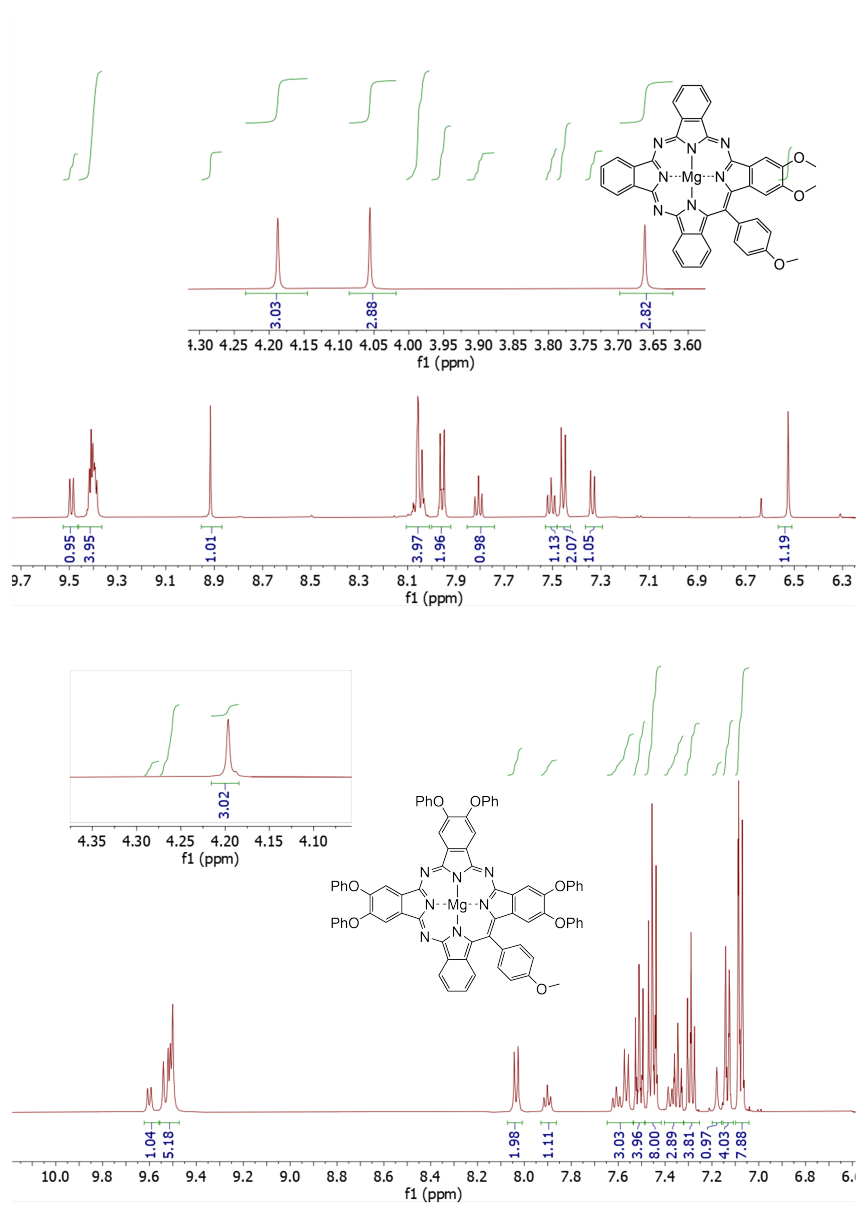


Figure 2.33: The  $^1\text{H}$  NMR spectra of 1:3 dimethoxy TBTAP (**53**) and 3:1 TBTAP (**54**)

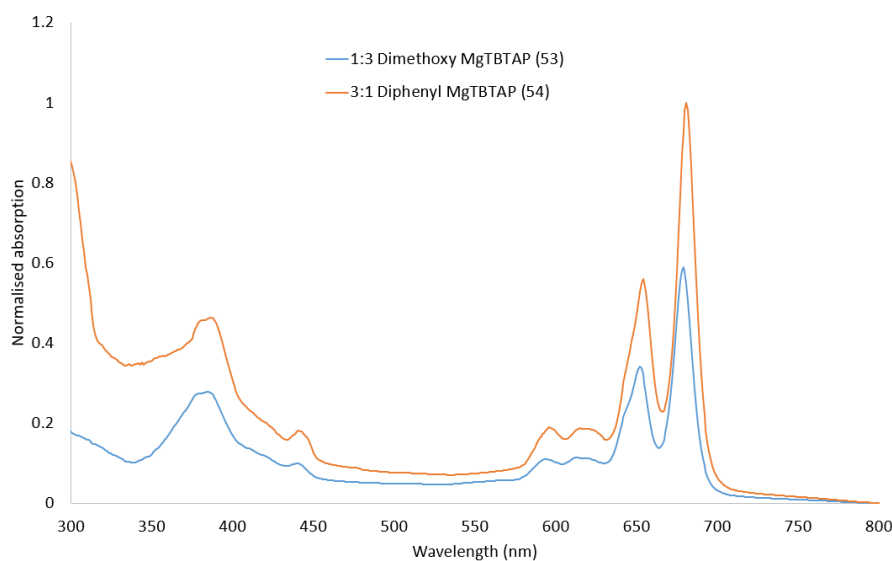


Figure 2.34: UV-Visible absorption spectra of MgTBTAPs (**53**) and (**54**).

The UV-Visible spectra (figure 2.35) are also concordant with MgTBTAPs, displaying similar absorption profiles to previously reported 3:1 MgTBTAPs.

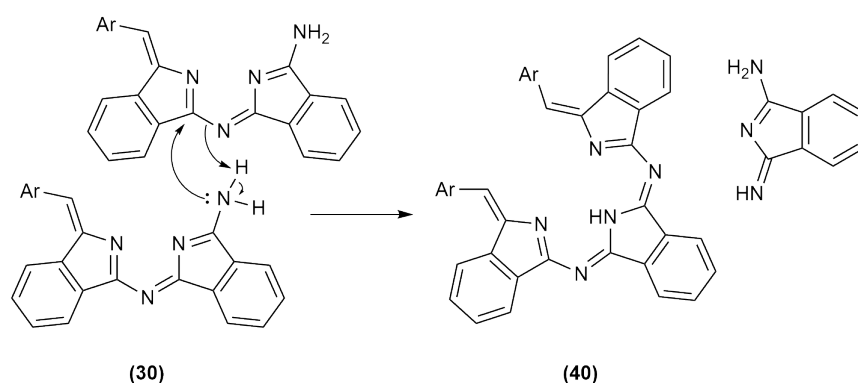
### 2.5.3 Discussion and mechanisms

With the unexpected result of the production of exclusively 3:1 MgTBTAPs from the previously designed pathway, new mechanisms must be proposed to explain this result. Clearly the reaction is not following the predicted and designed pathway, (**30**) and its derivatives may react via a number of pathways to produce different results. These pathways shall be proposed in this chapter and subsequently thermodynamically investigated via computational methods in a later chapter.

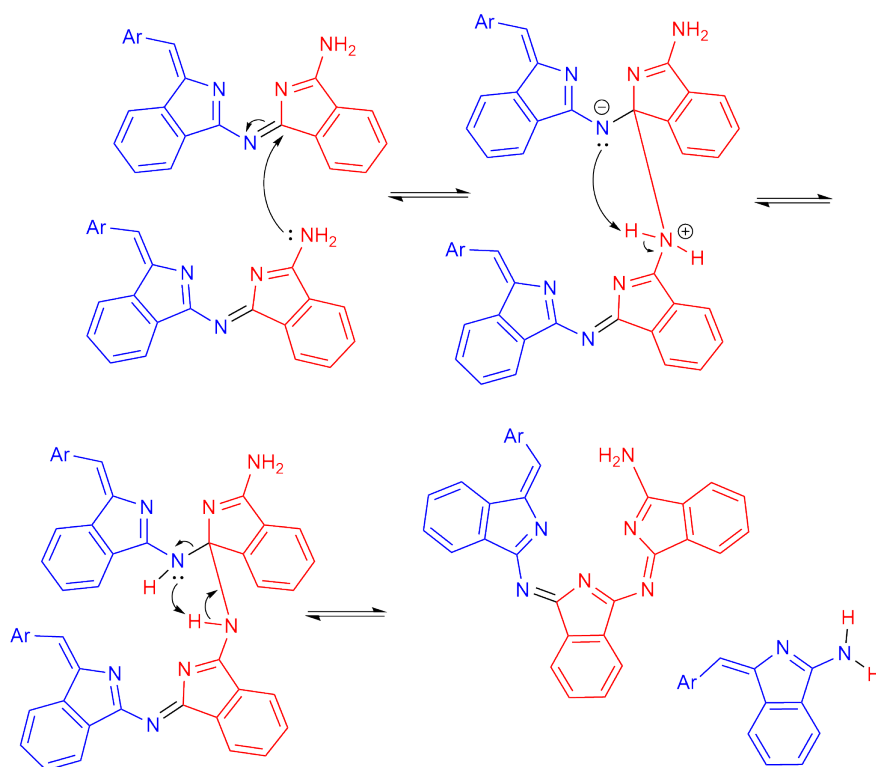
As previously described there is clear evidence two units of (**30**) may react to form the displacement product (**40**) with elimination of 1,3-diiminoisindoline as shown in scheme 2.58.

In order to form 3:1 TBTAPs from starting material (**30**) a reaction analogous to the above elimination must occur, but with elimination of aminoisindoline to build the 3:1 TBTAP in sequence (scheme 2.59 and 2.60). The formation of (**40**) at low temperature suggests that the pathway proposed below has higher thermodynamic or kinetic barriers.

The pathway is likely facilitated by coordination to magnesium, templating the macrocycle and reducing entropic and kinetic barriers. From this mechanistic investigation it is clear a complex but predictable set of equilibria exists between the dimer starting material and various other condensation/elimination products.



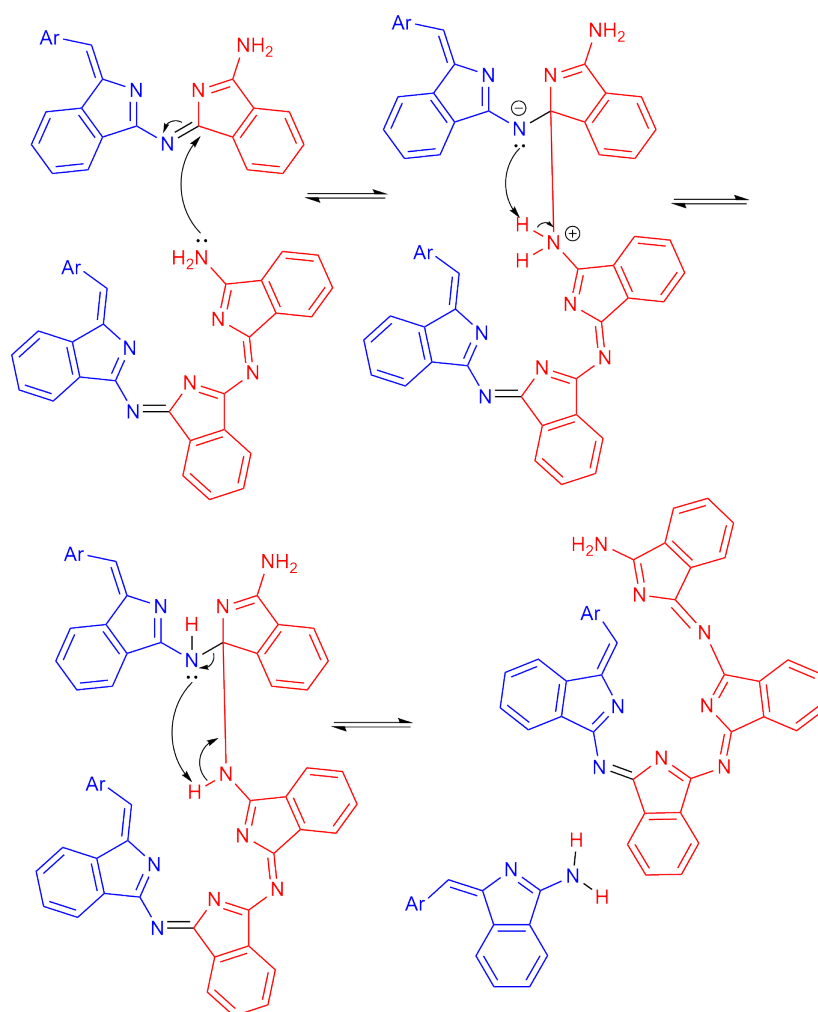
Scheme 2.58: The hypothesised mechanism for the formation of **(40)** with elimination of 1,3-diiminoisindoline.



Scheme 2.59: Hypothesised mechanism for the condensation of two units of **(30)** with elimination of aminoisindoline.

### MALDI-TOF analysis of aliquoted reaction samples.

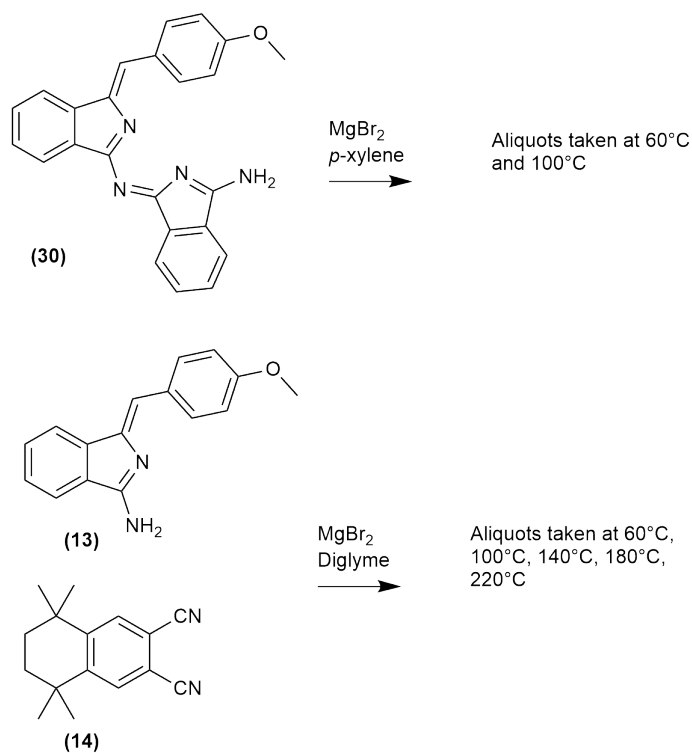
In order to obtain evidence to support the pathways proposed above, a series of reactions were performed at increasing temperatures with analysis by



Scheme 2.60: Hypothesised mechanism for the addition of one more unit of (30) to the 3 membered chain with elimination of aminoisindoline.

MALDI-TOF. It is expected analysis of these crude reaction mixtures will identify the intermediates proposed, as well as potentially revealing other species not yet considered by this work.

Both the pathway from condensation product **(30)**, and the conventional pathway from aminoisoindoline **(13)** and phthalonitrile **(14)** was examined as shown in scheme 2.61. The pathway from **(30)** was examined at low temperature, with reactions performed at 60°C and 100°C. The conventional pathway utilized a reaction with the temperature gradually increased and aliquots taken at 60°C, 100°C, 140°C, 180°C and 220°C.



Scheme 2.61: Pathways to be analysed by MALDI-TOF MS.

The first reaction examined was from intermediate **(30)**, aliquots were taken at 60°C and 100°C. Analysis by MALDI-TOF revealed very similar mixtures of compounds in both aliquots, and a representative spectrum is shown in figure 2.36.

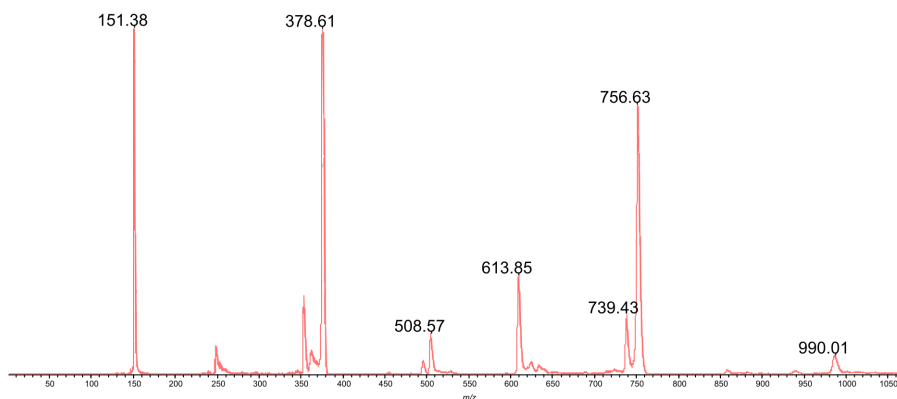


Figure 2.35: MALDI-TOF analysis of crude reaction mixtures from **(30)**.

### Evidence of 3:1 TBTAP formation pathway

Figure 2.35 shows several key peaks from the spectrum and the likely corresponding structures. The starting material **(30)** is clearly visible with a molecular ion peak visible at 378.61  $m/z$ . The presence of materials **(48)** and **(40)** at 508 and 611  $m/z$  respectively clearly support the mechanisms and reactivity proposed in schemes 2.61 and 2.62. A trace peak is clearly visible at 250  $m/z$ , corresponding to aminoisoindoline, and again corroborating the proposed mechanism to produce **(48)**.

The formation of **(40)** and **(48)** is supported by the likely presence of the structures identified in figure 2.38 (756.30  $m/z$ ). Both of these structures are condensation intermediates of two units of **(30)**, attacking at different positions to eliminate either 1,3-diiminoisoindoline or aminoisoindoline to form products **(40)** or **(48)** respectively. Unfortunately, due to the identical mass of both species it is impossible to elucidate if both are in fact present in the reaction. Additionally, the possibility of this peak being a [2M] MS dimer of **(30)** must be considered; a pure sample of **(30)** was also analysed by MALDI-TOF under the same laser power and a trace [2M] peak was observed. It is therefore impossible to conclude at this stage if the peak at 756  $m/z$  is in fact one or both of the proposed intermediates, or simply a [2M] dimer, or combination thereof.

From product **(48)**, another unit of **(30)** can be attacked, again with elimination of aminoisoindoline, to yield the 3:1 open chain TBTAP (scheme 2.60). This species has an exact mass of 634.20, with the intermediate species having an exact mass of 883.34. Unfortunately the intermediate was not observed by MALDI-TOF. There is a trace peak at 634  $m/z$  that could correspond to the 3:1 open chain intermediate (figure 2.36). This could be due to a number of reasons; firstly, MALDI-TOF is an ionising mass spectroscopy technique, ionisation of the proposed structure could result in fragmentation, and hence the species may not be observable. Secondly, once formed, the tetrameric species might rapidly undergo macrocyclization with elimination of ammonia to yield MgTBTAP; if

this is a highly favourable process the concentration of this species will be very low.

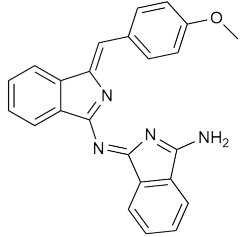
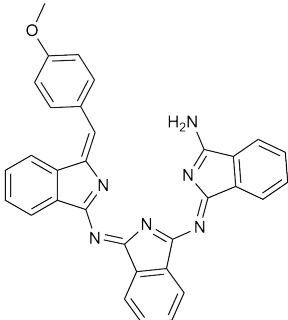
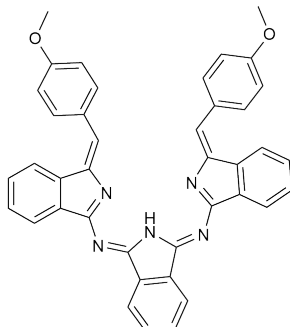
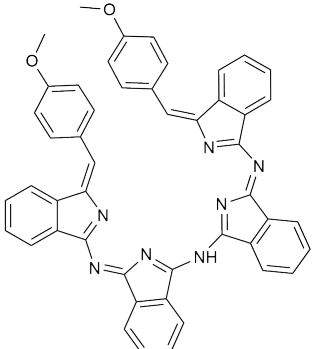
Structure	Exact Mass	Structure	Exact Mass
 <p>(30)</p>	378.15	 <p>(48)</p>	508.20
 <p>(40)</p>	611.23	 <p>(49)</p>	739.27

Figure 2.36: Table of masses observed and likely corresponding structures.

### Evidence of 2:2 TBTAP formation pathway

Another structure can be elucidated from the MALDI-TOF data, the 2+2 condensation product (**49**) of (**30**) with elimination of ammonia. The presence of this structure in the reaction mixture supports the pathways to 2:2 TBTAPs proposed in chapter 2 (schemes 2.13 - 15). Additionally, the peak at 990.01 m/z in the MALDI spectra corresponds to another possible structure, the condensation of (**30**) with (**40**), which with the elimination of aminoindoline, will again yield the 2+2 tetramer (**49**). While these species are observed in the reaction mixture, experimentally 2:2 TBTAPs are not produced utilizing substituted derivatives. This suggests TBTAP macrocyclization with elimination of ammonia is a more favourable process than with elimination of an aromatic fragment.

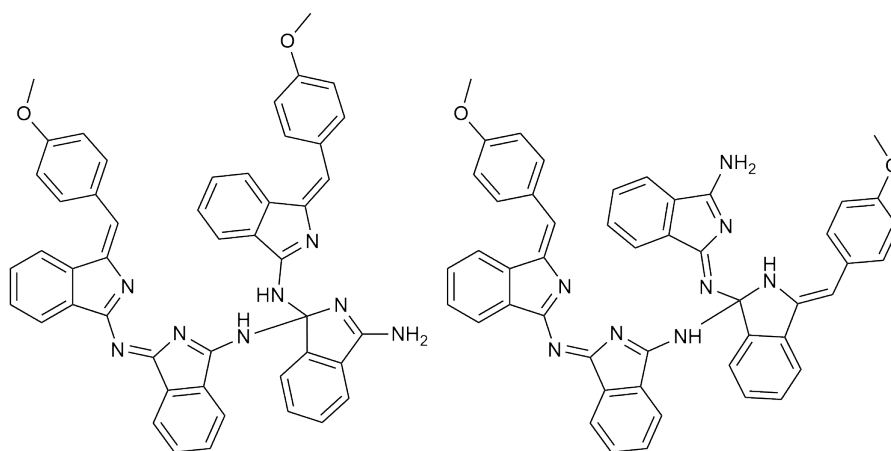


Figure 2.37: Structures of intermediates proposed in figures 2.92 and 2.93. These structures both have an exact mass of 756.30.

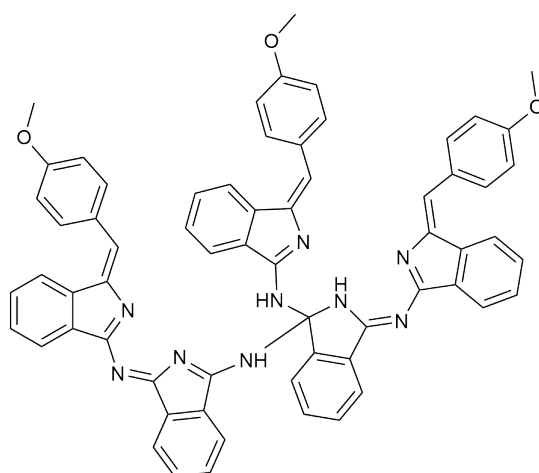


Figure 2.38: Structure of the hypothesised intermediate resulting from the condensation of **(30)** and **(40)**, with an exact mass of 989.38.

#### Evidence of 2:2 TBTAP formation pathway via aminoisoindoline (**13**) and phthalonitrile (**14**)

The MALDI-TOF spectra (figure 2.39) reveals a similar set of intermediates to the previous study, with aminoisoindoline (**13**) and phthalonitrile (**14**) (exact mass of 250.11 and 238.15 respectively) initially undergoing condensation to form product **(32)** (exact mass of 488). As expected, the trimeric product **(33)** is also present, further supporting the observed reactivity of **(32)**.

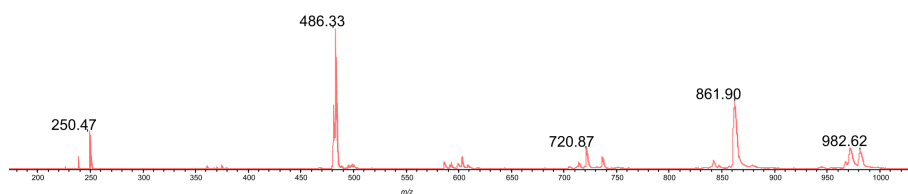


Figure 2.39: MALDI-TOF MS spectra of crude reaction mixture after 40 minutes at 220°C.

Structure	Exact Mass	Structure	Exact Mass
<p>(32)</p>	488.26	<p>(33)</p>	721.34

Figure 2.40: Table of masses observed and likely corresponding structures.

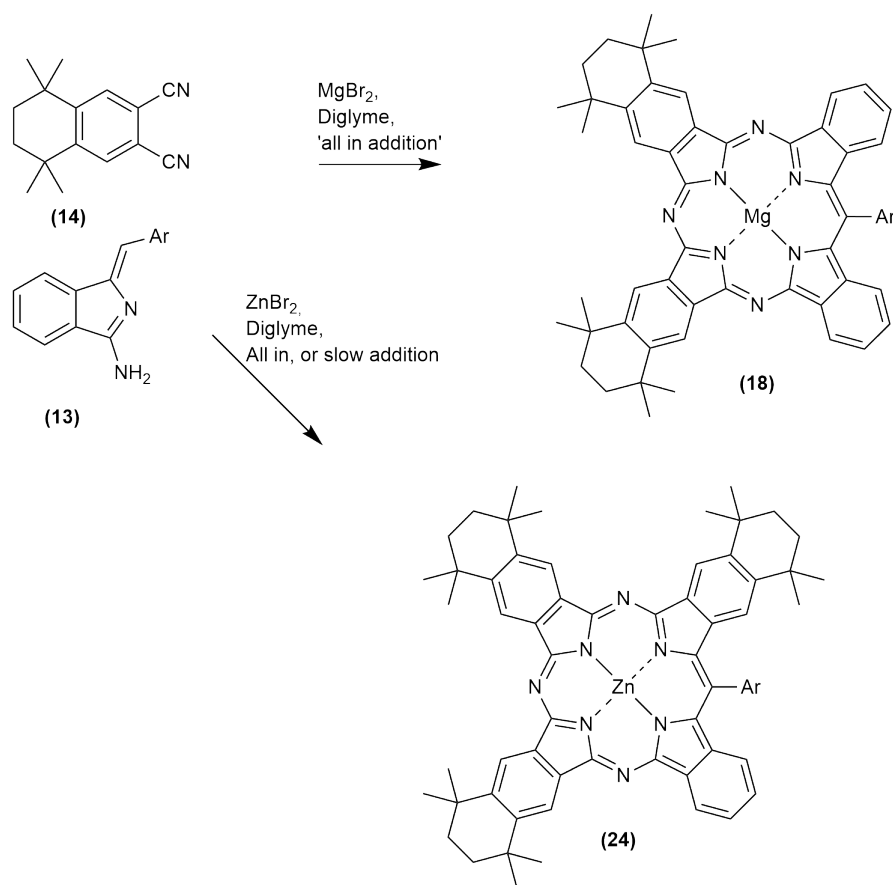
The 2:2 MgTBTAP product (**18**) is visible, with an exact mass of 862.41. Additionally the peak at approx 970 likely correspond to either a trace quantity of the 3:1 MgTBTAP product, or the open chain 3:1 TBTAP not coordinated to magnesium. Again, these results support previously observed reactivity and proposed mechanisms. The 2+2 condensation product was not observed by MALDI-TOF, again this may be due to fragmentation, however could also be due to the high reaction temperatures, and hence likely rapid macrocyclization to the 2:2 TBTAP product.

## 2.6 Conclusions and future work

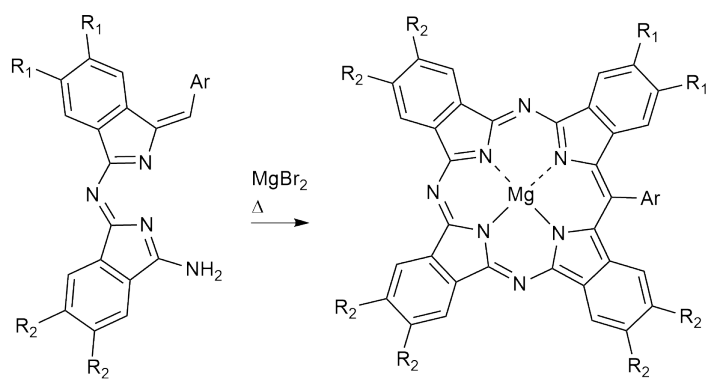
### 2.6.1 Synthetic methods for selective synthesis of 2:2 and 3:1 TBTAPs

This work has facilitated a range of new and exciting precursors, conditions and pathways suitable for the synthesis of complex TBTAP derivatives. Through the use of different starting materials and conditions, a range of substitution patterns may be controllably and selectively obtained in much higher yields. For a macrocyclic synthetic pathway the ability to selectively place substituents at various positions on a porphyrinoid is very rarely enjoyed with traditional synthesis methods and opens the door to new & highly specialised asymmetric systems.

Combined with the Cammidge groups previous work a diverse TBTAP ‘toolkit’ is now further expanded, with full control of *meso* substitution, peripheral substitution with symmetrical, 3:1 or 2:2 substitution patterns, and metal and axial substitution using traditional phthalocyanine chemistry methods. Schemes 2.62 and 2.63 below summarise new synthetic methodology for the selective synthesis of 2:2 and 3:1 TBTAPs from aminoisindoline and phthalonitrile.



Scheme 2.62: Selective synthesis of 2:2 substituted ABBA MgTBTAP and 3:1 ABBA ZnTBTAP systems.



Scheme 2.63: Synthesis of 3:1 ABBA TBTAP systems from derivatives of (30)

While control of 2:2 vs 3:1 TBTAP formation was obtained via the conventional pathways, new methodology from **(30)** and derivatives now allow the selective synthesis of 3:1 MgTBTAPs at much milder conditions and with far better yields, a summary of which is shown in scheme 2.64. Additionally, the parent structure MgTBTAP may be synthesised in much higher yields than previously obtained. It is assumed at this stage the synthesis of symmetrically substituted TBTAPs via symmetrical derivatives of **(30)** ( $R_1 = R_2$ ) will also be accessible in much better yields than with the previous pathway.

The selective and high yielding formation of 3:1 MgTBTAPs from **(30)** and derivatives, as shown in scheme 2.64, represents a new pathway to this class of compound previously observed in only trace - 1% yields with statistical condensations. These novel materials may now be prepared in 20-30 % yield, under much milder conditions than previous procedures. The use of *p*-xylene at reflux (140°C vs diglyme at 220°C) also has numerous advantages, the lower temperatures used should facilitate cleaner reactions with less side product formation or material decomposition. The lower temperatures also open the door to the synthesis of TBTAP derivatives containing more thermally sensitive functionalities that would otherwise degrade under the harsher reaction conditions.

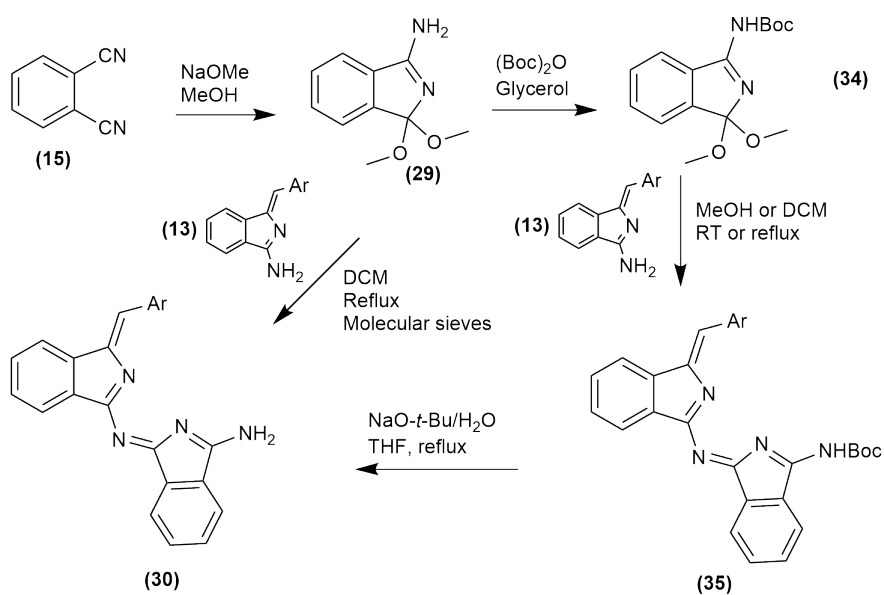
While the goal of stepwise construction of TBTAPs was not achieved due to the unpredicted reactivity of materials under the required conditions, the new materials and procedures developed offer useful insight and provide an exciting basis for future work. Stepwise construction may be afforded by various protection and activation methods, the use of better leaving groups to direct attack is of particular interest. This will be preliminarily explored *in silico* in a later chapter.

The new procedures afford TBTAPs selectively in much better yields with far milder conditions, this simplifies purification, improves efficiency, and may facilitate the synthesis of less thermally stable derivatives. In conclusion this work is a huge step towards fully controllable and high yielding synthesis of a suite of TBTAP derivatives.

## 2.6.2 Synthetic methods for stepwise assembly of macrocyclic building blocks

### Summary of synthetic methodology for **(30)** and derivatives.

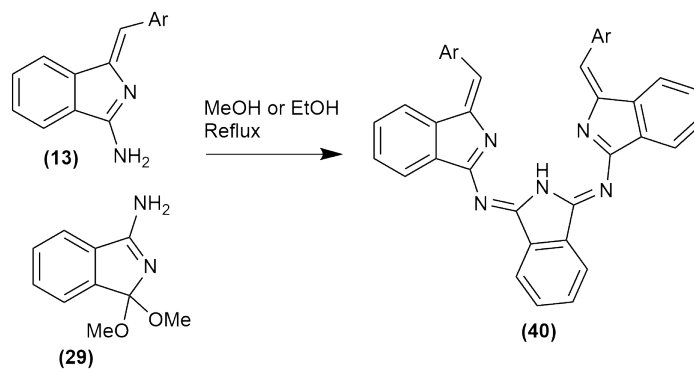
Shown in scheme 2.65 is a summary of the pathways developed in this work. These pathways are fully compatible with all derivatives utilised, however the full scope of possible derivatives has not yet been explored.



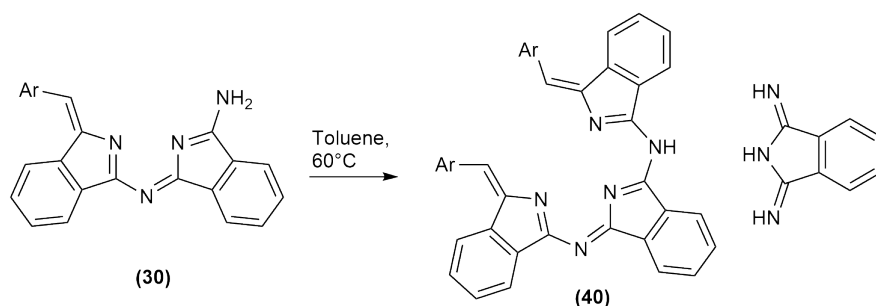
Scheme 2.64: Summary of synthetic methods to (30) and derivatives.

#### Summary of synthetic methodology for (40) and derivatives

While synthesised as a mostly unwanted side product in this work, (40) and its derivatives are also a novel and potentially highly useful macrocyclic building block.



Scheme 2.65: Formation of (40) and derivatives from aminoisindolines and dimethoxyindolines.



Scheme 2.66: Scheme for the formation of **(40)** with elimination of 1,3-diiminoisoindoline.

### 2.6.3 Future work

#### Expansion of derivatives via conventional selective pathways

The range of derivatives utilised with the selective 2:2 and 3:1 pathways presented in schemes 2.62 and 2.63 should be expanded in future studies to confirm the result is reliable and consistent, regardless of sterics or electronics at the peripheral positions. This work is limited in that it has only utilised tetrahydrotetramethylnaphthyl derivatives (**14**), this derivative was chosen as it gave a mixture of both 2:2 and 3:1 TBTAPs in previous studies. With the original study producing a mixture of both products, control has now been obtained that should likely carry over throughout a range of derivatives.

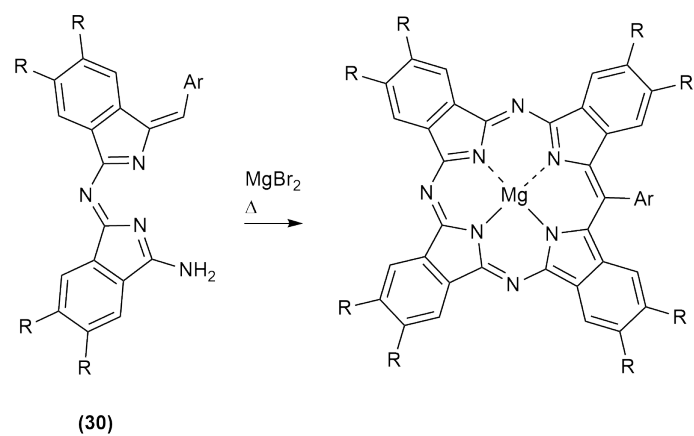
#### Expansion of 3:1 derivatives via **(30)** and related materials

The work throughout section 2.5.2 (scheme 2.64) explored a simple selection of derivatives; again, this may be further expanded by future work to encompass a wider range of functionalities, producing a new selection of novel 3:1 MgTBTAPs. Symmetrical derivatives should be explored, producing symmetrical TBTAPs (scheme 2.68). While many of these symmetrical, peripherally substituted, TBTAPs are not novel compounds, the new methodology may afford them in much higher yields.

The methodology may also be further expanded to include derivatives where neither  $R_1$  or  $R_2 = H$  (scheme 2.64). This would facilitate a novel new series of 3:1 substituted MgTBTAPs.

#### Activation or protection to facilitate selective 2:2 formation

As described in section 2.5, **(30)** was designed and expected to undergo a homocondensation with elimination of ammonia to yield 2:2 TBTAPs. Instead, 3:1 TBTAPs were obtained as described by schemes 2.56 and 2.57. This is due to **(30)** possessing 3 positions vulnerable to nucleophilic attack, shown in figure 2.42 and marked with \*. Attack by the nucleophilic amine of another unit of **(30)** at position C would yield the targeted 2:2 TBTAP, but as shown in section 2.5.3, attack at positions A or B occurs readily.



Scheme 2.67: Scheme for the synthesis of symmetrical TBTAPs from symmetrical derivatives of (30).

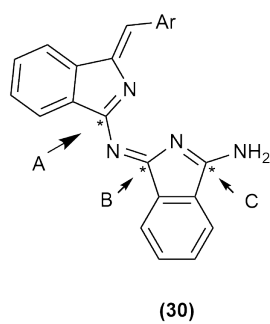
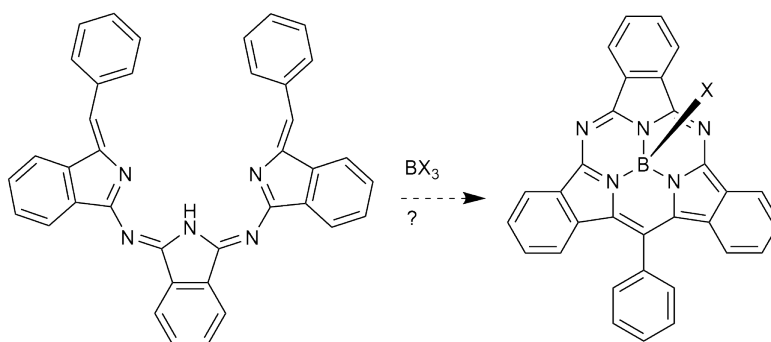


Figure 2.41: Positions susceptible to nucleophilic attack.

A potential method to circumvent this would be to activate the amine on one equivalent of (30) as a leaving group, hence directing attack from the amine of one unit of (30) towards position C on the activated derivative.

### Potential application of (40) and derivatives

While (40) was obtained as an undesired side product in these studies, there is clear potential application for these materials. In chapter 3 their potential as a SubTBDAP precursor shall be explored.



Scheme 2.68: Potential macrocyclization of trimeric side products to SubTB-DAPs.

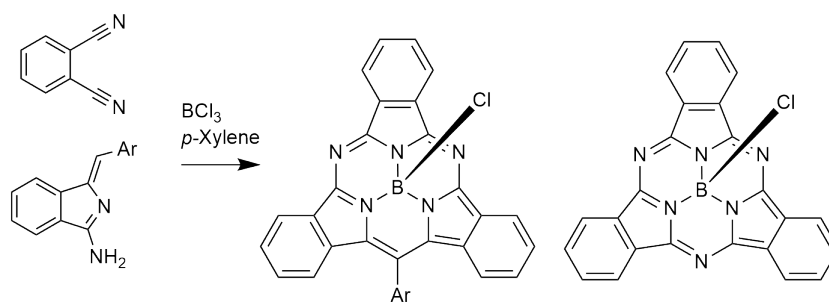
## Chapter 3

# Mechanistic investigations into SubTBDAP formation

### 3.1 Introduction

With previous work successfully investigating and diversifying synthetic routes to TBTAPs, and with SubTBDAP synthesis utilising the same aminoisoindoline precursors, these new methodologies were applied to SubTBDAP synthesis in an attempt to gain higher yields and better selectivity and diversity of products.

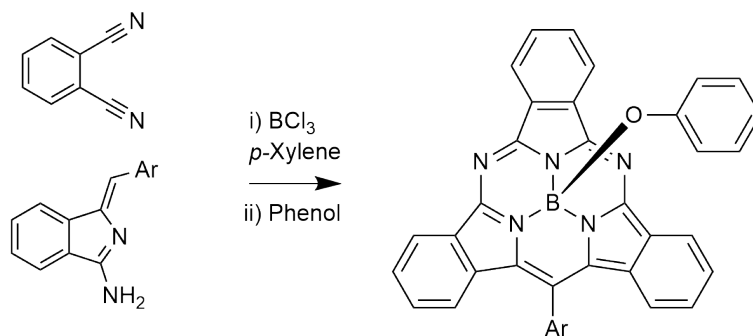
As previously discussed SubTBDAPs were first successfully synthesised in 2015 by the Cammidge group, utilising the reaction of aminoisoindoline and phthalonitrile with boron trichloride in xylene.<sup>30</sup> These are the optimum conditions for SubPc-Cl formation as determined by earlier studies.<sup>128</sup> This reaction, as expected, produced a significant amount of the homo-macrocyclization product SubPc-Cl, as well as the hybrid macrocyclic SubTBDAP-Cl product (scheme 3.1).



Scheme 3.1: Synthesis of SubPc-Cl and SubTBDAP-Cl from aminoisoindoline and phthalonitrile under optimum SubPc-Cl formation conditions.

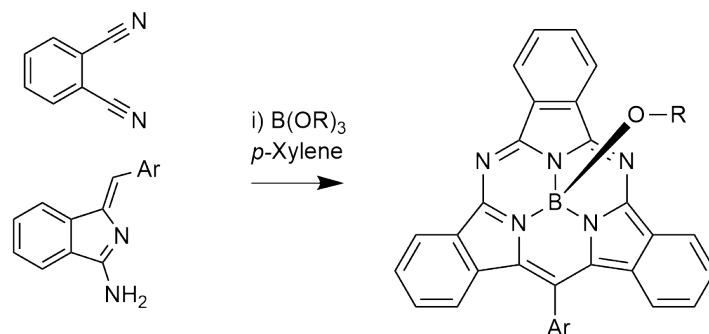
While the original studies identified the formation of SubTBDAP-Cl via MALDI-TOF evidence, the instability of the axial chloride ligand meant at-

tempts to isolate the new macrocycle resulted in hydrolysis or other displacements, giving a mixture of difficult to separate products.<sup>30</sup> This trend is well observed in SubPc chemistry, with water or alcohols readily displacing axial halides. Substitution with aliphatic or aromatic alcohols produce species with much better axial stability, eliminating purification issues such as hydrolysis on silica gel etc.<sup>128–130</sup>



Scheme 3.2: Synthesis of SubPc-OPh via addition of phenol to the reaction mixture.

With adjustments to the SubTBDAP procedure more stable and easily isolable derivatives can be synthesised. Utilizing either  $\text{BCl}_3$  followed by addition of an alcohol, commonly phenol, to displace the chloride (scheme 3.2). Or directly, by using a borate derivative ( $\text{B(OR)}_3$ ) as the templating and macrocyclization agent (scheme 3.3). These modifications were used to produce a range of axially and meso substituted SubTBDAPs, utilising different borates and aminoisindolines respectively.<sup>30</sup>



Scheme 3.3: Synthesis of SubPc-OR derivatives from borates, R = OMe, OPh, OBu, *Oi*-Pr.

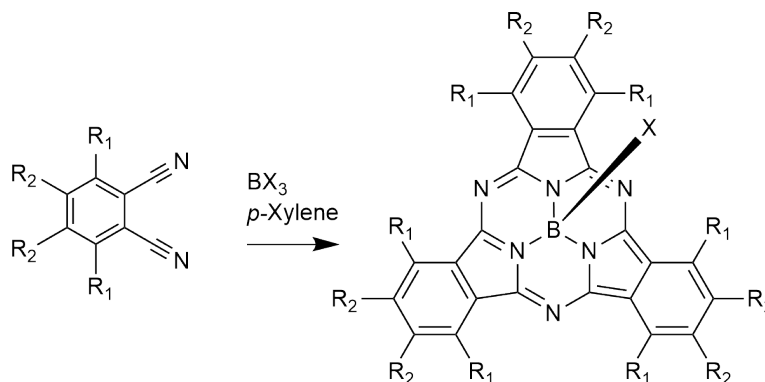
Exploration of the literature reveals the derivatives produced by the Cambridge group in 2015 are still the only published examples of SubTBDAPs since

their first synthesis. As with the various porphyrinoid and hybrid macrocycles previously explored; it is anticipated that the further functionalisation of SubTBDAPs will allow for more complex, modified, and specifically tuned systems to be investigated. The ability to produce SubTBDAP derivatives functionalised at the peripheral and non-peripheral ring positions, as well as *meso* and apical functionalisation will reveal the full scope of this species properties and adaptability.

## 3.2 Aims

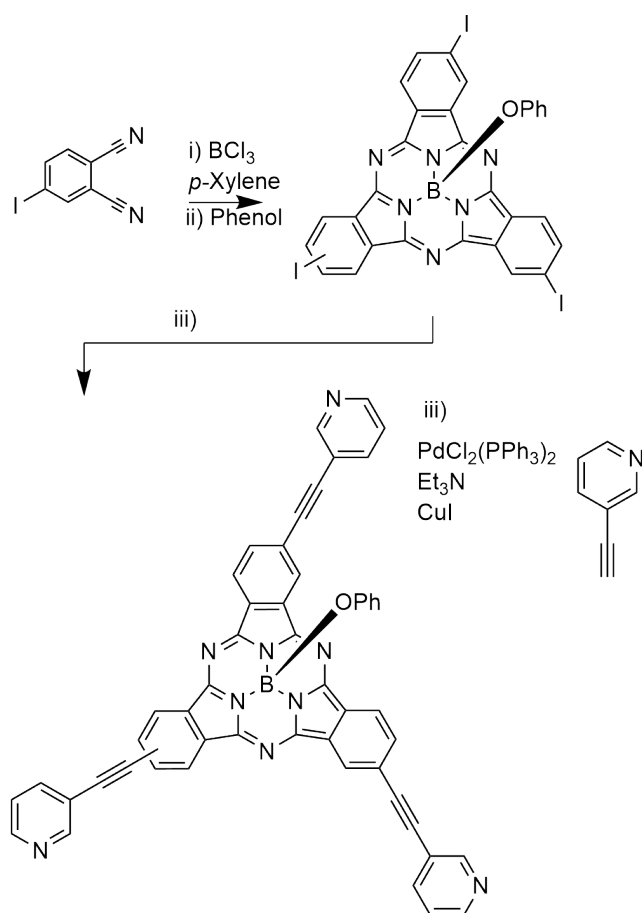
### 3.2.1 Peripherally and non-peripherally substituted SubTBDAPs via conventional pathways

With no previous exploration of peripherally and non-peripherally substituted SubTBDAPs being undertaken, part of this work aims to explore these functionalisation options. Phthalocyanine, TBTAP, and SubPc synthesis from phthalonitriles easily allows insertion of different functional groups via the use of phthalonitrile derivatives. SubPc synthesis appears versatile in the ability to include a wide range of electronically and sterically demanding fragments.



Scheme 3.4: Synthesis of symmetrical peripherally ( $R_2$ ) and non-peripherally ( $R_1$ ) substituted SubPcs.

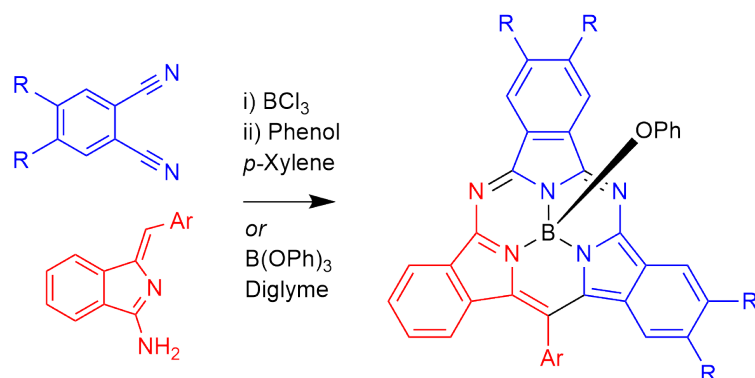
Scheme 3.4 shows the synthesis of substituted SubPcs from symmetrical phthalonitriles. Mono-substituted phthalonitriles may also be used. Functionalisation at these positions opens a range of synthetic options, as touched on in earlier discussions. Groups may be used to directly tune the properties of the macrocycle, or be used for incorporation to, or the formation of, larger systems, an example of which is shown below in scheme 3.5.



Scheme 3.5: An example of a tri-substituted SubPc, designed as a nanoparticle encapsulant during previous work in the Cammidge group. The ability to include easily displaceable halide substituents at the peripheral positions opens up the possibility of palladium catalysed cross-coupling reactions to further functionalise the macrocycle.

This part of the work will use phthalonitrile derivatives synthesised in the previous chapter to attempt synthesis of substituted SubTBDAPs via the conventional aminoisoindoline pathway as outlined below. As with TBTAP synthesis, the assumption at this stage is that the macrocyclization process is initiated by aminoisoindoline, resulting in the substitution pattern shown in scheme 3.6.

While this substitution pattern is assumed at this stage, confirming the structure of the product or products isolated from the reaction will provide valuable mechanistic insight into the series of steps that produce SubTBDAPs.



Scheme 3.6: Formation of substituted SubTBDAPs, the symmetrical homo-macrocyclization SubPc products are also expected to be produced as side products.

### 3.2.2 SubTBDAP synthesis from newly developed species

As discussed in the previous chapter, during the initial experiments that successfully first synthesised SubTBDAPs, an interesting potential intermediate was identified and isolated from the reaction mixture. This structure was characterised by x-ray crystallography and determined to be the condensation ‘trimer’ of phthalonitrile with 2 equivalents of aminoisoindoline, the structure of which is shown in figure 3.1.<sup>64</sup>

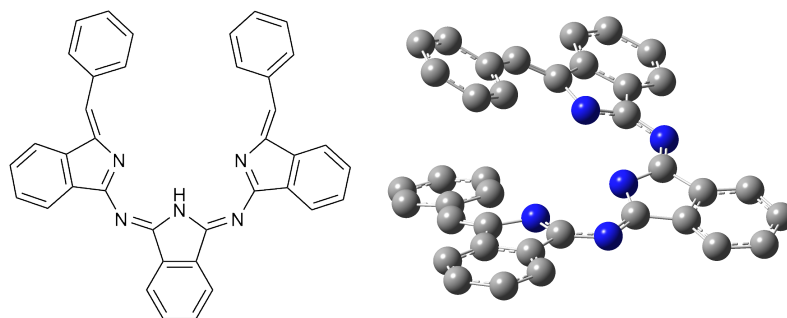
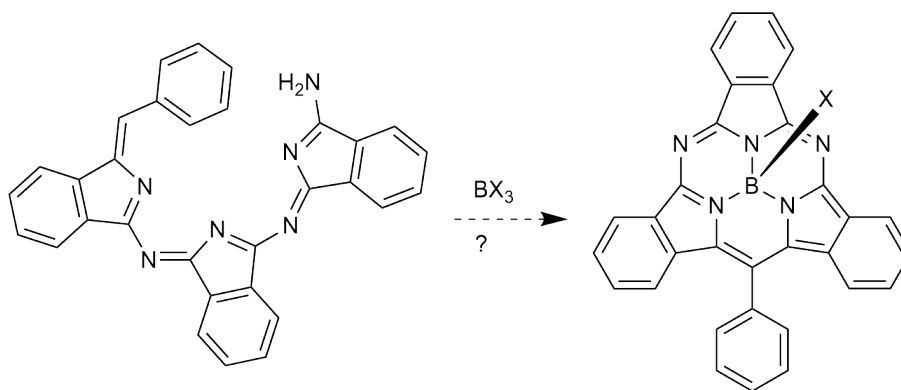


Figure 3.1: The ‘trimer’ condensation product of phthalonitrile and aminoisoindoline previously isolated and characterised.<sup>64</sup>

The right hand optimised structure above shows the planar distorted helical like conformation of the trimer, with both alkene bonds adopting the Z geometry the structure distorts to accommodate the overlapping phenyl fragments. The potential of this structure to macrocyclize to a SubTBDAP with elimination of an aromatic fragment is clear. The initial investigations reported that the concentration of the trimer appeared to decrease throughout the course of the

reaction, however it is unclear at this time if the structure is indeed a precursor to macrocyclization, or simply a condensation side product. With the methodology previously developed this trimer, as well as related species, can be synthesised selectively and subjected to the macrocyclization reaction conditions.

An alternative trimeric structure could also be a precursor to SubTBDAP formation, the linear condensation of two units of phthalonitrile by aminoisoindoline, shown in scheme 3.7. Rather than the elimination of an aromatic fragment to yield SubTBDAP, this precursor would eliminate ammonia on macrocyclization. This structure may also be synthesised via new methods from the previous chapter. The ability to selectively synthesise these potential TBDAPs precursors means that if they can be successfully macrocyclized to SubTBDAPs, the substitution pattern can be controlled.



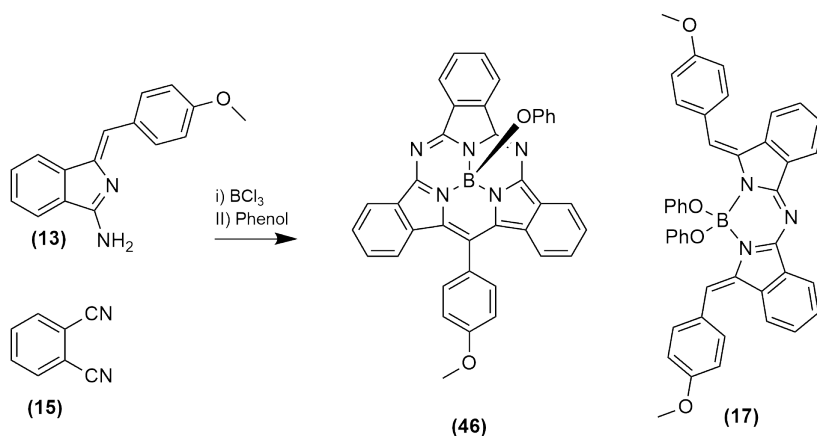
Scheme 3.7: A potential SubTBDAP formation pathway.

## 3.3 Results and discussion

### 3.3.1 Repeat of previously optimised procedures

Investigations began with repeating the previously optimised and published SubTBDAP synthesis. As discussed in the previous chapter, the required aminoisoindoline starting materials were synthesised via the previously developed pathways in good yields with easy purification. With these precursors available initial attempts at the SubTBDAP synthesis were undertaken.

The first attempts utilizing  $\text{BCl}_3$  were unsuccessful in producing isolable SubTBDAP. Evidence of SubTBDAP formation was visible on TLC, with the formation of a brightly coloured pink spot with strong yellow fluorescence, however clearly in very low yield, with a complex mixture of degraded material and side products. The photoinstability of SubPcs is well known, with hybrid counterparts displaying generally reduced photostability. Ensuring light was blocked from the reaction vessel and avoiding direct sunlight or use of fluorescent lights during workup and isolation was the first variable to be explored in achieving a reliable synthesis.



Scheme 3.8: Scheme for SubTBDAP formation

These modifications appeared to have no effect on the yield of macrocyclic products, with azaBODIPY being the major product despite several repeats of the reaction (scheme 3.8). As with SubPcs, it was discovered during initial reaction screening that small changes to reagent ratios can have a significant effect on the reaction outcome. Results can vary from decomposed tars to azaBODIPYs and SubPcs to SubTBDAPs.<sup>30</sup> With azaBODIPYs comprising the major product it was decided to increase the equivalents of phthalonitrile in an attempt to avoid homocondensation of the aminoisoindoline. Pre-heating of the oil bath used for the reaction was also explored, with the hypothesis that a slow increase to the reaction temperature could promote the homocondensation of aminoisoindoline before the macrocyclization process could initiate.

Despite these further modifications azaBODIPY remained the major product, with small quantities of SubPc and suspected SubTBDAP visible on TLC. These results prompted investigating the starting materials and reagents used. The aminoisoindoline had been synthesised and characterised as the correct material, phthalonitrile was recrystallised from a commercial source as previous studies had obtained greater yields with recrystallised phthalonitrile.<sup>30</sup> It was finally determined that the commercially obtained  $\text{BCl}_3$  solution had hydrolysed significantly while stored.  $\text{B(OH)}_3$  has been investigated and deemed unsuitable for use in SubPc and SubTBDAP synthesis.<sup>64</sup> With a new source of  $\text{BCl}_3$  the reaction was repeated and successfully produced the desired SubTBDAP and SubPc side product in similar yields to previously reported reactions. It is therefore clear the macrocyclization is very sensitive to water or hydrolysis of the  $\text{BCl}_3$ .

The reaction was also performed using  $\text{B(OPh)}_3$  as the borate source, and again gave the desired products with slightly reduced yield. Once again the  $\text{B(OPh)}_3$  has been in storage for some time, inevitably resulting in some hydrolysis to  $\text{B(OH)}_3$ , however still yielded an isolable quantity of SubTBDAP in this case.

### Characterisation and properties of SubTBDAP-OPh

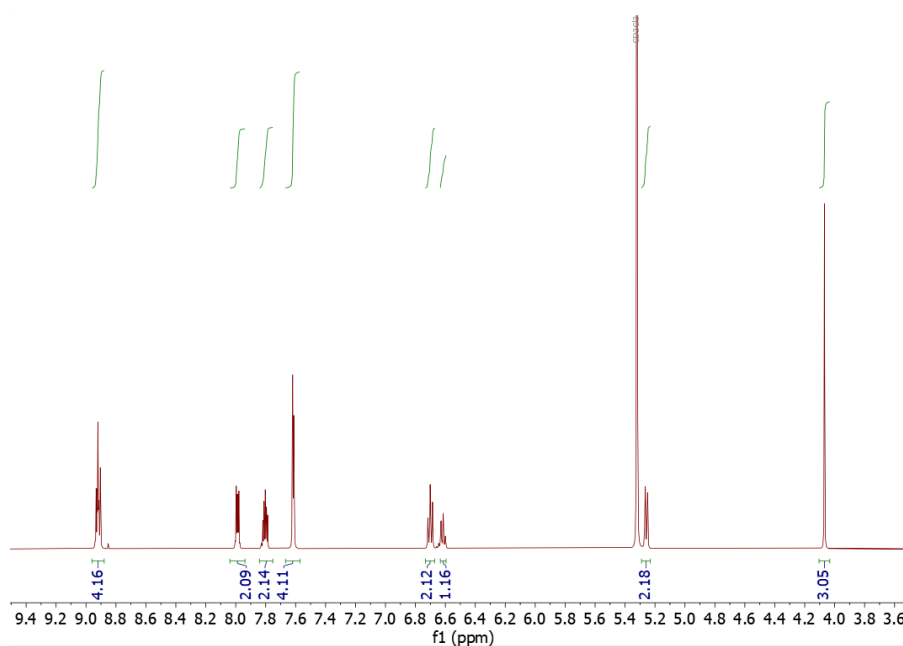


Figure 3.2:  $^1\text{H}$  NMR spectra of SubTBDAP-OPh (**46**).

The above spectra is concordant with both literature data and the structure of SubTBDAP (**46**). While the axial phenol fragment is visible on NMR, the

*ortho* and *meta* signals of the *meso* methoxytolyl fragment are not observable without the use of variable temperature NMR due to fast rotation of the *meso* substituent. The methoxy signal remains observable however, due to the lack of rotation at the *para* position.

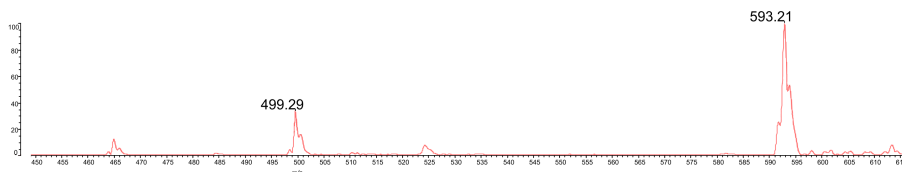
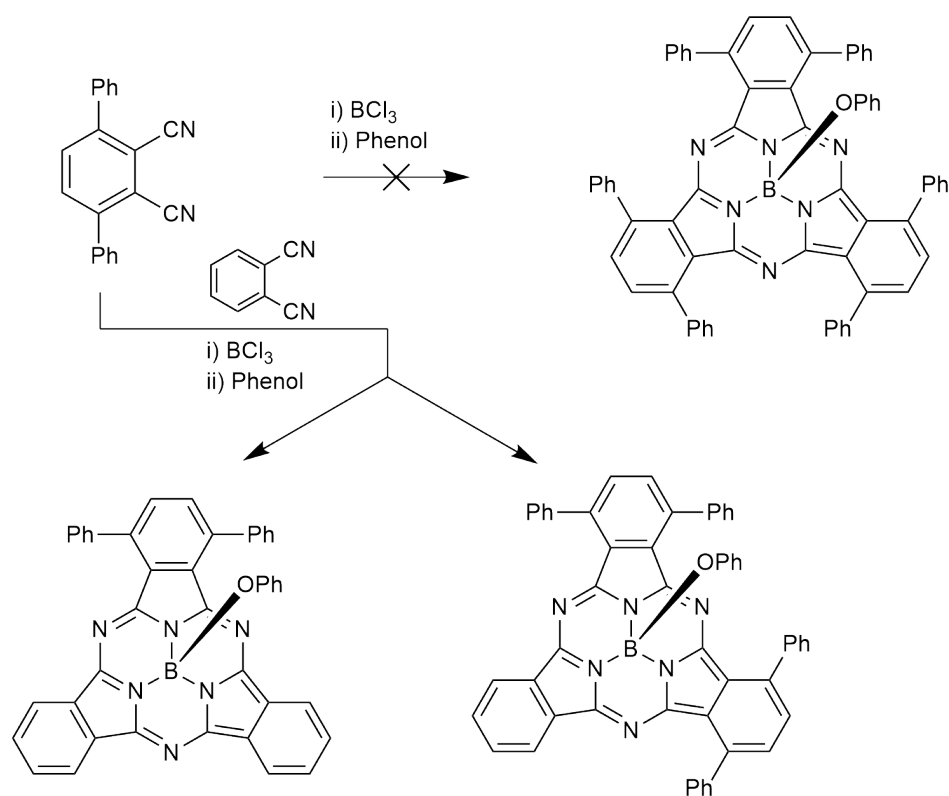


Figure 3.3: MALDI-TOF spectra of SubTBDAP (**46**)

Again the MALDI-TOF spectra is concordant with the structure of SubTBDAP (**46**), with peaks visible for the parent ion (593  $m/z$ ), as well as the [SubTBDAP-B]<sup>+</sup> fragment at 500  $m/z$ . UV-Vis data was also concordant with previous literature data (figure 3.5).

### 3.3.2 Attempted synthesis of non-peripherally substituted SubTBDAPs via conventional pathways

After initial repeats of the SubTBDAP procedure proved successful with fresh boron sources and strict anhydrous conditions, investigations could move forward with attempting to include peripheral and non-peripheral functionalisation in SubTBDAP synthesis. Following previous work from UEA developing pathways to 3,6 substituted aryl phthalonitriles,<sup>131,132</sup> and the subsequent synthesis of di and tetraphenyl SubPcs (scheme 3.9), non-peripheral phenyl SubTBDAPs were targeted. Previous SubPc synthetic investigations had revealed significantly reducing yield with further non-peripheral substitution, and hence steric strain, and no macrocyclic product for the symmetrical hexaphenyl SubPc. It is therefore anticipated the targeted tetraphenyl SubTBDAP may be inaccessible, the diphenyl SubTBDAP was therefore also targeted as it should be a significantly less sterically strained system.

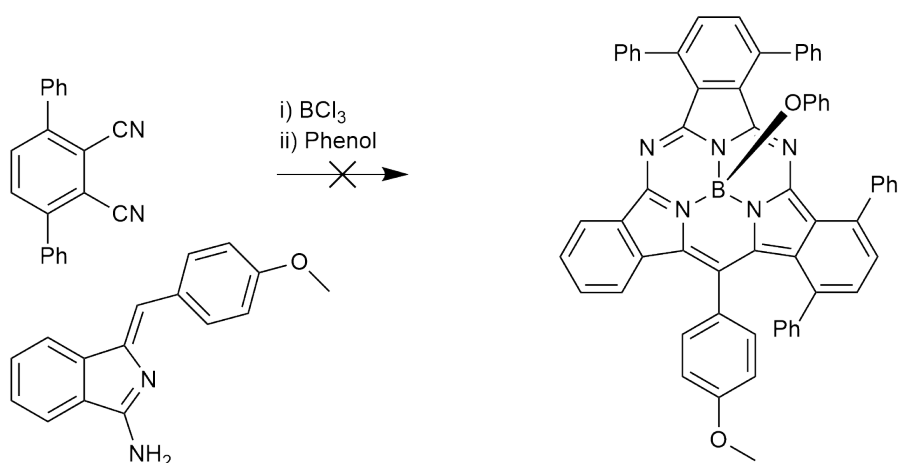


Scheme 3.9: Non-peripheral phenyl substituted SubPc synthesis. The hexaphenyl SubPc was not thermally/kinetically accessible, tetraphenyl SubPc was synthesised in poor yield, and diphenyl SubPc was synthesised in good yield. This clearly shows the trend of significantly decreased yield as steric crowding increases.

### Tetraphenyl-SubTBDAP

Scheme 3.10 shows a pathway for the first attempted non-peripherally substituted SubTBDAP synthesis, utilizing 3,6-diphenylphthalonitrile and aminoisoindoline. The expected product is the tetraphenyl SubTBDAP, formed from linear addition of 2 units of phthalonitrile to one equivalent of aminoisoindoline. The formation of diphenyl SubTBDAP would indicate macrocyclization via the elimination of an aromatic fragment as outlined in figure 3.1.

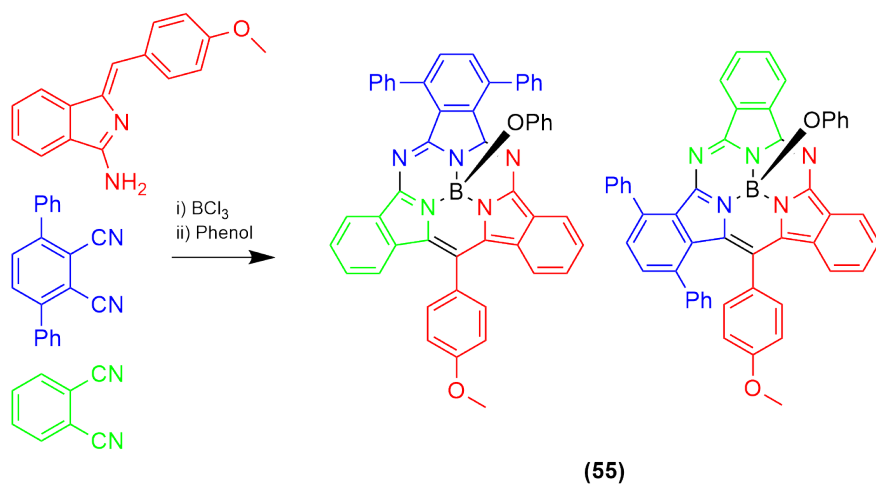
Attempts via both the  $\text{BCl}_3$  and  $\text{B(OPh)}_3$  mediated pathways did not yield any macrocyclic products, with azaBODIPY formation and decomposed material visible on TLC. This is likely due to the very high degree of steric crowding present in the product, making the macrocyclization transition state inaccessible. Higher boiling point solvents may overcome this, however, would also likely result in increased decomposition also, lowering yield.



Scheme 3.10: Scheme and proposed product for this SubTBDAP reaction.

### Diphenyl-SubTBDAP

With the previous synthesis unsuccessful due to steric factors, the less strained diphenyl SubTBDAP was targeted. Unfortunately, in order to achieve this, a mixed macrocyclization between aminoisoindoline, phthalonitrile, and 3,6-diphenylphthalonitrile is required (scheme 3.11). This is likely to produce a larger mixture of products, and a lower yield of the target diphenyl SubTBDAP.



Scheme 3.11: Scheme for the formation of diphenyl SubTBDAP, the expected side products are SubTBDAP, SubPc, diphenyl SubPc, and tetraphenyl SubPc. The two possible regioisomers of diphenyl SubTBDAP are also shown.

It was anticipated two different diphenyl SubTBDAPs may be produced, as shown in scheme 3.11. It is likely only the left hand structure will be produced

however, due to the higher strain associated with having non-peripheral phenyl groups interacting with the *meso*-phenyl group, significantly raising the energy of both the final structure, and macrocyclization transition state.

Attempts at the reaction appeared promising, with multiple pink fluorescent spots visible on TLC, 2 of which possessed the bright yellow fluorescence typically associated with SubTBDAPs. MALDI-TOF analysis of the reaction mixture revealed the presence of SubPc, SubTBDAP, and the target diphenyl SubTBDAP. It appeared the yield for the diphenyl SubTBDAP was significantly lower than for the SubPc and SubTBDAP side products, with a yield estimated at approximately 1 mg from a typical scale reaction. While separation was achieved on TLC, less success was achieved with prep scale silica gel column chromatography, with the mixture of SubTBDAP and diphenyl SubTBDAP proving very difficult to separate. While identified by MALDI-TOF as the correct product, not enough could be isolated successfully to facilitate recrystallisation and thus reliable NMR & UV-Vis characterisation. This additionally means while the product was identified as diphenyl-SubTBDAP (**55**), the regioisomer produced could not be elucidated.

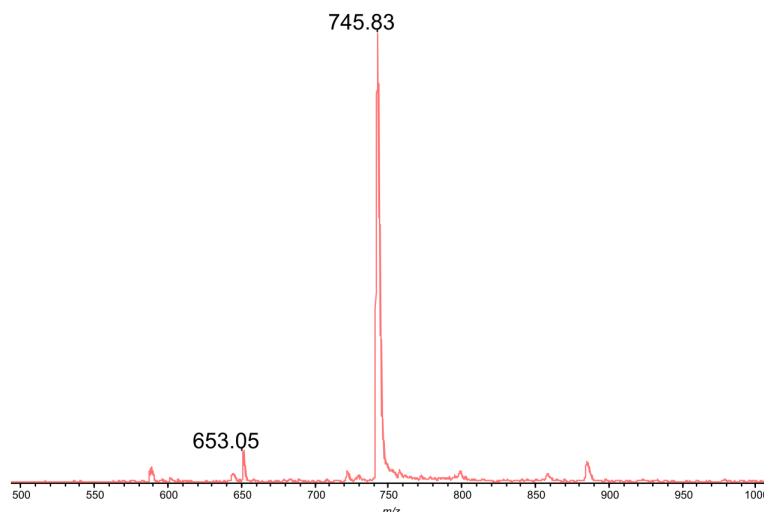
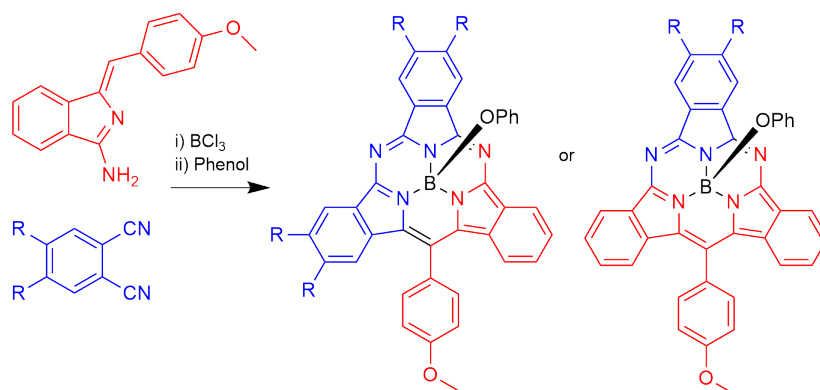


Figure 3.4: MALDI-TOF spectra for diphenyl-SubTBDAP (**55**). Again the parent ion (745  $m/z$ ) and [SubTBDAP-B]<sup>+</sup> (652  $m/z$ ) peaks are visible.

**Conclusions** It appears from these attempted syntheses the inclusion of large non-peripheral groups in SubTBDAPs results in significantly reduced yield, with no reactions producing significant, isolable yields. This can likely be attributed to higher energy transition states and intermediates associated with the formation of non-peripherally substituted porphyrinoids, therefore reducing the rate of reaction along this pathway, and promoting the formation of less sterically demanding SubPcs.

### 3.3.3 Peripherally substituted SubTBDAPs via conventional pathways

With attempts at non-peripherally substituted SubTBDAPs not producing any significant yields due to steric factors, it was decided to pursue the synthesis of sterically non-demanding peripherally substituted SubTBDAPs (scheme 3.12). As well as expanding functionalisation options for SubTBDAPs, these experiments, if successful, will provide crucial mechanistic insight through the product formed.

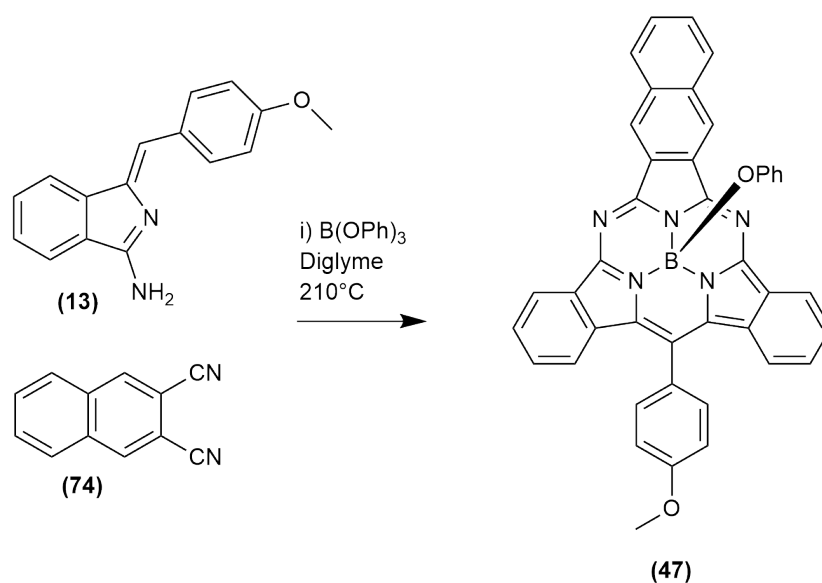


Scheme 3.12: Scheme for the synthesis of peripherally substituted SubTBDAPs.

Two possible SubTBDAP macrocyclization precursors/pathways were presented in figures 3.1 and scheme 3.7; the formation of di-substituted SubTBDAPs would support a pathway via the trimeric species presented in figure 3.1, and the formation of tetra-substituted SubTBDAPs would support the pathway presented in scheme 3.7. These mechanistic insights will be critical in designing SubTBDAP synthesis from pre assembled intermediates.

It is anticipated synthesising these SubTBDAPs should be much more straightforward, with sterics not preventing macrocyclization of tetra substituted derivatives a single phthalonitrile can be used, reducing the amount of possible macrocyclic products to 3, simplifying purification and improving yield of the target material.

The first attempted reaction utilised unsubstituted aminoisindoline (**13**) with 1,2-dicyanonaphthalene under the standard conditions previously reported.<sup>64</sup> The reaction appeared promising, with a pink spot possessing the characteristic yellow fluorescence visible by TLC analysis. After the reaction period the crude residue was subject to the standard work up procedure and an isolable, but significantly lower than previously reported, yield of bright pink material obtained via sequential column chromatography. The reaction is summarised by scheme 3.13.



Scheme 3.13: Successful synthesis of naphthyl substituted SubTBDAP (47).

Both the isolated product and crude mixture was characterised by MALDI-TOF and the pure product by UV-Vis spectroscopy (figure 3.5), which revealed the presence of the mono-substituted naphthyl SubTBDAP shown above in scheme 3.13. Notably, the utilisation of  $B(OPh)_3$  resulted in this being the sole macrocyclic product formed. It was reported previously that borates are not reactive enough to initiate SubPc macrocyclization under these reaction conditions, reducing unwanted side products.<sup>64</sup>

The isolated product was also analysed by  $^1H$  NMR, which revealed a  $C_s$  symmetric structure, confirming the substitution pattern shown above. This result is not only the first example of a peripherally substituted SubTBDAP with a procedure that selectively produces the  $C_s$  symmetric regioisomer, but also provides the mechanistic insight required to develop stepwise pathways.

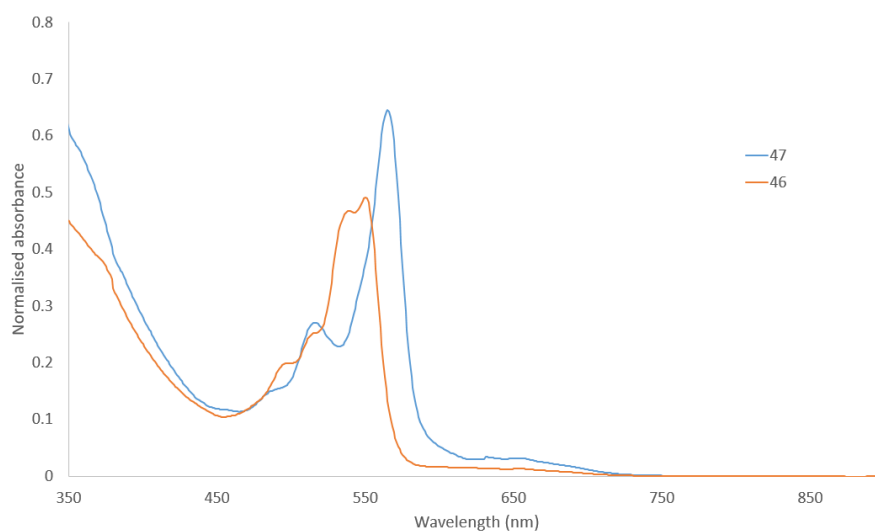


Figure 3.5: UV-Vis spectra of SubTBDAP-OPh (**46**) and naphthyl substituted SubTBDAP-OPh (**47**).

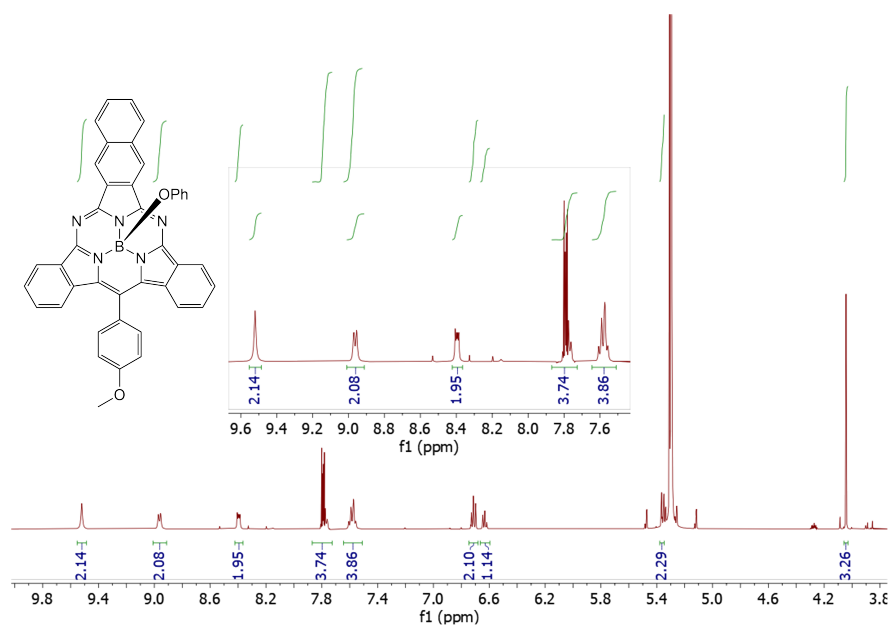
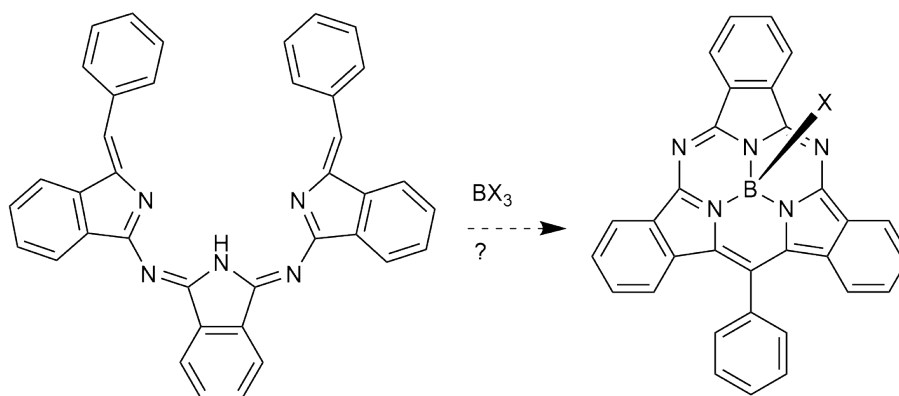


Figure 3.6:  $^1\text{H}$  NMR of naphthyl-SubTBDAP (**47**)

### Mechanistic insight and next steps

These results contradict the original hypothesis that aminoisoindoline acts as an initiator for the macrocyclization, with sequential addition of two units of phthalonitrile followed by macrocyclization to yield the SubTBDAP. Instead,

the formation of the Cs symmetric SubTBDAPs shows that two of the isoindole type fragments originated from the aminoisoindoline reagent, and one from phthalonitrile. Therefore the macrocyclization clearly follows an unexpected pathway, with similarities to the ABBA TBTAP formation pathway explored earlier. In order to produce the substitution pattern observed the reaction likely proceed via a ‘trimer’ type species shown below in scheme 3.14.

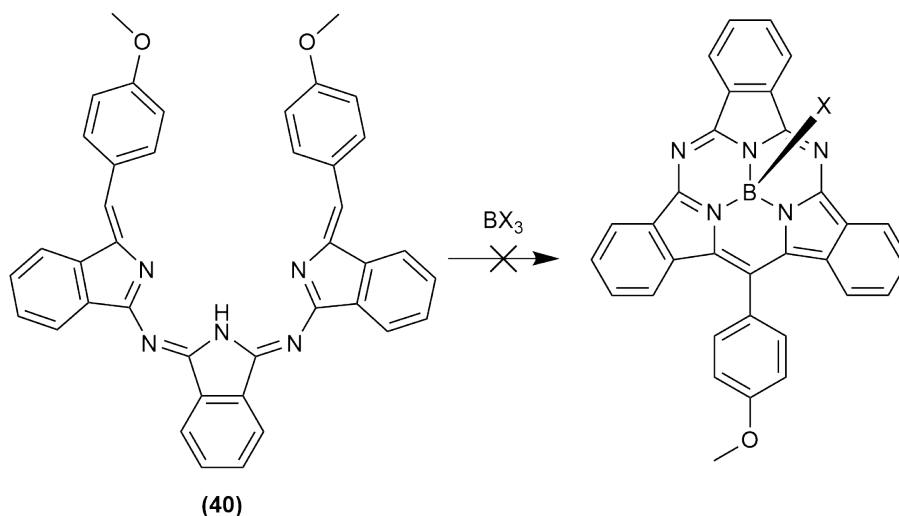


Scheme 3.14: Proposed macrocyclization of the ‘trimer’ to SubTBDAP with elimination of an aromatic fragment.

At this stage it is unclear if the species presented in scheme 3.14 directly macrocyclizes to SubTBDAP, or is simply observed as part of a more complex pathway resulting in the formation of Cs symmetric SubTBDAPs. This discovery is extremely interesting in the context of stepwise construction of SubTBDAP macrocycles, as the ‘trimers’ are now easily synthetically available. If they can be macrocyclized directly, a complete pathway for the controlled, stepwise assembly and cyclization of SubTBDAPs will have been developed.

### 3.3.4 Attempted SubTBDAP synthesis from ‘trimer’

With the previous results providing strong evidence to support a hypothesised macrocyclization from, or via, the ‘trimer’ in scheme 3.14, the next step of investigations was to subject (**40**) to the reaction conditions for SubTBDAP formation. Unfortunately despite multiple attempts under varying conditions no macrocyclic products were observed on TLC or by MALDI-TOF (scheme 3.15). Both  $\text{BCl}_3$  and  $\text{B}(\text{OPh})_3$  mediated pathways were investigated with variations in temperature and equivalents of the boron source, with no success.



Scheme 3.15: Failed synthesis of SubTBDAPs from trimers.

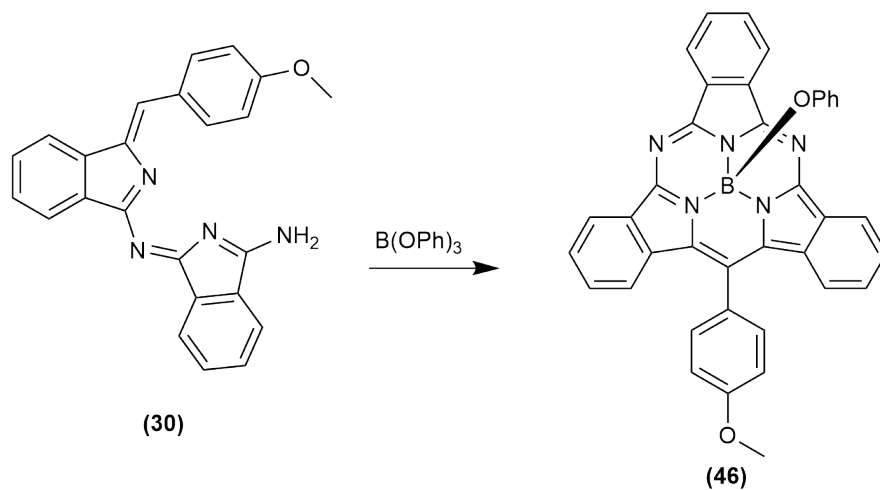
This result is unexpected, as previous evidence strongly suggests reaction via a symmetrical ‘trimer’ to form Cs symmetric SubTBDAPs. The only logical conclusion is that the reaction does proceed via ‘trimer’ (**40**), however an aromatic fragment is eliminated earlier in the pathway, rather than during macrocyclization, forming an unknown species that readily macrocyclizes to the Cs product.

### 3.3.5 SubTBDAP from unsubstituted dimer

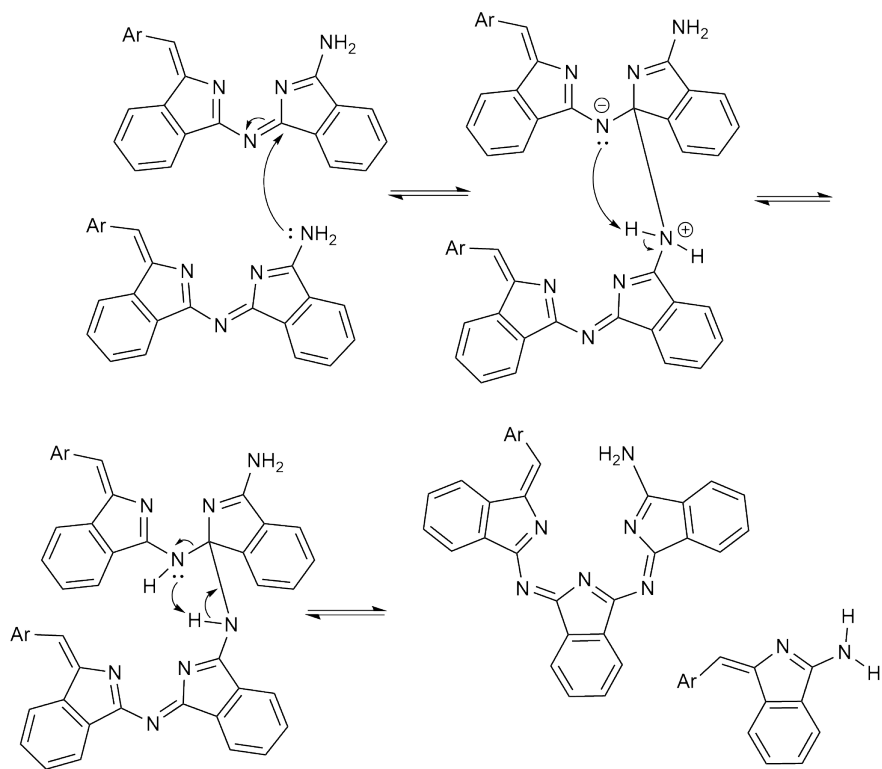
Condensation product (**30**) was also subjected to the reaction conditions, as it is now well established these structures form trimeric species they may also prove useful in forming SubTBDAPs.

Subjecting (**30**) to the reaction conditions described in scheme 3.16 produced SubTBDAP in an excellent yield of 20%, much higher than the best previously reported procedure. It is peculiar that the reaction proceeds readily from (**30**), but not trimeric structure (**40**), however does share similarities with previous work synthesising TBTAPs from (**30**). At this stage the most plausible explanation is that (**30**) undergoes a similar pathway to 3:1 (ABBB) TBTAP formation,

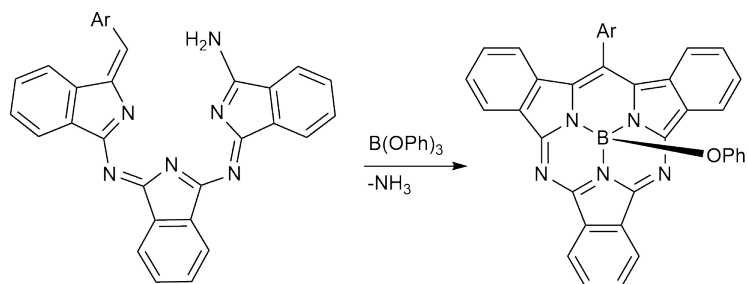
resulting in ABB SubTBDAPs via macrocyclization with elimination of ammonia (schemes 3.17 - 18). However, until this work is expanded with substituted derivatives of **(30)** to 'tag' each isoindole fragment, this is speculative.



Scheme 3.16: Successful and highly yielding synthesis of SubTBDAP from condensation product **(30)**.



Scheme 3.17: The proposed reaction mechanism between two units of **(30)** to form the alternative open chain ABB trimeric structure.

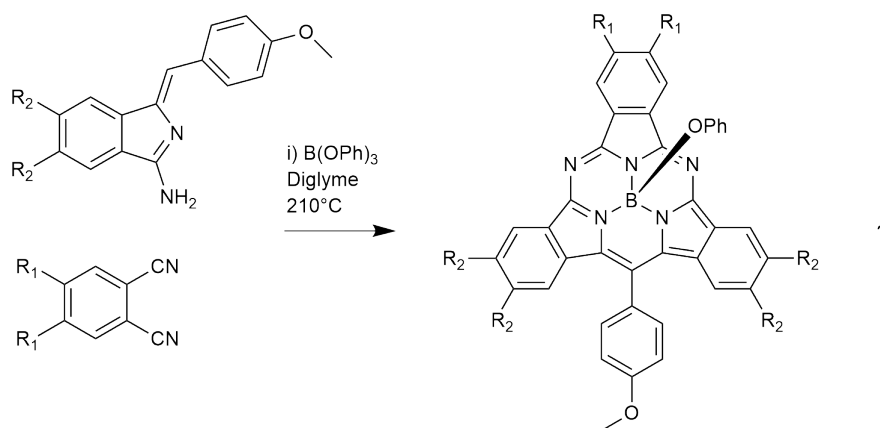


Scheme 3.18: Hypothesised macrocyclization of the open chain ABB 'trimer' to yield SubTBDAP with elimination of ammonia.

### 3.4 Conclusions and future work

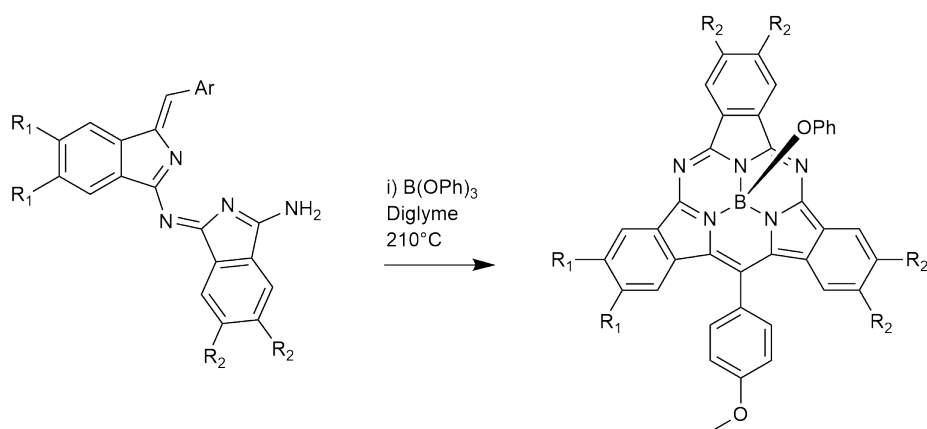
This work represents the first successful synthesis of peripherally substituted SubTBDAPs and mechanistic explorations with respect to SubTBDAP formation. The scope of SubTBDAP functionalisation was expanded to include peripheral functionalities, and a new, high yielding, synthesis was developed from the higher order intermediates developed. This offers exciting new synthetic opportunities, and has generated a significant amount of future work.

While Cs symmetric naphthyl SubTBDAP (**47**) was successfully synthesised as the first example of a substituted SubTBDAP, yielding crucial mechanistic insight, expanding this pathway to the range of derivatives initially planned has unfortunately not been achieved within this work. Future work should target a series of functionally and electronically diverse derivatives of both aminoisoindolines and phthalonitriles, which will ensure robustness of the procedure. Based on this work and its conclusions only Cs symmetric SubTBDAPs should be produced, however as seen on numerous occasions throughout these mechanistic explorations, delicate thermodynamic balances often exist, which may be influenced by sterics or electronics of the substrates utilised to produce different or unexpected products.



Scheme 3.19: Synthesis of Cs, ABA, SubTBDAPs from aminoisoindoline and phthalonitrile.

This work has confirmed that SubTBDAPs may not be synthesised from isolated trimeric species such as **(40)**, and therefore the macrocyclization step does not proceed via elimination of an aromatic fragment. However SubTBDAP may be synthesised in excellent yields from **(30)**. Plausible mechanisms have been proposed in the discussion above. This new procedure and insight may provide an extremely powerful and efficient route to ABB SubTBDAP derivatives, however this needs to be tested with a series of SubTBDAPs from derivatives of **(30)**.



Scheme 3.20: Synthesis of SubTBDAP derivatives from **(30)**, with the hypothesised substitution pattern shown.

## Chapter 4

# DFT studies on key proposed structures and pathways

### 4.1 Introduction

#### 4.1.1 Aims

With previous experiments producing differing results due to competing pathways, it is clear that delicate thermodynamic and kinetic balances between possible reaction pathways have significant impacts on the result. This chapter aims to explore these balances and support experimentally observed data through the use of *in silico* methods to analyse the thermodynamic landscape of selected reactions. Additionally once pathways have been identified and models produced, if concordant with experimental data, modifications to intermediates and structures for future work may be screened *in silico*. These modifications could include modifications of electronics through functional groups, or the use of different leaving groups to activate and promote desired pathways.

These aims will be achieved through the systematic production of models for the proposed pathways of each side product and product observed experimentally, accompanied by computational thermodynamic analysis of starting materials, products, intermediates and possible transition states. With this data potential energy diagrams for each reaction pathway may be produced and compared.

#### 4.1.2 Pathways to be targeted

##### **Aminoisoindoline homocondensation**

Often observed as a side product, as well as serving as a model condensation reaction between two amine bearing isoindole fragments, the thermodynamics of this reaction were explored.

### Condensation of (30)

With strong evidence of equilibrium behaviour between the starting materials and products this pathway was explored to confirm experimental observations.

### Condensation and elimination pathways between two units of (30)

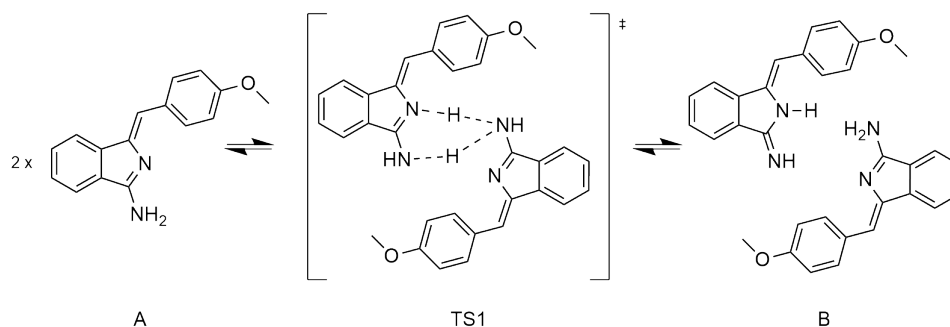
With multiple elimination pathways observed experimentally, this pathway shall be examined in order to gain more insight into the thermodynamics of competing condensations/eliminations. The charge distribution and hence activation of electrophilic carbons shall be examined. It is anticipated this analysis may give insight into the unexpected formation of 3:1 ABBB TBTAPs from (30).

#### 4.1.3 Methods

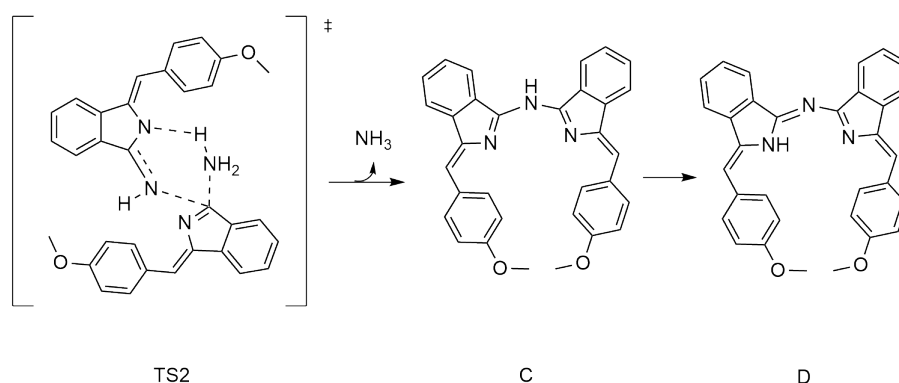
This work was performed with the Gaussian16 software package, utilizing the B3LYP/6-31+g(d,p) level of theory. Reagents, intermediates and products were optimised to global minima, confirmed by vibrational analysis. Transition states were confirmed to be saddle points by the presence of a single imaginary vibration in the optimised structure. Atomic partial charges are calculated via NBO methods. Where applicable, solvent effects were included in calculations utilising the PCM method.

## 4.2 Aminoisoindoline homocondensation

Commonly observed as a side product, analysis of the homocondensation pathway is not only important for obtaining overall thermodynamic landscape, but also serves as a model reaction for other condensations involving 2 terminal amines, such as the theoretical 2+2 TBTAP addition from (30). It was found the reaction likely proceeds via an initial proton transfer on one of the aminoisoindoline species to form a terminal imine with increased nucleophilicity. Following this proton transfer step, attack by the newly formed imine on another aminoisoindoline unit facilitates the homocondensation with elimination of ammonia (scheme 4.1 and 4.2).



Scheme 4.1: Initial proton transfer to form the more activated imine B.



Scheme 4.2: Homocondensation with elimination of ammonia to form azadipyrromethene C, which further tautomerizes to final structure D.

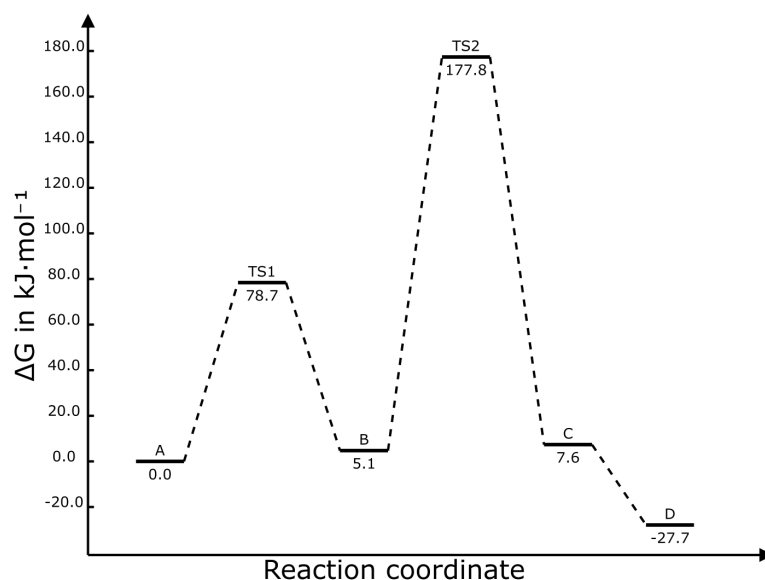


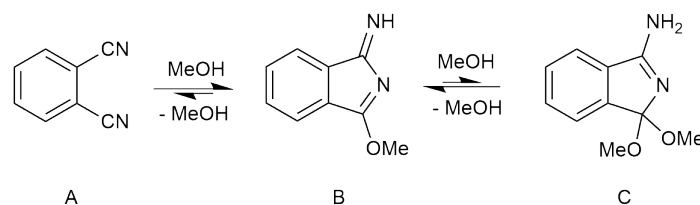
Figure 4.1: Potential energy diagram for the reaction presented above.

From figure 4.1 it can be seen that while the pathway possesses a large activation energy between species B and C,  $\Delta G < 0$  for the reaction pathway. This means under the reaction conditions there is a small thermodynamic driving force to the product. Species A, B and C are likely in equilibrium with similar concentrations due to the very similar values for  $\Delta G$ . While the reaction favours the formation of azadipyrromethene D, the small  $\Delta G$  between D and C means the reverse reaction also proceeds readily, as long as ammonia is present.

This suggests that reactions that form excessive and unwanted homocondensation products are likely driven by the elimination and off gassing of ammonia

from the reaction vessel, as with ammonia present the reaction will be reversible, albeit at a slower rate than the forward reaction. This conclusion is supported by the previously developed selective synthesis of aminoisindoline homocondensation products, a procedure that utilises the slow evaporation of the reaction solvent under a stream of  $N_2$  to facilitate homocondensation products in high yield. The methodology used appears to be utilised to encourage the off gassing of ammonia, and hence drive the reaction to completion. This offers an explanation as to why homocondensation products of aminoisindoline were less often observed in this work, reactions were most commonly performed in sealed glass tubes, hence retaining the produced ammonia in the reaction vessel and facilitating the reverse reaction of the equilibrium, regenerating aminoisindoline that will eventually be used in the reaction.

### 4.3 Synthesis of dimethoxyisindolines



Scheme 4.3: Series of equilibria that form dimethoxyisindoline.

The formation of dimethoxyisindolines proceeds via the consecutive addition of two equivalents of methanol to phthalonitrile, facilitated by a sub-stoichiometric quantity of sodium methoxide in methanol, which is regenerated by the reaction. The reaction should be reversible and consist of a series of equilibria as shown in scheme 4.3.

The free energies of the proposed structures were calculated and are presented in figure 4.2. It is clear from this data that the formation of methoxyisindoline B is a favourable and spontaneous process, the formation of dimethoxyisindoline C however results in an increase in  $\Delta G$ , and hence is non-spontaneous.

This supports experimental observations, which gave the impression an equilibrium exists between the species. The parent structure was easily synthesised with an optimised procedure to afford the desired dimethoxyisindoline driven by precipitation from the reaction mixture. Substituted derivatives were much harder to isolate in good yields, presumably due to the increased solubility of the targeted dimethoxy substituted isindoline, hence the targeted product remaining in solution and the reverse reactions occurring readily.

Observations of NMR spectra offer additional support; freshly synthesised materials and prepared samples allowed the collection of clean spectra that

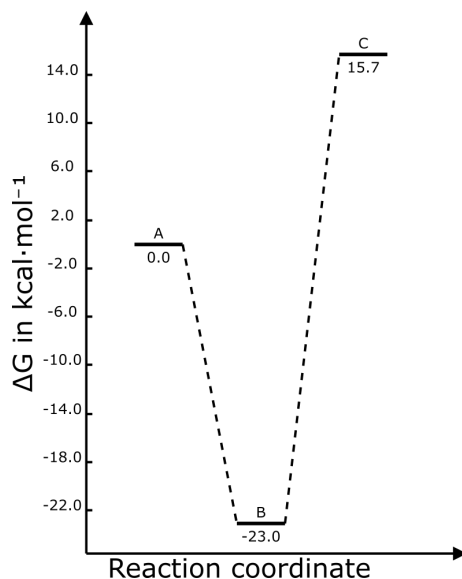
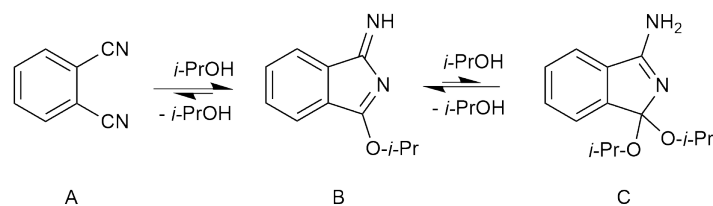


Figure 4.2: Potential energy diagram for dimethoxyisindoline formation. Solvent = methanol.

correlated with the structure of the product, with minimal side products or impurities visible. The use of older materials or NMR samples resulted in complex spectra that were clearly a mixture of products and very difficult to analyse. This suggests that in solution dimethoxyisindoline C may spontaneously eliminate methanol to form methoxyisindoline B. It is therefore important to consider the potential reactivity of both species B and C in subsequently analysed pathways.

#### Analysis of isopropylisindoline formation



Scheme 4.4: Formation of isopropylisindoline.

While these species were not utilised in this work they may be useful structures in future work. The original study that synthesised dimethoxyisindolines also synthesised iso-propyl derivatives, however only monosubstituted isopropylisindoline was isolated by the investigations.

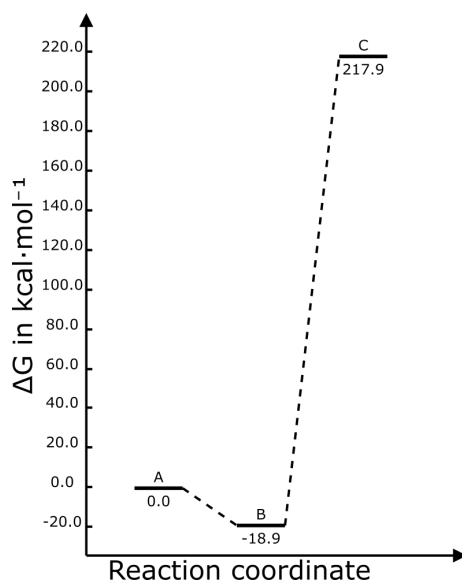
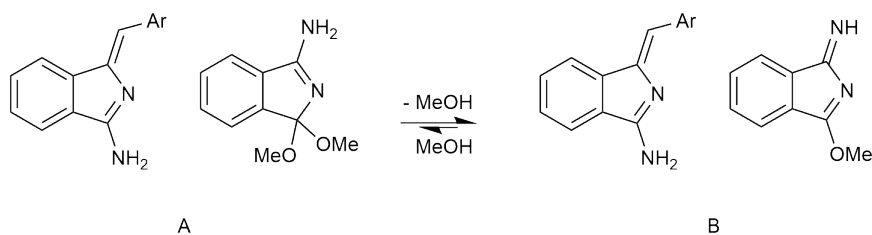


Figure 4.3: Potential energy diagram for the formation of di-isopropylisoindoline. Solvent = iso-propanol.

Again, the calculated free energy of the pathway (scheme 4.4 and figure 4.3) supports the spontaneous formation of isopropylisoindoline, the experimentally observed product. The further substitution to form di-isopropylisoindoline is clearly a very unfavourable process, with a large increase in  $\Delta G$ . This is likely due to very high steric crowding associated with the product.

#### 4.4 Synthesis of (30) and equilibrium

As observed experimentally, the formation of (30) and derivatives from aminoisoindoline and dimethoxyisoindoline appears to proceed under equilibrium conditions, resulting in poor yields and a mixture of products with substituted derivatives utilizing standard methodology.



Scheme 4.5: Dissociation of dimethoxyisoindoline to methoxyisoindoline and methanol.

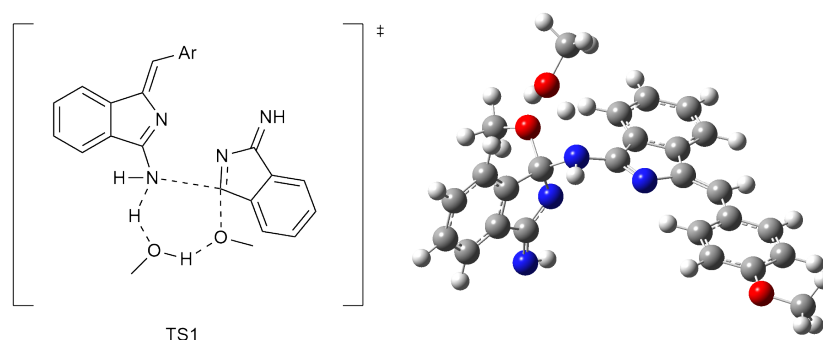
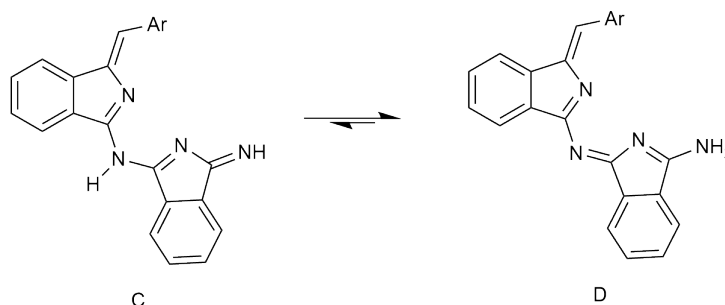


Figure 4.4: Hypothesised 6-membered cyclic transition state for the condensation of aminoisoindoline and methoxyisoindoline.

The first part of this pathway involves the dissociation of dimethoxyisoindoline A to methoxyisoindoline B and methanol, with a  $\Delta G$  of  $-38.7 \text{ kJ}\cdot\text{mol}^{-1}$  (scheme 4.5). From B the nucleophilic amine of aminoisoindoline attacks methoxyisoindoline via TS1 (figure 4.4) to produce C, final proton transfer yields **(30)** D (scheme 4.6). Two transition states were explored: the intramolecular elimination of methanol between aminoisoindoline and methoxyisoindoline via a 4 membered cyclic transition state, and the same transfer assisted by an additional molecule of methanol via a 6 membered cyclic transition state. It was found an additional molecule of methanol acting as a proton transfer agent significantly reduced the  $\Delta G^\ddagger$  of the pathway (figure 4.5).



Scheme 4.6: Tautomerization to form the final condensation product D.

Condensation product **(30)** (D) has a  $\Delta G$  of  $-31.3 \text{ kJ}\cdot\text{mol}^{-1}$ , very similar to the  $\Delta G$  of structure (B), assuming equilibrium conditions this means there is no thermodynamic driving force to product (D). This again supports experimental observations, where the precipitation of **(30)** from solution appeared to drive the reaction to completion, and higher solubility derivatives were produced in poor yield due to the desired product remaining in solution and hence undergoing reverse reactions.

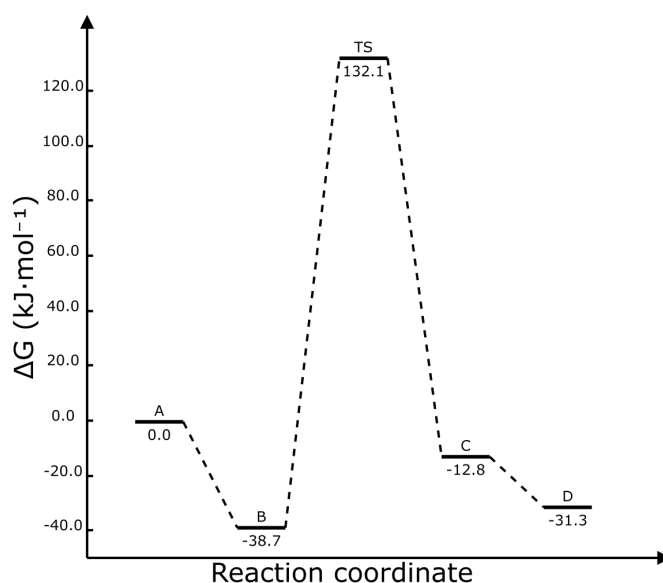


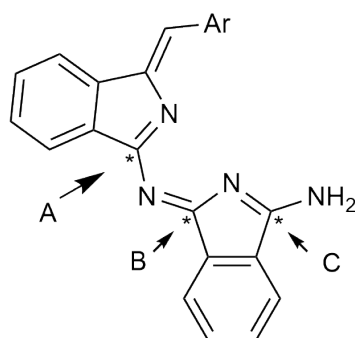
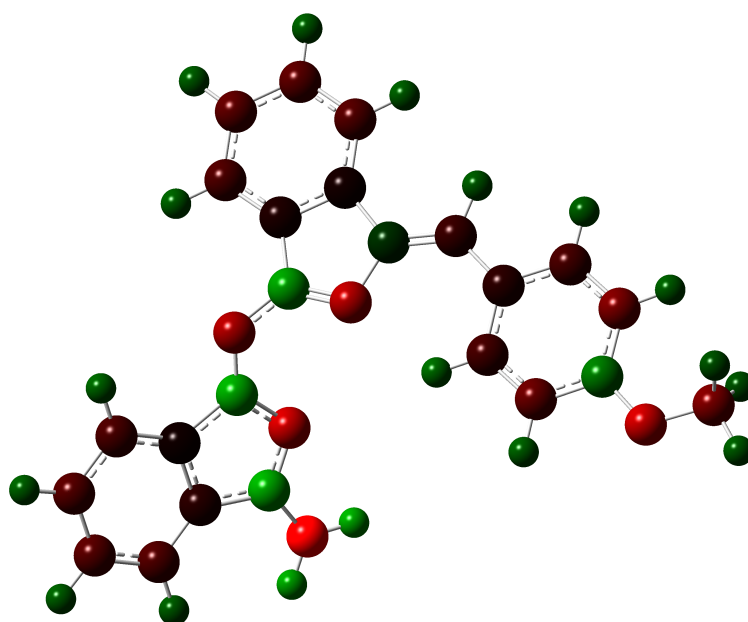
Figure 4.5: Potential energy diagram for the pathway presented above.

This analysis supports the proposed equilibrium, and improved yields through the elimination of methanol from the reaction mixture. From the data and experimental observations it is clear this condensation must be driven forward by either low solubility and hence precipitation of the product, or removal of methanol to prevent reverse reactions.

## 4.5 Homocondensations of (30) at different positions

As shown in section 2.5, (30) may react with itself at different positions to yield different products with different species eliminated. This section aims to map the thermodynamics of competing reactions and eliminations.

Natural bond orbital (NBO) analysis of (30) was used to obtain partial atomic charges for the structure, shown in figure 4.6. In chapter 2 observed reactivity and proposed mechanisms meant (30) must undergo homocondensations at each of the 3 positions labelled with \* in figure 4.6 to produce the range of species observed. NBO analysis supports these observations and proposed mechanisms with all 3 carbon atoms possessing very similar atomic charges, and hence susceptibility to nucleophilic attack. This indicates that electronically at least, nucleophilic attack is almost equally likely at all 3 positions, correlating experimental observations.

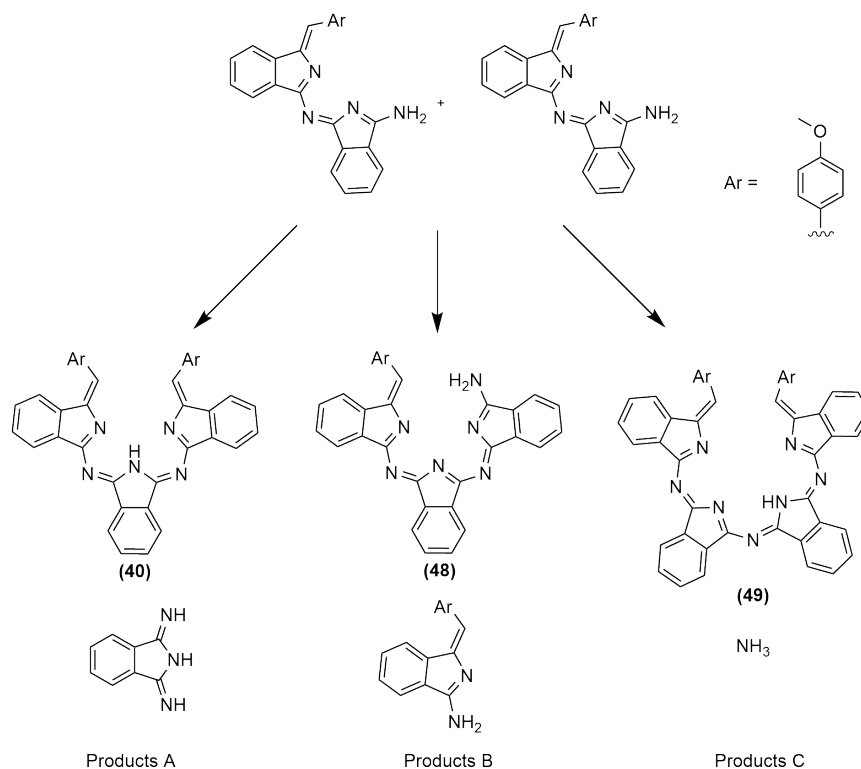


(30)

Figure 4.6: NBO analysis of charge distribution in (30). Red indicates increased electron density, green indicates reduced electron density, and black indicates neutral.

The reactivity of (30) has been thoroughly explored in chapter 2, both through experimentally isolated and characterised products, and likely products observed by MALDI-TOF spectroscopy of crude reaction mixtures. It is now well established that (30) reacts readily under mild conditions to produce the range of products described. This section therefore aims to analyse which product is thermodynamically favourable, with the assumption that all reactions are reversible and transition states are accessible.

If this analysis reveals no significant thermodynamic preference in the products it is logical to assume all species presented previously exist in solution, and therefore the favoured macrocyclic product is controlled by terminal leaving group.



Scheme 4.7: Scheme for the formation of various products from two units of condensation dimer (**30**).

As can be clearly seen from the potential energy diagram (figure 4.7), with the assumption that all possible condensations are thermally accessible and in equilibrium, trimeric product (**40**) is by far the thermodynamically preferred product. This strongly supports experimental observations in section 2.5, where attempted low temperature homocondensations of (**30**) to yield the ABBA tetramer (**49**) instead yielded the trimeric displacement product (**40**) in high yields.

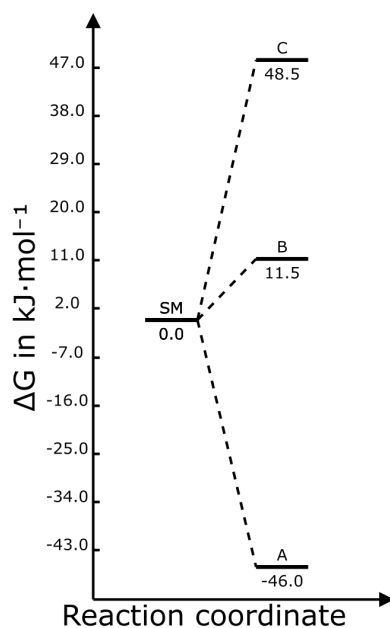


Figure 4.7: Potential energy diagram for the pathway presented in scheme 4.7.

This analysis also supports the unexpected formation of 3:1 ABBB TBTAPs from derivatives of **(30)** (section 2.5.2); while the pathway was originally designed with the expectation **(30)** would undergo homocondensation with elimination of ammonia to produce the ABBA tetramer, and hence 2:2 ABBA TBTAP, 3:1 ABBB TBTAPs were formed instead. A critical intermediate in the proposed pathway to 3:1 TBTAPs, as well as SubTBDAP formation from **(30)**, is the ABB ‘trimer’ **(48)**. Again, this analysis supports the formation of **(48)** over ABBA tetramer **(49)**, with **(48)** having a significantly lower  $\Delta G$ .

## 4.6 Conclusions

While this preliminary computational study supports some of the observed experimental results, the ultimate goal of a full thermodynamic analysis of competing macrocyclization pathways was not achieved. The potential for computational methods in supporting future work is clear however, and could provide crucial thermodynamic insight and *in silico* screening of designed pathways.

# Chapter 5

## Experimental

### 5.1 General Methods

Reagents and solvents were purchased from commercial sources and used without further purification, unless otherwise stated. Phthalonitrile was always recrystallized from xylene. Water and air sensitive reactions were carried out under an inert atmosphere, normally N<sub>2</sub>. Removal of solvents was carried out using a Buchi rotary evaporator under reduced pressure.

<sup>1</sup>H NMR and <sup>13</sup>C NMR were obtained using a Bruker Ascend™ 500 spectrometer at 500 and 125.7 MHz respectively. Norell S500 or 508 quartz NMR tubes were used. Signals are quoted in ppm and δ downfield from TMS. Coupling constants, J, are given in Hertz. Deuterated solvents were used and NMR experiments performed at 298°K.

IR spectra were recorded using a Perkin-Elmer Spectrum BX FT-IR spectrometer. UV-Vis spectra were recorded using a Hitachi U-3310 spectrophotometer in the solvent stated. Thin layer chromatography was performed with Alugram Sil G/UV254, and the compounds visualised with 254 or 365 nm UV light. Column chromatography was performed using silica gel 60 Å mesh 70 - 230 eluting with the solvent system stated, under ambient temperature and occasionally elevated pressure (hand pump). Solvent ratios are given as v:v. Melting points were recorded using a Reichart Thermovar microscope with a thermopar based control system. Microwave reaction were carried out using a Biotage Initiator+ system. MALDI-TOF spectra were recorded using a Shimadzu AXIMA Performance instrument.

### 5.2 Phthalonitriles and bromobenzonitriles

#### 5.2.1 6,7-Dicyano-1,2,3,4-tetrahydro-1,1,4,4-tetramethylnaphthalene (14)

##### 2,5-Dichloro-2,5-dimethylhexane

Following the procedure developed by Shudo *et al.*, concentrated hydrochloric acid (50 mL) cooled in an ice bath and 2,5-dimethyl-hexane-2,5-diol (5.0 g,

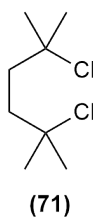


Figure 5.1: 2,5-Dichloro-2,5-dimethylhexane

34.2 mmol) was added with stirring.<sup>133</sup> The suspension was stirred at 0°C for 30 minutes before being left to stir at RT overnight. The off white precipitate was filtered and washed with H<sub>2</sub>O before being dissolved in DCM (50 mL) and washed with H<sub>2</sub>O. The organic phase was collected and the aqueous extracted further with DCM (2 x 50 mL). The organic phases were combined, dried with MgSO<sub>4</sub> and the solvent removed. The resulting crystalline product was recrystallised from methanol to give the *title compound* as colourless crystals (5.72 g, 91 %).

<sup>1</sup>H NMR (500 MHz, CDCl<sub>3</sub>) δ 1.98 (s, 4H), 1.57 (s, 12H)

<sup>13</sup>C NMR (125.7 MHz, CDCl<sub>3</sub>) δ 70.8, 41.5, 32.8

MP: 64-65°C (lit. 65°C)<sup>134</sup>

#### 1,1,4,4-Tetramethyl-1,2,3,4-tetrahydronaphthalene

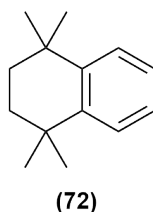


Figure 5.2: 1,1,4,4-Tetramethyl-1,2,3,4-tetrahydronaphthalene

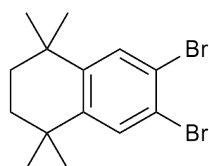
Utilizing Brusons' adaptation of Friedel-Crafts alkylation<sup>135</sup> a solution of 2,5-dichloro-2,5-dimethylhexane (1.0 g, 5.4 mmol) was prepared in benzene (50 mL). The solution was stirred at 50°C and AlCl<sub>3</sub> (0.29 g, 2.2 mmol) added in portions over 30 min. The solution was stirred at 50°C overnight then checked by <sup>1</sup>H NMR, if the reaction was incomplete small portions of AlCl<sub>3</sub> were added until NMR indicated completion. The solution was cooled to RT and poured into dilute HCl. The mixture was extracted with DCM (3 x 50 mL), the organic phases were combined and washed with H<sub>2</sub>O (50 mL), Na<sub>2</sub>CO<sub>3</sub> solution (50 mL)

then dried over MgSO<sub>4</sub>. The solvent was removed to yield the *title compound* as a pale yellow oil (0.87 g, 86 %)

<sup>1</sup>H NMR (500 MHz, CDCl<sub>3</sub>) δ 7.31 (dd, J = 5.9, 3.4 Hz, 2H), 7.12 (dd, J = 5.9, 3.4 Hz, 2H), 1.69 (s, 4H), 1.28 (s, 12H)

<sup>13</sup>C NMR (125.7 MHz, CDCl<sub>3</sub>) δ 144.8, 126.6, 125.6, 35.1, 34.2, 32.1

#### 6,7-Dibromo-1,1,4,4-tetramethyl-1,2,3,4-tetrahydronaphthalene



(67)

Figure 5.3: 6,7-Dibromo-1,1,4,4-tetramethyl-1,2,3,4-tetrahydronaphthalene

To a solution of 1,1,4,4-tetramethyl-1,2,3,4-tetrahydronaphthalene (4.8 g, 25.5 mmol) in DCM (75 mL) was added iron powder (170 mg) and I<sub>2</sub> (65 mg). The solution was cooled to 0°C and Br<sub>2</sub> (2.65 mL, 51 mmol) was added dropwise over 30 min. The resulting solution was stirred at RT overnight and added to a solution of Na<sub>2</sub>S<sub>2</sub>O<sub>5</sub> and NaHCO<sub>3</sub> to neutralise excess Br<sub>2</sub>. Brine was added and the mixture extracted with DCM (3 x 250 mL), the organics were dried with MgSO<sub>4</sub> and the solvent removed to yield a yellow/brown solid. Purification was achieved with silica gel chromatography eluting with PE:DCM (3:2) to yield the *title compound* as an off white solid (8.3 g, 94 %).

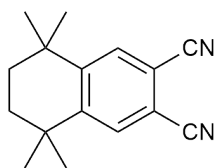
<sup>1</sup>H NMR (500 MHz, CDCl<sub>3</sub>) δ 7.51 (s, 2H), 1.66 (s, 4H), 1.26 (s, 12H).

<sup>13</sup>C NMR (125.7 MHz, CDCl<sub>3</sub>) δ 146.3, 131.8, 121.5, 34.9, 34.6, 31.7

MP: 113-115°C (lit. 111-112°C)<sup>136</sup>

#### 6,7-Dicyano-1,1,4,4-tetramethyl-1,2,3,4-tetrahydronaphthalene (14)

To a solution of 6,7-dibromo-1,1,4,4-tetramethyl-1,2,3,4-tetrahydronaphthalene (5.5 g, 16 mmol) in anhydrous *p*-xylene (30 mL) was added finely ground and oven dried K<sub>3</sub>[Fe(CN)<sub>6</sub>] (2.4 g, 3.2 mmol), CuI (304 mg, 1.6 mmol) and 1-butylimidazole (4.4 mL, 32 mmol). The suspension was refluxed for 72 hr then cooled to RT. Et<sub>2</sub>O (100 mL) was added and the solution filtered. The solution was washed with H<sub>2</sub>O (3 x 50 mL) and brine (2 x 50 mL). The organic phase was collected and dried over MgSO<sub>4</sub>, the solvent was removed to yield an off white solid. The crude product was subjected to silica gel chromatography eluting with PE/Et<sub>2</sub>O, 7:1, recrystallisation from MeOH yielded the *title compound* as a colourless solid (2.9 g, 76 %).<sup>137</sup>



(14)

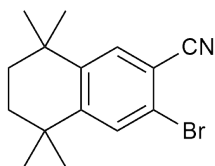
Figure 5.4: 6,7-Dicyano-1,1,4,4-tetramethyl-1,2,3,4-tetrahydronaphthalene

$^1\text{H}$  NMR (500 MHz,  $\text{CDCl}_3$ )  $\delta$  7.71 (s, 2H), 1.72 (s, 4H), 1.30 (s, 12H).

$^{13}\text{C}$  NMR (125.7 MHz,  $\text{CDCl}_3$ )  $\delta$  151.9, 132.7, 116.1, 112.6, 35.1, 34.0, 31.4

MP: 204-206 °C (lit. 206-208°C)<sup>138</sup>

### 5.2.2 6-Bromo-7-cyano-1,2,3,4-tetrahydro-1,1,4,4-tetramethylnaphthalene



(56)

Figure 5.5: 6,7-Dicyano-1,1,4,4-tetramethyl-1,2,3,4-tetrahydronaphthalene

The *title compound* was obtained as a side product from the dicyanation of 6,7-dibromo-1,1,4,4-tetramethyl-1,2,3,4-tetrahydronaphthalene. Alternatively the *title compound* may be selectively synthesised utilizing a modified procedure.

To a solution of 6,7-dibromo-1,1,4,4-tetramethyl-1,2,3,4-tetrahydronaphthalene (5.5 g, 16 mmol) in anhydrous *p*-xylene (30 mL) was added finely ground and oven dried  $\text{K}_3[\text{Fe}(\text{CN})_6]$  (1.2 g, 1.6 mmol),  $\text{CuI}$  (152 mg, 0.8 mmol) and 1-butylimidazole (2.2 mL, 16 mmol). The suspension was refluxed for 72 hr then cooled to RT.  $\text{Et}_2\text{O}$  (100 mL) was added and the solution filtered. The solution was washed with  $\text{H}_2\text{O}$  (3 x 50 mL) and brine (2 x 50 mL). The organic phase was collected and dried over  $\text{MgSO}_4$ , the solvent was removed to yield an off white solid. The crude product was subjected to silica gel chromatography eluting with PE/ $\text{Et}_2\text{O}$ , 7:1, recrystallisation from MeOH yielded the *title compound* as a colourless solid (3.9 g, 84 %)

$^1\text{H}$  NMR (500 MHz,  $\text{CDCl}_3$ )  $\delta$  7.57 (s, 1H), 7.54 (s, 1H), 1.68 (s, 4H), 1.27 (s, 6H), 1.26 (s, 6H)

$^{13}\text{C}$  NMR (125.7 MHz,  $\text{CDCl}_3$ )  $\delta$  152.8, 145.5, 133.2, 131.4, 121.5, 117.8, 112.9, 35.0, 34.4, 31.6, 31.5

MP: 157-159°C (lit. 158-159°C)<sup>139</sup>

### 5.2.3 4,5-Diphenoxyphthalonitrile

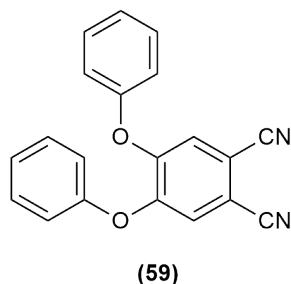


Figure 5.6: 4,5-Diphenoxyphthalonitrile

A solution of 4,5-dichlorophthalonitrile (1.0 g, 5.1 mmol), phenol (1.4 g, 15 mmol) and  $\text{K}_2\text{CO}_3$  (3.0 g, 22 mmol) in anhydrous DMF (30 mL) was heated to 110°C overnight.<sup>140</sup> The solution was cooled and added to  $\text{H}_2\text{O}$  (100 mL). The precipitate was filtered, washed with  $\text{H}_2\text{O}$  and recrystallised from MeOH to yield the *title compound* as colourless crystals (1.4 g, 87 %)

$^1\text{H}$  NMR (500 MHz,  $\text{CDCl}_3$ )  $\delta$  7.59 – 7.52 (m, 4H), 7.39 (ddt,  $J = 7.8, 7.1, 1.1$  Hz, 2H), 7.35 (s, 2H), 7.21 – 7.14 (m, 4H)

$^{13}\text{C}$  NMR (125.7 MHz,  $\text{CDCl}_3$ )  $\delta$  156.4, 154.2, 132.8, 128.4, 124.5, 122.2, 116.9, 112.5

MP: 151 - 153 °C (lit. 149-150°C)<sup>140</sup>

### 5.2.4 4,5-Dimethoxyphthalonitrile

#### 1,2-Dibromo-4,5-dimethoxybenzene

1,2-Dimethoxybenzene (40 g, 0.29 mol) was dissolved in DCM (300 mL) and the solution cooled to 0°C.  $\text{Br}_2$  (33 mL, 0.64 mol) was added dropwise over 2 hr and the solution further stirred for 1 hr while warming to RT. The solution was washed with aqueous  $\text{Na}_2\text{S}_2\text{O}_3$  (200 mL),  $\text{H}_2\text{O}$  (200 mL) and saturated NaCl solution (200 mL). The aqueous solutions were combined and extracted further with DCM (2 x 200 mL). The organics were combined and dried with  $\text{MgSO}_4$  and the solvent removed. The crude residue was recrystallised from MeOH to yield the *title compound* as a colourless crystalline solid (79 g, 93 %).<sup>141</sup>

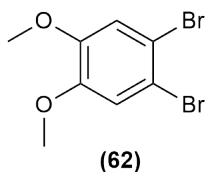


Figure 5.7: 1,2-Dibromo-4,5-dimethoxybenzene

$^1\text{H}$  NMR (500 MHz,  $\text{CDCl}_3$ )  $\delta$  7.05 (s, 2H), 3.85 (s, 6H)

$^{13}\text{C}$  NMR (125.7 MHz,  $\text{CDCl}_3$ )  $\delta$  148.9, 116.0, 114.9, 56.3

MP: 87-90 °C (lit. 90°C)<sup>142</sup>

#### 4,5-Dimethoxyphthalonitrile

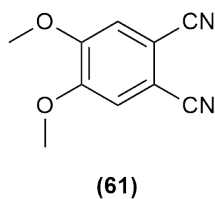


Figure 5.8: 4,5-Dimethoxyphthalonitrile

To a solution of 1,2-dibromo-4,5-dimethoxybenzene (9.5 g, 32 mmol) in anhydrous *p*-xylene (60 mL) was added finely ground and oven dried  $\text{K}_3[\text{Fe}(\text{CN})_6]$  (4.8 g, 6.4 mmol),  $\text{CuI}$  (608 mg, 3.2 mmol) and 1-butylimidazole (8.4 mL, 64 mmol). The suspension was refluxed for 72 hr then cooled to RT.  $\text{Et}_2\text{O}$  (100 mL) was added and the solution filtered. The solution was washed with  $\text{H}_2\text{O}$  (3 x 50 mL) and brine (2 x 50 mL). The organic phase was collected and dried over  $\text{MgSO}_4$ , the solvent was removed to yield an off white solid. The crude product was subjected to silica gel chromatography eluting with DCM/PE 1:2  $\rightarrow$  DCM/PE 1:1  $\rightarrow$  DCM, recrystallisation from MeOH yielded the *title compound* as a colourless solid (4.1 g, 68 %).<sup>137</sup>

$^1\text{H}$  NMR (500 MHz,  $\text{CDCl}_3$ )  $\delta$  7.15 (s, 2H), 3.97 (s, 6H)

$^{13}\text{C}$  NMR (125.7 MHz,  $\text{CDCl}_3$ )  $\delta$  152.7, 115.9, 114.9, 109.2, 56.8

MP: 180-183°C (lit. 179 - 181°C)<sup>143</sup>

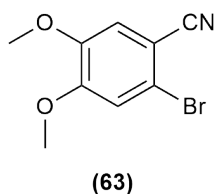


Figure 5.9: 2-Bromo-4,5-dimethoxybenzonitrile

### 5.2.5 2-Bromo-4,5-dimethoxybenzonitrile

The *title compound* was obtained as a side product from the dicyanation of 1,2-dibromo-4,5-dimethoxybenzene. Alternatively the *title compound* may be selectively synthesised via a modified procedure.

To a solution of 1,2-dibromo-4,5-dimethoxybenzene (4.8 g, 16 mmol) in anhydrous *p*-xylene (30 mL) was added finely ground and oven dried  $K_3[Fe(CN)_6]$  (1.2 g, 1.6 mmol), CuI (304 mg, 1.6 mmol) and 1-butylimidazole (4.2 mL, 32 mmol). The suspension was refluxed for 72 hr then cooled to RT.  $Et_2O$  (100 mL) was added and the solution filtered. The solution was washed with  $H_2O$  (3 x 50 mL) and brine (2 x 50 mL). The organic phase was collected and dried over  $MgSO_4$ , the solvent was removed to yield an off white solid. The crude product was subjected to silica gel chromatography eluting with DCM/PE 1:2  $\rightarrow$  DCM/PE 1:1  $\rightarrow$  DCM, recrystallisation from MeOH yielded the *title compound* as a colourless solid (2.9 g, 75 %).<sup>137</sup>

$^1H$  NMR (500 MHz,  $CDCl_3$ )  $\delta$  7.07 (s, 1H), 7.05 (s, 1H), 3.93 (s, 3H), 3.88 (s, 3H)

$^{13}C$  NMR (125.7 MHz,  $CDCl_3$ )  $\delta$  153.3, 148.7, 117.8, 117.7, 115.6, 115.4, 107.1, 56.6, 56.5

MP: 120-124°C (lit. 117°C)<sup>144</sup>

### 5.2.6 4,5-Dimethylphthalonitrile

#### 1,2-Dibromo-4,5-dimethylbenzene

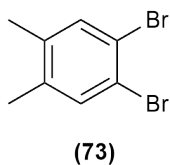


Figure 5.10: 1,2-Dibromo-4,5-dimethylbenzene

A solution of I<sub>2</sub> (200 mg) in *o*-xylene (46 mL, 0.38 mol) was cooled to 0°C and Br<sub>2</sub> (40 mL) was added dropwise over 2 hr. The mixture was left to stir at RT overnight then dissolved in Et<sub>2</sub>O (300 mL). The solution was washed with 2M NaOH (2 x 100 mL) and H<sub>2</sub>O (2 x 200 mL). The organics were dried with MgSO<sub>4</sub> and the solvent removed to yield a red/pink oil. Recrystallisation from MeOH yielded the *title compound* as off white crystals (64 g, 64 %).<sup>145</sup>

<sup>1</sup>H NMR (500 MHz, CDCl<sub>3</sub>) δ 7.30 (s, 2H), 2.11 (s, 6H).

<sup>13</sup>C NMR (125.7 MHz, CDCl<sub>3</sub>) δ 137.7, 134.2, 121.1, 19.1.

MP: 84-86 °C (lit. 88°C)<sup>146</sup>

#### 4,5-Dimethylphthalonitrile

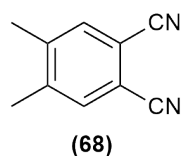


Figure 5.11: 4,5-Dimethylphthalonitrile

To a solution of 1,2-dibromo-4,5-dimethylbenzene (8.4 g, 32 mmol) in anhydrous *p*-xylene (60 mL) was added finely ground and oven dried K<sub>3</sub>[Fe(CN)<sub>6</sub>] (4.8 g, 6.4 mmol), CuI (608 mg, 3.2 mmol) and 1-butylimidazole (8.4 mL, 64 mmol). The suspension was refluxed for 72 hr then cooled to RT. Et<sub>2</sub>O (100 mL) was added and the solution filtered. The solution was washed with H<sub>2</sub>O (3 x 50 mL) and brine (2 x 50 mL). The organic phase was collected and dried over MgSO<sub>4</sub>, the solvent was removed to yield an off white solid. The crude product was subjected to silica gel chromatography eluting with DCM/PE 1:1, recrystallisation from MeOH yielded the *title compound* as a colourless solid (3.8 g, 77 %).<sup>137</sup>

<sup>1</sup>H NMR (500 MHz, CDCl<sub>3</sub>) δ 7.55 (s, 2H), 2.38 (s, 6H)

<sup>13</sup>C NMR (125.7 MHz, CDCl<sub>3</sub>) δ 143.6, 134.4, 115.8, 113.2, 20.2

MP: 170-174 °C (lit. 175 - 177°C)<sup>143</sup>

#### 5.2.7 2-Bromo-4,5-dimethylbenzonitrile

The *title compound* was obtained as a side product of the dicyanation of 1,2-dibromo-4,5-dimethylbenzene, alternatively the *title compound* may be selectively synthesised utilizing a modified procedure.

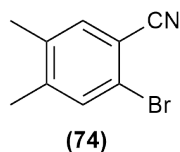


Figure 5.12: 2-Bromo-4,5-dimethylbenzonitrile

To a solution of 1,2-dibromo-4,5-dimethylbenzene (8.4 g, 32 mmol) in anhydrous *p*-xylene (60 mL) was added finely ground and oven dried  $\text{K}_3[\text{Fe}(\text{CN})_6]$  (2.4 g, 3.2 mmol), CuI (304 mg, 1.6 mmol) and 1-butylimidazole (4.2 mL, 32 mmol). The suspension was refluxed for 72 hr then cooled to RT.  $\text{Et}_2\text{O}$  (100 mL) was added and the solution filtered. The solution was washed with  $\text{H}_2\text{O}$  (3 x 50 mL) and brine (2 x 50 mL). The organic phase was collected and dried over  $\text{MgSO}_4$ , the solvent was removed to yield an off white solid. The crude product was subjected to silica gel chromatography eluting with DCM/PE 1:1, recrystallisation from MeOH yielded the *title compound* as a colourless solid (5.6 g, 83 %)

$^1\text{H}$  NMR (500 MHz,  $\text{CDCl}_3$ )  $\delta$  7.44 (s, 1H), 7.39 (s, 1H), 2.31 (s, 3H), 2.29 (s, 3H)

$^{13}\text{C}$  NMR (125.7 MHz,  $\text{CDCl}_3$ )  $\delta$  143.6, 136.4, 136.2, 134.7, 123.5, 117.0, 113.2, 21.1, 20.4

MP: 108-110 °C (lit. 106°C)<sup>147</sup>

## 5.2.8 3,6-Diphenylphthalonitrile

### Phthalonitrile-3,6-ditriflate

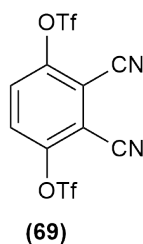


Figure 5.13: Phthalonitrile-3,6-ditriflate

2,3-Dicyanohydroquinone (5.1 g, 31 mmol) was dissolved in a solution of dry DCM (30 mL) and 2,6-lutidine (16 mL) under  $\text{N}_2$  and cooled to  $-78^\circ\text{C}$ . Trifluoromethanesulphonic anhydride (21 g, 75 mmol) was added dropwise over 30 min. The solution was warmed to RT and allowed to stir overnight. The

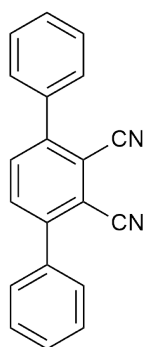
solution was added to DCM (200 mL) and washed with H<sub>2</sub>O (200 mL), 1M HCl (100 mL), 5% NaOH (100 mL) and brine (100 mL). The organics were collected, dried with MgSO<sub>4</sub> and the solvent removed to yield a pale yellow crystalline solid. Recrystallisation from toluene/cyclohexane (1:1) yielded the *title compound* as a colourless crystalline solid (8.0 g, 61%).<sup>131,132</sup>

<sup>1</sup>H NMR (500 MHz, CDCl<sub>3</sub>) δ 7.87 (s, 2H)

<sup>13</sup>C NMR (125.7 MHz, CDCl<sub>3</sub>) δ 149.0, 128.8, 118.6 (q, J = 321.4 Hz), 112.9, 109.4

MP: 107 - 109 °C (lit. 107.5 - 108.1°C)<sup>148</sup>

### 3,6-Diphenylphthalonitrile



(70)

Figure 5.14: 3,6-Diphenylphthalonitrile

To a solution of phthalonitrile-3,6-ditriflate (1.0 g, 2.4 mmol) in toluene/EtOH/H<sub>2</sub>O (3:3:1, 30 mL) LiCl (0.26 g) was added. The solution was degassed with argon for 30 min and Pd(DPPF)Cl<sub>2</sub> (80 mg, 5 mol %) was added. Benzeneboronic acid (0.85 g, 7 mmol) and Cs<sub>2</sub>CO<sub>3</sub> (2.6 g, 8 mmol) were added and the mixture stirred at RT overnight. The reaction was filtered and the solvent removed to yield a brown solid, the solid was dissolved in toluene/EtOAc (1:1, 100 mL) and washed with 10% KOH (2 x 50 mL), 1M HCl (50 mL) and brine (80 mL). The organics were dried over MgSO<sub>4</sub> and the solvent removed. Recrystallisation of the crude material from EtOH yielded the *title compound* as colourless needles (0.9 g, 65 %)

<sup>1</sup>H NMR (500 MHz, CDCl<sub>3</sub>) δ 7.80 (s, 2H), 7.63 – 7.58 (m, 4H), 7.58 – 7.50 (m, 6H)

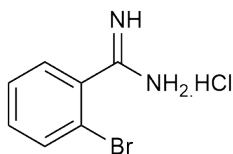
<sup>13</sup>C NMR (125.7 MHz, CDCl<sub>3</sub>) δ 145.9, 136.4, 134.1, 129.8, 129.2, 128.8, 115.8, 115.7

MP: 211 - 213 °C

## 5.3 Amidines and aminoisoindolines

### 5.3.1 (Z)-1-(Phenylmethylene)-1*H*-isoindol-3-amine

#### 2-Bromobenzamidinium hydrochloride (11)



(11)

Figure 5.15: 2-Bromobenzamidinium hydrochloride

To a solution of 2-bromobenzonitrile (3.7 g, 20.33 mmol) in dry THF (3 mL) was added a 1M solution of anhydrous  $\text{LiN}(\text{SiMe}_3)_2$  in THF (22 mmol, 1.1 eq). The reaction mixture was stirred at room temperature for 4 hrs. The reaction was then cooled in an ice bath and a 5M solution of HCl in *i*-PrOH was added (15 mL). The solution was left to stir at RT overnight, The precipitate was filtered and washed with  $\text{Et}_2\text{O}$  to yield the *title compound* as off white crystals (4.0 g, 84 %).<sup>114</sup>

$^1\text{H}$  NMR (500 MHz, Methanol- $d_4$ )  $\delta$  7.81 (dd,  $J = 7.3, 1.5$  Hz, 1H), 7.63-7.53 (m, 3H)

$^{13}\text{C}$  NMR (125.7 MHz, Methanol- $d_4$ )  $\delta$  168.0, 134.7, 134.5, 132.8, 130.7, 129.2, 120.8

MP: > 300°C (lit. > 250°C)<sup>149</sup>

#### (Z)-1-(Phenylmethylene)-1*H*-isoindol-3-amine (12)

A mixture of 2-bromobenzamidinium (706 mg, 3 mmol), BINAP (102 mg, 0.165 mmol) and  $\text{PdCl}_2(\text{MeCN})_2$  (39 mg, 0.15 mmol) was sealed in a microwave vessel with a stirrer bar and purged with  $\text{N}_2$ . A solution of ethynylbenzene (0.395 mL, 1.2 eq) and DBU (1.12 mL, 2.5 eq) in dry DMF (12 mL) was added. The vial was stirred at RT for 5 mins to allow a solution to form. The vial was then irradiated in a microwave reactor at 120°C for 1hr. After cooling EtOAc (50 mL) was added and the solution washed with a solution of  $\text{NaHCO}_3$  (75 mL x 3). The organic layer was dried with  $\text{MgSO}_4$ , filtered and concentrated. The crude residue was subject to column chromatography utilising PE:EtOAc (1:1) followed by EtOAc to afford an oily yellow substance that was recrystallised from DCM/petrol to yield the *title compound* as yellow needles (0.48 g, 73 %).<sup>115</sup>

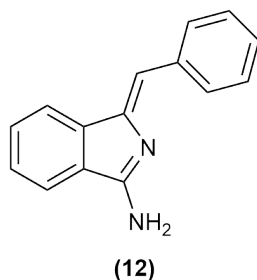


Figure 5.16: (Z)-1-(Phenylmethylene)-1*H*-isoindol-3-amine

$^1\text{H}$  NMR (500 MHz,  $\text{CDCl}_3$ )  $\delta$  8.14 (d,  $J = 7.7$  Hz, 2H), 7.83 (dt,  $J = 7.5$ , 0.9 Hz, 1H), 7.55 – 7.47 (m, 2H), 7.46 – 7.38 (m, 3H), 7.32 – 7.24 (m, 1H), 6.80 (s, 1H), 5.56 (br s, 2H)

$^{13}\text{C}$  NMR (125.7 MHz,  $\text{CDCl}_3$ )  $\delta$  165.1, 146.3, 142.5, 136.4, 130.7, 130.4, 129.4, 128.4, 127.3, 127.2, 119.7, 119.3, 114.7

MS (MALDI-TOF):  $m/z = 220.84$   $[\text{M}]^+$

Chemical formula and exact mass:  $\text{C}_{15}\text{H}_{12}\text{N}_2$ , 220.10  $\text{g}\cdot\text{mol}^{-1}$

**(Z)-1-[(4-Methoxy)benzylidene]-1*H*-isoindol-3-amine (13)**

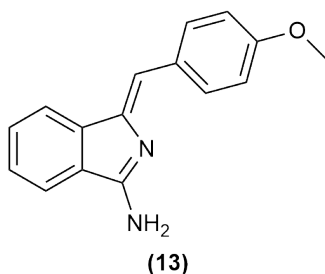


Figure 5.17: (Z)-1-[(4-Methoxy)benzylidene]-1*H*-isoindol-3-amine

A mixture of 2-bromobenzamidine (706 mg, 3 mmol), BINAP (102 mg, 0.165 mmol) and  $\text{PdCl}_2(\text{MeCN})_2$  (39 mg, 0.15 mmol) was sealed in a microwave vessel with a stirrer bar and purged with  $\text{N}_2$ . A solution of 1-ethynyl-4-methoxybenzene (0.49 mL, 1.2 eq) and DBU (1.12 mL, 2.5 eq) in dry DMF (12 mL) was added. The vial was stirred at RT for 5 mins to allow a solution to form. The vial was then irradiated in a microwave reactor at 120C for 1hr. After cooling EtOAc (50 mL) was added and the solution washed with a solution of  $\text{NaHCO}_3$  (75 mL x 3). The organic layer was dried with  $\text{MgSO}_4$ , filtered and concentrated. The crude residue was subject to column chromatography

utilising PE:EtOAc (1:1) followed by EtOAc to afford an oily yellow substance that was recrystallised from DCM/petrol to yield the title compound as yellow needles (0.57 g, 76 %).<sup>115</sup>

<sup>1</sup>H NMR (500 MHz, CDCl<sub>3</sub>)  $\delta$  8.16 – 8.10 (m, 2H), 7.81 (dt, J = 7.3, 1.1 Hz, 1H), 7.49 (td, J = 7.6, 0.9 Hz, 2H), 7.43 – 7.35 (m, 1H), 7.01 – 6.94 (m, 2H), 6.78 (s, 1H), 5.49 (br s, 2H), 3.88 (s, 3H).

<sup>13</sup>C NMR (125.7 MHz, CDCl<sub>3</sub>)  $\delta$  164.5, 159.2, 143.3, 139.6, 132.1, 130.8, 129.7, 129.0, 126.8, 123.8, 119.7, 118.8, 114.1, 55.4

MP: 152-154°C

MS (MALDI-TOF):  $m/z = 250.46 [M]^+$

Chemical formula and exact mass: C<sub>16</sub>H<sub>14</sub>N<sub>2</sub>O, 250.11 g.mol<sup>-1</sup>

### 5.3.2 (Z)-1-[(4-Methoxybenzylidene)]-5,5,8,8-tetramethyl-5H,6H,7H,8H-benzo[f]isoindol-3-amine

#### 6-Bromo-1,1,4,4-tetramethyl-1,2,3,4-tetrahydronaphthamide hydrochloride

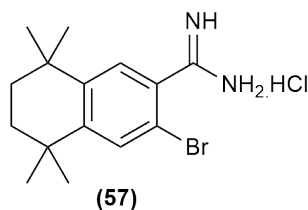


Figure 5.18: 1,1,4,4-Tetramethyl-1,2,3,4-tetrahydronaphthamide hydrochloride

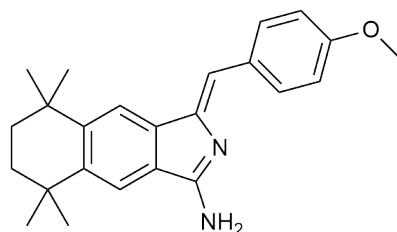
To a solution of 6-bromo-7-cyano-1,1,4,4-tetramethyl-1,2,3,4-tetrahydronaphthalene (3.5 g, 10.2 mmol) in dry THF (3 mL) was added a 1M solution of anhydrous LiN(SiMe<sub>3</sub>)<sub>2</sub> in THF (11 mL, 11 mmol). The reaction was stirred at RT for 4 hr, after which a 5M solution of HCl in *i*-PrOH (8 mL) and stirred overnight. The resulting precipitate was filtered and washed with Et<sub>2</sub>O to yield the *title compound* as colourless crystals (3.27 g, 93 %).<sup>114</sup>

<sup>1</sup>H NMR (500 MHz, Methanol-*d*<sub>4</sub>)  $\delta$  7.72 (s, 1H), 7.59 (s, 1H), 1.76 (s, 4H), 1.34 (s, 6H), 1.32 (s, 6H)

<sup>13</sup>C NMR (125.7 MHz, Methanol-*d*<sub>4</sub>)  $\delta$  169.8, 154.2, 154.1, 148.0, 134.2, 131.6, 130.8, 119.0, 36.9, 36.8, 36.7, 36.5, 32.9, 32.9

MP: 152-154 °C (lit. 153 - 155°C)<sup>139</sup>

**(Z)-1-[(4-Methoxybenzylidene)]-5,5,8,8-tetramethyl-5H,6H,7H,8H-benzo[f]isoindol-3-amine**



**(28)**

Figure 5.19: (Z)-1-[(4-Methoxybenzylidene)]-5,5,8,8-tetramethyl-5H,6H,7H,8H-benzo[f]isoindol-3-amine

A mixture of 6-bromo-1,1,4,4-tetramethyl-1,2,3,4-tetrahydronaphthamide hydrochloride (1.0 g, 3 mmol), BINAP (102 mg, 0.165 mmol) and PdCl<sub>2</sub>(MeCN)<sub>2</sub> (39 mg, 0.15 mmol) was sealed in a microwave vessel with a stirrer bar and purged with N<sub>2</sub>. A solution of 1-ethynyl-4-methoxybenzene (0.49 mL, 1.2 eq) and DBU (1.12 mL, 2.5 eq) in dry DMF (12 mL) was added. The vial was stirred at RT for 5 mins to allow a solution to form. The vial was then irradiated in a microwave reactor at 120C for 1hr. After cooling EtOAc (50 mL) was added and the solution washed with a solution of NaHCO<sub>3</sub> (75 mL x 3). The organic layer was dried with MgSO<sub>4</sub>, filtered and concentrated. The crude residue was subject to column chromatography utilising PE:EtOAc (1:1) followed by EtOAc to afford an oily yellow substance that was recrystallised from DCM/petrol to yield the title compound as yellow needles (0.61 g, 56 %).<sup>115</sup>

<sup>1</sup>H NMR (500 MHz, CDCl<sub>3</sub>) δ 8.06 (d, J = 8.5 Hz, 2H), 7.72 (s, 1H), 7.42 (s, 1H), 6.92 (d, J = 8.5 Hz, 2H), 6.68 (s, 1H), 3.85 (s, 3H), 1.75 (s, 4H), 1.39 (s, 6H), 1.34 (s, 6H)

<sup>13</sup>C NMR (125.7 MHz, CDCl<sub>3</sub>) δ 164.5, 158.7, 147.0, 145.1, 144.5, 140.1, 131.6, 129.7, 117.7, 117.3, 113.8, 113.5, 55.3, 35.1, 35.1, 35.0, 34.8, 32.6, 32.4

MP: 200-204 °C (lit. 202 - 205°C)<sup>139</sup>

MS (MALDI-TOF): *m/z* = 360.88 [M]<sup>+</sup>

Chemical formula and exact mass: C<sub>24</sub>H<sub>28</sub>N<sub>2</sub>O, 360.22 g.mol<sup>-1</sup>

### 5.3.3 (Z)-5,6-Dimethoxy-1-[(4-methoxy)benzylidene]-1*H*-isoindol-3-amine

#### 2-Bromo-4,5-dimethoxybenzamidinium hydrochloride

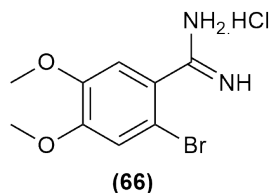


Figure 5.20: 2-Bromo-4,5-dimethoxybenzamidinium hydrochloride

To a solution of 2-bromo-4,5-dimethoxybenzimidine (3.0 g, 10.2 mmol) in dry THF (3 mL) was added a 1M solution of anhydrous  $\text{LiN}(\text{SiMe}_3)_2$  in THF (11 mL, 11 mmol). The reaction was stirred at RT for 4 hr, after which a 5M solution of HCl in *i*-PrOH (8 mL) and stirred overnight. The resulting precipitate was filtered and washed with  $\text{Et}_2\text{O}$  to yield the *title compound* as colourless crystals (2.5 g, 82 %).<sup>114</sup>

$^1\text{H}$  NMR (500 MHz,  $\text{MeOH-}d_4$ )  $\delta$  7.32 (s, 1H), 7.20 (s, 1H), 3.91 (s, 3H), 3.88 (s, 3H)

$^{13}\text{C}$  NMR (125.7 MHz,  $\text{MeOH-}d_4$ )  $\delta$  168.4, 154.2, 150.9, 125.1, 118.2, 114.0, 112.8, 57.6, 57.5

MP: 150-154 °C (lit. 148 - 150°C)<sup>139</sup>

#### (Z)-5,6-Dimethoxy-1-[(4-methoxy)benzylidene]-1*H*-isoindol-3-amine

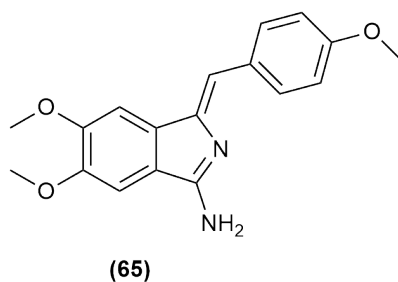


Figure 5.21: (Z)-5,6-Dimethoxy-1-[(4-methoxy)benzylidene]-1*H*-isoindol-3-amine

A mixture of 2-bromo-4,5-dimethoxybenzimidine hydrochloride (0.89 g, 3 mmol), BINAP (102 mg, 0.165 mmol) and PdCl<sub>2</sub>(MeCN)<sub>2</sub> (39 mg, 0.15 mmol) was sealed in a microwave vessel with a stirrer bar and purged with N<sub>2</sub>. A solution of 1-ethynyl-4-methoxybenzene (0.49 mL, 1.2 eq) and DBU (1.12 mL, 2.5 eq) in dry DMF (12 mL) was added. The vial was stirred at RT for 5 mins to allow a solution to form. The vial was then irradiated in a microwave reactor at 120C for 1hr. After cooling EtOAc (50 mL) was added and the solution washed with a solution of NaHCO<sub>3</sub> (75 mL x 3). The organic layer was dried with MgSO<sub>4</sub>, filtered and concentrated. The crude residue was subject to column chromatography utilising PE:EtOAc (1:1) followed by EtOAc to afford an oily yellow substance that was recrystallised from DCM/petrol to yield the title compound as yellow needles (1.6 g, 63 %).<sup>115</sup>

<sup>1</sup>H NMR (500 MHz, CDCl<sub>3</sub>) δ 7.90 (d, J = 8.5 Hz, 2H), 7.21 (s, 1H), 7.16 (s, 1H), 6.94 (d, J = 8.5 Hz, 2H), 6.61 (s, 1H), 4.02 (s, 3H), 3.95 (s, 3H), 3.84 (s, 3H)

<sup>13</sup>C NMR (125.7 MHz, CDCl<sub>3</sub>) δ 163.9, 158.8, 151.2, 149.3, 143.2, 136.1, 131.4, 128.9, 122.4, 114.7, 114.0, 102.0, 56.3, 56.2, 55.5

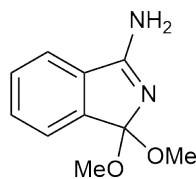
MP: 219-223 °C (lit. 220 - 223°C)<sup>139</sup>

MS (MALDI-TOF): *m/z* = 310.70 [M]<sup>+</sup>

Chemical formula and exact mass: C<sub>18</sub>H<sub>18</sub>N<sub>2</sub>O<sub>3</sub>, 310.13 g.mol<sup>-1</sup>

## 5.4 Dimethoxyindolines

### 5.4.1 1-Imino-3,3-dimethoxyisoindoline (29)



(29)

Figure 5.22: 1-Imino-3,3-dimethoxyisoindoline

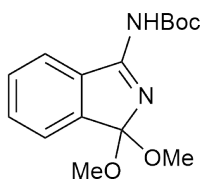
Sodium metal (2 g, 0.09 mol) was dissolved in MeOH (70 mL), the solution was cooled to RT and phthalonitrile (10 g, 78 mmol) was added. The solution was stirred until a precipitate formed, this was filtered, washed with H<sub>2</sub>O and dried under vacuum to yield the *title compound* as a pale green crystalline solid (8.0 g, 54 %).<sup>121</sup>

$^1\text{H}$  NMR (500 MHz,  $\text{CDCl}_3$ )  $\delta$  7.54 (dt,  $J = 7.3, 1.1$  Hz, 1H), 7.50 – 7.42 (m, 3H), 3.37 (s, 6H)

$^{13}\text{C}$  NMR (125.7 MHz,  $\text{CDCl}_3$ )  $\delta$  134.2, 131.7, 131.2, 130.9, 129.8, 123.5, 122.7, 120.6, 51.4, 50.6

MP: Decomposes

#### 5.4.2 N-Boc 1-imino-3,3-dimethoxyisoindoline (34)



(34)

Figure 5.23: N-Boc 1-imino-3,3-dimethoxyisoindoline

1-Amino-3,3-dimethoxyisoindoline (1.0 g, 5.2 mmol) was added to a solution of di-tert-butyl dicarbonate (1.2 g, 5.5 mmol) in glycerol (10 mL). The solution was stirred vigorously overnight at RT. The solution was then extracted with hexane/EtOAc (9:1) (3 x 50 mL). The organics were dried over  $\text{MgSO}_4$  and the solvent removed to yield the *title compound* as a colourless oil (1.42 g, 94 %).<sup>122</sup>

$^1\text{H}$  NMR (500 MHz,  $\text{CDCl}_3$ )  $\delta$  9.30 (s, 1H), 7.96 – 7.91 (m, 1H), 7.54 (td,  $J = 7.4, 1.1$  Hz, 1H), 7.47 - 7.40 (m, 2H), 3.23 (s, 6H), 1.51 (s, 9H)

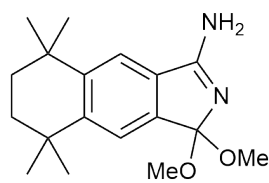
$^{13}\text{C}$  NMR (125.7 MHz,  $\text{CDCl}_3$ )  $\delta$  164.9, 139.9, 134.1, 133.0, 130.7, 127.7, 124.2, 122.5, 112.6, 51.9, 28.2, 27.5, 14.3.

MP: < 25°C

FT-IR: (ATR),  $\nu$  ( $\text{cm}^{-1}$ ): 1768 (C=O), 1084 (C-O, ether)

#### 5.4.3 1-Imino-5,5,8,8-tetramethyl-5H,6H,7H,8H-12,12-dimethoxyisoindoline (31)

To a solution of 6,7-dicyano-1,1,4,4-tetramethyl-1,2,3,4-tetrahydronaphthalene (2.0 g, 8.4 mmol) in MeOH (10 mL) was added NaOMe (0.54 g, 10 mmol). The solution was stirred at RT overnight and the precipitate filtered and washed with  $\text{H}_2\text{O}$ . The precipitate was dried under vacuum to yield the *title compound* as an off white solid (1.6 g, 63 %).<sup>121</sup>



(31)

Figure 5.24: 1-Imino-5,5,8,8-tetramethyl-5H,6H,7H,8H-12,12-dimethoxyisoindoline

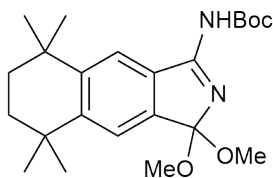
$^1\text{H}$  NMR (500 MHz,  $\text{CDCl}_3$ )  $\delta$  7.49 (s, 1H), 7.32 (s, 1H), 5.61 (s, 2H), 3.40 (s, 6H), 1.73 (s, 4H), 1.33 (s, 12H)

$^{13}\text{C}$  NMR (125.7 MHz,  $\text{CDCl}_3$ )  $\delta$  136.0, 133.6, 133.1, 132.8, 132.0, 124.9, 123.8, 121.3, 52.3, 51.0, 35.3, 34.9, 31.8, 31.6

MP: decomposes

FT-IR: (ATR),  $\nu$  ( $\text{cm}^{-1}$ ): 3430 (N-H), 1077 (C-O, ether)

#### 5.4.4 NBoc 1-Imino-5,5,8,8-tetramethyl-5H,6H,7H,8H-12,12-dimethoxyisoindoline (36)



(36)

Figure 5.25: NBoc 1-Imino-5,5,8,8-tetramethyl-5H,6H,7H,8H-12,12-dimethoxyisoindoline (36)

To a solution of tetramethyldimethoxyindoline (1.5 g, 5 mmol) in glycerol (10 mL) was added di-tert-butyl-dicarbonate (1.2 g, 5.5 mmol). The solution was stirred at RT overnight, then extracted with hexane/EtOAc (9:1) (3 x 50 mL). The organics were collected and dried over  $\text{MgSO}_4$  and the solvent removed to yield the *title compound* as a colourless oil (1.8 g, 91 %).<sup>122</sup>

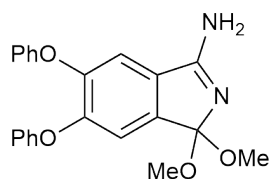
$^1\text{H}$  NMR (500 MHz,  $\text{CDCl}_3$ )  $\delta$  9.34 (s, 1H), 7.62 (s, 1H), 7.43 (s, 1H), 3.31 (s, 6H), 1.81 (s, 4H), 1.54 (s, 9H), 1.34 (s, 12H)

$^{13}\text{C}$  NMR (125.7 MHz,  $\text{CDCl}_3$ )  $\delta$  165.4, 136.7, 134.2, 133.9, 133.2, 132.6, 125.7, 124.2, 121.4, 52.1, 50.7, 35.3, 35.1, 32.0, 31.9, 28.6, 27.9, 14.4

MP: < 25°C

FT-IR: (ATR),  $\nu$  ( $\text{cm}^{-1}$ ): 1770 (C=O), 1085 (C-O, ether)

#### 5.4.5 1-Imino-4,5-diphenoxy-8,8-dimethoxyisoindoline



(60)

Figure 5.26: 1-Imino-4,5-diphenoxy-8,8-dimethoxyisoindoline

To a solution of 4,5-diphenoxyphthalonitrile (2.6 g, 8.4 mmol) in MeOH (10 mL) was added NaOMe (0.54 g, 10 mmol). The solution was stirred at RT overnight and the precipitate filtered and washed with  $\text{H}_2\text{O}$ . The precipitate was dried under vacuum to yield the *title compound* as an off white solid (2.1 g, 68 %).<sup>121</sup>

$^1\text{H}$  NMR (500 MHz,  $\text{CDCl}_3$ )  $\delta$  7.54 - 7.48 (m, 4H), 7.32 (dt, 2H), 7.20 - 7.14 (m, 4H), 7.12 (s, 1H), 7.04 (s, 1H), 3.42 (s, 6H)

$^{13}\text{C}$  NMR (125.7 MHz,  $\text{CDCl}_3$ )  $\delta$  154.1, 152.7, 130.7, 130.2, 129.6, 129.2, 127.0, 126.8, 124.5, 122.2, 121.4, 119.1, 52.3, 51.9

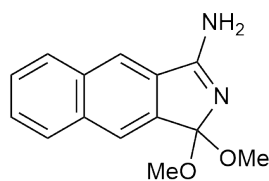
MP: decomposes

FT-IR: (ATR),  $\nu$  ( $\text{cm}^{-1}$ ): 3420 (N-H), 1105 (C-O, ether)

#### 5.4.6 1-Imino-3,3-dimethoxybenzo(F)isoindoline (41)

To a solution of 2,3-dicyanonaphthalene (1.5 g, 8.4 mmol) in MeOH (10 mL) was added NaOMe (0.54 g, 10 mmol). The solution was stirred at RT overnight and the precipitate filtered and washed with  $\text{H}_2\text{O}$ . The precipitate was dried under vacuum to yield the *title compound* as an off white solid (1.6 g, 80 %).<sup>121</sup>

$^1\text{H}$  NMR (500 MHz,  $\text{MeOH-}d_4$ )  $\delta$  8.58 (s, 1H), 8.07 (s, 1H), 8.02 (dd, J = 8.2, 3.5 Hz, 2H), 7.71 - 7.59 (m, 2H), 3.35 (s, 6H)



(41)

Figure 5.27: 1-Imino-3,3-dimethoxybenzo(F)isoindoline

$^{13}\text{C}$  NMR (125.7 MHz, MeOH- $d_4$ )  $\delta$  146.3, 140.4, 140.0, 139.2, 138.4, 137.9, 137.6, 137.0, 136.5, 135.3, 124.9, 121.2, 54.2, 53.0

MP: decomposes

FT-IR: (ATR),  $\nu$  ( $\text{cm}^{-1}$ ): 3435 (N-H), 1085 (C-O, ether)

## 5.5 Aminoisoindoline & dimethoxyisoindoline dimeric condensation products

**Procedure A** Procedure A utilises dimethoxyisoindolines and aminoisoindolines in MeOH at room temperature

**Procedure B** Procedure B utilises NBoc protected dimethoxyisoindoline derivatives and aminoisoindolines in EtOH at reflux.

**Procedure C** Procedure C utilises aminoisoindoline, phthalonitrile and NaOMe to form the dimethoxyisoindoline *in situ*.

**Procedure D** Procedure D utilises aminoisoindoline and dimethoxyisoindoline in dry DCM with molecular sieves to remove MeOH.

**Procedure E** Procedure E utilises NBoc protected products, deprotection with NaOt-Bu/ $\text{H}_2\text{O}$  yields the target materials.

### 5.5.1 Condensation product (30)

**Procedure A** A solution of (1Z)-1-[(4-methoxyphenyl)methylene]-1*H*-isoindol-3-amine (0.25 g, 1 mmol) and 1,1-dimethoxy-1*H*-isoindol-3-amine (0.19 g, 1 mmol) in MeOH (5 mL) was stirred at RT overnight. Upon completion the solvent was removed and the residue recrystallised from EtOAc to yield the (30) as a dark orange solid (0.28 g, 74 %)

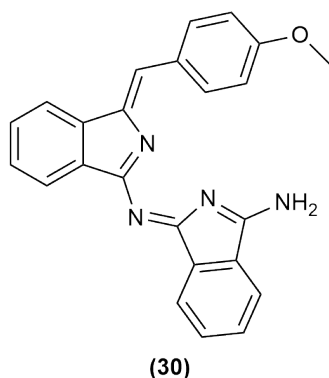


Figure 5.28: Condensation product **(30)**

**Procedure C** To a solution of (1*Z*)-1-[(4-methoxyphenyl)methylene]-1*H*-isoindol-3-amine (0.25 g, 1 mmol) and phthalonitrile (0.13 g, 1 mmol) in MeOH (10 mL) was added NaOMe (65 mg, 1.2 mmol). The solution was stirred at RT overnight and the precipitate filtered to yield the *title compound* as a dark orange solid (0.16 g, 41 %)

**Procedure E** To a solution of **(35)** (1 mmol, 0.48 g) in THF (5 mL) was added Na*Ot*-*Bu* (3 eq, 0.29 g) and H<sub>2</sub>O (1 eq, 0.02 mL). The solution was heated to reflux for 6 hrs, cooled, and worked up as previously described to yield the *title compound* as a dark orange solid (0.26 g, 68 %)

<sup>1</sup>H NMR (500 MHz, DMSO-*d*<sub>6</sub>) δ 8.26 (d, *J* = 8.7 Hz, 2H), 8.13 (d, *J* = 7.5 Hz, 1H), 8.07 (d, *J* = 8.0 Hz, 1H), 7.91 (d, *J* = 7.5 Hz, 1H), 7.78 (d, *J* = 7.5 Hz, 1H), 7.68 (td, *J* = 7.5, 1.1 Hz, 1H), 7.61 (td, *J* = 7.5, 1.1 Hz, 1H), 7.43 (t, *J* = 7.3 Hz, 1H), 7.37 (t, *J* = 7.3 Hz, 1H), 7.24 (s, 1H), 7.05 (d, *J* = 8.7 Hz, 2H), 3.81 (s, 3H)

<sup>13</sup>C NMR (125.7 MHz, DMSO-*d*<sub>6</sub>) δ 160.1, 154.3, 153.9, 146.9, 144.1, 128.4, 123.3, 119.8, 119.0, 118.2, 117.4, 117.2, 116.8, 113.4, 55.7

MP: 168 - 172 °C

MS (MALDI-TOF): *m/z* = 378.94 [M]<sup>+</sup>

Chemical formula and exact mass: C<sub>24</sub>H<sub>18</sub>N<sub>4</sub>O, 378.15 g.mol<sup>-1</sup>

UV-Vis: λ<sub>max</sub> (nm) (ε (dm<sup>3</sup>.mol<sup>-1</sup>.cm<sup>-1</sup>)) = 440 (6.16.10<sup>3</sup>), 332 (1.06.10<sup>4</sup>), 260 (1.54.10<sup>4</sup>)

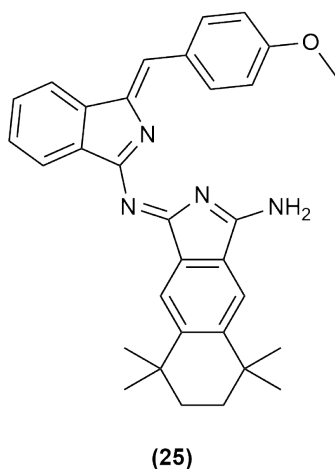


Figure 5.29: Condensation product **(25)**

### 5.5.2 Condensation product **(25)**

**Procedure A** A solution of (1Z)-1-[(4-methoxyphenyl)methylene]-1*H*-isindol-3-amine (0.31 g, 1.24 mmol) and 1-imino-5,5,8,8-tetramethyl-5*H*,6*H*,7*H*,8*H*-12,12-dimethoxyisoindoline (0.37 g, 1.24 mmol) in MeOH (5 mL) was stirred at RT overnight. Upon completion the solvent was removed and the residue purified by column chromatography eluting with DCM:hexane 2:3. The red/orange fraction was collected and recrystallised from EtOAc to yield the **(25)** as a dark orange solid (0.12 g, 20%)

**Procedure D** To a solution of (1Z)-1-[(4-methoxyphenyl)methylene]-1*H*-isindol-3-amine (0.25 g, 1 mmol) and 1-imino-5,5,8,8-tetramethyl-5*H*,6*H*,7*H*,8*H*-12,12-dimethoxyisoindoline (0.30 g, 1 mmol) in dry DCM (10 mL) was added oven dried molecular sieves. The solution was heated to reflux overnight. Upon completion the dark red solution was decanted and the sieves rinsed several times with DCM. The organics were combined and the solvent removed. The crude solid was recrystallised from DCM/hexane to yield the *title compound* as a dark orange solid (0.24 g, 48 %)

**Procedure E** To a solution of **(37)** (1 mmol, 0.59 g) in THF (5 mL) was added NaO*t*-Bu (3 eq, 0.29 g) and H<sub>2</sub>O (1 eq, 0.02 mL). The solution was heated to reflux for 6 hrs, cooled, and worked up as previously described to yield the *title compound* as a dark orange solid (0.32 g, 65 %)

<sup>1</sup>H NMR (500 MHz, DMSO-*d*<sub>6</sub>) δ 8.11 – 8.02 (m, 4H), 7.84 (d, J = 7.4 Hz, 2H), 7.47 (m, 2H), 7.16 (s, 1H), 7.08 – 7.03 (m, 2H), 3.91 (s, 3H), 1.77 (s, 4H), 1.43 (s, 6H), 1.39 (s, 6H)

<sup>13</sup>C NMR (125.7 MHz, DMSO-*d*<sub>6</sub>) δ 161.8, 153.1, 152.9, 146.9, 144.5, 129.0, 122.3, 119.3, 119.1, 116.2, 115.4, 115.1, 114.9, 111.2, 55.7, 33.4, 33.1, 32.8, 31.2, 31.0

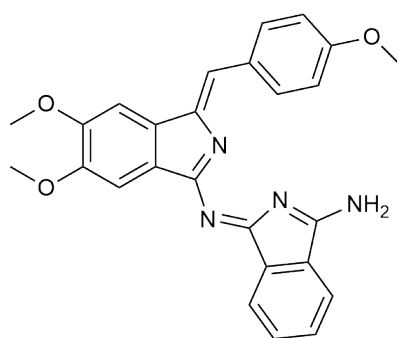
MP: 148 - 154 °C

MS (MALDI-TOF):  $m/z = 488.65 [M]^+$

Chemical formula and exact mass:  $C_{32}H_{32}N_4O$ , 488.26 g.mol<sup>-1</sup>

UV-Vis:  $\lambda_{\max}$  (nm) ( $\epsilon$  (dm<sup>3</sup>.mol<sup>-1</sup>.cm<sup>-1</sup>)) = 442 (6.88.10<sup>3</sup>), 334 (1.19.10<sup>4</sup>), 260 (1.68.10<sup>4</sup>)

### 5.5.3 Condensation product (42)



(42)

Figure 5.30: Condensation product (42)

**Procedure D** To a solution of (Z)-5,6-Dimethoxy-1-[(4-Methoxy)benzylidene]-1*H*-isoindol-3-amine (0.31 g, 1 mmol) and 1-imino-3,3-dimethoxyisoindoline (0.19 g, 1 mmol) in dry DCM (10 mL) was added oven dried molecular sieves. The solution was heated to reflux overnight. Upon cooling the dark red solution was decanted and the molecular sieves washed several times with DCM. The organics were combined, the solvent removed, and the crude product recrystallised from DCM/hexane to yield the *title compound* as a dark orange solid (0.19 g, 43 %)

<sup>1</sup>H NMR (500 MHz, DMSO-*d*<sub>6</sub>)  $\delta$  8.35 – 8.31 (m, 1H), 8.00 – 7.91 (m, 3H), 7.69 – 7.64 (m, 3H), 7.45 (s, 1H), 7.16 (s, 1H), 7.03 (d,  $J = 8.6$  Hz, 2H), 4.16 (s, 3H), 3.94 (s, 3H), 3.89 (s, 3H)

<sup>13</sup>C NMR (125.7 MHz, DMSO-*d*<sub>6</sub>)  $\delta$  158.2, 150.7, 148.8, 145.9, 144.2, 143.8, 135.1, 134.9, 130.9, 127.6, 127.0, 125.7, 124.3, 117.8, 117.4, 115.2, 113.8, 112.3, 111.8, 57.4, 56.8, 53.1

MP: 195 - 199°C

MS (MALDI-TOF):  $m/z = 437.28 [M]^+$

Chemical formula and exact mass: C<sub>26</sub>H<sub>22</sub>N<sub>4</sub>O<sub>3</sub>, 438.17 g.mol<sup>-1</sup>

UV-Vis:  $\lambda_{\max}$  (nm) ( $\epsilon$  (dm<sup>3</sup>.mol<sup>-1</sup>.cm<sup>-1</sup>)) = 437 (5.96.10<sup>3</sup>), 330 (1.02.10<sup>4</sup>), 263 (1.37.10<sup>4</sup>)

#### 5.5.4 Condensation product (43)

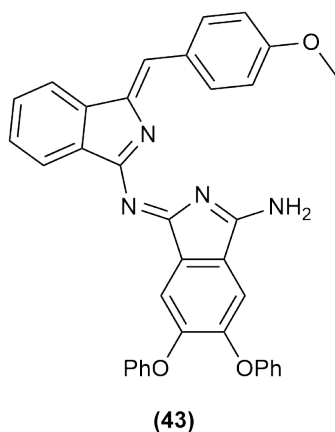


Figure 5.31: Condensation product **(43)**

**Procedure D** To a solution of (1Z)-1-[(4-methoxyphenyl)methylene]-1H-isindol-3-amine (0.25 g, 1 mmol) and 1-imino-4,5-diphenoxy-8,8-dimethoxyisoindoline (0.38 g, 1 mmol) in dry DCM (10 mL) was added oven dried molecular sieves. The solution was heated at reflux overnight. Once complete the dark red solution was decanted and the sieves rinsed with DCM several times. The organics were combined and the solvent removed. The crude residue was recrystallised from DCM/hexane to yield the *title compound* as a dark orange solid (0.25 g, 44 %)

<sup>1</sup>H NMR (500 MHz, DMSO-*d*<sub>6</sub>)  $\delta$  8.23 (d, *J* = 8.6 Hz, 2H), 8.19 – 8.15 (m, 2H), 7.94 (d, *J* = 7.7 Hz, 1H), 7.82 (d, *J* = 4.4 Hz, 1H), 7.41 – 7.27 (m, 3H), 7.14 – 6.97 (m, 8H), 6.96 – 6.91 (m, 2H), 6.66 (s, 1H), 3.79 (s, 3H)

<sup>13</sup>C NMR (125.7 MHz, DMSO-*d*<sub>6</sub>)  $\delta$  156.4, 150.2, 149.8, 147.6, 146.6, 146.3, 138.4, 136.8, 134.2, 132.0, 130.6, 130.5, 126.7, 119.6, 119.1, 119.0, 118.3, 114.2, 57.2

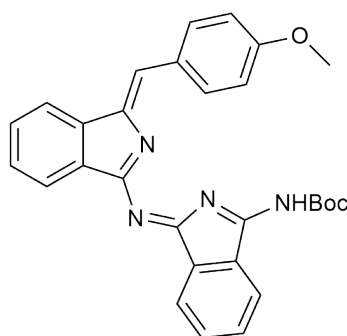
MP: 173 - 178°C

MS (MALDI-TOF): *m/z* = 563.71 [M]<sup>+</sup>

Chemical formula and exact mass: C<sub>36</sub>H<sub>26</sub>N<sub>4</sub>O<sub>3</sub>, 562.20 g.mol<sup>-1</sup>

UV-Vis:  $\lambda_{\max}$  (nm) ( $\epsilon$  (dm<sup>3</sup>.mol<sup>-1</sup>.cm<sup>-1</sup>)) = 446 (6.34.10<sup>3</sup>), 336 (1.13.10<sup>4</sup>), 262 (2.41.10<sup>4</sup>)

### 5.5.5 NBoc protected condensation product (35)



(35)

Figure 5.32: NBoc protected condensation product (35)

**Procedure B** A solution of (1*Z*)-1-[(4-methoxyphenyl)methylene]-1*H*-isoindol-3-amine (0.25 g, 1 mmol) and N-Boc 1-imino-3,3-dimethoxyisoindoline (0.29 g, 1 mmol) in EtOH (10 mL) was heated to reflux overnight. The solution was cooled to RT and the solvent removed. The crude residue was subject to silica gel chromatography eluting with DCM/PE (3:2). The intensely red fraction was collected and the solvent removed to yield the *title compound* as a dark red solid (0.18 g, 38 %)

<sup>1</sup>H NMR (500 MHz, CDCl<sub>3</sub>)  $\delta$  8.32 (d, *J* = 8.6 Hz, 2H), 8.20 (d, *J* = 7.5 Hz, 1H), 8.16 – 8.09 (m, 1H), 7.98 (d, *J* = 7.5 Hz, 1H), 7.85 (d, *J* = 7.5 Hz, 1H), 7.78 – 7.71 (m, 1H), 7.71 – 7.66 (m, 1H), 7.54 – 7.41 (m, 2H), 7.31 (s, 1H), 7.13 (dd, *J* = 8.0, 6.0 Hz, 2H), 3.88 (s, 3H), 1.63 (s, 9H)

<sup>13</sup>C NMR (125.7 MHz, CDCl<sub>3</sub>)  $\delta$  166.2, 158.2, 152.3, 152.0, 145.4, 145.1, 127.9, 122.6, 119.7, 117.6, 117.2, 114.8, 54.6, 28.5, 14.0

MP: 162 - 167 °C

MS (MALDI-TOF): *m/z* = 479.11 [M]<sup>+</sup>

Chemical formula and exact mass: C<sub>29</sub>H<sub>26</sub>N<sub>4</sub>O<sub>3</sub>, 478.20 g.mol<sup>-1</sup>

FT-IR: (ATR),  $\nu$  (cm<sup>-1</sup>): 1776 (C=O)

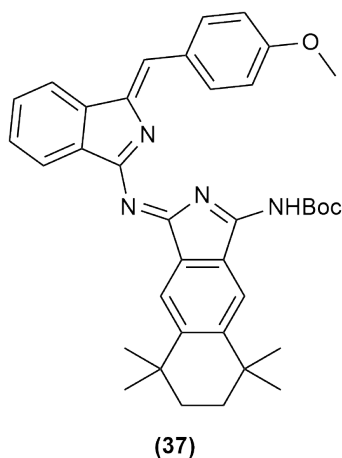


Figure 5.33: NBoc protected condensation product **(37)**

### 5.5.6 NBoc protected condensation product **(37)**

**Procedure C** A solution of (1*Z*)-1-[(4-methoxyphenyl)methylene]-1*H*-isindol-3-amine (0.16 g, 0.64 mmol) and NBoc 1-imino-5,5,8,8-tetramethyl-5*H*,6*H*,7*H*,8*H*-12,12-dimethoxyisindoline (0.24 g, 0.64 mmol) in EtOH (10 mL) was heated to reflux overnight. The solution was cooled to RT and the solvent removed. The crude residue was subject to silica gel chromatography eluting with DCM/PE (3:2). The intensely red fraction was collected and the solvent removed to yield the *title compound* as a dark red solid (0.10 g, 26 %)

$^1\text{H}$  NMR (500 MHz,  $\text{CDCl}_3$ )  $\delta$  8.35 (d,  $J = 8.4$  Hz, 2H), 8.14 (s, 1H), 8.09 (s, 1H), 8.04 (d,  $J = 7.4$  Hz, 1H), 7.94 (s, 1H), 7.90 – 7.83 (m, 1H), 7.54 – 7.43 (m, 1H), 7.31 (s, 1H), 7.14 (d,  $J = 8.4$  Hz, 2H), 3.90 (s, 3H), 1.78 (s, 4H), 1.60 (s, 9H), 1.38 (s, 12H)

$^{13}\text{C}$  NMR (125.7 MHz,  $\text{CDCl}_3$ )  $\delta$  168.0, 159.7, 153.4, 153.0, 144.3, 144.1, 128.6, 124.1, 123.6, 123.1, 118.9, 118.4, 115.7, 55.3, 33.6, 33.2, 33.0, 31.4, 28.6, 14.8

MP: 128 - 134 °C

MS (MALDI-TOF):  $m/z = 589.24$   $[\text{M}]^+$

Chemical formula and exact mass:  $\text{C}_{47}\text{H}_{40}\text{N}_4\text{O}_3$ , 588.31  $\text{g}\cdot\text{mol}^{-1}$

FT-IR: (ATR),  $\nu$  ( $\text{cm}^{-1}$ ): 1782 (C=O)

## 5.6 Trimeric condensation products

**Procedure A** Procedure A utilises dimethoxyisoindolines and aminoisoindolines in MeOH at reflux.

**Procedure B** Procedure B is the homocondensation of **(30)** to yield **(40)** with the elimination of diiminoisoindoline.

### 5.6.1 Condensation product **(33)**

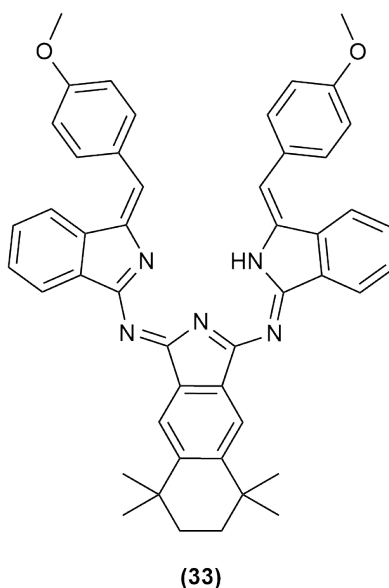


Figure 5.34: Condensation product **(33)**

**Procedure A** A solution of (1Z)-1-[(4-methoxyphenyl)methylene]-1H-indol-3-amine (0.5 g, 2 mmol) and 1-imino-5,5,8,8-tetramethyl-5H,6H,7H,8H-12,12-dimethoxyisoindoline (0.30 g, 1 mmol) in MeOH (10 mL) was heated to reflux overnight. Upon cooling the solvent was removed and the crude residue purified by silica gel chromatography eluting with DCM/hexane (3:2). The first brown fraction was collected and recrystallised from DCM/hexane to yield the *title compound* as a dark brown solid (0.52 g, 72 %)

**Procedure B** A solution of **(32)** (0.26 g, 0.53 mmol) in toluene (10 mL) was heated to 100°C overnight. Upon cooling the solvent was removed and the crude residue purified by silica gel chromatography eluting with EtOAc/hexane (2:3). The first brown fraction was collected, the solvent removed, and the residue recrystallised from DCM/hexane to yield the *title compound* as a dark brown solid (55 mg, 68 %).



$^{13}\text{C}$  NMR (125.7 MHz,  $\text{CDCl}_3$ )  $\delta$  161.0, 153.2, 152.4, 141.2, 140.9, 139.5, 131.1, 126.9, 121.0, 109.6, 64.2

MP: 200 - 203°C

MS (MALDI-TOF):  $m/z = 610.78$   $[\text{M}]^+$

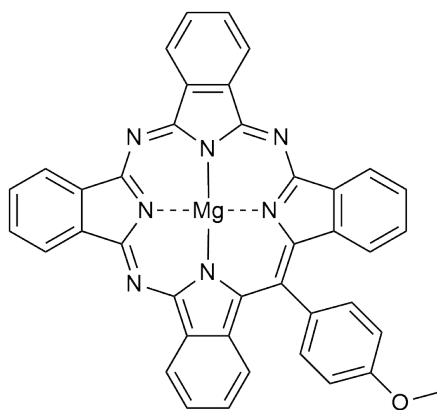
Chemical formula and exact mass:  $\text{C}_{40}\text{H}_{29}\text{N}_5\text{O}_2$ , 611.23  $\text{g}\cdot\text{mol}^{-1}$

UV-Vis:  $\lambda_{\text{max}}$  (nm) ( $\epsilon$  ( $\text{dm}^3\cdot\text{mol}^{-1}\cdot\text{cm}^{-1}$ )) = 475 ( $4.93\cdot 10^3$ ), 400 ( $9.57\cdot 10^3$ ), 347 ( $1.29\cdot 10^4$ ), 264 ( $2.01\cdot 10^4$ )

## 5.7 TBTAPs

Procedure A utilises aminoisoindolines and phthalonitrile with the original procedures. Procedure B utilises aminoisoindolines and phthalonitriles with modified versions of the original procedure. Procedure C utilises (**30**) and derivatives with the newly developed methodology.

### 5.7.1 MgTBTAP (16)



(16)

Figure 5.36: MgTBTAP (**16**)

**Procedure A** A suspension of phthalonitrile (154 mg, 3 eq.) and  $\text{MgBr}_2$  (110 mg, 1.5 eq.) in dry diglyme (0.5 mL) was heated in an oil bath at  $220^\circ\text{C}$  under an argon atmosphere for 10 min. A solution of aminoisoindoline (100 mg, 1 eq.) and phthalonitrile (51 mg, 1 eq.) in dry diglyme (1 mL) was then added dropwise over 1 hr. After addition the reaction was refluxed for 30 min. A final solution of DABCO (67.5 mg, 1.5 eq.) and phthalonitrile (51 mg, 1 eq.) in dry diglyme (0.5 mL) was added dropwise over 1 hr, followed by a further 30 min reflux. A stream of argon was passed through the reaction vessel to remove the solvent. The crude mixture was cooled to room temperature and dissolved in a mixture of DCM/MeOH (50 mL, 1:1) with the aid of sonication. The solvent was removed *in vacuo* and the residue purified by silica gel chromatography, firstly with DCM/ $\text{NEt}_3$ /THF (10:1:4). The collected green fractions were resubjected to a column eluted with PE/THF/MeOH (10:3:1) to obtain the pure green product. The material was recrystallised from DCM/MeOH to yield the title compound as dark crystals with a purple reflex (43 mg, 17 %).

**Procedure C** Condensation product (**30**) (180 mg, 2 eq) was added to a solution of  $\text{MgBr}_2$  (44 mg, 1 eq) in *p*-xylene (3 mL) and heated to reflux for 3 hr. After the reaction was complete the solvent was removed *in vacuo*, and the crude mixture dissolved in DCM/MeOH (50 mL, 1:1) with the aid

of sonication. The crude mixture was loaded on silica and purified by silica gel chromatography utilizing DCM/ $\text{NEt}_3$ /THF (10:1:4). The green fractions were collected and subjected to a second column chromatography eluting with PE/THF/MeOH (10:3:1). The green fractions were then recrystallised from DCM/MeOH to yield the *title compound* as a dark green solid (62 mg, 40 %)

$^1\text{H}$  NMR (500 MHz, Acetone- $d_6$ )  $\delta$  9.48 (d,  $J = 7.6$  Hz, 2H), 9.41 – 9.38 (m, 4H), 8.15 – 8.09 (m, 4H), 7.93 (d,  $J = 8.3$  Hz, 2H), 7.86 (t,  $J = 7.3$  Hz, 2H), 7.55 (t,  $J = 7.3$  Hz, 2H), 7.45 (d,  $J = 8.3$  Hz, 2H), 7.10 (d,  $J = 8.1$  Hz, 2H), 4.10 (s, 3H)

$^{13}\text{C}$  NMR (125.7 MHz, Acetone- $d_6$ )  $\delta$  163.4, 158.2, 155.0, 154.3, 145.6, 142.6, 142.5, 141.7, 141.0, 137.6, 136.4, 132.1, 131.5, 130.4, 129.7, 128.9, 128.2, 124.3, 124.0, 123.8, 116.2, 56.4

MP:  $> 300^\circ\text{C}$  (lit.  $> 300^\circ\text{C}$ )<sup>139</sup>

UV-Vis:  $\lambda_{\text{max}}$  (nm) ( $\epsilon$  ( $\text{dm}^3 \cdot \text{mol}^{-1} \cdot \text{cm}^{-1}$ )) = 676 ( $2.93 \cdot 10^5$ ), 652 ( $1.72 \cdot 10^5$ ), 596 ( $3.76 \cdot 10^4$ ), 447 ( $4.71 \cdot 10^4$ ), 390 ( $1.36 \cdot 10^5$ )

MALDI-TOF:  $m/z = 641.49$   $[\text{M}]^+$  (100%)

Chemical formula and exact mass:  $\text{C}_{40}\text{H}_{23}\text{MgN}_7\text{O}$ ,  $641.18 \text{ g} \cdot \text{mol}^{-1}$

### 5.7.2 2:2 MgTBTAP (18)

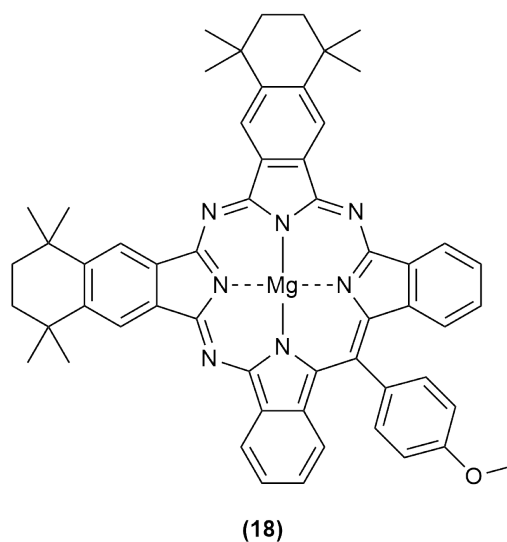


Figure 5.37: 2:2 MgTBTAP (18)

**Procedure A** A suspension of tetramethylphthalonitrile (**14**) (286 mg, 3 eq.) and MgBr<sub>2</sub> (110 mg, 1.5 eq.) in dry diglyme (0.5 mL) was heated in an oil bath at 220°C under an argon atmosphere for 10 min. A solution of aminoisoindoline (100 mg, 1 eq.) and tetramethylphthalonitrile (**14**) (95 mg, 1 eq.) in dry diglyme (1 mL) was then added dropwise over 1 hr. After addition the reaction was refluxed for 30 min. A final solution of DABCO (67.5 mg, 1.5 eq.) and phthalonitrile (95 mg, 1 eq.) in dry diglyme (0.5 mL) was added dropwise over 1 hr, followed by a further 30 min reflux. A stream of argon was passed through the reaction vessel to remove the solvent. The crude mixture was cooled to room temperature and dissolved in a mixture of DCM/MeOH (50 mL, 1:1) with the aid of sonication. The solvent was removed *in vacuo* and the residue purified by silica gel chromatography, firstly with DCM/NEt<sub>3</sub>/THF (10:1:4). The collected green fractions were resubjected to a column eluted with PE/THF/MeOH (20:3:1) to obtain the pure green product as the second green fraction. The material was recrystallised from DCM/MeOH to yield the title compound as dark crystals with a purple reflex (10.3 mg, 3.0 %).

**Procedure B** A suspension of tetramethylphthalonitrile (**14**) (190 mg, 1 eq), aminoisoindoline (**13**) (200 mg, 1 eq), MgBr<sub>2</sub> (110 mg) and DABCO (67.5 mg) was heated to reflux in diglyme (3 mL) for 3 hrs. Work up and purification was performed as above to yield the *title compound* as dark crystals with a purple reflex (28 mg, 8 %).

<sup>1</sup>H NMR (500 MHz, THF-*d*<sub>8</sub>) δ 9.62 – 9.53 (m, 2H), 9.48 (m, 4H), 8.06 – 7.97 (m, 2H), 7.86 (t, J = 7.2 Hz, 2H), 7.56 (ddd, J = 8.1, 6.8, 1.1 Hz, 2H), 7.53 – 7.46 (m, 2H), 7.20 (d, J = 8.1 Hz, 2H), 4.19 (s, 3H), 2.08 (s, 8H), 1.80 (s, 24H).

<sup>13</sup>C NMR (125.7 MHz, THF-*d*<sub>8</sub>) δ 160.7, 156.8, 153.2, 151.7, 146.8, 146.6, 141.0, 140.7, 139.1, 138.7, 136.0, 134.0, 126.8, 126.5, 126.3, 125.1, 122.7, 121.2, 121.0, 115.4, 56.7, 36.8, 36.6, 33.2

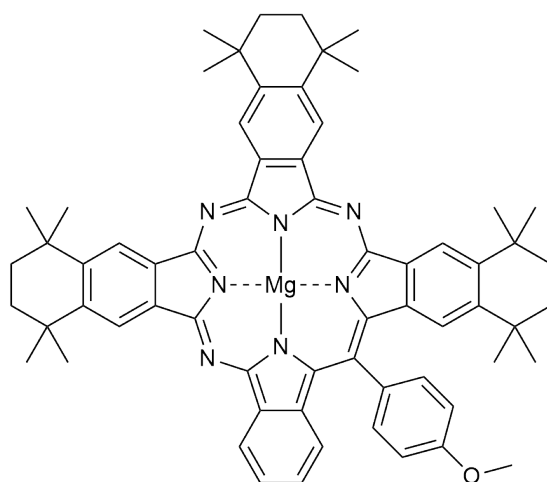
MP: > 300 °C (lit. > 300°C)<sup>139</sup>

UV-Vis: λ<sub>max</sub> (nm) (ε (dm<sup>3</sup>.mol<sup>-1</sup>.cm<sup>-1</sup>)) = 681 (2.14.10<sup>5</sup>), 656 (1.43.10<sup>5</sup>), 462 (4.02.10<sup>4</sup>), 390 (7.21.10<sup>4</sup>)

MALDI-TOF: *m/z* = [M]<sup>+</sup> 860.70 (100%) Chemical formula and exact mass: C<sub>56</sub>H<sub>51</sub>MgN<sub>7</sub>O, 861.40 g.mol<sup>-1</sup>

### 5.7.3 3:1 MgTBTAP (**19**)

**Procedure B** A suspension of tetramethylphthalonitrile (**14**) (286 mg, 3 eq.) and MgBr<sub>2</sub> (110 mg, 1.5 eq.) in dry diglyme (0.5 mL) was heated in an oil bath at 220°C under an argon atmosphere for 10 min. A solution of aminoisoindoline (100 mg, 1 eq.) and tetramethylphthalonitrile (**14**) (95 mg, 1 eq.) in dry diglyme (1 mL) was then added dropwise over 3 hr. After addition the reaction was refluxed for 30 min. A final solution of DABCO (67.5 mg, 1.5 eq.) and tetramethylphthalonitrile (**14**) (95 mg, 1 eq.) in dry diglyme (0.5 mL) was



(19)

Figure 5.38: 3:1 MgTBTAP (19)

added dropwise over 3 hr, followed by a further 30 min reflux. A stream of argon was passed through the reaction vessel to remove the solvent. The crude mixture was cooled to room temperature and dissolved in a mixture of DCM/MeOH (50 mL, 1:1) with the aid of sonication. The solvent was removed *in vacuo* and the residue purified by silica gel chromatography, firstly with DCM/NEt<sub>3</sub>/THF (10:1:4). The collected green fractions were resubjected to a column eluted with PE/THF/MeOH (20:3:1) to obtain the pure green product as the first green fraction. The material was recrystallised from DCM/MeOH to yield the title compound as dark crystals with a purple reflex. (21 mg, 6 %)

**Procedure C** A solution of (32) (233 mg, 2 eq) was added to a solution of MgBr<sub>2</sub> (44 mg, 1 eq) in *p*-xylene (3 mL) and heated to reflux for 3 hr. After the reaction was complete the solvent was removed *in vacuo*, and the crude mixture dissolved in DCM/MeOH (50 mL, 1:1) with the aid of sonication. The crude mixture was loaded on silica and purified by silica gel chromatography utilizing DCM/NEt<sub>3</sub>/THF (10:1:4). The green fractions were collected and subjected to a second column chromatography eluting with PE/THF/MeOH (10:3:1). The green fractions were then recrystallised from DCM/MeOH to yield the *title compound* as a dark green solid (70 mg, 30 %)

<sup>1</sup>H NMR (500 MHz, THF-*d*<sub>8</sub>) δ 9.57 (d, J = 7.5 Hz, 1H), 9.52 – 9.41 (m, 5H), 8.03 (d, J = 8.3 Hz, 1H), 7.86 (t, J = 7.2 Hz, 1H), 7.61 – 7.52 (m, 3H), 7.37 (d, J = 8.3 Hz, 1H), 7.16 (s, 1H), 4.20 (s, 4H), 2.08 (s, 12H), 1.81 (s, 24H), 1.35 (s, 12H).

<sup>13</sup>C NMR (125.7 MHz, THF-*d*<sub>8</sub>) δ 161.7, 153.7, 153.4, 152.3, 147.4, 147.0, 146.8, 144.8, 144.3, 142.6, 142.0, 140.5, 139.8, 139.2, 138.8, 138.6, 137.9, 136.2,

134.0, 127.2, 126.9, 125.4, 124.3, 123.5, 121.8, 121.6, 121.4, 120.5, 115.2, 56.1, 36.7, 36.6, 36.4, 36.1, 35.4, 35.3, 33.2, 33.2, 32.9, 32.5

MP: > 300 °C (lit. > 300°C)<sup>139</sup>

UV-Vis:  $\lambda_{\max}$  (nm) ( $\epsilon$  (dm<sup>3</sup>.mol<sup>-1</sup>.cm<sup>-1</sup>)) = 686 (5.42.10<sup>4</sup>), 662 (3.31.10<sup>4</sup>), 443 (7.06.10<sup>3</sup>), 396 (1.83.10<sup>4</sup>)

MALDI-TOF:  $m/z$  = 970.83 [M]<sup>+</sup> (100%)

Chemical formula and exact mass: C<sub>64</sub>H<sub>65</sub>MgN<sub>7</sub>O, 971.51 g.mol<sup>-1</sup>

#### 5.7.4 3:1 ZnTBTAP (24)

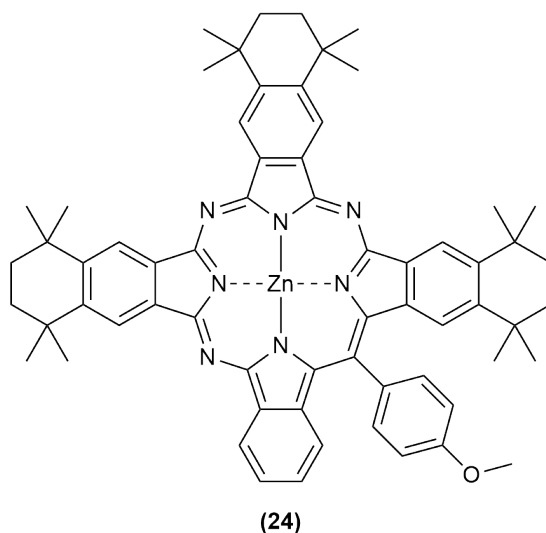


Figure 5.39: 3:1 ZnTBTAP (**24**)

**Procedure B** A suspension of tetramethylphthalonitrile (**14**) (286 mg, 3eq) and ZnBr<sub>2</sub> (135 mg, 1.5 eq.) in dry diglyme (0.5 mL) was heated in an oil bath at 220°C under an argon atmosphere for 10 min. A solution of aminoisoindoline (100 mg, 1 eq.) and tetramethylphthalonitrile (**14**) (95 mg, 1 eq.) in dry diglyme (1 mL) was then added dropwise over 3 hr. After addition the reaction was refluxed for 30 min. A final solution of DABCO (67.5 mg, 1.5 eq.) and tetramethylphthalonitrile (**14**) (95 mg, 1 eq.) in dry diglyme (0.5 mL) was added dropwise over 3 hr, followed by a further 30 min reflux. A stream of argon was passed through the reaction vessel to remove the solvent. The crude mixture was cooled to room temperature and dissolved in a mixture of DCM/MeOH (50 mL, 1:1) with the aid of sonication. The solvent was removed *in vacuo* and the residue purified by silica gel chromatography, firstly with DCM/NEt<sub>3</sub>/THF (10:1:4). The collected green fractions were resubjected to a column eluted with

PE/THF/MeOH (10:3:1) to obtain the pure green product. The material was recrystallised from DCM/MeOH to yield the title compound as dark crystals with a purple reflex (28 mg, 7 %)

$^1\text{H}$  NMR (500 MHz, THF- $d_8$ )  $\delta$  9.60 (d,  $J = 7.8$  Hz, 1H), 9.56 – 9.47 (m, 5H), 8.03 (d,  $J = 8.5$  Hz, 2H), 7.90 (t,  $J = 7.0$  Hz, 1H), 7.61 (t,  $J = 7.0$  Hz, 1H), 7.56 (d,  $J = 8.5$  Hz, 2H), 7.38 (d,  $J = 7.8$  Hz, 1H), 7.18 (s, 1H), 4.20 (s, 3H), 2.09 (s, 12H), 1.81 (s, 24H), 1.35 (s, 6H), 1.29 (s, 6H)

$^{13}\text{C}$  NMR (125.7 MHz, THF- $d_8$ )  $\delta$  163.3, 153.2, 152.4, 152.3, 147.8, 147.1, 145.8, 144.8, 144.1, 141.6, 141.0, 140.7, 139.6, 139.2, 138.7, 137.6, 136.8, 136.2, 134.2, 127.1, 125.9, 125.4, 124.9, 123.5, 121.7, 121.6, 121.1, 120.5, 115.1, 56.8, 36.8, 36.4, 36.0, 35.6, 35.1, 33.1, 32.8, 32.3

MP: > 300°C

UV-Vis:  $\lambda_{\text{max}}$  (nm) ( $\epsilon$  ( $\text{dm}^3 \cdot \text{mol}^{-1} \cdot \text{cm}^{-1}$ )) = 684 ( $4.69 \cdot 10^4$ ), 660 ( $2.74 \cdot 10^4$ ), 441 ( $6.35 \cdot 10^3$ ), 415 ( $1.62 \cdot 10^4$ )

MALDI-TOF:  $m/z = 1010.17$  [ $\text{M}$ ] $^+$  (100%)

Chemical formula and exact mass:  $\text{C}_{64}\text{H}_{65}\text{ZnN}_7\text{O}$ , 1011.45  $\text{g} \cdot \text{mol}^{-1}$

### 5.7.5 1:3 MgTBTAP (53)

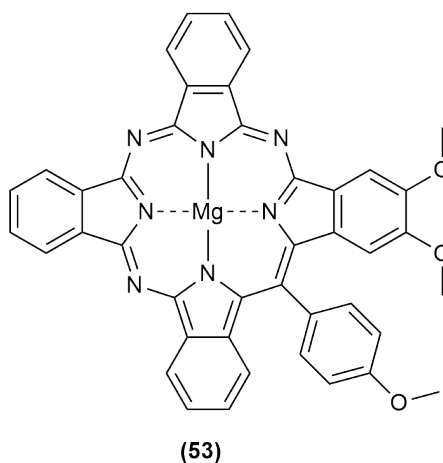


Figure 5.40: 1:3 MgTBTAP (53)

**Procedure C** A solution of **(42)** (209 mg, 2 eq) was added to a solution of MgBr<sub>2</sub> (44 mg, 1 eq) in *p*-xylene (3 mL) and heated to reflux for 3 hr. After the reaction was complete the solvent was removed *in vacuo*, and the crude mixture dissolved in DCM/MeOH (50 mL, 1:1) with the aid of sonication. The crude mixture was loaded on silica and purified by silica gel chromatography utilizing DCM/NEt<sub>3</sub>/THF (10:1:4). The green fractions were collected and subjected to a second column chromatography eluting with PE/THF/MeOH (10:3:1). The green fractions were then recrystallised from DCM/MeOH to yield the *title compound* as a dark green solid (58 mg, 34 %)

<sup>1</sup>H NMR (500 MHz, THF-*d*<sub>8</sub>) δ 9.61 (d, J = 7.6 Hz, 1H), 9.55 – 9.48 (m, 4H), 9.03 (s, 1H), 8.21 – 8.15 (m, 4H), 8.07 (d, J = 8.4 Hz, 2H), 7.92 (t, J = 7.3 Hz, 1H), 7.62 (t, J = 7.3 Hz, 1H), 7.57 (d, J = 8.4 Hz, 2H), 7.45 (d, J = 8.0 Hz, 1H), 6.64 (s, 1H), 4.30 (s, 3H), 4.17 (s, 3H), 3.78 (s, 3H)

<sup>13</sup>C NMR (125.7 MHz, CDCl<sub>3</sub>) δ 162.0, 154.5, 151.4, 144.0, 140.5, 136.7, 134.2, 129.9, 129.8, 129.6, 128.0, 127.5, 127.3, 123.7, 123.6, 115.5, 107.9, 105.0, 56.6, 56.2, 56.0

MP: > 300°C

UV-Vis: λ<sub>max</sub> (nm) (ε (dm<sup>3</sup>.mol<sup>-1</sup>.cm<sup>-1</sup>)) = 674 (8.41.10<sup>4</sup>), 648 (3.92.10<sup>4</sup>), 442 (1.05.10<sup>4</sup>), 401 (2.79.10<sup>4</sup>)

MALDI-TOF: *m/z* = 700.38 [M]<sup>+</sup> (100%)

Chemical formula and exact mass: C<sub>42</sub>H<sub>27</sub>MgN<sub>7</sub>O<sub>3</sub>, 701.20 g.mol<sup>-1</sup>

### 5.7.6 3:1 MgTBTAP (54)

**Procedure C** A solution of **(43)** (270 mg, 2 eq) was added to a solution of MgBr<sub>2</sub> (44 mg, 1 eq) in *p*-xylene (3 mL) and heated to reflux for 3 hr. After the reaction was complete the solvent was removed *in vacuo*, and the crude mixture dissolved in DCM/MeOH (50 mL, 1:1) with the aid of sonication. The crude mixture was loaded on silica and purified by silica gel chromatography utilizing DCM/NEt<sub>3</sub>/THF (10:1:4). The green fractions were collected and subjected to a second column chromatography eluting with PE/THF/MeOH (10:3:1). The green fractions were then recrystallised from DCM/MeOH to yield the *title compound* as a dark green solid (96 mg, 34 %).

<sup>1</sup>H NMR (500 MHz, THF-*d*<sub>8</sub>) δ 9.60 (d, J = 7.5 Hz, 1H), 9.56 – 9.47 (m, 5H), 8.08 – 8.01 (m, 2H), 7.90 (t, J = 7.2 Hz, 1H), 7.63 – 7.58 (m, 1H), 7.58 – 7.55 (m, 2H), 7.53 – 7.49 (m, 4H), 7.48 – 7.43 (m, 8H), 7.40 – 7.32 (m, 3H), 7.31 – 7.27 (m, 4H), 7.18 (s, 1H), 7.16 – 7.11 (m, 4H), 7.08 (dd, J = 8.1, 1.2 Hz, 8H), 4.20 (s, 3H)

<sup>13</sup>C NMR (125.7 MHz, THF-*d*<sub>8</sub>) δ 164.1, 154.4, 153.6, 153.1, 152.9, 147.9, 146.2, 144.2, 143.6, 141.2, 140.7, 140.2, 139.9, 139.4, 138.9, 137.2, 127.8, 127.3, 127.2, 124.8, 124.3, 122.4, 122.1, 120.4, 120.2, 115.3, 55.9

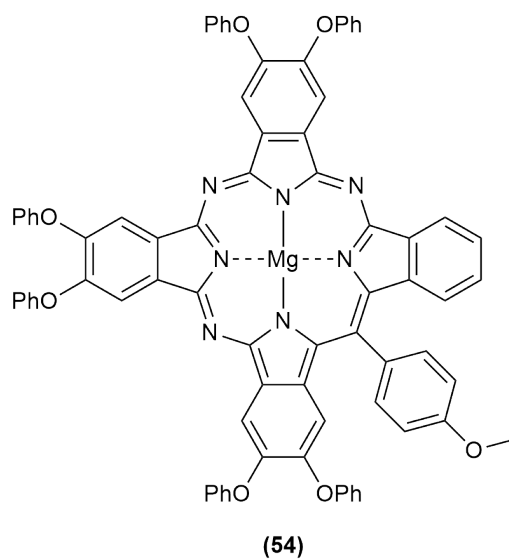


Figure 5.41: 3:1 MgTBTAP (**54**)

MP: > 300°C

UV-Vis:  $\lambda_{\max}$  (nm) ( $\epsilon$  (dm<sup>3</sup>.mol<sup>-1</sup>.cm<sup>-1</sup>)) = 682 (9.81.10<sup>4</sup>), 655 (5.04.10<sup>4</sup>), 443 (1.92.10<sup>4</sup>), 389 (4.30.10<sup>4</sup>)

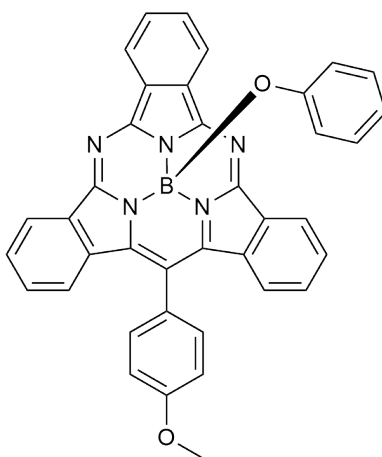
MALDI-TOF:  $m/z$  = 1192.42 [M]<sup>+</sup> (100%)

Chemical formula and exact mass: C<sub>76</sub>H<sub>47</sub>MgN<sub>7</sub>O<sub>7</sub>, 1193.34 g.mol<sup>-1</sup>

## 5.8 SubTBDAPs

Procedure A utilises the original procedure with  $\text{BCl}_3$  as the boron source. Procedure B utilises the original procedure with  $\text{B}(\text{OPh})_3$  as the boron source.<sup>30</sup> Procedure C utilises new intermediate (30) with  $\text{B}(\text{OPh})_3$  as the boron source.

### 5.8.1 SubTBDAP-OPh (46)



(46)

Figure 5.42: SubTBDAP-OPh (46)

**Procedure A** (Z)-1-[(4-Methoxy)benzylidene]-1*H*-isoindol-3-amine (58 mg, 1 eq) and phthalonitrile (60 mg, 2 eq), was dissolved in *p*-xylene (3 mL) in a sealed glass tube under argon.  $\text{BCl}_3$  was added dropwise as a 1M solution in *p*-xylene (0.47 mL, 0.47 mmol, 2 eq) and the reaction tube sealed. The reaction was heated to reflux for 3 hours, after which an excess of phenol (0.22 g, 10 eq) was added to the reaction. The solution was refluxed overnight, after which the solvent was removed and the crude residue subjected to silica gel chromatography eluting with EtOAc/hexane (2:7). The pink fractions were collected and subjected to a second column, eluting with 1:3:2 diethyl ether/hexane/DCM. Recrystallisation from DCM/hexane yielded the *title compound* as dark red crystals (14 mg, 10 %).

**Procedure B** To a solution of (Z)-1-[(4-Methoxy)benzylidene]-1*H*-isoindol-3-amine (112 mg, 1 eq) and phthalonitrile (173 mg, 3 eq) in dry diglyme (3.3 mL) in a sealed glass tube was added  $\text{B}(\text{OPh})_3$  (263 mg, 2 eq). The solution was degassed with dry  $\text{N}_2$  then heated to 200°C for 3 hours. The mixture was cooled and EtOAc added (50 mL), the solution was then washed with saturated  $\text{NaHCO}_3$  (3 x 75 mL). The organics were dried with  $\text{MgSO}_4$  and the solvent removed. The crude residue was subjected to silica gel chromatography eluting with EtOAc/hexane (2:7). The pink fractions were collected and subjected to a

second column, eluting with 1:3:2 diethyl ether/hexane/DCM. Recrystallisation from DCM/hexane yielded the *title compound* as dark red crystals (21 mg, 8 %).

**Procedure C** To a solution of **(30)** (170 mg, 1 eq) in dry diglyme (2 mL) in a sealed glass tube was added B(OPh)<sub>3</sub> (130 mg, 1 eq). The tube was purged with N<sub>2</sub> and the mixture stirred briefly at RT, a blood red solution formed. The vessel was placed in an oil bath at RT and heated to 200°C for 3 hours. Upon cooling the crude reaction mixture was diluted with EtOAc (50 mL) and washed with saturated NaHCO<sub>3</sub> (3 x 75 mL). The organics were dried with MgSO<sub>4</sub> and the solvent removed *in vacuo*. The crude residue was subjected to silica gel chromatography eluting with EtOAc/hexane (2:7). The pink fractions were collected and subjected to a second column, eluting with 1:3:2 diethyl ether/hexane/DCM. Recrystallisation from DCM/hexane yielded the *title compound* as dark red crystals (28 mg, 21 %).

<sup>1</sup>H NMR (500 MHz, Methylene Chloride-*d*<sub>2</sub>, 298 K)  $\delta$  8.96 – 8.88 (m, 4H), 7.99 (dd, J = 5.9, 3.0 Hz, 2H), 7.80 (dt, J = 8.0, 4.0 Hz, 2H), 7.62 (d, J = 4.3 Hz, 4H), 6.70 (t, J = 7.5 Hz, 2H), 6.62 (t, J = 7.5 Hz, 1H), 5.26 (dd, J = 7.5, 1.6 Hz, 2H), 4.07 (s, 3H)

<sup>13</sup>C NMR (125.7 MHz, CDCl<sub>3</sub>)  $\delta$  163.7, 152.8, 152.2, 136.2, 135.0, 134.8, 131.3, 130.0, 128.8, 128.2, 127.4, 127.2, 126.6, 126.1, 123.1, 122.8, 121.4, 120.5, 116.1, 56.6

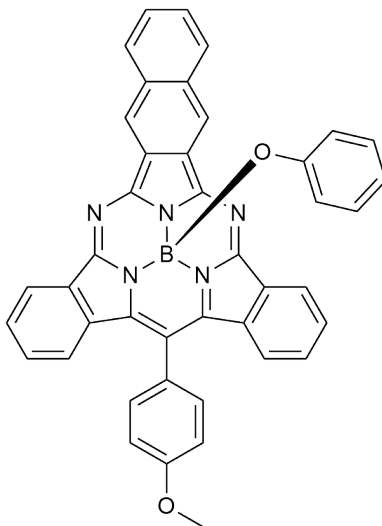
MP: 296 - 299 °C (lit. 300°C)<sup>30</sup>

UV-Vis:  $\lambda_{\max}$  (nm) ( $\epsilon$  (dm<sup>3</sup>.mol<sup>-1</sup>.cm<sup>-1</sup>)) = 550 (4.74.10<sup>4</sup>), 539 (4.52.10<sup>4</sup>), 510 (2.28.10<sup>4</sup>), 336 (5.08.10<sup>4</sup>)

MALDI-TOF:  $m/z$  = 593.68 [M]<sup>+</sup> (100%)

Chemical formula and exact mass: C<sub>38</sub>H<sub>25</sub>BN<sub>5</sub>O<sub>2</sub>, 594.21 g.mol<sup>-1</sup>

### 5.8.2 Naphthyl-SubTBDAP-OPh (47)



(47)

Figure 5.43: Naphthyl-SubTBDAP-OPh (47)

**Procedure B** To a solution of (*Z*)-1-[(4-Methoxy)benzylidene]-1*H*-isoindol-3-amine (112 mg, 1 eq) and 6,7-dicyanonaphthalene (250 mg, 3 eq) in dry diglyme (3.3 mL) in a sealed glass tube was added B(OPh)<sub>3</sub> (263 mg, 2 eq). The solution was degassed with dry N<sub>2</sub> then heated to 200°C for 3 hours. The mixture was cooled and EtOAc added (50 mL), the solution was then washed with saturated NaHCO<sub>3</sub> (3 x 75 mL). The organics were dried with MgSO<sub>4</sub> and the solvent removed. The crude residue was subjected to silica gel chromatography eluting with EtOAc/hexane (2:7). The pink fractions were collected and subjected to a second column, eluting with 1:3:2 diethyl ether/hexane/DCM. Recrystallisation from DCM/hexane yielded the *title compound* as dark red crystals (26 mg, 9 %).

<sup>1</sup>H NMR (500 MHz, Methylene Chloride-*d*<sub>2</sub>, 298 K) δ 9.52 (s, 2H), 8.96 (d, *J* = 8.5 Hz, 2H), 8.40 (dd, *J* = 6.3, 3.4 Hz, 2H), 7.83 – 7.74 (m, 4H), 7.63 – 7.53 (m, 4H), 6.75 – 6.67 (m, 2H), 6.63 (t, *J* = 7.5 Hz, 1H), 5.36 (d, *J* = 7.5 Hz, 2H), 4.04 (s, 3H)

<sup>13</sup>C NMR (125.7 MHz, CDCl<sub>3</sub>) δ 167.4, 162.2, 151.3, 151.1, 137.4, 136.4, 135.3, 132.8, 131.0, 130.6, 129.5, 129.3, 128.2, 128.0, 127.3, 127.1, 123.0, 122.7, 121.9, 121.3, 115.3, 57.0

MP: > 300°C

UV-Vis:  $\lambda_{\max}$  (nm) ( $\epsilon$  (dm<sup>3</sup>.mol<sup>-1</sup>.cm<sup>-1</sup>)) = 565 (4.56.10<sup>4</sup>), 516 (1.92.10<sup>4</sup>),  
343 (3.12.10<sup>4</sup>)

MALDI-TOF:  $m/z = 643.98$  [M]<sup>+</sup> (100%)

Chemical formula and exact mass: C<sub>42</sub>H<sub>27</sub>BN<sub>5</sub>O<sub>2</sub>, 644.23 g.mol<sup>-1</sup>

# Bibliography

- (1) M. O. Senge, N. N. Sergeeva and K. J. Hale, *Chemical Society Reviews*, 2021, **50**, 4730–4789.
- (2) T. D. Lash, *Journal of Porphyrins and Phthalocyanines*, 2011, **15**, 1093–1115.
- (3) C. G. Claessens, D. González-Rodríguez and T. Torres, *Chemical Reviews*, 2002, **102**, 835–854.
- (4) S. Saito and A. Osuka, *Angewandte Chemie International Edition*, 2011, **50**, 4342–4373.
- (5) T. Woller, P. Geerlings, F. De Proft, B. Champagne and M. Alonso, *Molecules*, 2018, **23**.
- (6) E. V. Antina, E. V. Balantseva and M. B. Berezin, *Russian Journal of General Chemistry*, 2011, **81**, 1222–1230.
- (7) A. K. Sobbi, D. Wöhrle and D. Schlottwein, *Journal of the Chemical Society, Perkin Transactions 2*, 1993, 481–488.
- (8) E. Secret, M. Maynadier, A. Gallud, A. Chaix, E. Bouffard, M. Gary-Bobo, N. Marcotte, O. Mongin, K. El Cheikh, V. Hugues, M. Auffan, C. Frochot, A. Morère, P. Maillard, M. Blanchard-Desce, M. J. Sailor, M. Garcia, J.-O. Durand and F. Cunin, *Advanced Materials*, 2014, **26**, 7643–7648.
- (9) K. S. Kim, J. M. Lim, A. Osuka and D. Kim, *Journal of Photochemistry and Photobiology C: Photochemistry Reviews*, 2008, **9**, 13–28.
- (10) A. Chaudhary, A. Srinivasan and T. K. Chandrashekar, in *Handbook of Porphyrin Science*, ch. 169, pp. 271–366.
- (11) S. Bhattacharya, C. Biswas, S. S. K. Raavi, J. Venkata Suman Krishna, N. Vamsi Krishna, L. Giribabu and V. R. Soma, *The Journal of Physical Chemistry C*, 2019, **123**, 11118–11133.
- (12) A. van As, C. C. Joubert, B. E. Buitendach, E. Erasmus, J. Conradie, A. N. Cammidge, I. Chambrier, M. J. Cook and J. C. Swarts, *Inorganic Chemistry*, 2015, **54**, 5329–5341.
- (13) S. Khene, A. N. Cammidge, M. J. Cook and T. Nyokong, *Journal of Porphyrins and Phthalocyanines*, 2007, **11**, 761–770.
- (14) L. Tejerina, S. Yamamoto, I. López-Duarte, M. V. Martínez-Díaz, M. Kimura and T. Torres, *Helvetica Chimica Acta*, 2020, **103**, e2000085.
- (15) J. H. Helberger and A. von Rebay, *Justus Liebigs Annalen der Chemie*, 1937, **531**, 279–287.

- (16) C. E. Dent, *Journal of the Chemical Society*, 1938, 1–6.
- (17) P. A. Barrett, R. P. Linstead, G. A. P. Tuey and J. M. Robertson, *Journal of the Chemical Society*, 1939, 1809–1820.
- (18) P. A. Barrett, R. P. Linstead, F. G. Rundall and G. A. P. Tuey, *Journal of the Chemical Society*, 1940, 1079–1092.
- (19) R. P. Linstead and F. T. Weiss, *Journal of the Chemical Society*, 1950, 2975–2981.
- (20) G. Quirion, M. Poirier, M. Ogawa and B. Hoffman, *Solid State Communications*, 1987, **64**, 613–616.
- (21) K. Liou, M. Y. Ogawa, T. P. Newcomb, G. Quirion, M. Lee, M. Poirier, W. P. Halperin, B. M. Hoffman and J. A. Ibers, *Inorganic Chemistry*, 1989, **28**, 3889–3896.
- (22) W. B. Euler, J. Martinsen, L. J. Pace, B. M. Hoffman and J. A. Ibers, *Molecular Crystals and Liquid Crystals*, 1982, **81**, 231–242.
- (23) C. C. Leznoff and N. B. McKeown, *The Journal of Organic Chemistry*, 1990, **55**, 2186–2190.
- (24) N. E. Galanin, E. V. Kudrik and G. P. Shaposhnikov, *Russian Journal of Organic Chemistry*, 2002, **38**, 1200–1203.
- (25) A. N. Cammidge, M. J. Cook, D. L. Hughes, F. Nekelson and M. Rahman, *Chemical Communications*, 2005, 930–932.
- (26) A. N. Cammidge, I. Chambrier, M. J. Cook, D. L. Hughes, M. Rahman and L. Sosa-Vargas, *Chemistry – A European Journal*, 2011, **17**, 3136–3146.
- (27) J. Mack, L. Sosa-Vargas, S. J. Coles, G. J. Tizzard, I. Chambrier, A. N. Cammidge, M. J. Cook and N. Kobayashi, *Inorganic Chemistry*, 2012, **51**, 12820–12833.
- (28) A. Díaz-Moscoso, G. J. Tizzard, S. J. Coles and A. N. Cammidge, *Angewandte Chemie International Edition*, 2013, **52**, 10784–10787.
- (29) N. Alharbi, A. Díaz-Moscoso, G. J. Tizzard, S. J. Coles, M. J. Cook and A. N. Cammidge, *Tetrahedron*, 2014, **70**, Special Memorial Issue for Professor Sandy McKillop, 7370–7379.
- (30) S. Remiro-Buenamañana, A. Díaz-Moscoso, D. L. Hughes, M. Bochmann, G. J. Tizzard, S. J. Coles and A. N. Cammidge, *Angewandte Chemie International Edition*, 2015, **54**, 7510–7514.
- (31) M. Gouterman, G. H. Wagnière and L. C. Snyder, *Journal of Molecular Spectroscopy*, 1963, **11**, 108–127.
- (32) Z. Zhao, A. N. Cammidge and M. J. Cook, *Chemical Communications*, 2009, 7530–7532.
- (33) D. Chiabrando, F. Vinchi, V. Fiorito, S. Mercurio and E. Tolosano, *Frontiers in Pharmacology*, 2014, **5**, 61.
- (34) T. G. Traylor, *Pure and Applied Chemistry*, 1991, **63**, 265–274.
- (35) L. Yin, N. Wu, J. C. Curtin, M. Qatanani, N. R. Szwergold, R. A. Reid, G. M. Waitt, D. J. Parks, K. H. Pearce, G. B. Wisely and M. A. Lazar, *Science*, 2007, **318**, 1786–1789.

- (36) M.-A. Gilles-Gonzalez and G. Gonzalez, *Journal of Inorganic Biochemistry*, 2005, **99**, Heme-diatomic interactions, Part 1, 1–22.
- (37) W. Arnold and J. R. Azzi, *Proceedings of the National Academy of Sciences*, 1968, **61**, 29–35.
- (38) P. Rothmund, *Journal of the American Chemical Society*, 1936, **58**, 625–627.
- (39) P. Rothmund, *Journal of the American Chemical Society*, 1935, **57**, 2010–2011.
- (40) J. S. Lindsey, I. C. Schreiman, H. C. Hsu, P. C. Kearney and A. M. Marguerettaz, *The Journal of Organic Chemistry*, 1987, **52**, 827–836.
- (41) J. S. Lindsey and R. W. Wagner, *The Journal of Organic Chemistry*, 1989, **54**, 828–836.
- (42) A. Braun and J. Tcherniac, *Berichte der deutschen chemischen Gesellschaft*, 1907, **40**, 2709–2714.
- (43) C. E. Dent, R. P. Linstead and A. R. Lowe, *Journal of the Chemical Society*, 1934, 1033–1039.
- (44) R. P. Linstead and A. R. Lowe, *Journal of the Chemical Society*, 1934, 1022–1027.
- (45) J. M. Robertson, *Journal of the Chemical Society*, 1935, 615–621.
- (46) C. D. Molek, J. A. Halfen, J. C. Loe and R. W. McGaff, *Chem. Commun.*, 2001, 2644–2645.
- (47) A. Meller and A. Ossko, *Monatshefte für Chemie / Chemical Monthly*, 1972, **103**, 150–155.
- (48) H. Kietaihl, *Monatshefte für Chemie / Chemical Monthly*, 1974, **105**, 405–418.
- (49) G. de la Torre, P. Vázquez, F. Agulló-López and T. Torres, *Chemical Reviews*, 2004, **104**, 3723–3750.
- (50) T. Nyokong, *Coordination Chemistry Reviews*, 2007, **251**, 37th International Conference on Coordination Chemistry, Cape Town, South Africa, 1707–1722.
- (51) A. Ogunsipe, J.-Y. Chen and T. Nyokong, *New Journal of Chemistry*, 2004, **28**, 822–827.
- (52) J. He, G. Benkő, F. Korodi, T. Polívka, R. Lomoth, B. Åkermark, L. Sun, A. Hagfeldt and V. Sundström, *Journal of the American Chemical Society*, 2002, **124**, 4922–4932.
- (53) N. Kobayashi, H. Ogata, N. Nonaka and E. A. Luk'yanets, *Chemistry – A European Journal*, 2003, **9**, 5123–5134.
- (54) L. Sambrotta, I. Rezzano, G. Buldain and B. Frydman, *Tetrahedron*, 1989, **45**, 6645–6652.
- (55) H. Shang, Z. Xue, K. Wang, H. Liu and J. Jiang, *Chemistry – A European Journal*, 2017, **23**, 8644–8651.
- (56) A. M. Pereira, A. R. Soares, M. J. Calvete and G. de la Torre, *Journal of Porphyrins and Phthalocyanines*, 2009, **13**, 419–428.

- (57) L. Liu, L.-P. Guo, X.-J. Bo, J. Bai and X.-J. Cui, *Analytica Chimica Acta*, 2010, **673**, 88–94.
- (58) G. De La Torre, M. V. Martínez-Díaz and T. Torres, *Journal of Porphyrins and Phthalocyanines*, 1999, **03**, 560–568.
- (59) Q. M. Zhang, H. Li, M. Poh, F. Xia, Z.-Y. Cheng, H. Xu and C. Huang, *Nature*, 2002, **419**, 284–287.
- (60) H. He, A. G. Sykes, P. S. May and G. He, *Dalton Transactions.*, 2009, 7454–7461.
- (61) S. F. Zhu Peihua, Wang Yucheng, *pat.*, CN106317091A, 2016.
- (62) R.-S. Lin, M.-R. Li, Y.-H. Liu, S.-M. Peng and S.-T. Liu, *Inorganica Chimica Acta*, 2010, **363**, 3523–3529.
- (63) N. Alharbi, G. J. Tizzard, S. J. Coles, M. J. Cook and A. N. Cammidge, *Tetrahedron*, 2015, **71**, Special Memorial Issue for Professor Alan Katritzky, 7227–7232.
- (64) S. Remiro-Buenamañana, A. Díaz-Moscoso, D. L. Hughes, M. Bochmann, G. J. Tizzard, S. J. Coles and A. N. Cammidge, *Angewandte Chemie (International ed. in English)*, 2015, **54**, 7510–7514.
- (65) S. R. Buenamañana, Ph.D. Thesis, School of Chemistry University of East Anglia, Norwich, United Kingdom, 2015.
- (66) M. J. Ahrens, L. E. Sinks, B. Rybtchinski, W. Liu, B. A. Jones, J. M. Giaimo, A. V. Gusev, A. J. Goshe, D. M. Tiede and M. R. Wasielewski, *Journal of the American Chemical Society*, 2004, **126**, 8284–8294.
- (67) T. G. Goodson, *Accounts of Chemical Research*, 2005, **38**, 99–107.
- (68) D. Chen, Y. Kusakabe, Y. Ren, D. Sun, P. Rajamalli, Y. Wada, K. Suzuki, H. Kaji and E. Zysman-Colman, *The Journal of Organic Chemistry*, 2021, **86**, 11531–11544.
- (69) A. Sautter, B. K. Kaletaş, D. G. Schmid, R. Dobraua, M. Zimine, G. Jung, I. H. M. van Stokkum, L. De Cola, R. M. Williams and F. Würthner, *Journal of the American Chemical Society*, 2005, **127**, 6719–6729.
- (70) H. Langhals, *Helvetica Chimica Acta*, 2005, **88**, 1309–1343.
- (71) W. T. Hadmojo, U.-H. Lee, D. Yim, H. W. Kim, W.-D. Jang, S. C. Yoon, I. H. Jung and S.-Y. Jang, *ACS Applied Materials & Interfaces*, 2018, **10**, 41344–41349.
- (72) W. T. Hadmojo, D. Yim, S. Sinaga, W. Lee, D. Y. Ryu, W.-D. Jang, I. H. Jung and S.-Y. Jang, *ACS Sustainable Chemistry & Engineering*, 2018, **6**, 5306–5313.
- (73) H. Yin, J. K. W. Ho, V. Piradi, S. Chen, X. Zhu and S. K. So, *Small Methods*, 2020, **4**, 2000136.
- (74) V. Y. Merritt, *IBM Journal of Research and Development*, 1978, **22**, 353–371.
- (75) C. W. Tang, *Applied Physics Letters*, 1986, **48**, 183–185.
- (76) J. Nelson, *Current Opinion in Solid State and Materials Science*, 2002, **6**, 87–95.

- (77) M. Senge, M. Fazekas, E. Notaras, W. Blau, M. Zawadzka, O. Locos and E. Ni Mhuircheartaigh, *Advanced Materials*, 2007, **19**, 2737–2774.
- (78) G. de la Torre, P. Vázquez, F. Agulló-López and T. Torres, *Journal of Materials Chemistry*, 1998, **8**, 1671–1683.
- (79) S. Mathews, S. C. Kumar, L. Giribabu and S. V. Rao, *Materials Letters*, 2007, **61**, 4426–4431.
- (80) Y. Chen, M. Hanack, W. J. Blau, D. Dini, Y. Liu, Y. Lin and J. Bai, *Journal of Materials Science*, 2006, **41**, 2169.
- (81) X. Zhang, L. Yu, C. Zhuang, T. Peng, R. Li and X. Li, *ACS Catalysis*, 2014, **4**, 162–170.
- (82) X. Zhang, T. Peng, L. Yu, R. Li, Q. Li and Z. Li, *ACS Catalysis*, 2015, **5**, 504–510.
- (83) J. R. Darwent, P. Douglas, A. Harriman, G. Porter and M.-C. Richoux, *Coordination Chemistry Reviews*, 1982, **44**, 83–126.
- (84) I. Arslan and I. Balcioglu, *Dyes and Pigments*, 1999, **43**, 95–108.
- (85) G. Mele, R. Del Sole, G. Vasapollo, E. Garcia-López, L. Palmisano and M. Schiavello, *Journal of Catalysis*, 2003, **217**, 334–342.
- (86) A. Alinsafi, F. Evenou, E. Abdulkarim, M. Pons, O. Zahraa, A. Benhammou, A. Yaacoubi and A. Nejmeddine, *Dyes and Pigments*, 2007, **74**, 439–445.
- (87) K. Ishii, *Coordination Chemistry Reviews*, 2012, **256**, 19th International Symposium on the Photophysics and Photochemistry of Coordination Compounds, 1556–1568.
- (88) O. L. Kaliya, E. A. Lukyanets and G. N. Vorozhtsov, *Journal of Porphyrins and Phthalocyanines*, 1999, **03**, 592–610.
- (89) N. Corrigan, J. Xu and C. Boyer, *Macromolecules*, 2016, **49**, 3274–3285.
- (90) H. Abrahamse and M. R. Hamblin, *Biochemical Journal*, 2016, **473**, 347–364.
- (91) E. B. Agyekum, C. Nutakor, A. M. Agwa and S. Kamel, *Membranes (Basel)*, 2022, **12**.
- (92) A. M. Oliveira, R. R. Beswick and Y. Yan, *Current Opinion in Chemical Engineering*, 2021, **33**, 100701.
- (93) P. Chatterjee, M. S. K. Ambati, A. K. Chakraborty, S. Chakraborty, S. Biring, S. Ramakrishna, T. K. S. Wong, A. Kumar, R. Lawaniya and G. K. Dalapati, *Energy Conversion and Management*, 2022, **261**, 115648.
- (94) J. Krämer, R. Kang, L. M. Grimm, L. De Cola, P. Picchetti and F. Biedermann, *Chemical Reviews*, 2022, **122**, 3459–3636.
- (95) L. K. Kumawat, N. Mergu, A. K. Singh and V. K. Gupta, *Sensors and Actuators B: Chemical*, 2015, **212**, 389–394.
- (96) R. Sessoli, D. Gatteschi, A. Caneschi and M. A. Novak, *Nature*, 1993, **365**, 141–143.
- (97) J. Lu, M. Guo and J. Tang, *Chemistry – An Asian Journal*, 2017, **12**, 2772–2779.

- (98) D. González-Lucas, S. C. Soobrattee, D. L. Hughes, G. J. Tizzard, S. J. Coles and A. N. Cammidge, *Chemistry – A European Journal*, 2020, **26**, 10724–10728.
- (99) J. H. Helberger, *Justus Liebigs Annalen der Chemie*, 1937.
- (100) N. E. Galanin, E. V. Kudrik and G. P. Shaposhnikov, *Russian Journal of General Chemistry*, 2004, **74**, 282–285.
- (101) V. V. Kalashnikov, V. E. Pushkarev and L. G. Tomilova, *Mendeleev Communications*, 2011, **21**, 92–93.
- (102) W. B. Dandliker, M. L. Hsu and W. P. Murphy, *pat.*, WO/2006/001944, 2005.
- (103) I. S. Han, *pat.*, WO2004041828A1, 2002.
- (104) L. Jian, *pat.*, US20210261589A1, 2020.
- (105) K. Hiromitsu, E. Taro, K. Akiko and A. Takashi, *pat.*, US9505941B2, 2018.
- (106) L. Jian and W. Zixing, *pat.*, WO2010105141A3, 2010.
- (107) L. Huang, C. D. Park, T. Fleetham and J. Li, *Applied Physics Letters*, 2016, **109**, 233302.
- (108) A. N. Cammidge, I. Chambrier, M. J. Cook, E. H. Langner, M. Rahman and J. C. Swarts, *Journal of Porphyrins and Phthalocyanines*, 2011, **15**, 890–897.
- (109) N. B. Chaure, A. N. Cammidge, I. Chambrier and A. K. Ray, *Journal of Applied Physics*, 2018, **124**, 235501.
- (110) S. M. Borisov, G. Zenkl and I. Klimant, *ACS Applied Materials & Interfaces*, 2010, **2**, 366–374.
- (111) F. Gao, C.-L. Yang, M.-S. Wang, X.-G. Ma and W.-W. Liu, *Spectrochimica Acta Part A: Molecular and Biomolecular Spectroscopy*, 2018, **195**, 176–183.
- (112) A. N. Cammidge, I. Chambrier, M. J. Cook, D. L. Hughes, M. Rahman and L. Sosa-Vargas, *Chemistry – A European Journal*, 2011, **17**, 3136–3146.
- (113) G. E. Morse and T. P. Bender, *ACS Applied Materials & Interfaces*, 2012, **4**, PMID: 22979940, 5055–5068.
- (114) R. T. Boéré, R. T. Oakley and R. W. Reed, *Journal of Organometallic Chemistry*, 1987, **331**, 161–167.
- (115) M. Hellal and G. D. Cuny, *Tetrahedron Letters*, 2011, **52**, 5508–5511.
- (116) R. Chinchilla and C. Nájera, *Chem. Soc. Rev.*, 2011, **40**, 5084–5121.
- (117) E. D. Becker and R. B. Bradley, *The Journal of Chemical Physics*, 1959, **31**, 1413–1414.
- (118) T. V. Melenchuk, E. A. Danilova and M. K. Islyaikin, *Russian Journal of General Chemistry*, 2010, **80**, 1369–1372.
- (119) M. A. Tyutina, T. V. Kudayarova and E. A. Danilova, *Russian Journal of General Chemistry*, 2017, **87**, 1737–1741.

- (120) T. Fukuda, Y. Kikukawa, A. Fuyuhiko, N. Kobayashi and N. Ishikawa, *Chemistry Letters*, 2014, **43**, 925–927.
- (121) I. Chambrier and M. J. Cook, *Journal of Chemical Research, Synopses*, 1990.
- (122) A. P. Ingale, V. K. More, U. S. Gangarde and S. V. Shinde, *New Journal of Chemistry*, 2018, **42**, 10142–10147.
- (123) C. G. McPherson, N. Caldwell, C. Jamieson, I. Simpson and A. J. B. Watson, *Organic and Biomolecular Chemistry*, 2017, **15**, 3507–3518.
- (124) Z. Cheraiet, S. Ouarna, S. Hessainia, M. Berredjem and N.-E. Aouf, *ISRN Organic Chemistry*, 2012, 404235.
- (125) G. Pavan Kumar, D. Rambabu, M. V. Basaveswara Rao and M. Pal, *Journal of Chemistry*, 2013, **2013**, 916960.
- (126) R. Varala, S. Nuvula and S. R. Adapa, *The Journal of Organic Chemistry*, 2006, **71**, 8283–8286.
- (127) N. J. Tom, W. M. Simon, H. N. Frost and M. Ewing, *Tetrahedron Letters*, 2004, **45**, 905–906.
- (128) C. G. Claessens, D. González-Rodríguez, B. del Rey, T. Torres, G. Mark, H.-P. Schuchmann, C. von Sonntag, J. G. MacDonald and R. S. Nohr, *European Journal of Organic Chemistry*, 2003, 2547–2551.
- (129) K. Adachi and H. Watarai, *Chemistry – A European Journal*, 2006, **12**, 4249–4260.
- (130) J. Guilleme, D. González-Rodríguez and T. Torres, *Angewandte Chemie International Edition*, 2011, **50**, 3506–3509.
- (131) J. Cook, Michael and J. Heeney, Martin, *pat.*, WO0142368A1, 2001.
- (132) M. J. Gentian AS, Cook and I. Fernandes, *pat.*, WO02096913A1, 2002.
- (133) H. Kagechika, E. Kawachi, Y. Hashimoto, K. Shudo and T. Himi, *Journal of Medicinal Chemistry*, 1988, **31**, 2182–2192.
- (134) L. Schmerling and J. P. West, *Journal of the American Chemical Society*, 1952, **74**, 2885–2889.
- (135) H. A. Bruson and J. W. Kroeger, *Journal of the American Chemical Society*, 1940, **62**, 36–44.
- (136) I. Rose, C. G. Bezzu, M. Carta, B. Comesaña-Gándara, E. Lasseguette, M. C. Ferrari, P. Bernardo, G. Clarizia, A. Fuoco, J. C. Jansen, K. E. Hart, T. P. Liyana-Arachchi, C. M. Colina and N. B. McKeown, *Nature Materials*, 2017, **16**, 932–937.
- (137) T. Schareina, A. Zapf, W. Mägerlein, N. Müller and M. Beller, *Chemistry – A European Journal*, 2007, **13**, 6249–6254.
- (138) S. A. Mikhalenko, L. I. Solov'eva and E. A. Luk'yanets, *Journal of the Russian Chemical Society*, 1988, **58**, 2618–19.
- (139) F. Alkorbi, A. Díaz-Moscoso, J. Gretton, I. Chambrier, G. J. Tizzard, S. J. Coles, D. L. Hughes and A. N. Cammidge, *Angewandte Chemie International Edition*, 2021, **60**, 7632–7636.
- (140) D. Wöhrle, M. Eskes, K. Shigehara and A. Yamada, *Synthesis*, 1993, 194–196.

- (141) T. Wenderski, K. M. Light, D. Ogrin, S. G. Bott and C. J. Harlan, *Tetrahedron Letters*, 2004, **45**, 6851–6853.
- (142) M. Kohn and L. Steiner, *The Journal of Organic Chemistry*, 1947, **12**, 30–33.
- (143) J. Metz, O. Schneider and M. Hanack, *Inorganic Chemistry*, 1984, **23**, 1065–1071.
- (144) V. Wentworth and O. L. Brady, *Journal of the Chemical Society, Perkin Transactions 1*, 1920, **117**, 1040–1045.
- (145) J. Li, H. Lin, J. Huang and J. Yin, *Dyes and Pigments*, 2019, **170**, 107564.
- (146) W. H. Mills and I. G. Nixon, *Journal of the Chemical Society*, 1930, 2510–2524.
- (147) A. Brandstrom and S. A. I. Carlsson, *Acta Chemica Scandinavica*, 1967, **21**, 983–92.
- (148) J. H. van Tonder, N. Loganathan, M. Gohain and B. C. B. Bezuidenhoudt, *Zeitschrift für Kristallographie - New Crystal Structures*, 2014, **229**, 357–358.
- (149) S. Dalai, V. N. Belov, S. Nizamov, K. Rauch, D. Finsinger and A. de Meijere, *European Journal of Organic Chemistry*, 2006, 2753–2765.

## Chapter 6

# Appendix

### 6.1 Publications

VIP **Phthalocyanine Hybrids** Very Important PaperHow to cite: *Angew. Chem. Int. Ed.* **2021**, *60*, 7632–7636

International Edition: doi.org/10.1002/anie.202016596

German Edition: doi.org/10.1002/ange.202016596

**Complementary Syntheses Giving Access to a Full Suite of Differentially Substituted Phthalocyanine-Porphyrin Hybrids**

Faeza Alkorbi, Alejandro Díaz-Moscoso,\* Jacob Gretton, Isabelle Chambrier, Graham J. Tizzard, Simon J. Coles, David L. Hughes, and Andrew N. Cammidge\*

**Abstract:** Phthalocyanines and porphyrins are often the scaffolds of choice for use in widespread applications. Synthetic advances allow bespoke derivatives to be made, tailoring their properties. The selective synthesis of unsymmetrical systems, particularly phthalocyanines, has remained a significant unmet challenge. Porphyrin-phthalocyanine hybrids offer the potential to combine the favorable features of both parent structures, but again synthetic strategies are poorly developed. Here we demonstrate strategies that give straightforward, controlled access to differentially substituted meso-aryl-tetrabenzotriazaporphyrins by reaction between an aryl-aminoisoindole (A) initiator and a complementary phthalonitrile (B). The choice of precursors and reaction conditions allows selective preparation of 1:3 Ar-ABBB and, uniquely, 2:2 Ar-ABBA functionalized hybrids.

Phthalocyanines (Pc) and porphyrins are among the most widely studied functional organic materials. Porphyrin derivatives are widespread in nature and perform crucial life-sustaining functions. Synthetic porphyrins and phthalocyanines are diversely used across chemical, biological and other advanced technology fields. Their popularity stems from a combination of general molecular properties such as light absorption and stability (a direct consequence of their extended aromaticity), and the ability to tune their physico-chemical properties through a number of complementary strategies such as metal ion incorporation, perturbation of the core, and/or introduction of appropriate substituents.<sup>[1]</sup>

Hybrid structures, intermediate between Pc and porphyrins (Figure 1), were recognized as important scaffolds during the birth of Pc chemistry, and were discussed in Linstead's and

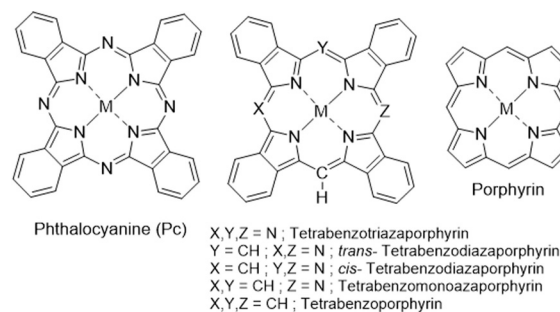


**Figure 1.** Molecular structures of phthalocyanine (Pc), porphyrin, and their hybrids.

Dent's original seminal series of papers in the 1930s.<sup>[2]</sup> The hybrids possess complementary and superior characteristics to their parents, bridging the Pc and porphyrin systems and allowing precise tuning of their properties for specific applications.<sup>[3]</sup> However, scarce synthetic availability of hybrid materials has limited the study of their scope. Synthetic procedures are mostly derived from the original methods from the 1930s, employing a carbon-based nucleophile to initiate reaction with a phthalonitrile (Pn) co-reactant.<sup>[3]</sup> These strategies generally have poor yields and selectivity, leading most investigations to focus on hybrid structures bearing only simple or no substituents on the macrocycle or the meso-carbon position. Interest in functional hybrids has been growing recently. We<sup>[4]</sup> and others<sup>[5]</sup> have refined C-nucleophile procedures, extending studies to include substituents at the Pn and meso-sites, and controlling product distribution through stoichiometry and reaction conditions. Access to the full range of (separable and processable) hybrids has further revealed their enhanced behavior as device components.<sup>[6]</sup> More innovative synthetic inventions have recently started to redefine the field, charting the first steps towards controlled synthesis of di-<sup>[7]</sup> and triaza<sup>[8]</sup> hybrids.

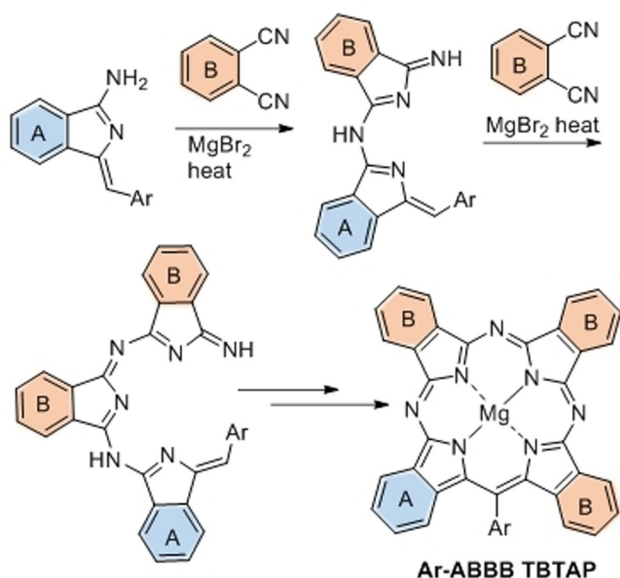
Our synthesis of meso-aryl tetrabenzotriazaporphyrins (TBTAPs) provided, for the first time, scalable access to these hybrid structures functionalized at the meso position.<sup>[8]</sup> Based on the proposed mechanism, we recognized that our synthetic protocol had the potential to introduce different benzo fragments (A and B) around the macrocycle in a regiospecific manner, in addition to the meso functionality (Scheme 1). Such structural control has been long pursued in normal Pc chemistry with only limited advances.<sup>[9]</sup> In the hybrid series, success would deliver materials that are unavailable in general Pc chemistry, but also offer the opportunity to further exploit the possibilities provided by the meso-substituent.

[\*] Dr. F. Alkorbi, Dr. A. Díaz-Moscoso, J. Gretton, Dr. I. Chambrier, Dr. D. L. Hughes, Prof. A. N. Cammidge  
 School of Chemistry, University of East Anglia  
 Norwich Research Park, Norwich NR4 7TJ (UK)  
 E-mail: a.diaz.moscoso@csic.es  
 a.cammidge@uea.ac.uk

Dr. G. J. Tizzard, Prof. S. J. Coles  
 UK National Crystallography Service  
 Chemistry University of Southampton  
 Southampton SO17 1BJ (UK)

Supporting information and the ORCID identification number(s) for the author(s) of this article can be found under:  
<https://doi.org/10.1002/anie.202016596>.

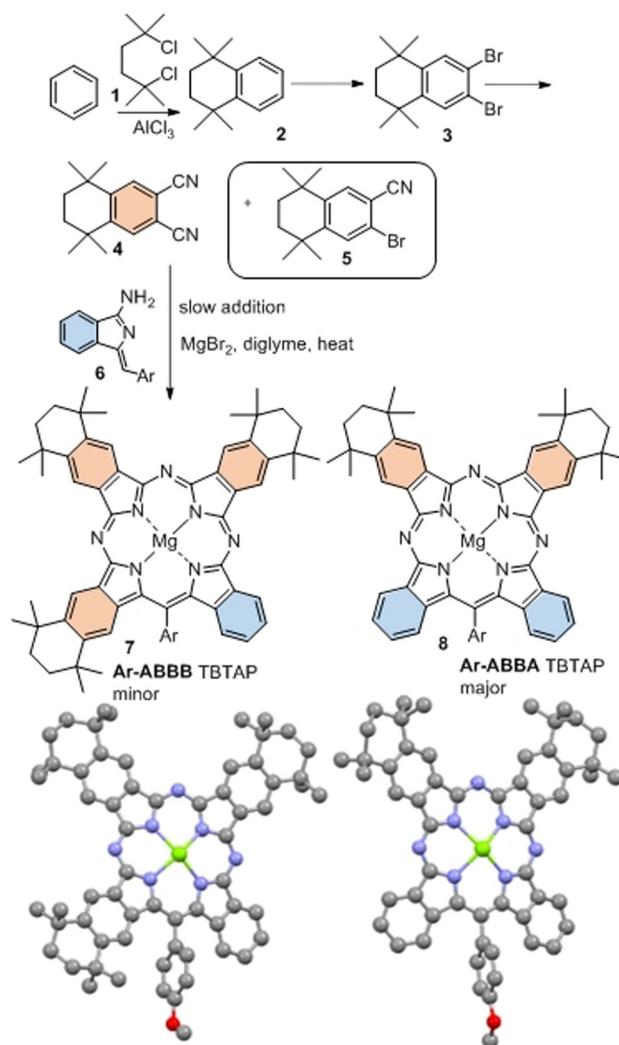
© 2021 The Authors. Angewandte Chemie International Edition published by Wiley-VCH GmbH. This is an open access article under the terms of the Creative Commons Attribution License, which permits use, distribution and reproduction in any medium, provided the original work is properly cited.



**Scheme 1.** The synthesis of *meso*-aryl TBTAPs from reaction between aminoisoindole initiator<sup>[10]</sup> (providing the A ring) and phthalonitrile (providing the B ring).<sup>[8]</sup>

Our first attempts to investigate the potential to introduce substituents onto TBTAP hybrids employed commercially available 4-*tert*-butylphthalonitrile,<sup>[11]</sup> a widely used precursor in Pc chemistry that imparts good solubility to the final macrocycles. According to our proposed mechanism for this reaction, we expected to obtain a 1:3 peripheral substitution pattern (Scheme 1). However, reaction with our aminoisoindole co-reactant under the conditions optimized for TBTAP synthesis produced a complex mixture of products. Therefore, we shifted our strategy to symmetrically disubstituted Pns in order to simplify characterization and analysis. Several examples leading to peripheral substitution were chosen, avoiding steric clashes with substituents on the new *meso*-carbon.<sup>[4,8]</sup> Initial investigations used the Pn derivative **4**, derived from tetramethyl tetralin, synthesized from benzene by Friedel–Crafts alkylation,<sup>[12]</sup> bromination,<sup>[12,13]</sup> and cyanation.<sup>[13b,14]</sup> An initial test reaction was performed using Pn **4** alone under the reaction conditions (MgBr<sub>2</sub> in diglyme at reflux) to ensure that Pc formation did not occur directly at a competitive rate, as already shown for the unsubstituted phthalonitrile.<sup>[8]</sup> TBTAP hybrid formation was then attempted following the previously optimized procedure, essentially by slowly adding aminoisoindole “initiator” **6** to a mixture of Pn **4** (3–5 equiv) and MgBr<sub>2</sub> in refluxing diglyme (Scheme 2).

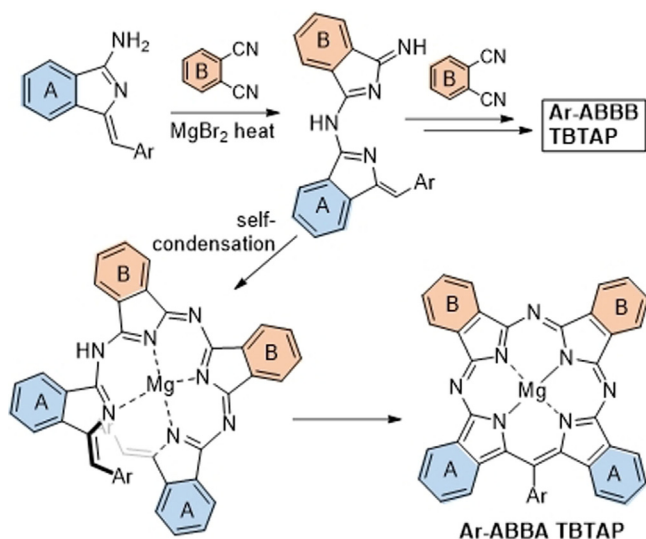
Macrocycle formation proceeded smoothly but two distinct hybrid products were isolated. The first product was characterized as the expected Ar-ABBB (1:3) TBTAP hybrid **7** that likely results from the proposed sequential addition of aminoisoindole to 3 Pn units, followed by cyclization and aromatization (Scheme 1). However, this component was the minor product. The dominant product was identified as the unique Ar-ABBA (2:2) TBTAP hybrid **8**, produced as a single regioisomer. It is theoretically possible that this unexpected product is an artifact produced from the Ar-ABBB hybrid **7**



**Scheme 2.** Hybrid synthesis from a substituted phthalonitrile, uncovering an alternative pathway leading to Ar-ABBA TBTAP hybrid (Ar = 4-methoxyphenyl); crystal structures of hybrids **7** and **8** (solvent molecules omitted for clarity).

by a retro-Friedel Crafts (de)alkylation under the reaction conditions. Although unlikely, this possibility was eliminated in a test experiment whereby Ar-ABBB hybrid **7** was isolated and subjected to the reaction conditions (MgBr<sub>2</sub> in refluxing diglyme). No reaction took place and it was therefore clear that the Ar-ABBA hybrid **8** results from an alternative, dominant reaction sequence.

The most likely mechanism leading to hybrid **8** is shown in Scheme 3. It has the same first step as the mechanism proposed in Scheme 1, involving the initial addition of aminoisoindole to Pn rendering an AB subunit (like all intermediates in Schemes 1 and 3, this is expected to be complexed to magnesium ion that is omitted for clarity), but the pathways then diverge. Addition of this intermediate to a second Pn eventually leads to the 1:3 ABBB hybrid but this appears to be a slow step. Self-condensation of two AB intermediates (through loss of NH<sub>3</sub>) likely dominates, leading then to cyclization and aromatization via loss of a benzyl

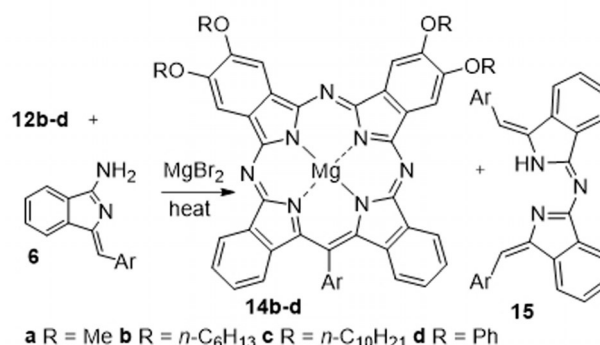
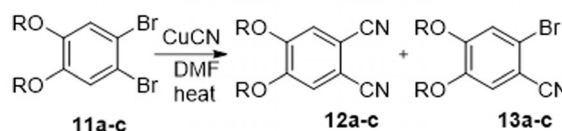
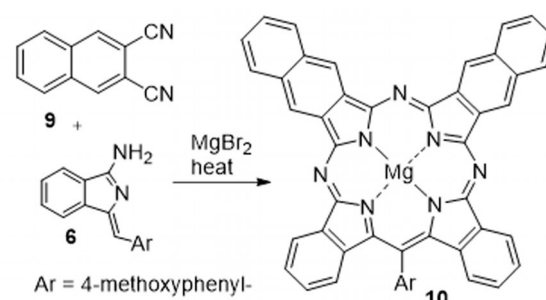


**Scheme 3.** Proposed mechanistic pathway leading to **Ar-ABBA** TBTAP hybrids.

fragment. Of course, both pathways lead to the same product if unsubstituted Pn is employed as co-reactant. Further support for this proposed sequence was provided by the results observed from changing the reaction stoichiometry and protocol. Switching to 2:2 aminoindolenone:Pn stoichiometry and/or increasing the rate of addition (including reactions where all starting materials are mixed prior to heating) increased the relative proportion of **Ar-ABBA** 2:2 TBTAP hybrid in the isolated macrocyclic product mixture. However, in such reactions the overall yield of both hybrids is reduced because self-condensation of aminoindolenone starts to compete with addition to Pn.

The reaction, therefore, offers potential to produce two separate classes of TBTAP hybrids, both largely unprecedented. Two further series of experiments were carried out to demonstrate the scope. Firstly, alternative Pn derivatives were employed. 2,3-Naphthalonitrile **9** is commercially available and underwent macrocyclization with aminoindolenone **6** (Scheme 4). Naphthalonitrile **9** appears to be more reactive than Pn **4** and the reaction is complicated by competing formation of naphthalocyanine (MgNPc). Nevertheless, **Ar-ABBA** TBTAP hybrid **10** was formed and isolated as the dominant hybrid once again. As expected,  $\pi$ -extended mixed hybrid ( $C_{2v}$  symmetry) shows a split, red-shifted Q-band absorption at 709 and 681 nm.

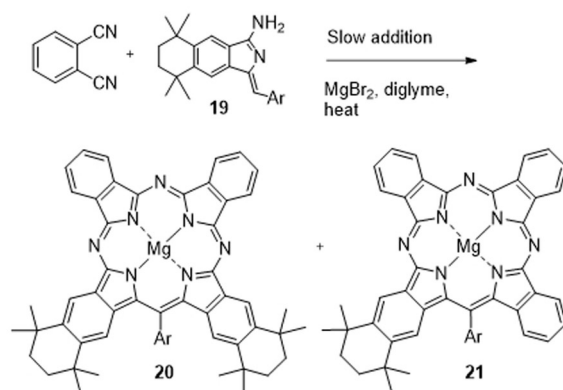
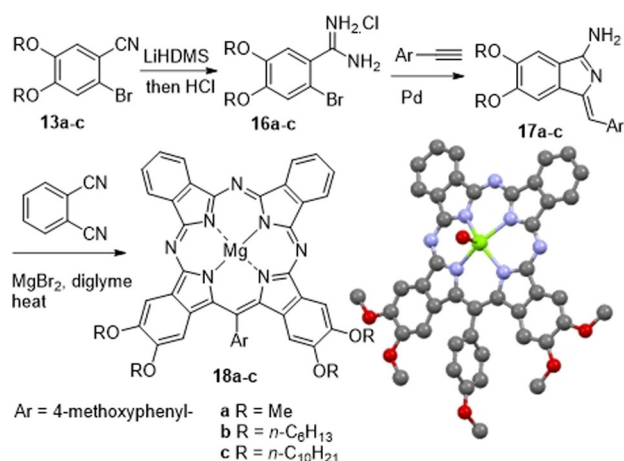
The second class of Pn selected were the 4,5-dialkoxy derivatives **12**. In Pc chemistry these Pns are widely employed.<sup>[15]</sup> They are known to be relatively easy to prepare at scale, and within the Pc series the alkoxy substituents modify the electronic, solubility and self-assembly properties. The synthesis of the Pns and hybrids is shown in Scheme 4. Cyanation<sup>[14]</sup> of dibromobenzene precursors **11** was carefully controlled to prevent excessive Pc formation under the reaction conditions. Stopping the reaction before completion resulted in a mixture of mono- (**13**) and dinitriles (**12**), but was a desirable outcome because we required the bromobenzonitrile derivatives for subsequent experiments (vide infra).



**Scheme 4.** The synthesis of naphthyl (**10**, top) and tetraalkoxy/phenoxy (**14**, bottom) **Ar-ABBA** TBTAP hybrids.

Dialkoxyphthalonitriles **12a–c** were first shown not to react to form MgPcs in refluxing diglyme in the presence of  $MgBr_2$ , allowing our standard reaction conditions to be employed for hybrid synthesis. Reaction of dimethoxy-Pn **12a** with aminoindolenone, however, failed to produce significant quantities of macrocycle (hybrid or Pc) and instead yielded significant quantities of condensation product **15** (plus unreacted Pn), presumably due to solubility issues. Longer chain dihexyloxy- and didecyloxy-Pn (**12b** and **12c**, and diphenoxy-Pn (**12d**, prepared from 4,5-dichlorophthalonitrile), reacted smoothly, however, using the single-operation procedure whereby a mixture of aminoindolenone, Pn and  $MgBr_2$  were heated directly in diglyme. Once again, the dominant macrocyclic product isolated from these reactions was the **Ar-ABBA** TBTAP. Separation proved to be challenging, but the pure **Ar-ABBA** hybrids **14b–d** could be isolated and characterized.

In all experiments described so far, an identical aminoindolenone reactant was employed. Aminoindolenone **6** has no substituents on the indolenone fragment so delivers unsubstituted rings (“A”) into the **Ar-ABBA** hybrids. Alternative substitution patterns become available if the indolenone fragment is itself functionalized, and in such cases the syntheses will deliver hybrids with substituents on the rings adjacent to the *meso*-Ar. This complementary sequence has been demonstrated using the precursor bromobenzonitriles prepared as



**Scheme 5.** Complementary synthesis of TBTAP hybrids to introduce substituents adjacent to the *meso*-carbon.

part of the earlier Pn synthesis, and is indeed a powerful approach (Scheme 5).

Bromobenzonitriles **13a–c** were converted to the corresponding amidine hydrochloride salts (**16a–c**) by treatment with LiHDMS followed by HCl workup.<sup>[16]</sup> The amidines were converted to aminoisindolenes (**17a–c**) by reaction with 4-methoxyphenyl acetylene under palladium catalysis.<sup>[17]</sup> In accordance with our previous results, reaction of these substituted aminoisindolenes with phthalonitrile in a single operation led to formation of the complementary (*meso*-adjacent) Ar-ABBA TBTAP hybrids **18a–c** as the dominant macrocyclic products, alongside traces of the 1:3 Ar-ABBB TBTAP and phthalocyanine (identified by MALDI-MS). Ar-ABBA hybrids **18a–c** were isolated pure by chromatography and recrystallization. In the case of the methoxy-substituted TBTAP **18a**, crystals suitable for X-ray diffraction were obtained and the crystal structure is also shown in Scheme 5.

Unlike the dialkoxy derivatives, aminoisindolene **19** (prepared from bromobenzonitrile **5** by the same reaction sequence described for **17**) is freely soluble in diglyme enabling the reaction to be performed by slow addition (syringe pump) to phthalonitrile and therefore allowing the sequential addition mechanism to compete more effectively. Under these conditions the 1:3 TBTAP hybrid **21** could indeed also be isolated, although it remains a minor component compared to the Ar-ABBA 2:2 hybrid **20**. This

effectively completes the series and demonstrates that the full suite of hybrid structures can be accessed at will (Figure 2).

In conclusion, two pathways are proposed for the synthesis of an important class of functionalized phthalocyanine-porphyrin hybrids (TBTAPs). The materials are novel in their own right, but more importantly, the syntheses offer control and variation over structural and substituent modifications, a goal not yet achieved even within the extensively investigated chemistry of the parent phthalocyanines. Differential substitution can be controlled leading to a full range of complementary functionality, at the *meso*-carbon itself (ideal for attachment of these functional antennae<sup>[18]</sup> molecules) and at one or both of the adjacent or opposite benzo sites to the *meso*-carbon (controlling molecular electronic character but also permitting design of super- and supramolecular functional assemblies<sup>[19]</sup>).

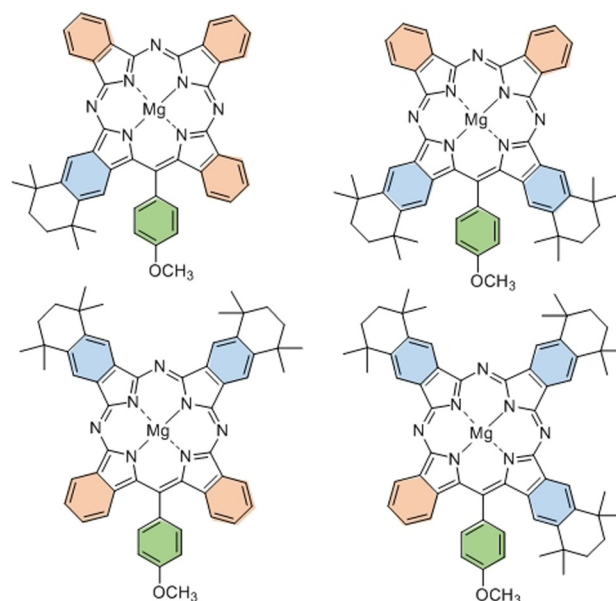


**Figure 2.** Suite of TBTAP hybrids that can now be synthesized controlling the *meso*-aryl, adjacent, and opposite benzo-substituents.

### Acknowledgements

Support from Najran University, Saudi Arabia (F.A.), UEA (I.C.), EU (A.D.M.) and EPSRC (the National Crystallography and Mass Spectrometry Services) are gratefully acknowledged.

### Conflict of interest

The authors declare no conflict of interest.

**Keywords:** hybrids · phthalocyanines · porphyrinoids · selectivity

[1] a) *The Porphyrin Handbook*, Vol. 1–20 (Eds.: K. M. Kadish, K. M. Smith, R. Guilard), Academic Press, Amsterdam, 2000;

- b) *Handbook of porphyrin science: with applications to chemistry, physics, materials science, engineering, biology and medicine, Vol. 1–45* (Eds.: K. M. Kadish, K. M. Smith, R. Guilard), World Scientific, New Jersey, **2010**.
- [2] a) C. E. Dent, *J. Chem. Soc.* **1938**, 1–6; b) P. A. Barrett, R. P. Linstead, G. A. P. Tuey, J. M. Robertson, *J. Chem. Soc.* **1939**, 1809–1820; c) P. A. Barrett, R. P. Linstead, F. G. Rundall, G. A. P. Tuey, *J. Chem. Soc.* **1940**, 1079–1092.
- [3] a) A. N. Cammidge, I. Chambrier, M. J. Cook, L. Sosa-Vargas in *Handbook of Porphyrin Science Vol. 16* (Eds.: K. M. Kadish, K. M. Smith, R. Guilard), World Scientific Publishing Company, **2012**, pp. 331–404; b) V. V. Kalashnikov, V. E. Pushkarev, L. G. Tomilova, *Russ. Chem. Rev.* **2014**, *83*, 657–675.
- [4] a) A. N. Cammidge, M. J. Cook, D. L. Hughes, F. Nekelson, M. Rahman, *Chem. Commun.* **2005**, 930–932; b) A. N. Cammidge, I. Chambrier, M. J. Cook, D. L. Hughes, M. Rahman, L. Sosa-Vargas, *Chem. Eur. J.* **2011**, *17*, 3136–3146.
- [5] a) C. C. Leznoff, N. B. McKeown, *J. Org. Chem.* **1990**, *55*, 2186–2190; b) N. E. Galanin, E. V. Kudrik, G. P. Shaposhnikov, *Russ. J. Gen. Chem.* **2004**, *74*, 282–285; c) N. E. Galanin, L. A. Yakubov, E. V. Kudrik, G. P. Shaposhnikov, *Russ. J. Gen. Chem.* **2008**, *78*, 1436–1440; d) V. V. Kalashnikov, V. E. Pushkarev, L. G. Tomilova, *Mendeleev Commun.* **2011**, *21*, 92–93.
- [6] a) Q.-D. Dao, K. Watanabe, H. Itani, L. Sosa-Vargas, A. Fujii, Y. Shimizu, M. Ozaki, *Chem. Lett.* **2014**, *43*, 1761–1763; b) N. B. Chaure, A. N. Cammidge, I. Chambrier, M. J. Cook, A. K. Ray, *ECS J. Solid State Sci. Technol.* **2015**, *4*, 3086–3090; c) Q.-D. Dao, A. Fujii, H. Itani, Y. Shimizu, M. Ozaki, *Jpn. J. Appl. Phys.* **2020**, *59*, 101003.
- [7] a) D. S. Andrianov, V. B. Rybakov, A. V. Cheprakov, *Chem. Commun.* **2014**, *50*, 7953–7955; b) M. Umetani, G. Kim, T. Tanaka, D. Kim, A. Osuka, *J. Org. Chem.* **2020**, *85*, 3849–3857.
- [8] A. Díaz-Moscoso, G. J. Tizzard, S. J. Coles, A. N. Cammidge, *Angew. Chem. Int. Ed.* **2013**, *52*, 10784–10787; *Angew. Chem.* **2013**, *125*, 10984–10987.
- [9] V. N. Nemykin, S. V. Dudkin, F. Dumoulin, C. Hirel, A. G. Gürek, V. Ahsen, *ARKIVOC* **2014**, 142–204.
- [10] Aminoisoindolene derivatives have subsequently been employed as initiators in the synthesis of expanded and contracted macrocycles, and in the synthesis of benzo-fused azadipyrromethene derivatives; a) T. Furuyama, T. Sato, N. Kobayashi, *J. Am. Chem. Soc.* **2015**, *137*, 13788–13791; b) S. Remiro-Buenamañana, A. Díaz-Moscoso, D. L. Hughes, M. Bochmann, G. J. Tizzard, S. J. Coles, A. N. Cammidge, *Angew. Chem. Int. Ed.* **2015**, *54*, 7510–7514; *Angew. Chem.* **2015**, *127*, 7620–7624; c) A. Díaz-Moscoso, E. Emond, D. L. Hughes, G. J. Tizzard, S. J. Coles, A. N. Cammidge, *J. Org. Chem.* **2014**, *79*, 8932–8936; d) Y. V. Zatsikha, L. I. Sharmova, T. S. Blesener, I. A. Kuzmin, Y. V. Germanov, D. E. Herbert, V. N. Nemykin, *J. Org. Chem.* **2019**, *84*, 14540–14557.
- [11] L. Tejerina, S. Yamamoto, I. López-Duarte, M. V. Martínez-Díaz, M. Kimura, T. Torres, *Helv. Chim. Acta* **2020**, *103*, e2000085.
- [12] I. Rose, C. G. Bezzu, M. Carta, B. Comesaña-Gándara, E. Lasseguette, M. C. Ferrari, P. Bernardo, G. Clarizia, A. Fuoco, J. C. Jansen, K. E. Hart, T. P. Liyana-Arachchi, C. M. Colina, N. B. McKeown, *Nat. Mater.* **2017**, *16*, 932–937.
- [13] a) P. R. Ashton, U. Girreser, D. Giuffrida, F. H. Kohnke, J. P. Mathias, F. M. Raymo, A. M. Z. Slawin, J. F. Stoddart, D. J. Williams, *J. Am. Chem. Soc.* **1993**, *115*, 5422–5429; b) M. Hanack, P. Haisch, H. Lehmann, L. R. Subramanian, *Synthesis* **1993**, *4*, 387–390.
- [14] G. P. Ellis, T. M. Romney-Alexander, *Chem. Rev.* **1987**, *87*, 779–794.
- [15] a) J. F. van der Pol, E. Neeleman, J. W. Zwikker, W. Drenth, R. J. M. Nolte, *Recl. Trav. Chim. Pays-Bas* **1988**, *107*, 615–620; b) N. B. McKeown, *Phthalocyanine materials: synthesis, structure, and function*, Cambridge University Press, Cambridge, **1998**; c) X. Jiang, D. Wang, Z. Yu, W. Ma, H.-B. Li, X. Yang, F. Liu, A. Hagfeldt, L. Sun, *Adv. Energy Mater.* **2019**, *9*, 1803287.
- [16] S. Dalai, V. N. Belov, S. Nizamov, K. Rauch, D. Finsinger, A. de Meijere, *Eur. J. Org. Chem.* **2006**, 2753–2765.
- [17] M. Hellal, G. D. Cuny, *Tetrahedron Lett.* **2011**, *52*, 5508–5511.
- [18] X. F. Chen, M. E. El-Khouly, K. Ohkubo, S. Fukuzumi, D. K. P. Ng, *Chem. Eur. J.* **2018**, *24*, 3862–3872.
- [19] S. Jin, M. Supur, M. Addicoat, K. Furukawa, L. Chen, T. Nakamura, S. Fukuzumi, S. Irle, D. Jiang, *J. Am. Chem. Soc.* **2015**, *137*, 7817–7827.

Manuscript received: December 14, 2020

Accepted manuscript online: January 11, 2021

Version of record online: March 1, 2021



Ultrafast Dynamics Hot Paper

How to cite: *Angew. Chem. Int. Ed.* **2021**, *60*, 10568–10572

International Edition: doi.org/10.1002/anie.202101572

German Edition: doi.org/10.1002/ange.202101572

# Ultrafast Excimer Formation and Solvent Controlled Symmetry Breaking Charge Separation in the Excitonically Coupled Subphthalocyanine Dimer

Palas Roy, Giovanni Bressan, Jacob Gretton, Andrew N. Cammidge, and Stephen R. Meech\*

**Abstract:** Knowledge of the factors controlling excited state dynamics in excitonically coupled dimers and higher aggregates is critical for understanding natural and artificial solar energy conversion. In this work, we report ultrafast solvent polarity dependent excited state dynamics of the structurally well-defined subphthalocyanine dimer,  $\mu$ -OSubPc<sub>2</sub>. Stationary electronic spectra demonstrate strong exciton coupling in  $\mu$ -OSubPc<sub>2</sub>. Femtosecond transient absorption measurements reveal ultrafast excimer formation from the initially excited exciton, mediated by intramolecular structural evolution. In polar solvents the excimer state decays directly through symmetry breaking charge transfer to form a charge separated state. Charge separation occurs under control of solvent orientational relaxation.

Self-assembled chromophore aggregates play central roles in light harvesting and energy transport processes which underpin photosynthesis, solar energy conversion and molecular electronics.<sup>[1]</sup> Co-facial molecular homodimers are the fundamental unit of such aggregates and exhibit a range of phenomena including: exciton formation and decay, which is critical in efficient energy transport; relaxation to excimers, which act as trap states, disrupting exciton diffusion; symmetry breaking charge separation, a model system for the primary step in bacterial photosynthesis.<sup>[2]</sup> In this work we probe ultrafast dynamics in the structurally well-defined  $\mu$ -oxo-subphthalocyanine dimer ( $\mu$ -OSubPc<sub>2</sub>), resolving sequential exciton relaxation to form an excimer, and observing its subsequent decay in polar solvents by symmetry breaking charge separation. While important intermediates in the decay dynamics of excitonically coupled dimers have been studied previously, most notably in perylene derivatives,<sup>[3]</sup> the rigid and soluble  $\mu$ -OSubPc<sub>2</sub> allows observation of discrete

spectra for each state and their sequential kinetics in real-time under solvent control. Thus, this study of  $\mu$ -OSubPc<sub>2</sub> permits the real time characterization of relaxation through the key intermediates of photoexcited dimers; the observation of these states suggests potential applications in photovoltaic cells.

Boron SubPc has three conjugated heteroaromatic rings, in contrast to the four familiar in phthalocyanines, and consequently adopts a bowl-like rather than planar structure. It has an intense blue-green absorption, making it a particularly useful chromophore for solar energy harvesting.<sup>[4]</sup> The oxygen bridged dimer,  $\mu$ -OSubPc<sub>2</sub>, has been synthesized and structurally characterized as a co-facial non-co-planar dimer with approximate C<sub>2v</sub> symmetry (Figure 1 a).<sup>[5]</sup> The electronic spectra of  $\mu$ -OSubPc<sub>2</sub> have been studied.<sup>[6]</sup> The absorption shows strong exciton coupling, yielding an intense blue shifted spectrum, while the emission spectra are broad and featureless and the quantum yield is low, suggestive of excimer formation (Figure 1 b). Beyond that, the photophysics of  $\mu$ -OSubPc<sub>2</sub> are uncharacterized. In the following we show that the rigid structure and good solubility of  $\mu$ -OSubPc<sub>2</sub> allows us to solvent tune its photophysics and thus unambiguously resolve the dynamics of the full range of excited state processes in excitonically coupled dimers.

Figure 1 b shows that the absorption spectrum of the dimer has its peak absorbance blue shifted by 1110 cm<sup>-1</sup> with

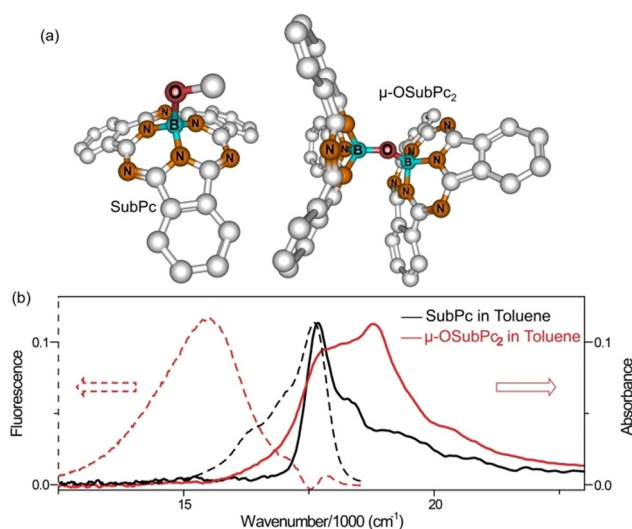


**Figure 1.** a) DFT optimized chemical structure of the SubPc monomer and  $\mu$ -OSubPc<sub>2</sub> dimer. b) Absorption (solid lines) and emission ( $\lambda_{\text{ex}} = 530$  nm, dash lines) spectra of monomer (black) and  $\mu$ -OSubPc<sub>2</sub> dimer (red) in toluene. Spectra are shown peak normalized.

[\*] Dr. P. Roy, Dr. J. Gretton, Prof. Dr. A. N. Cammidge, Prof. Dr. S. R. Meech  
School of Chemistry, University of East Anglia  
Norwich NR4 7TJ (UK)  
E-mail: s.meech@uea.ac.uk

Dr. G. Bressan  
Department of Life Sciences, Imperial College London  
London SW7 2BX (UK)

Supporting information and the ORCID identification number(s) for the author(s) of this article can be found under:  
<https://doi.org/10.1002/anie.202101572>.

© 2021 The Authors. Angewandte Chemie International Edition published by Wiley-VCH GmbH. This is an open access article under the terms of the Creative Commons Attribution License, which permits use, distribution and reproduction in any medium, provided the original work is properly cited.

respect to the monomer, indicating interchromophore coupling. In the calculated structure (Figure 1 a) the B–B distance is 0.265 nm, the shortest distance between  $\pi$  systems is 0.36 nm, and the monomer extinction coefficient is  $9 \times 10^4 \text{ M}^{-1} \text{ cm}^{-1}$ , putting  $\mu\text{-OSubPc}_2$  in the region where strong dipole-dipole coupling is expected. The spectroscopy of such molecular dimers (and higher aggregates) was elucidated by Kasha, who showed that the monomer absorption is split into two exciton states in the dimer.<sup>[7]</sup> For co-facial dimers, where the transition dipole moment is in the molecular plane (H-aggregates), the allowed (in-phase) exciton transition is blue shifted, while out-of-phase transitions to the lowest energy, red-shifted state are forbidden (in the absence of disorder). For dimers with an end-on alignment (J aggregates) the lowest energy exciton state is allowed. In  $\mu\text{-OSubPc}_2$  the centres of the rings are aligned as in an H-dimer, but the nonlinear B–O–B bridge imposes a pseudo  $C_{2v}$  structure (the individual SubPc units in the dimer undergo nearly barrierless rotation about the B–O bond, Supporting Information, Figure S1) yielding a non-parallel arrangement. In this case transitions to both the lower and upper exciton states are allowed, consistent with the simultaneous observation of a blue shifted maximum and absorption to the red of the monomer 0–0 transition in  $\mu\text{-OSubPc}_2$  (Figure 1 b).<sup>[7]</sup>

In contrast to the structured asymmetric absorption, the emission is broad and featureless, and exhibits a large Stokes loss. This spectrum is consistent with emission from an intramolecular excimer state, as detailed further below. Note that emission on the blue edge (near  $17610 \text{ cm}^{-1}$ ) is ill-defined in Figure 1 b because a trace-monomer impurity emission has been subtracted. This contribution is superficially similar to emission from a Frenkel exciton state (as has been seen in perylene dimers<sup>[3c]</sup>) but detailed analysis shows it to be a monomer contribution (Supplementary information Figure S2).

Transient absorption (TA) spectra (Figure 2) of  $\mu\text{-OSubPc}_2$  excited at 546 nm were measured with ca 100 fs time resolution between 400 and 1300 nm, in five solvents of widely varying polarity and solvation time, specifically: toluene (TL), methyl-tetrahydrofuran (MTHF), acetonitrile (ACN), *N,N*-dimethylformamide (DMF) and 1:1 TL/ACN mixture. Experimental details are described elsewhere and in the Supporting Information.<sup>[8]</sup> The TA of the SubPc mono-

mer has been published elsewhere<sup>[9]</sup> and is shown in the Supporting Information Figure S3 for reference. It shows an intense bleach at  $17690 \text{ cm}^{-1}$  and weaker induced absorption to the red ( $12000\text{--}17000 \text{ cm}^{-1}$ ) and blue (peaking at  $21200 \text{ cm}^{-1}$ ). The former decays in ca 2 ns as the bleach partially fills, while the latter does not evolve suggesting both singlet-singlet and triplet-triplet absorption contribute to that transient absorption, consistent with literature observations.<sup>[10]</sup> There is no TA observed for the monomer below  $11000 \text{ cm}^{-1}$ .

Figure 2 shows the TA for  $\mu\text{-OSubPc}_2$  in TL and DMF (data for MTHF, ACN and ACN/toluene mixtures are shown in the Supporting Information, Figure S4). In toluene (Figure 2 a) neither the bleach nor the TA, which appear promptly at  $16500$  and  $21500 \text{ cm}^{-1}$  respectively, evolve significantly in the first 10 ps. However, a negative feature appears on the picosecond timescale at  $14900 \text{ cm}^{-1}$ ; based on the absence of ground state absorption and the location of the excimer fluorescence this is consistent with stimulated emission from the excimer (Figure 1 b); the shift compared to Figure 1 b arises from the overlapping TA (Figure S7). At the same time a transient grows in the near IR (NIR) at  $9400 \text{ cm}^{-1}$ . A similar NIR transient was observed in the perylene excimer and was assigned as an excimer to charge transfer state transition.<sup>[3d,e]</sup> After about 10 ps all transient states relax toward the baseline, although the ground state does not fully recover, and at 3 ns there is a weak residual absorption at  $21600 \text{ cm}^{-1}$ , which is assigned to population of a long lived, possibly triplet

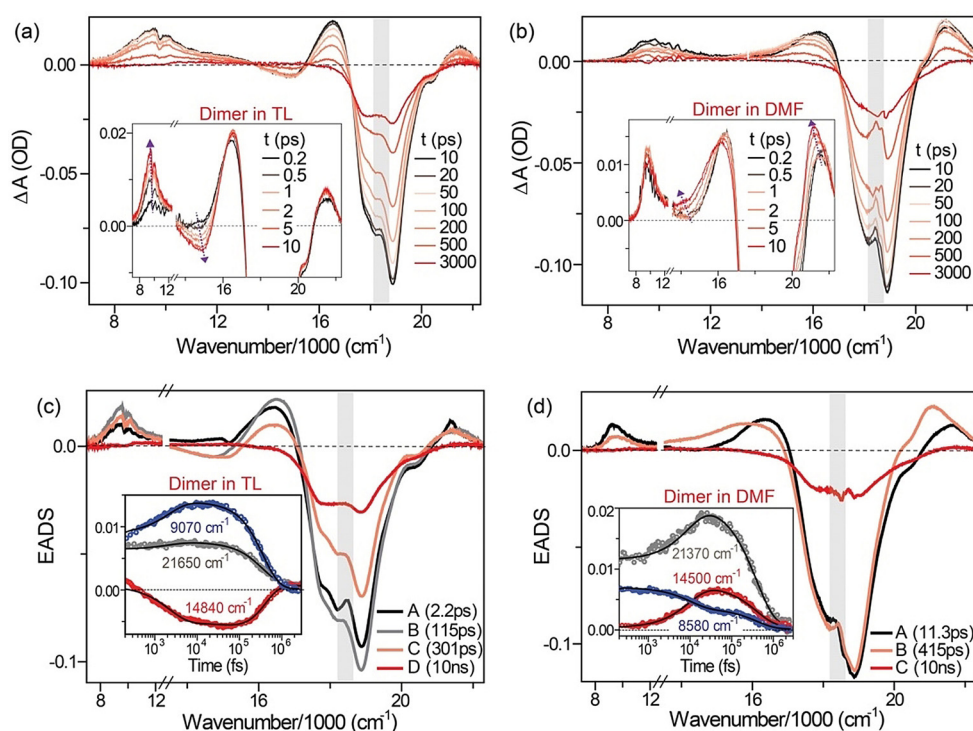


**Figure 2.** a,b) Transient absorption spectra of  $\mu\text{-OSubPc}_2$  dimer in toluene (TL) and DMF respectively at different timescales, with insets showing early time data. Excitation was at 546 nm and the dimer concentration was  $12 \mu\text{M}$ . c,d) EADS recovered from global analysis for the TA datasets in TL and DMF respectively. Inset shows data and global analysis fits at different probe wavenumbers. Note that data near  $18600 \text{ cm}^{-1}$  are perturbed by scattered light (shown by grey area).

state (the triplet TA is reported at  $21700\text{ cm}^{-1}$  in SubPc films).<sup>[10]</sup>

Figure 2b reveals very different behaviour for  $\mu$ -OSubPc<sub>2</sub> in DMF. In this case stimulated emission associated with excimer formation is not observed (consistent with the very weak broad steady state emission in this solvent, supplementary information Figure S2d,e). Instead the spectral evolution shows a picosecond rise in the transient absorption at  $21200\text{ cm}^{-1}$  and a broadening in the  $12000\text{--}17000\text{ cm}^{-1}$  transient, accompanied by a low amplitude rise in the NIR band, which probably reflects the same underlying broadening (see global analysis below). We note that in  $\mu$ -OSubPc<sub>2</sub> the NIR band does not shift with solvent polarity suggesting that in the  $\mu$ -OSubPc<sub>2</sub> dimer it is not a transition to a charge separated state.

In the weakly polar MTHF solvent intermediate behaviour is observed, with both stimulated emission due to excimer formation along with a slower rise and broadening in the transients in both visible and NIR (See the Supporting Information, Figure S4b). For polar ACN the spectral evolution is the same as for DMF, but significantly faster (See the Supporting Information, Figure S4c).

Quantitative analysis of the TA dynamics was performed by global analysis,<sup>[11]</sup> where time resolved data were analyzed with a sequential model, for which only one or two intermediate states (for polar and nonpolar solvents, respectively) plus a final state were required to obtain an accurate fit. The resulting evolution associated difference spectra (EADS) for toluene and DMF are shown in Figures 2c and d, respectively, while those for MTHF and acetonitrile are given in the Supporting Information, Figure S5, and all kinetic data are tabulated in the Supporting Information (Table S1). To show the quality of fit, the single wavelength data for key transients are plotted in the inset of Figure 2c and d, including the fitted function from the global analysis.

In nonpolar toluene the first two components are required to describe the formation of the excimer stimulated emission (at  $14840\text{ cm}^{-1}$ , Figure 2), which initially appears in 2.2 ps. Significantly, the NIR absorption ( $9070\text{ cm}^{-1}$ ) appears promptly on population of the dimer excited state, although it grows in amplitude as the stimulated emission develops. Thus, this NIR TA is evidently a dimer band rather than one specifically associated with the excimer, although the observed time dependence shows that its transition moment depends on the state (exciton or excimer) of the dimer. The second slower component in excimer formation is essential for a good fit (see the Supporting Information, Figure S6a) and appears in evolution of both the stimulated emission and the  $16500\text{ cm}^{-1}$  transient absorption. We assign this slower component to reorganization in the excimer structure during its lifetime. The rigid  $\mu$ -OSubPc<sub>2</sub> structure leaves little room for major structural reorganization. One possibility is evolution in the angle formed by the two rings, which would require solvent displacement. Alternatively, it is possible that in place of the free rotation about the O–B bonds observed in the ground state (Figure S2), the excimer has a favoured low energy orientation of the two rings, which is adopted in ca 100 ps. After this excimer reorganization the only further evolution observed in toluene is a 301 ps uniform decay in

population, which yields a final long lived state with a spectrum similar to that of the SubPc triplet.<sup>[10]</sup>

In contrast, global analysis of  $\mu$ -OSubPc<sub>2</sub> in polar DMF has only a single intermediate which forms in 10 ps, (Figure 2d). This is characterized by the absence of a stimulated emission contribution from the excimer, and a strong rising component at  $21370\text{ cm}^{-1}$ , accompanied by a broadening of the transient absorption on the low wavenumber side of the bleach, and a decrease in amplitude of the NIR band (which however persists). We assign these kinetics to polar solvent induced symmetry breaking charge separation in the  $\mu$ -OSubPc<sub>2</sub>. The growth in absorption around  $21370\text{ cm}^{-1}$  and  $14500\text{ cm}^{-1}$ , which extends across much of the visible range, is consistent with the spectrum of the SubPc cation observed in a mixed SubPc:C<sub>60</sub> film, where electron transfer occurs;<sup>[10]</sup> in that film characteristic TAs of the transient cation at  $19200$  and  $14000\text{ cm}^{-1}$  are reported, while the chemically oxidized SubPc shows a strong absorption around  $15000\text{ cm}^{-1}$ . The spectrum of reduced SubPc was observed in a photoelectron transfer and pulse radiolysis study, revealing a strong feature near  $21000\text{ cm}^{-1}$ , as seen here in the TA.<sup>[12]</sup> Thus, comparison with the available literature is consistent with charge separation in the  $\mu$ -OSubPc<sub>2</sub> dimer.

The TA data in the intermediate polarity solvent MTHF again requires two intermediate components for a successful fit (see Supporting Information, Figure S6b), but the spectroscopic behaviour is quite distinct from that in toluene. The first 1.3 ps relaxation reflects formation of the excimer stimulated emission, but the subsequent 7 ps step is associated with a small rise in the transient absorption near  $21500\text{ cm}^{-1}$  and a broadening in the transient spectrum around  $15000\text{ cm}^{-1}$  (see also the Supporting Information, Figures S4, S5). This second step is therefore associated with formation of the charge separated (CS) state from the excimer or, since transient spectra of both persist throughout the subsequent 282 ps decay, it is more likely that on the 7 ps timescale an equilibrium is established between excimer and CS state.

The kinetics in acetonitrile provide further support for symmetry breaking charge separation in polar media. The spectral evolution is essentially identical to that in DMF, but the kinetics are on a faster time scale. We assign this difference to solvent control of symmetry breaking charge separation. The mean solvation time of acetonitrile (0.26 ps) is faster than that of DMF (0.9 ps) in line with this assignment.<sup>[13]</sup> However, these times are clearly both faster than observed for formation of the CS state. These solvation times are dominated by a fast inertial (librational) solvation component. A recent measurement and simulation of charge transfer state formation in bianthryl suggests that the solvent librational component is not effective in stabilizing charge separation.<sup>[14]</sup> In bianthryl the slower diffusive orientational solvent modes were shown to be critical in the stabilization. Extending that argument to  $\mu$ -OSubPc<sub>2</sub>, we have for ACN a 0.6 ps diffusive response, which is close to the 1.2 ps observed. For DMF the slower solvation dynamics are more complex, with components of 2 and 30 ps contributing, both notably longer than for ACN.<sup>[13]</sup> Thus, the observed kinetics are consistent with the symmetry breaking decay of the excimer to form the CS state being under the control of

diffusive polar solvent reorientation. The asymmetry required is introduced by a fluctuation in the polar solvent environment surrounding the symmetric excimer. The same mechanism has been shown to operate for charge separation in quadrupolar chromophores.<sup>[15]</sup> These conclusions are summarized in Figure 3.

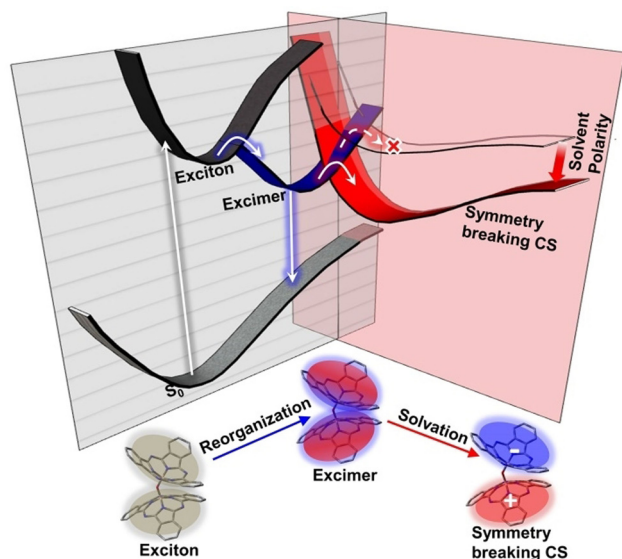


**Figure 3.** Schematic representation of  $\mu$ -OSubPc<sub>2</sub> photophysics. Direct excitation is to a Frenkel exciton state, where excitation is shared over the dimer. This is followed by sequential formation of the  $\mu$ -OSubPc<sub>2</sub> excimer and its decay by symmetry breaking charge separation to form a charge separated state, which is accessible only in polar solvent. The first step thus involves an evolution in the wavefunction of the Frenkel exciton state to favor charge resonance forms in the excimer. This involves evolution on intramolecular coordinates. The excimer subsequently decays along a solvation coordinate in polar solvents, with the initial step arising from an asymmetric fluctuation in the solvent environment.

In summary, the transient excited state dynamics of the strongly excitonically coupled, structurally well-defined  $\mu$ -OSubPc<sub>2</sub> have been recorded in a range of solvents. The formation of an excimer state from the initially excited dimer was observed to occur on a picosecond timescale. In solvents of moderate to high polarity, solvent orientational fluctuations introduce an asymmetry which promotes ultrafast decay of the excimer to a CS state. The observation of these sequential steps in a single structurally well-defined dimer suggests  $\mu$ -OSubPc<sub>2</sub> is a good candidate for modelling excited state dynamics in excitonically coupled dimers. Further, we note that the  $\mu$ -OSubPc<sub>2</sub> itself has a potentially important role to play in photovoltaic devices. Its intense blue shifted broad absorption is helpful for harvesting solar energy,<sup>[16]</sup> and its ability to yield intramolecular charge separation in asymmetric environments is useful in photovoltaic applications, because CS state formation may reduce the binding energy of charge carriers, which can thus be more easily dissociated and extracted in photovoltaic devices.<sup>[17]</sup>

## Acknowledgements

We are grateful to EPSRC for financial support (grants to SRM, EP/R042357/1, EP/J009148/1).

## Conflict of interest

The authors declare no conflict of interest.

**Keywords:** excimer · excited states · subphthalocyanine · symmetry breaking charge separation · ultrafast dynamics

- [1] a) P. D. Frischmann, K. Mahata, F. Würthner, *Chem. Soc. Rev.* **2013**, *42*, 1847–1870; b) J. L. McHale, *J. Phys. Chem. Lett.* **2012**, *3*, 587–597; c) M. R. Wasielewski, *Acc. Chem. Res.* **2009**, *42*, 1910–1921.
- [2] a) N. J. Hestand, F. C. Spano, *Chem. Rev.* **2018**, *118*, 7069–7163; b) P. D. Harvey, C. Stern, C. P. Gros, R. Guillard, *Coord. Chem. Rev.* **2007**, *251*, 401–428; c) J. D. Schultz, A. F. Coleman, A. Mandal, J. Y. Shin, M. A. Ratner, R. M. Young, M. R. Wasielewski, *J. Phys. Chem. Lett.* **2019**, *10*, 7498–7504.
- [3] a) C. Kaufmann, W. Kim, A. Nowak-Krol, Y. Hong, D. Kim, F. Würthner, *J. Am. Chem. Soc.* **2018**, *140*, 4253–4258; b) M. Son, K. H. Park, C. Z. Shao, F. Würthner, D. Kim, *J. Phys. Chem. Lett.* **2014**, *5*, 3601–3607; c) J. Sung, P. Kim, B. Fimmel, F. Würthner, D. Kim, *Nat. Commun.* **2015**, *6*, 8646d; J. Sung, A. Nowak-Krol, F. Schlosser, B. Fimmel, W. Kim, D. Kim, F. Würthner, *J. Am. Chem. Soc.* **2016**, *138*, 9029–9032; e) K. E. Brown, W. A. Salamant, L. E. Shoer, R. M. Young, M. R. Wasielewski, *J. Phys. Chem. Lett.* **2014**, *5*, 2588–2593; f) E. A. Margulies, L. E. Shoer, S. W. Eaton, M. R. Wasielewski, *Phys. Chem. Chem. Phys.* **2014**, *16*, 23735–23742; g) R. M. Young, M. R. Wasielewski, *Acc. Chem. Res.* **2020**, *53*, 1957–1968.
- [4] a) H. Gommans, T. Aernouts, B. Verreert, P. Heremans, A. Medina, C. G. Claessens, T. Torres, *Adv. Funct. Mater.* **2009**, *19*, 3435–3439; b) C. G. Claessens, D. González-Rodríguez, T. Torres, *Chem. Rev.* **2002**, *102*, 835–854.
- [5] a) Y. Yasuhiro, M. Tomohiro, *Bull. Chem. Soc. Jpn.* **2011**, *84*, 1208–1214; b) M. V. Fulford, A. J. Lough, T. P. Bender, *Acta Crystallogr. Sect. B* **2012**, *68*, 636–645; c) M. Geyer, F. Plenzig, J. Rauschnabel, M. Hanack, B. del Rey, A. Sastre, T. Torres, *Synthesis* **1996**, 1139–1151.
- [6] J. D. Dang, M. V. Fulford, B. A. Kamino, A. S. Paton, T. P. Bender, *Dalton Trans.* **2015**, *44*, 4280–4288.
- [7] M. Kasha, H. R. Rawls, M. Ashraf El-Bayoumi, *Pure Appl. Chem.* **1965**, *11*, 371–392.
- [8] C. R. Hall, J. Conyard, I. A. Heisler, G. Jones, J. Frost, W. R. Browne, B. L. Feringa, S. R. Meech, *J. Am. Chem. Soc.* **2017**, *139*, 7408–7414.
- [9] G. Bressan, A. N. Cammidge, G. A. Jones, I. A. Heisler, D. Gonzalez-Lucas, S. Remiro-Buenamañana, S. R. Meech, *J. Phys. Chem. A* **2019**, *123*, 5724–5733.
- [10] D. B. Sulas, E. J. Rabe, C. W. Schlenker, *J. Phys. Chem. C* **2017**, *121*, 26667–26676.
- [11] J. J. Snellenburg, S. P. Liptenok, R. Seger, K. M. Mullen, I. H. M. van Stokkum, *J. Stat. Software* **2012**, *49*, 1–22.
- [12] A. Medina, C. G. Claessens, G. M. A. Rahman, A. M. Lamsabhi, O. M.ó, M. Yáñez, D. M. Guldi, T. Torres, *Chem. Commun.* **2008**, 1759–1761.
- [13] M. L. Horng, J. A. Gardecki, A. Papazyan, M. Maroncelli, *J. Phys. Chem.* **1995**, *99*, 17311–17337.
- [14] C. Lee, C. H. Choi, T. Joo, *Phys. Chem. Chem. Phys.* **2020**, *22*, 1115–1121.

- [15] a) B. Dereka, M. Koch, E. Vauthey, *Acc. Chem. Res.* **2017**, *50*, 426–434; b) B. Dereka, A. Rosspeintner, Z. Li, R. Liska, E. Vauthey, *J. Am. Chem. Soc.* **2016**, *138*, 4643–4649.
- [16] J. S. Castrucci, R. K. Garner, J. D. Dang, E. Thibau, Z.-H. Lu, T. P. Bender, *ACS Appl. Mater. Interfaces* **2016**, *8*, 24712–24721.
- [17] a) Y. Tamai, *Polym. J.* **2020**, *52*, 691–700; b) I. Hwang, S. Beaupré, M. Leclerc, G. D. Scholes, *Chem. Sci.* **2012**, *3*, 2270–2277; c) T. M. Clarke, J. R. Durrant, *Chem. Rev.* **2010**, *110*, 6736–6767.
- Manuscript received: February 1, 2021  
Accepted manuscript online: February 19, 2021  
Version of record online: March 30, 2021
-